FACILITY FORM 602

N69-23419 (ACCESSION NUMBER)

(THRU)

218 (PAGES)

1 (CODE)

CR #108696 (NASA CR OR TMX OR AD NUMBER)

28 (CATEGORY)

PRINCETON UNIVERSITY

DEPARTMENT OF
AEROSPACE AND MECHANICAL SCIENCES

NASA Research Grant NGL-31-001-005
(Supplement 6)

Prepared for
National Aeronautics
and Space Administration

CURRENT PATTERN AND GAS FLOW STABILIZATION IN PULSED PLASMA ACCELERATORS

Report 857*

Prepared by Alan C Eckbreth
Alan C. Eckbreth

Approved by R. G. Jahn
Robert G. Jahn
Professor of Aerospace Sciences
and Research Leader

*This report is a reproduction in entirety of the Ph.D. dissertation of Mr. Alan C. Eckbreth. It is submitted to the sponsor and to the distribution list in this form both as a presentation of the technical material, and as an indication of the academic program supported by this Grant.

December 1968

School of Engineering and Applied Science
Department of Aerospace and Mechanical Sciences
Guggenheim Aerospace Propulsion Laboratories
PRINCETON UNIVERSITY
Princeton, New Jersey

ABSTRACT

Spatial stabilization of the formerly propagating current patterns in the exhaust plume of a linear pinch discharge device fitted with an anode exhaust orifice has led to the construction of a parallel-plate accelerator in which this phenomenon can be more conveniently studied. Stabilization of a propagating current sheet driven by a 120,000 ampere x 20 μsec rectangular current pulse is precipitated by partially insulating the electrodes. Stabilization of the current sheet at the electrode-to-insulator discontinuity is studied with Kerr-cell discharge and wedge flow photography, magnetic and electric field probes, and terminal voltage measurements. These measurements indicate the stabilized discharge continues to accelerate gas through itself as long as gas from the prior prefilling of the discharge chamber remains. A shock tube gas injection technique is used to supply fresh gas to the stabilized current discharge. It is found that the current must be driven for hundreds of microseconds before a steady gas flow can be established in contrast to the tens of microseconds time scale required for electrodynamic stabilization. The quasi-steady flow mode in which both current pattern and gas flow stabilization coexist, is studied with the above mentioned diagnostic techniques, and the discharge is again found to accelerate the inlet flow.

TABLE OF CONTENTS

TABLE OF CONTENTS-contd.

LIST OF ILLUSTRATIONS

LIST OF ILLUSTRATIONS-cont'd

LIST OF ILLUSTRATIONS-cont'd

LIST OF ILLUSTRATIONS cont'd

Chapter I

A DISCUSSION OF STABILIZATION*

A. HISTORY OF THE EXPERIMENT

The Electric Propulsion Laboratory at Princeton University has been engaged for several years in a fundamental investigation of pulsed plasma propulsion. A pulsed plasma thruster must accomplish a sequence of three events: 1) The propellant, a plasma in this instance, must be created. 2) The plasma must be accelerated to a velocity in a propulsion range of interest. 3) This high velocity plasma must then be efficiently expelled from the engine.

1. Closed Chamber Current Sheet Studies

One suitable device on which to perform basic studies on the creation and acceleration of plasma is a linear or zeta pinch. This device is schematically illustrated in Figure I-1. It consists of a right circular cylindrically shaped main chamber created by two parallel circular electrodes separated by a cylindrical, insulated outer wall. Operational details of this and other experimental apparatus will be discussed in Chapter II.

---

*For the reader unaware of the attractiveness and feasibility of electric propulsion for space missions, or unaware of the physical fundamentals and classes of electric propulsion, references [1] and [2] are highly recommended.

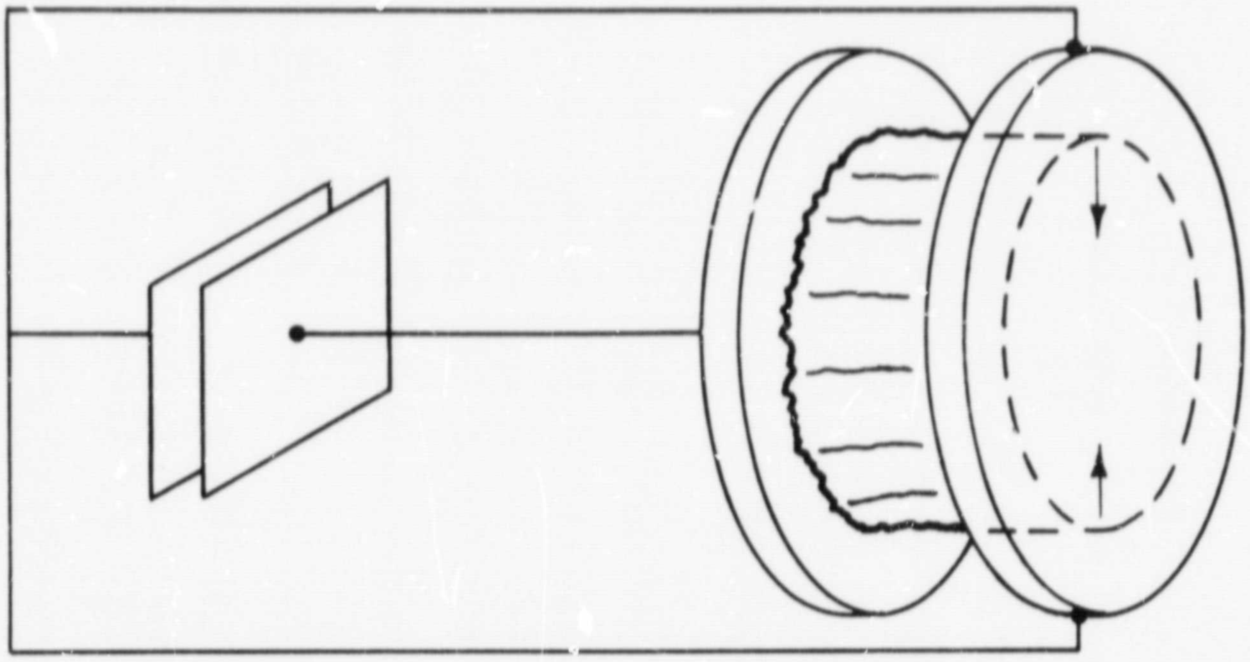

FIGURE I-1 LINEAR PINCH (SCHEMATIC)

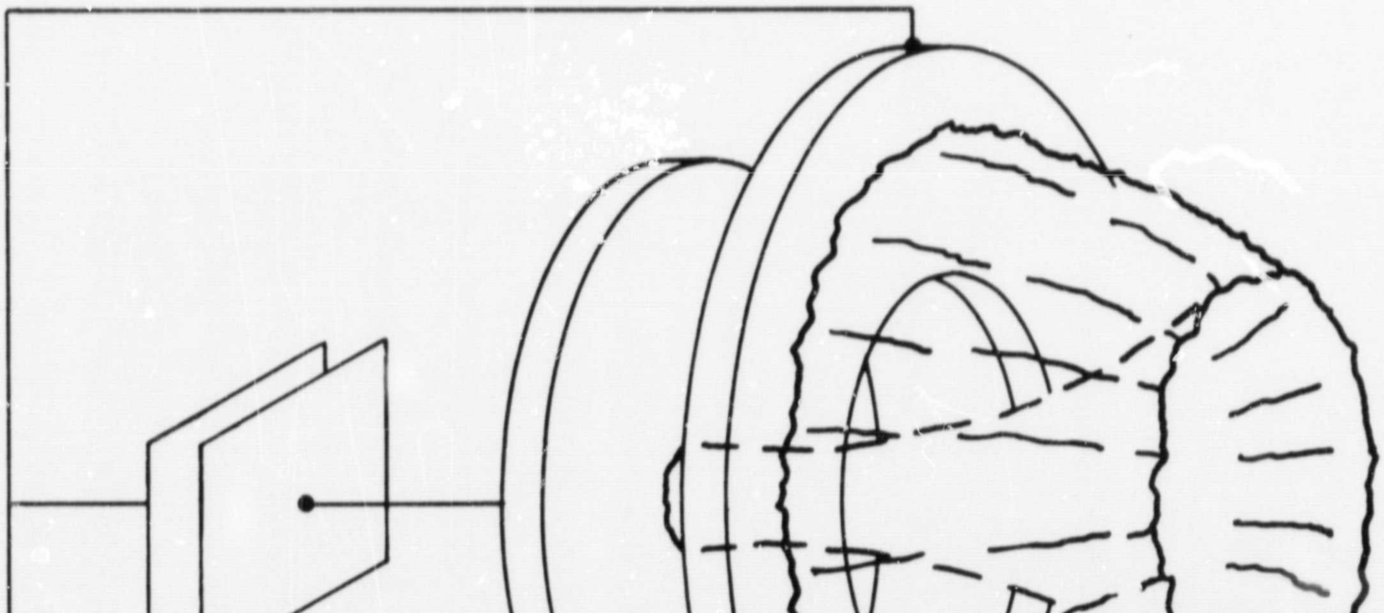

FIGURE I-2 ORIFICE PINCH (SCHEMATIC)

In operation, a cylindrical current sheet is formed at the outer wall of the discharge chamber and propagates radially inward due to the interaction of the discharge current and its self magnetic field, the familiar $\vec{j} \times \vec{B}$ force. This process continues until the sheet implodes on itself; this is the well known "pinch" process from which this device derives its name. As the current sheet drives inward, gas in its path is swept up and accelerated to sheet velocity.

One philosophy of pulsed plasma propulsion is to construct current sheets which behave as impermeable pistons sweeping up gas as they progress. One of the simplest models of the sheet [3], the snowplow model, assumes that the current sheet behaves dynamically in the above manner; the momentum equation resulting from this model when coupled with an appropriate circuit equation enable calculation of the inward trajectory of the sheet, that is, its radial position as a function of time. Departures of experimentally obtained trajectories from theoretically predicted ones, permit one to define a snowplow efficiency and to ascribe a certain leakiness to the supposed impermeable piston. Several closed chamber investigations have been completed in which the creation and acceleration phases were primarily studied, [4],[5] and others are currently being carried out.[6]

2. Orifice Pinch Exhaust Work

In an attempt to study the exhaust phase of the thruster sequence, the solid anode is replaced by an anode containing an orifice as shown in Figure I-2. A vacuum vessel is placed in front of the orifice in order that the plasma created in the pinch chamber can be expelled through the orifice. Typically, pinch devices are driven by currents exhibiting a damped, sinusoidal character whose half cycle time is comparable with pinch time, τ_p, the time it takes for the current to traverse the radius of the chamber from the outer wall to implosion at the center of the chamber. As the circuit current tends to zero, the current flowing in the exhaust plume tends to short circuit itself forming a series of current vortices which propagate downstream with the exhausted plasma.[7],[8]

In order to investigate what will occur if the circuit current does not tend to zero as the plasma is about to be exhausted, a series of experiments is conducted in which the orifice pinch device is driven with nearly rectangular current pulses whose pulse length, τ, is much greater than τ_p. The pulse lengths employed are in the tens of microseconds range. It is found that the current billows out into the exhaust vessel, as it does when driven by sinusoidal waveforms, but after a time, the current pattern ceases to propagate outward despite the presence of the force in an outward radial and axial direction. Instead, the current pattern undergoes a spatial stabilization for the duration of the current pulse, i.e. the current contours remain stationary with time. There are experimental indications, however, that despite the cessation of current propagation and hence "snowplowing" propulsion, that the current pattern stabilized discharge continues to accelerate gas through itself in a new mode.

3. Parallel Plate Geometry

In order to study this type of stabilization in a simpler geometry, a parallel plate accelerator shown schematically in Figure I-3a was constructed. In this device a plane current sheet initiates at the back wall and propagates down the accelerator away from the wall by the interaction of the current and its self magnetic field. Propagating current sheets are spatially stabilized by partially insulating the electrodes as shown in Figure I-3b. Experiments to be described later indicate that these stabilized current distributions also continue to accelerate matter through themselves.

Whether the matter accelerated by the stabilized current distribution is incompletely snowplowed gas, electrode or insulator material, or a combination of all three is not clear. Only by extending the rectangular current pulses to durations of hundreds of microseconds is it possible to feed the current zone with "fresh" gas, that is, gas never involved in the initiation and acceleration phases of the sheet. Until fresh gas is injected, the gas flow into the stabilized current zone is basically unsteady. With the advent of a

AP25 R 4444 68

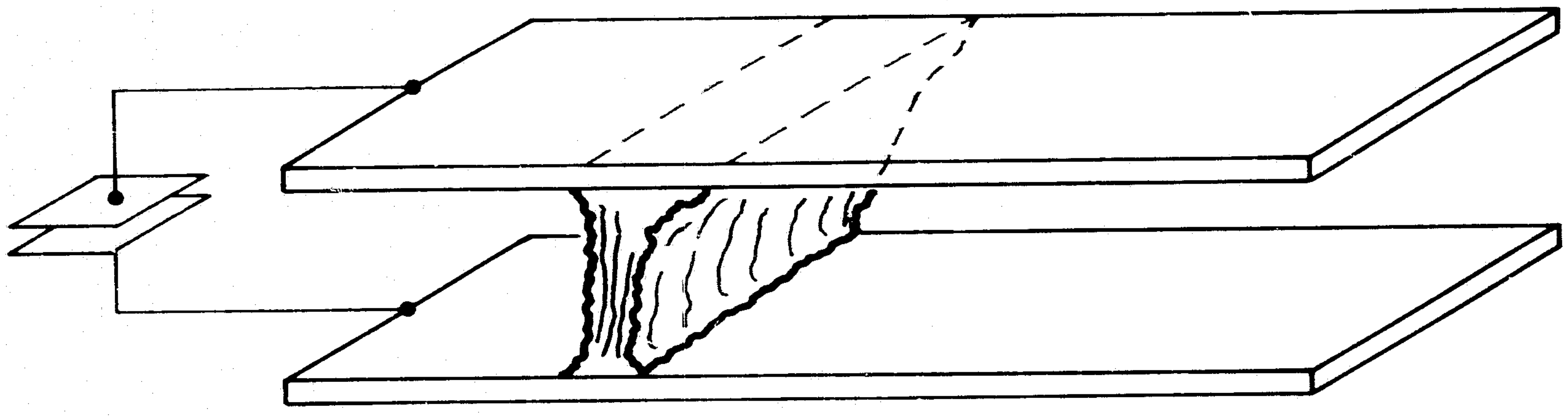

a) ALL METAL ELECTRODES

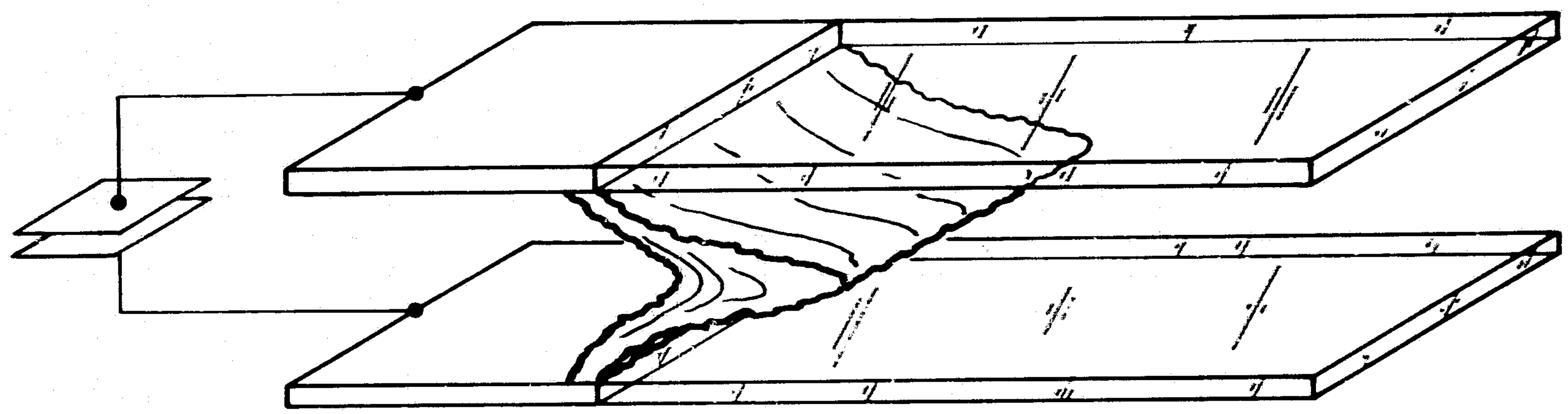

d) PARTIALLY INSULATED ELECTRODES

PARALLEL PLATE ACCELERATOR

FIGURE I-3

"fresh" gas flow to the discharge, a second kind of stabilization, a flow pattern or gasdynamic stabilization, can be identified.

B. STABILIZATION PHENOMENA

1. Types of Stabilization

This thesis studies the two above mentioned types of stabilization in pulsed plasma accelerators, namely, current pattern and gas flow stabilization. Altogether three types of stabilization may be defined: 1) current pattern or electrodynamic stabilization in which formerly convecting current distributions cease to propagate, 2) flow pattern or gasdynamic stabilization in which fresh gas is fed to the discharge, and 3) thermal pattern or thermodynamic stabilization* wherein all electrode temperatures stabilize and heat transfer to the electrodes remains constant.

2. Importance of Stabilization

Stabilizations in pulsed plasma accelerators are of interest because of the fundamental questions they pose: 1) Physically, why does current pattern stabilization occur at all, i.e. why does the current distribution cease to propagate and when can it be expected to occur? 2) What possible effect does current pattern stabilization have on the exhaust phase of a pulsed plasma accelerator? Is it desirable or undesirable? 3) What is the accelerating nature of a stabilized current distribution? How do the

---

*It should be pointed out that thermionic emission processes are not included in this category. The thermionic emisssion from the cathode stabilizes on a sub microsecond time scale. This is evident from resistive voltage drop measurements of the discharges.

accelerating characteristics of the stabilized phase compare with the pulsed phase which gives rise to it? 4) Is the establishment of the first two kinds of stabilization, current and flow pattern, a sufficient condition to allow for an accurate simulation of a completely steady state device? The work presented in this thesis is directed toward shedding some light on the first three questions.

The last question is a most difficult one to answer. An experiment is currently underway at Princeton, among other laboratories, in which an attempt is being made to simulate the steady state magnetoplasmadynamic arcjet [9] by establishing current pattern and gas flow stabilization in a pulsed plasma thruster of similar geometry. There are some steady state devices, most notably the MPD arcjet, whose environments are too hostile to permit interior diagnostic probing; consequently these devices are not very well understood. If these devices can be simulated in a pulsed mode, then many of the known transient diagnostic techniques can be employed in an attempt to gain fundamental physical insight into the operation of the devices. The results of the attempted MPD arc simulation at Princeton is the subject of a forthcoming Ph.D. thesis.[10]

C. TEMPORAL DOMAINS OF ELECTROMAGNETIC THRUSTERS

1. Accelerator Modes

Generally electromagnetic accelerators are classed either as steady or unsteady. In view of the three types of stabilization which have been discussed, four temporal domains may be identified in terms of the types of stabilization which occur in each: 1) pulsed mode - no stabilization at all occurs, 2) pulsed flow mode - only current pattern stabilization exists, 3) quasi-steady mode - both current pattern and flow stabilization are present, and 4) steady mode - all three types of stabilization occur. The first three domains may be placed under the general heading of unsteady electromagnetic acceleration.

2. Comparative Advantages

There are qualities about the various temporal regimes which make some preferable to others as the mode in which to operate an actual space engine. In Jahn's book,[2] three potential advantages of pulsed accelerators over steady state devices are pointed out: 1) Thrust efficiency has been found to increase with increased current density. Steady state accelerators have upper limits on the current density based on material erosion and heating considerations. Operation in a pulsed, repetitive mode would enable operation at comparatively larger current densities, and hence much higher average thrust levels and, most probably, less electrode erosion. 2) Operation in the pulsed mode may prevent certain equilibrations between high energy ions and free electrons, which, if allowed to occur, would result in energy losses due to radiation and inelastic collisions. 3) Pulsed operation often results in desirable spatial nonuniformities such as the skin effect, which can be advantageous.

Among others, Ashby[11] points out the disadvantages of the pulsed mode relative to the quasi-steady mode:
1) The time for each pulse is limited by the transient time, typically 1 to 10 μsec, of the sheet along the electrodes. For practical space missions, tens and hundreds of millions of discharges will be required and adequate system reliability becomes a major problem. With quasi-steady operation the pulse time is typically a millisecond, hence three to four orders of magnitude, fewer discharges would be required and system reliability should be much higher.
2) In the pulsed mode, low inductance energy storage capacitor banks are required and rapid propellant switching must be employed. In quasi-steady operation, the capacitor bank can be operated at low voltage. It need not be closely coupled to the accelerator since many thrusters can be powered from the same source and slower gas handling systems can be tolerated. 3) The efficiency of quasi-steady accelerators should be higher since magnetic field energy is not being constantly fed into an expanding zone behind the current. Furthermore, the production of internal energy is generally less in the quasi-steady acceleration mode than that in which a current sheet propels a gas by snowplowing, the so-called dynamical inefficiency [12].

Naturally, steady state devices share many of the advantages that quasi-steady accelerators possess relative to the pulsed mode. It is also to be expected that the quasi-steady devices possess many of the advantages that pulsed systems have relative to steady state operation. It is clear, then, that quasi-steady operation may indeed optimize electromagnetic acceleration processes having many of the advantages of both pulsed and steady operation and apparently few of the disadvantages of each domain. Hence the establishment of the quasi-steady flow mode and its study, are of great interest. Achievement of this quasi-steady mode of operation by establishing both current pattern and gas flow stabilization, will be described later in this work.

Chapter II

EXPERIMENTAL APPARATUS

The various discharge geometries alluded to in the last chapter will now be discussed in greater detail along with the supporting equipment employed. In the next chapter, the various diagnostic techniques employed will be described establishing the foundation on which to discuss the experiments conducted.

A. LINEAR PINCH

The linear pinch has been the principle device employed at Princeton [13] to study the creation and acceleration of current sheets. It has been modified in a way to be discussed shortly for the first exhaust experiments. A schematic diagram of the linear pinch is shown in Figure II-1. The main chamber, in which the discharge occurs, consists of two planar, circular aluminum electrodes 5" in diameter separated by a 2" interelectrode gap. The electrode separation is maintained by the outer wall, a cylindrical insulator of either glass or plexiglass. The top electrode is maintained at ground potential and since the device is charged to negative voltages relative to ground, this becomes the anode during the first half cycle of the current waveform. The middle electrode is thus the cathode and a gas injection switch assembly [14] is positioned below the cathode as shown.

AP 25 R 4442 68

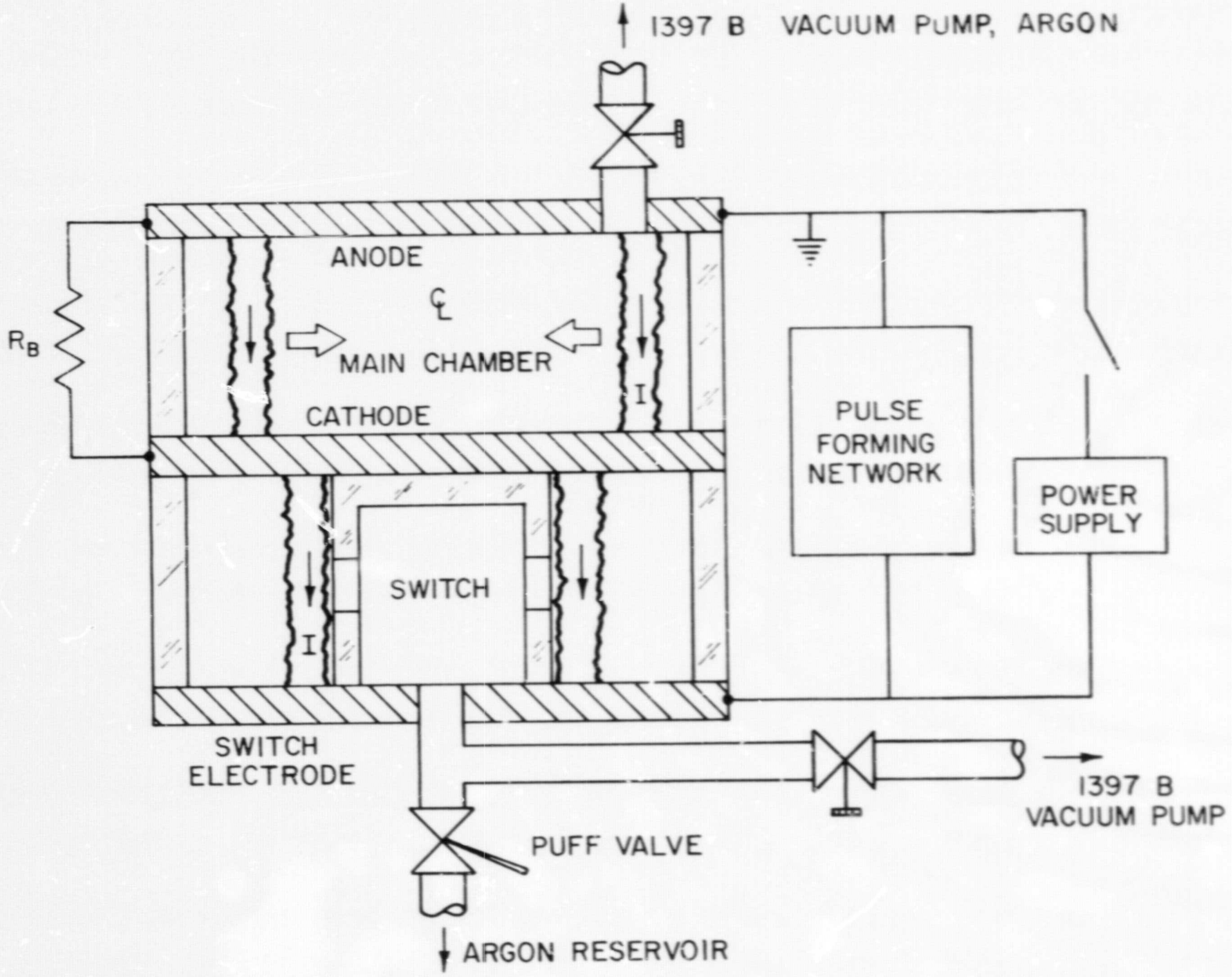

LINEAR PINCH (DETAILED SCHEMATIC)

FIGURE II-1

In operation, the main or pinch chamber is prefilled to the desired operating pressure, normally 100 μ argon and the switch chamber is evacuated. Pressure is monitored by a CVC Pirani Gauge, Type GP-140, and is calibrated using a standard McLoed gauge. The power supply charges the pulse forming network, be it a capacitor bank, LC ladder network, etc., and the switch electrode, the bottom electrode, to the desired initial voltage and is then switched off. To prevent the cathode potential from decreasing due to electrostatic induction as the switch electrode is charged, a ballast resistor R_B, typically $1000\,\Omega$, grounds the cathode to the anode. The switch is "closed" with a puff of gas; when the gas pressure reaches the equivalent 10,000 volt point on the Paschen curve, the switch discharge initiates. Since the switch discharge resistance is very low, generally less than a milliohm, the resistive voltage drop, IR, is quite small relative to the 10,000 volts initial charging voltage. Consequently, a high fraction of the initial voltage appears across the chamber electrodes which results in the initiation of the discharge. The discharge forms as a cylindrical sheet of current at the outermost wall of the pinch chamber; this particular configuration corresponds to a minimum in inductance and represents the lowest impedance path for the initiating discharge. Due to the interaction of the discharge current and its self magnetic field, the cylindrical sheet radially implodes on itself, the pinch effect. A shorting bar maintains the switch electrode at ground and shorts out the pulse forming network when the device is not in use. Additional details are available in [15] and [16].

B. ORIFICE PINCH AND EXHAUST VESSELS

The orifice pinch is a simple extension of the linear pinch wherein an anode containing a circular orifice replaces the original solid anode. The plasma created in the pinch chamber can thus be exhausted into an adjoining vacuum vessel and the ejection process can be systematically studied. The orifice pinch is shown in Figure II-2.

The first vacuum vessels used were made of pyrex, one being 6" in diameter and 24" long, the other 9" in diameter and 18" long. It became apparent, however, during the course of the work that these 6" and 9" ID vacuum vessels were too small and were interfering with the exhaust process.

To resolve this difficulty, a large plexiglass tank 3' in diameter and approximately 6' long was constructed.[17] This facility is pictured in Figure II-3. The tank is rough pumped with either a CVC 1397B (15 cfm) or a Kinney (45 cfm) pump and then further evacuated with a water cooled CVC 6" diffusion pump, Model PMC 6B equipped with a refrigerated baffle and roughed with a 1402B CVC forepump. The tank can be pumped as low as $3\text{x}10^{-6}$ mm Hg; in the work to be described, the tank is pumped down to 10^{-4} mm Hg before the discharge is initiated. Pressures are monitored with

APGS-PR 4001-64

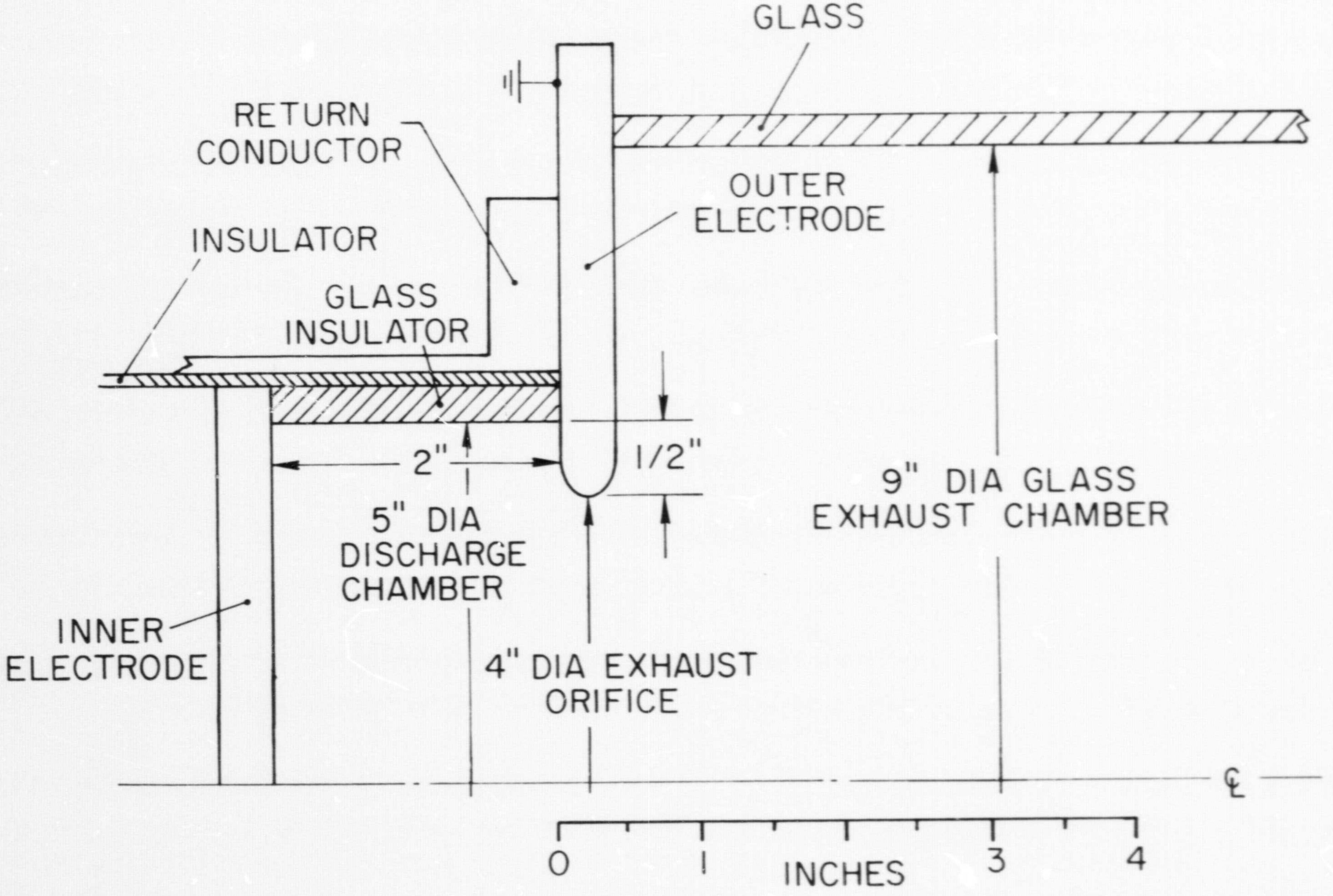

DISCHARGE CHAMBER WITH ORIFICE AND EXHAUST CHAMBER (SCHEMATIC)

FIGURE II-2

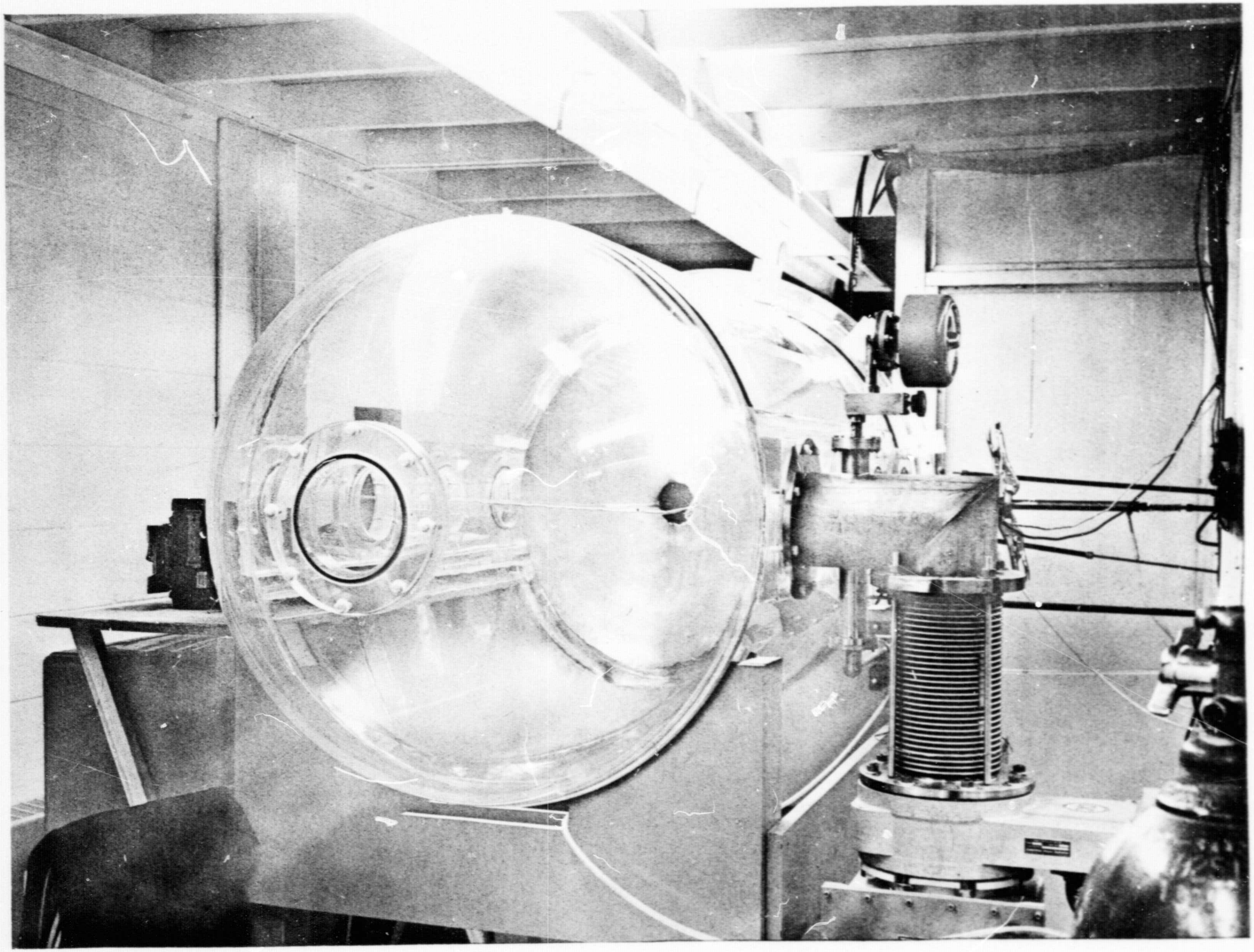

LARGE ANODE WITH EXHAUST ORIFICE INSIDE PLEXIGLAS VACUUM TANK

FIGURE II-3

a Pirani gauge and a vacuum ionization gauge CVC model GPH-100A. This tank is also fitted with an adjustable probe rake carriage shown in Figure II-4 so that probes may be accurately and reproducibly positioned in the pinch chamber and vacuum vessel. Position changes are accomplished by means of two exterior cranks, one for radial traverses and one for axial traverses.

Two distinct gas filling modes of operation are possible with the orifice pinch. In the "ambient" mode, both the pinch chamber and exhaust tank are prefilled to the desired operating pressure, typically 100μ, and then the device is operated like any linear pinch. In order to test the effect of back pressure on the exhaust phase and to simulate the space environment more closely, a "shock tube" mode of gas injection shown in Figure II-5 is employed. In this mode of operation both the pinch chamber and exhaust vessel are initially evacuated. The switch is charged to the desired operating voltage and the process is initiated by rupturing the shock tube diaphragm with a mechanical plunger. Gas flows are then established supplying the pinch and switch chambers. When the pressure in the switch reaches the proper point on the Paschen curve, the switch breaks down initiating the discharge in the main chamber. The amount of gas in the pinch chamber at breakdown can be varied depending on how the gas flows to the chamber and switch are synchronized;

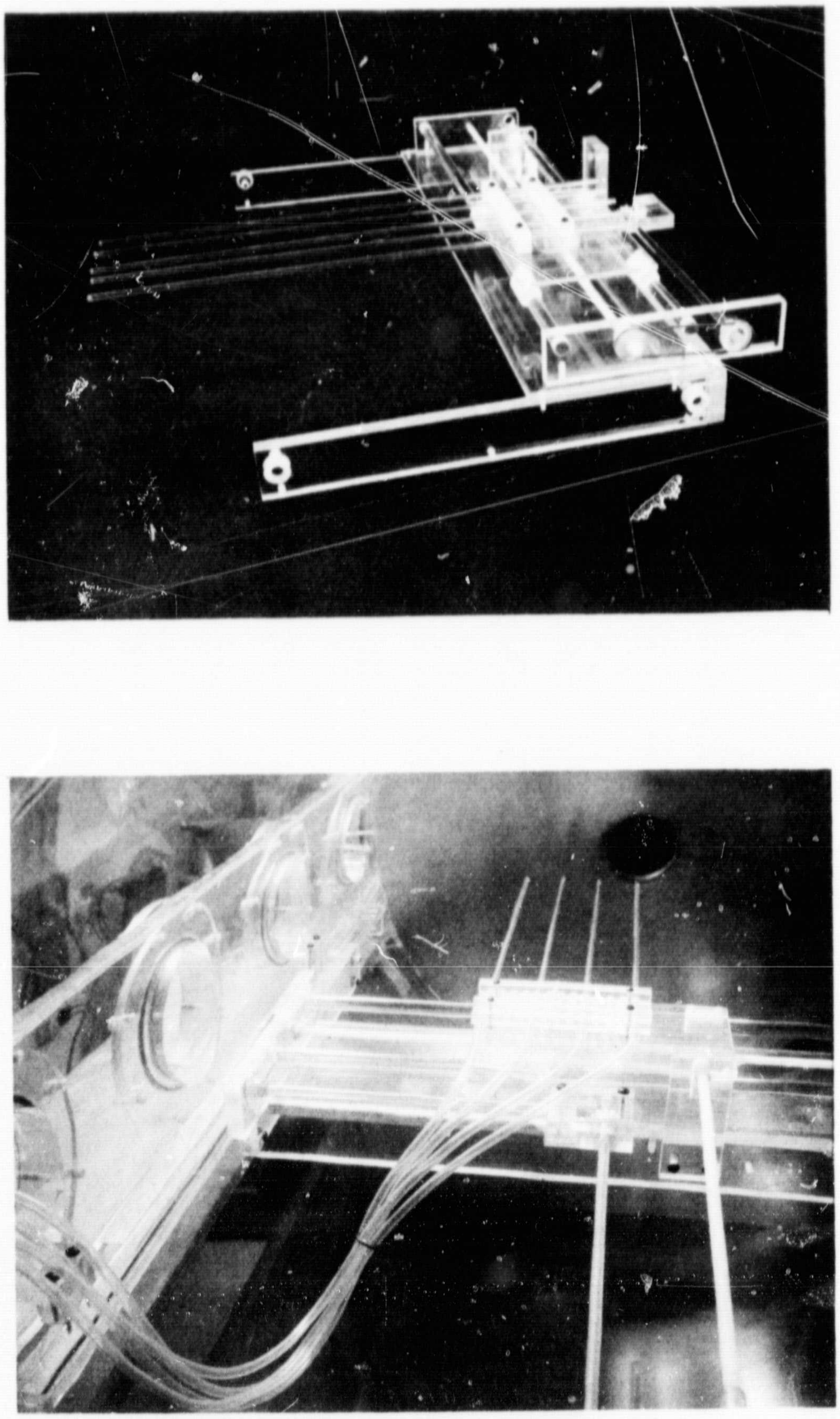

MULTIPLE PROBE ARRANGEMENT FOR PLEXIGLAS VACUUM TANK

FIGURE II-4

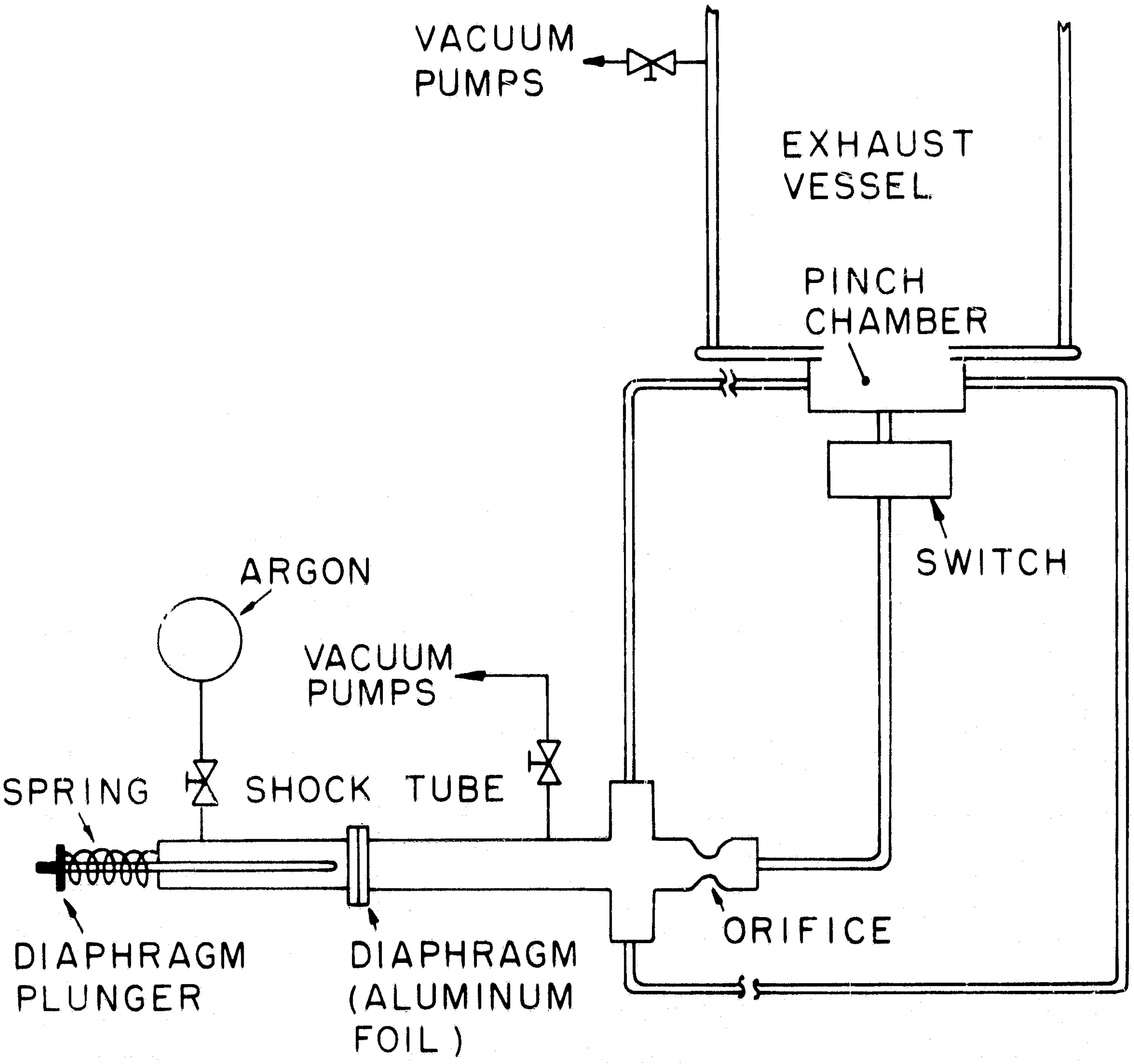

SCHEMATIC OF THE SHOCK TUBE
TRIGGERED GAS INJECTION SYSTEM

FIGURE II-5

AP25-4074-66

the synchronization of the flows can be varied by adjusting the size of the orifice leading to the switch. With this mode of gas injection, pressure in the tank remains quite low because of the large volumetric expansion from the pinch chamber to the exhaust vessel. This has been verified by direct measurement [18] using miniature fast ionization vacuum gauges. The average pressure in the discharge chamber at the time of discharge initiation is inferred by varying the switch orifice until similar behavior is found between the "shock tube" mode and a given pressure ambient filling. Kerr cell photography is the most commonly used diagnostic for the mean pressure determinations although magnetic probes can be used equally as well.

The shock tube which is used is quite small; it is about an inch in diameter and possesses 12" long driver and driven sections of stainless steel construction. Diaphragms cut from commercially available aluminum wrap are used. In all of the experiments to be described, the driver section pressure is 2 atm argon and the pressure in the driven section corresponded to that in the tank, 0.05μ; at this pressure the gas has a mean free path comparable with the tank dimensions and hence much larger than the diameter of the shock tube. When the diaphragm is ruptured, a 2 atm to vacuum interface is created. Classical gasdynamic shocks are not obtained in this situation, but rather a complicated effusion process evolves beginning as a free expansion. [19] [20] This system is used merely to inject gas into the system; no attempt is made to program or monitor the mass flow rate into the discharge. In view of the results to be presented later concerning gasdynamic flow stabilization to a current pattern stabilized discharge, the question of mass flow on a tens of microsecond time scale is a mute point. On this time scale and in the geometry under discussion, virtually no new mass is fed to the discharge after initiation.

C. PARALLEL PLATE ACCELERATOR

As mentioned in Chapter I, a parallel plate accelerator was constructed in order to provide a simpler geometry in which to achieve and study various types of stabilization.

1. Other Parallel Plate Devices

Parallel plate geometries have been used by several other investigators, either as electromagnetic shock tubes or pulsed plasma accelerators. The parallel plate configuration has, of course, been long used in steady state MHD accelerators and generators; these devices operate in substantially different regimes and will not be discussed.

Parallel plate devices have been used as electromagnetic shock tubes by Wright [21] in England and by a group at Risö, [22] [23] and treated analytically by Wright and Black, [24] and by Morse [25].

Parallel plate configurations have been employed primarily for plasma acceleration by Maes[26], Liebing [27], Dougal [28], Lie [29], MacLelland [30], and Lovberg [31]. Winicur [32] used the parallel plate configuration in a theoretical acceleration study. Burton [33] is currently using a parallel plate geometry to stabilize current sheets. It should be pointed out that in the above references, a rail gun has been classified as a parallel plate accelerator of small width.

Most of the parallel plate configurations are quite different in size from that in use here, employ different electrode materials, operate at different pressures and with different gases and are driven by widely varying current waveforms. Also to be noted is that only parallel plate geometries employing gases as opposed to vaporized metals are listed. In Table II-1 a comparative summary of all the parallel plate devices mentioned is presented. Findings of these various investigations will not be discussed in detail at this point, but will be referred to when appropriate.

2. Design Considerations

As is evident from Table II-1, parallel plate devices have been built in several different sizes. The dimensions of the Princeton device are based on the following criteria. The electrode spacing was selected to be 2"

TABLE II-1

Investigator	Dimensions L x W x H	Gas Type and Pressure	Electrode Material	Electrical Characteristics
Wright	1.57"x .78"x .78"	Deuterium .1mm Hg	Copper	10KV, 16µf, $L_o = 3 \times 10^{-9}$h
Riso	19.7"x 7.9"x 1.2"	Hydrogen .05 to 5mm Hg	Aluminum	15-25KV, 16-64µf
Maes	16"x 1/4" dia x 2-3"	Helium Puff 1.7×10^{-8} kg	?	5KV 15µf
Liebing	31.5"x 3.15"x 1.97"	Argon .02 to 3mm Hg	Copper	14KV, rectangular pulse 60,000 amps 35 µsec
Dougal	3"x 2.75"x 1.3"	Deuterium .2 to .7mm Hg	Stainless Steel	20KV, sine pulse 50,000 amps 10 µsec
Lie	3.15"x 2.36"x 1.38"	Helium .5mm Hg	Copper	10KV, 15µf
MacLelland	11.8"x 1.97"x 1.97"	N_2, H_2, Ar .5mm Hg	Brass	8KV, sine pulse 20µf, 5 µsec
Lovberg	2.36"x 3.15"x 1.57"	Hydrogen .3mm Hg	Copper	16KV, sine pulse 3µf, 10^5 amp .8 µsec
Burton	10"x 4" x 4"	Argon .075-.6mm Hg	Brass	5KV, rectangular pulse 50,000 amps 35 µsec
Princeton	48"x 6"x 2"	Argon .1mm Hg	Aluminum	10KV, rectangular pulse 120,000 amps - 20 µsec to 4,000 amps - 600 µsec

because the bulk of the experience at Princeton has been with linear pinches employing a 2" gap. This is a convenient dimension over which to probe and photograph. More importantly, however, this dimension is large enough to prevent electrode sheaths and feet from dominating the physical event under investigation. The width of the accelerator was chosen to be 6". Here a compromise must be made between very large widths relative to the electrode gap which, of course, improve the two dimensionality of the device but, in turn, decrease the lineal current density, I/W, total current/accelerator width, which, if made too low, negatively affects the sweeping properties of the current sheet. Narrow channels must be avoided to minimize three dimensional effects such as the effect of fringing magnetic fields which tend to collapse the current sheet into a spoke or constricted arc as it propagates along the electrodes. From linear pinch experience, good, sweeping sheets are found at lineal current densities of 10^6 amps/meter. Invoking an I/W scaling between the pinch work and the parallel plate, good sweeping sheets, for the highest current levels contemplated, could be obtained for a width of 6". Invoking a more general scaling, such as $F(\xi)\Big/\frac{dm(\xi)}{d\xi}$ where ξ is a generalized spatial coordinate, F the driving force on the sheet and m the mass collected by the sheet, it can be shown that for uniform fillings at the same initial pressure in each geometry the more general scaling parameter reduces to matching the lineal current density.

The length of 48" was based on the anticipated maximum excursion of a perfectly snowplowing sheet driven by a current pulse with a linear rise for a time t_o to some constant current amplitude I lasting for a total pulse time $\tau_p \gg t_o$. Because of the impedance mismatch between the capacitor bank and the discharge, the current waveform is determined by the external circuit characteristics and is independent of the sheet dynamics. To first order, it can be shown that the distance over which the current sheet will propagate during the time of the pulse scales as the total initial electrical charge, CV_o, on the capacitor bank, which is constant despite the variety of rectangular current waveforms used. For the initial charge in use here, it is found that the sheet would generally progress about 2.5' during the time of the pulse. Since current sheets which do not snowplow perfectly propagate faster and hence farther due to a decreased mass loading, it was decided to extend the above dimension to 4' to prevent the sheet from reaching the downstream wall during the time of the pulse.

Aluminum was chosen to be the electrode material based also on past experience. Aluminum is advantageous to use because of its good electrical conductivity, its cleanliness, its ease of machining and in relation to the 4'x6" electrode dimension, its light weight. For the set of partially insulated electrodes to be described later, nylon was chosen as the insulating material.

Also to be considered is the question of side walls. The parallel plate accelerator [31] employed by Lovberg consisted of two small metal electrodes placed inside a vacuum chamber with no side walls in the vicinity of the plates. If the parallel plate accelerator under consideration were situated in such a way, quite a large tank would be required. Although the large dielectric vacuum tank could be used, several logistical problems, such as difficulty of probing, capacitor bank electrical connections and time sharing arose. If side walls are used, there is the advantage of constraining the flow to interact with the discharge current and not to leak around it. For these reasons, side walls were incorporated into the design. The metal electrodes serve as two walls of the vacuum system and are mounted on the top and bottom of a one-piece plexiglass rectangular housing which serves as the four side walls of the vacuum enclosure and provides the supporting structure for the electrodes. A schematic assembly of the parallel plate accelerator is shown in Figure II-6 along with the set of coordinates to be used in all the discussions to follow.

When the all metal electrodes are used, probes are inserted into the chamber through access ports drilled in the anode cover. Although this permits construction of small probes, the streamwise spatial resolution is poor, limited to a 1/2" at best; such a resolution requires

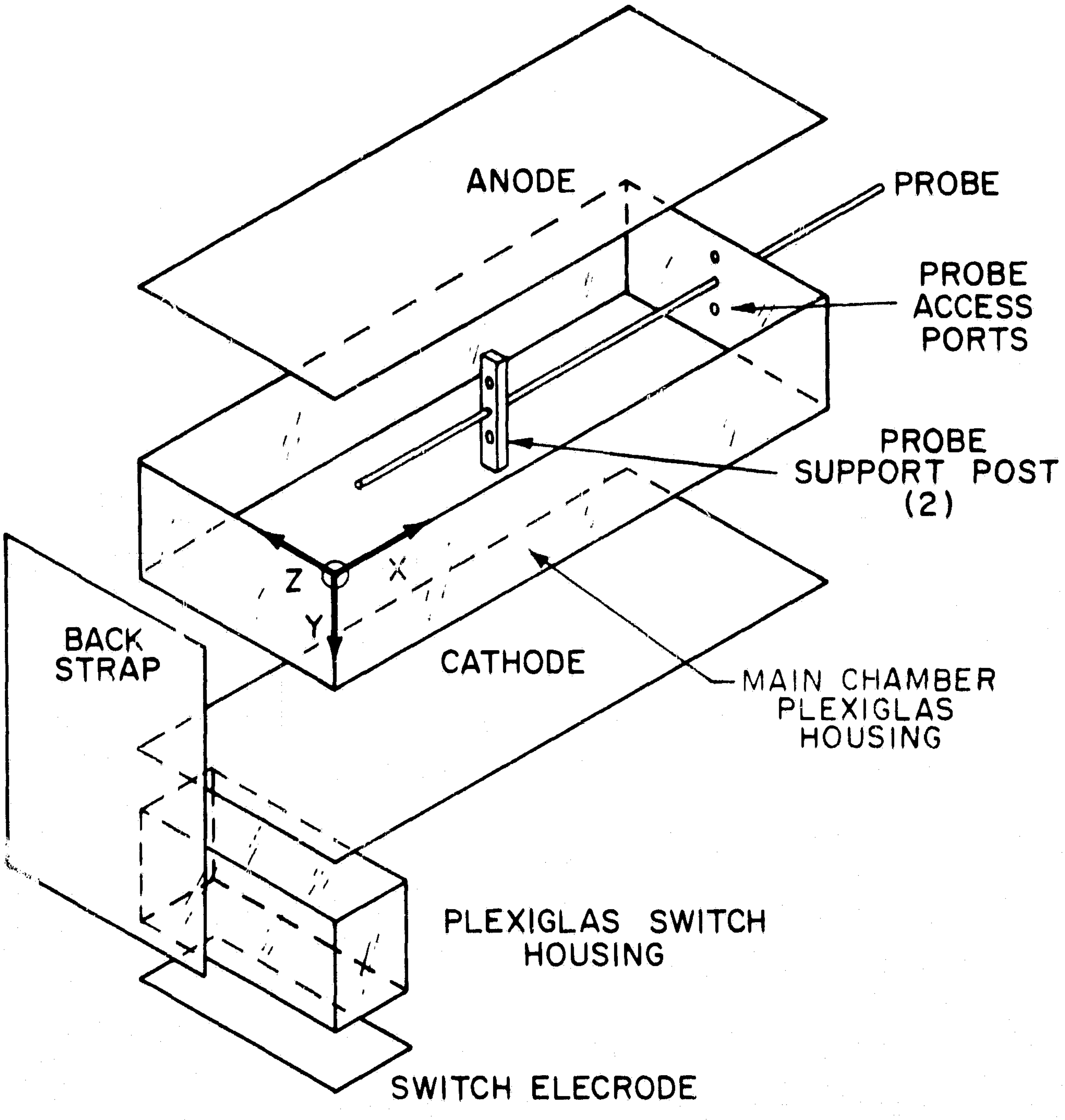

EXPLODED ASSEMBLY OF
PARALLEL PLATE ACCELERATOR

FIGURE II-6

dozens of probe holes. Furthermore when the partially insulated electrodes are used, there would be severe electrical insulation problems associated with probe ports through the insulated cover. This problem was circumvented by drilling 3 probe access ports at various heights in the front wall, at x=48", of the rectangular plexiglass housing. Long probes are required to reach the locations of interest generally in the region $0<x<12"$ but since the probes are brought in parallel to the plates in a streamwise direction, the spatial resolution in the streamwise direction can be made as fine as legitimatly allowed by the probe dimensions and the character of the phenomena under investigation. Two posts are placed in intermediate channel locations to support the probes and to enable precise positioning of the probe.

3. Description of the Device

Operationally the parallel plate accelerator functions in the same way as a linear pinch; it differs only in geometry. P photographs of the parallel plate accelerator are shown in Figure II-7. The device is shown schematically in Figure II-8a in its ambient mode of operation and in Figure II-8b in the shock tube gas injection mode.

In either mode of operation the switch is initially evacuated and the switch electrode charged to -10KV. The top plate of the accelerator serves as the anode and is

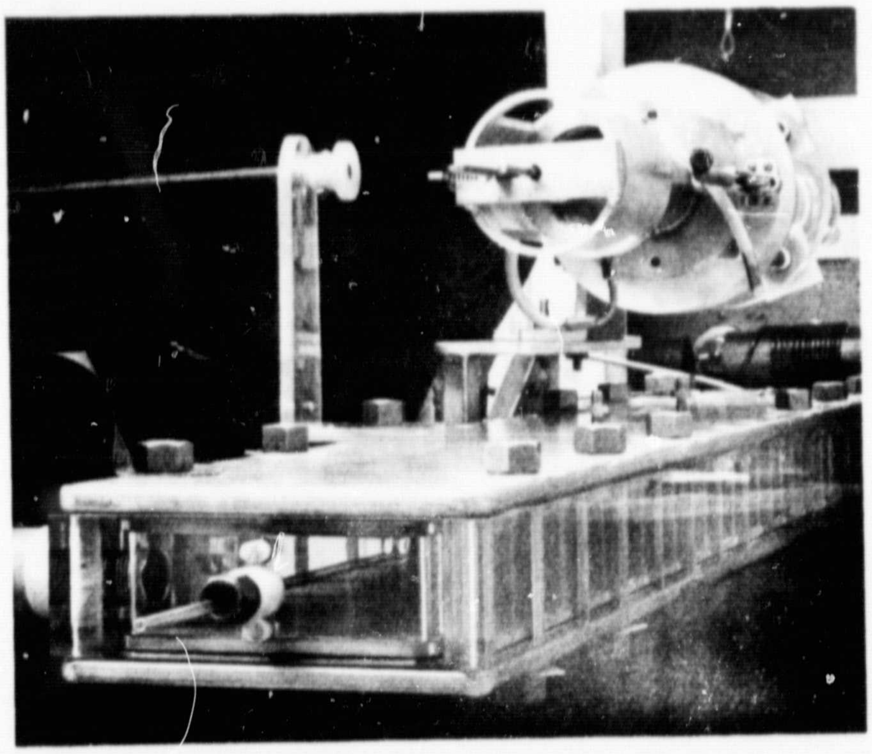

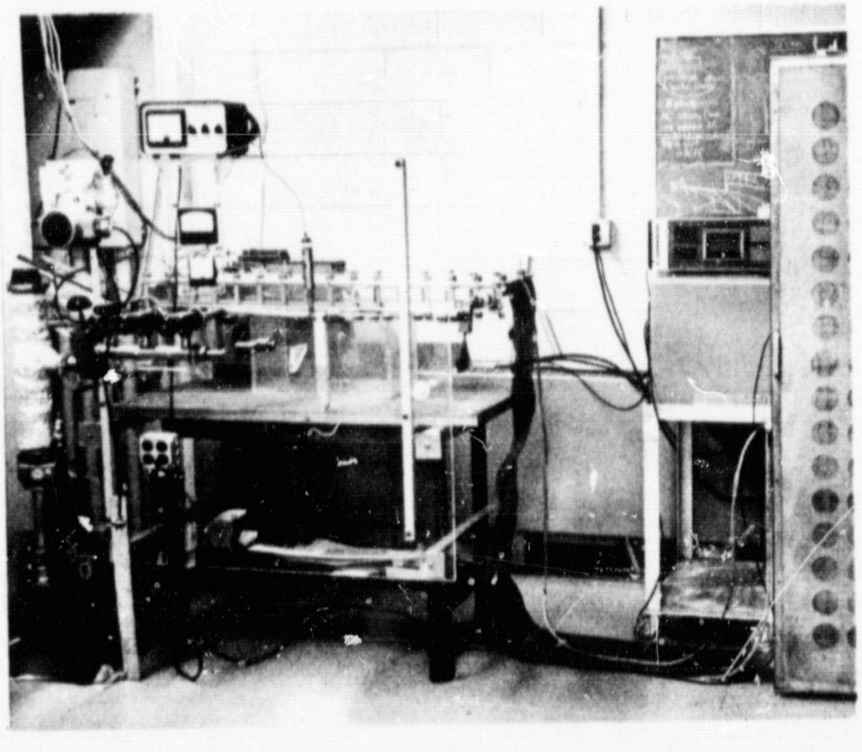

PHOTOGRAPHS OF PARALLEL PLATE ACCELERATOR

FIGURE II - 7

3P 25 A 4319 67

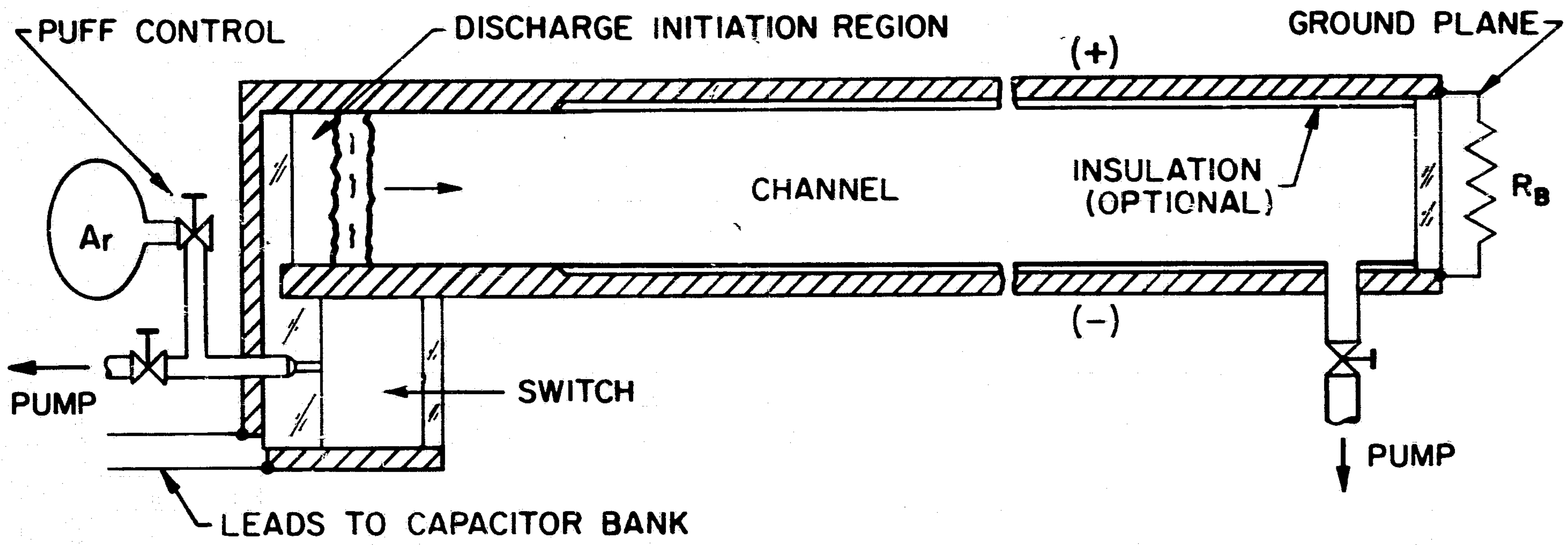

SCHEMATIC DIAGRAM OF PARALLEL PLATE ACCELERATOR

FIGURE II-8a

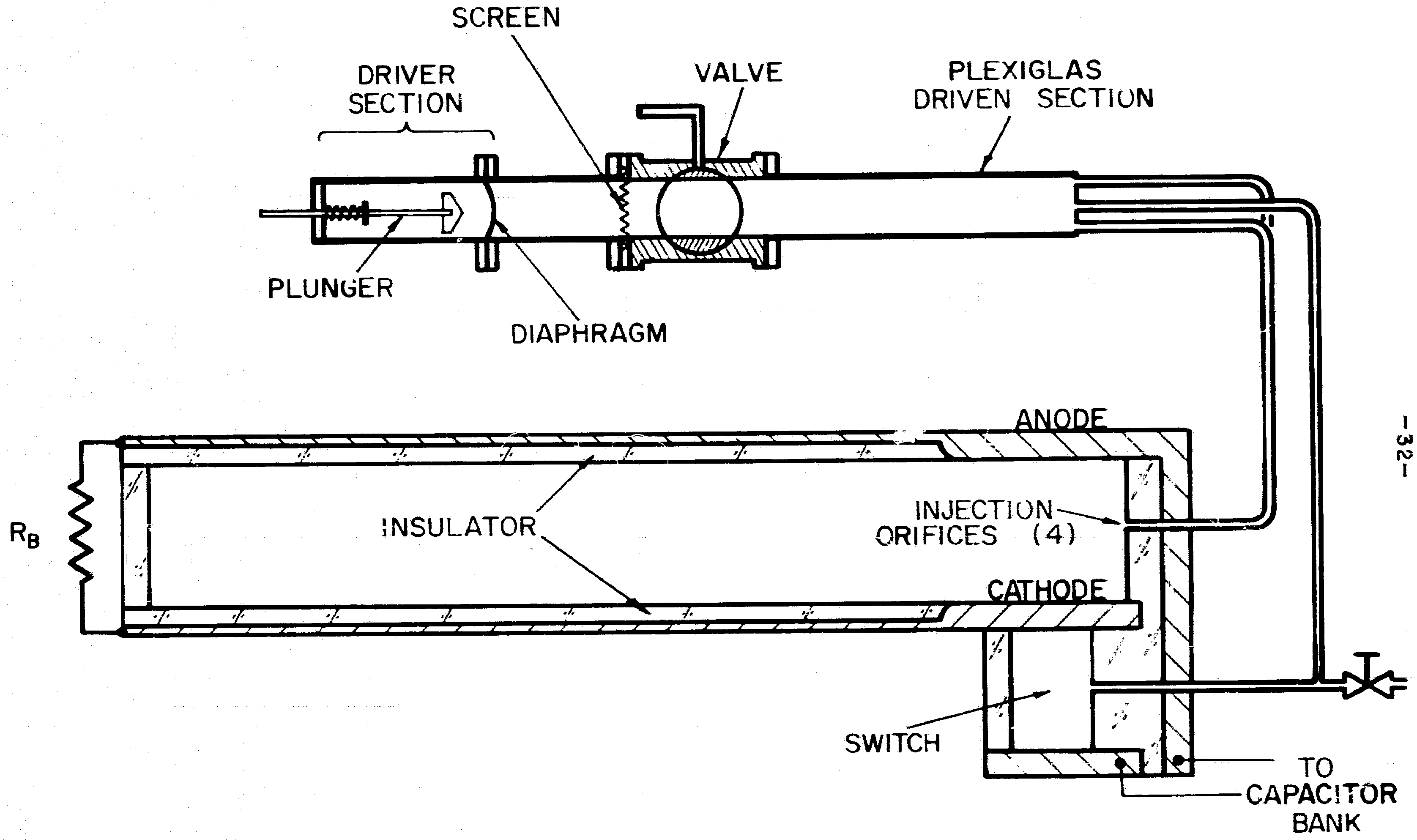

SHOCK TUBE GAS INJECTION SYSTEM

FIGURE II-8b

grounded. The bottom plate, the cathode, is kept at ground potential during the charging process through a 1000Ω ballast resistor, R_B. Gas is admitted to the switch either by a puff valve connected to an argon reservoir or from a tube leading from the driven section of the shock tube. At the proper point on the Paschen curve, the switch is closed transferring the high voltage to the cathode. This, in turn, breaks the gas down in the chamber in the form of a flat sheet of current at the back wall, at x=0", which is the position of minimum inductance. The current sheet then drives down the electrodes for the duration of the current pulse in the all metal electrode configuration, or is stabilized after a period of propagation in the partially insulated electrode configuration. These events will be described in detail in later chapters. The gas in the chamber at the time of breakdown is there either from a prefilling, the ambient mode, or from injection by the shock tube, the gas injection mode.

The shock tube employed is 2 1/2" in internal diameter, has a 6" long stainless steel driver section fitted with a diaphragm plunging mechanism, and an 18" driven section consisting of a 6" long ball valve and a 12" long plexiglass section. The plexiglass end wall, which is removable, contains 5 orifices. Four orifices feed separate 1/4" ID. tygon tubes which pass through the backstrap of the accelerator to 4 orifices in the back wall of the discharge chamber; the remaining orifice feeds a 1/2" ID tygon tube leading to the switch. Furthermore, constrictions can be inserted in the tygon tubes to regulate the flow; the flows to the chamber and switch can further be regulated relative to one another by varying the lengths of the tubes feeding the chamber and switch. The driver section pressure is 2 atm of argon in all of the experiments. Aluminum foil, .003" thick, soft temper, is used for the diaphragms.

Unlike the orifice pinch setup where diffusion pumps are used to evacuate the exhaust vessel, the parallel plate accelerator is pumped out with a roughing pump, a Welch 1397B Duo-Seal Vacuum Pump. With a liquid nitrogen cold trap, chamber pressures prior to filling or gas injection around 0.5 μ Hg are obtained. The background pressure is checked with a McLoed gauge. A Pirani gauge is generally used to monitor pressure.

D. CAPACITOR BANK AND PULSE FORMING

The capacitor bank used in all of the work to be described, unless otherwise noted, consisted of 40 BICC Fast Energy Storage Capacitors with an individual capacitance of 3.2 μf and a voltage rating of 30 KV* Since rectangular current pulses are desired, the capacitors are arranged in 4 rows of 10 capacitors as shown in Figure II-9. Each set of capacitors is connected in parallel with a series inductance

---

*We are indebted to the Plasma Physics Laboratory of Princeton University and the Atomic Energy Commission for the loan of these capacitors.

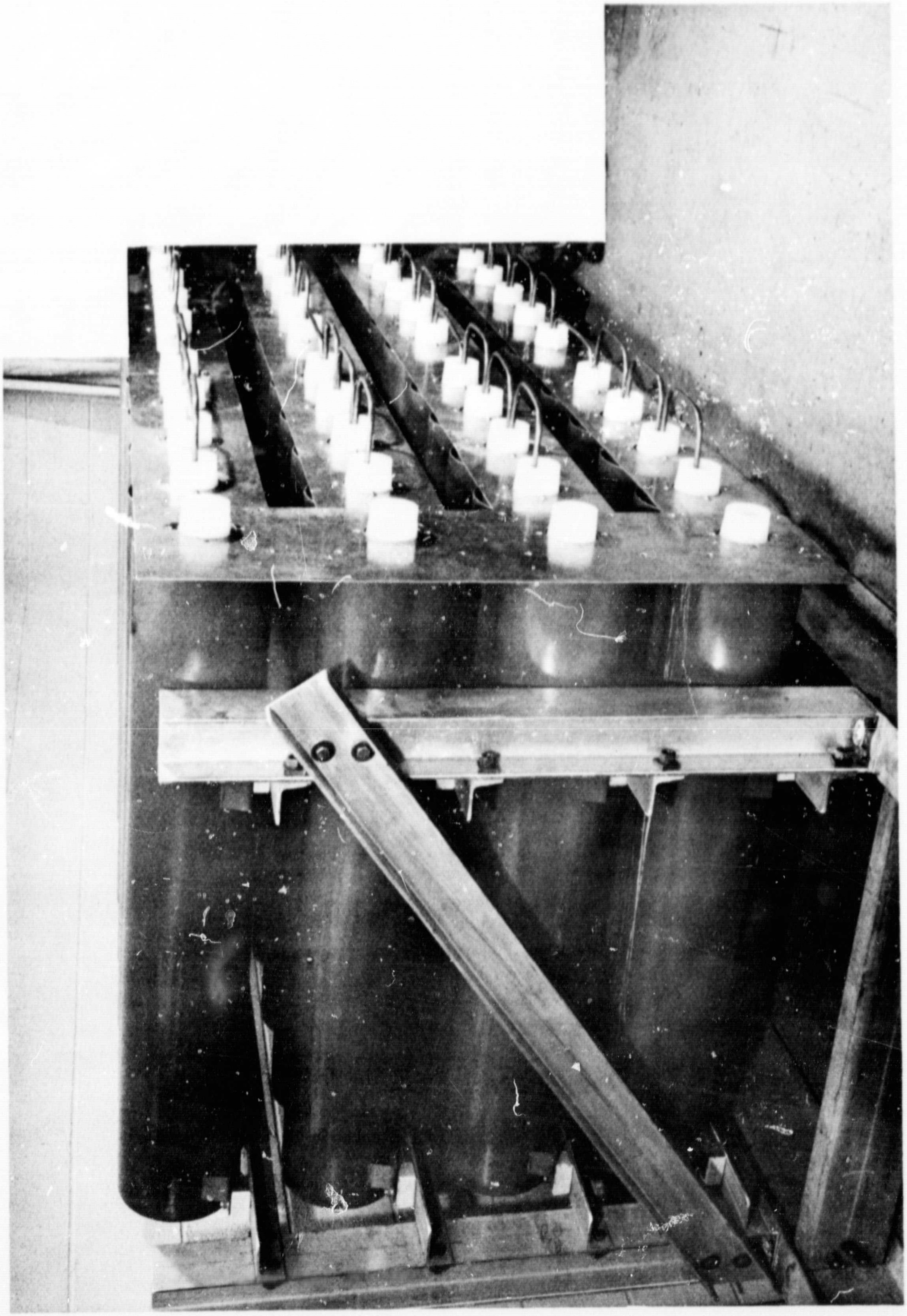

VIEW OF LONG PULSE NETWORK

FIGURE II-9

to form a LC ladder network. Such ladder networks, when charged to an initial voltage and discharged through a short, deliver a rectangular current pulse of amplitude $I_\ell = V_0/Z_\ell$ where $Z_\ell = [L/C]^{1/2}$ and duration $\tau_\ell = 2[LC]^{1/2}$ where L and C are the total inductance and capacitance respectively of the line.[34][35] When the 4 ladder networks are placed in parallel, the current delivered through the short is $4I_1$ and the pulse time is τ_ℓ. When the 4 ladders are connected in series, one obtains $I = I_1$ and $\tau = 4\tau_\ell$. Because the discharge impedance is much smaller than the line impedance, the discharge can be treated as a short relative to the external circuit parameters and the current is determined by the line characteristics and the initial voltage. Since LC ladder networks simulate transmission lines, the ladder network is referred to as the line. 10 KV is the normal and also the maximum operating voltage used. Using copper inductors shaped much like door handles, some of which can be seen in Figure II-9, pulses of 120,000 amperes for 20 μsec, 60,000 amps for 40 μsec and 30,000 amps for 80 μsec are obtained. When referring to rectangular current pulses the shorthand notation, I (kiloamps) /τ (μsec) will be employed; in reference to the above current pulses, one writes $^{120}/20$, $^{60}/40$ and $^{30}/80$. With inductors consisting of 13 turns of #8 TW wire wound on 4" OD plastic sewer pipe nominal pulses of $^{20}/125$, $^{10}/250$ and 5/500 are obtained. Using this technique, fairly good pulse shapes are obtained which are perfectly reproducible. With the present capacitor bank and a desired I/τ current pulse, the inductance required can be readily calculated. The inductance of a given coil or piece of rod is experimentally determined by inductively coupling into an unknown L- known C circuit with a sine wave generator and searching for resonance.

E. SUPPORTING EQUIPMENT

To record the data, type 551 or 555 dual beam Tektronix oscilloscopes are employed to monitor the data signal which is recorded by photographing it off the oscilloscope face. The oscilloscopes are housed in copper screenrooms fitted with power line filters to shield the oscilloscopes from any background noise and from noise generated during the course of the experiment. Noise, as used here, is considered to be any unwanted electromagnetic or electrostatic pickup whether it be truly spurious or due to fields and waves associated with the experiment.

Two different modes of grounding are employed during the experiments. When the diagnostics used are inductively coupled into the experimental apparatus, the diagnostics i.e. probe, oscilloscope and screenroom and the experimental apparatus i.e. accelerator, capacitor bank, power supply are separately grounded via direct earth grounds. Power line grounds are generally avoided. When the diagnostics are directly coupled e.g. voltage probe, a ground plane is employed between the screenroom and the accelerator.

A ground plane is a wide sheet of copper connecting the screenroom to the ground electrode, the anode in all cases. In this case, the direct earth ground from the screenroom is removed and the entire system is ground with one direct earth ground to the capacitor bank. Since all the systems are interconnected, all are grounded. The removal of the second earth ground when the ground plane is in use is to avoid the creation of a "ground loop". In high frequency electromagnetic work, changing magnetic fluxes can induce an emf about a loop, and all points of the loop, supposedly at ground, are not at the same potential; this is similar to how a radio loop antenna works. The induced emf's about the loop must not be allowed to occur in a situation where measurements are made relative to ground. The use of a ground plane with inductively coupled diagnostics is optional but here again care must be exercised to employ only one ground for the entire system. The use of a ground plane with directly coupled diagnostics is found to be mandatory.

CHAPTER III

DIAGNOSTICS

To study the various phenomena of interest, several types of diagnostics are employed. These diagnostic techniques will now be described in general. Since several variations of a particular type of probe are often used, specific details concerning particular probes will be discussed in connection with the appropriate experiment.

A few brief comments on the environmental conditions prevailing in the various discharge devices described in the preceding chapter should be made to describe the character of the probing regime. The initial voltage used in all of the experiments is 10,000 volts. After breakdown of the gas, the voltage across the electrodes is generally less than 1000 volts. The discharge is driven with rectangular current pulses ranging from 120,000 amperes for 20 μsec to about 5,000 amperes for 500 μsec. This predicates power levels in the gas from 0.2 to 84 megawatts; these power levels are, of course, sustained for very short times, so that the energy deposition into the gas varies from about 10^2 to 1.5×10^3 joules. Argon is used in the experiments and the initial pressure under ambient conditions is generally 100μ;

this corresponds to a density of 3.3×10^{15} particles/cm^3. Electron densities may range as high as 10^{16} particles/cm^3. Current sheet speeds up to 40,000 $^{\text{m}}$/sec are found with the largest amplitude current pulses. Generally, probe responses in the sub microsecond time range are required.

A. KERR CELL PHOTOGRAPHY

Kerr cell photography is employed to view directly the luminosity associated with the current distribution whether the current is moving, stabilized or in the process of stabilizing. It is also employed in an attempt to determine the nature of the flow field by investigating the luminosity generated by the interaction of the plasma flow and 15° half angle wedges placed in the flow. The physics of the Kerr cell shutter is explained in [36].

The Kerr cell used in these experiments is an Electro-Optical Instruments Model E-^{51}/A ^{W}/HN-22 ^{S}/N 6272. Two exposure times are available, 50 nanosec and 5 µsec. The former is used with the current pulses ranging from the ^{120}/20 through ^{30}/80, while the latter is employed for the ^{20}/125 through ^{5}/500 pulses.

The Kerr cell, employed as a fast shutter, is placed directly in front of a Graflex camera whose shutter is held open. In operation, the oscilloscope triggers at the time of discharge initiation and simultaneously delivers an output pulse which is fed to a Hewlett-Packard Model 214A pulse generator. The input pulse to the generator is amplified and delayed as desired relative to the initiation of the discharge; the output pulse is then fed to the Kerr cell electronics network "opening" the Kerr cell shutter. A voltage tap on the Kerr cell module feeds an indicator pulse back to the oscilloscope which is recorded and seen as small hash on the current waveform. In this manner, the precise time when the photograph is taken, can be recorded. By adjusting the delay in the pulse generator, a time sequence of photographs of the time history of the luminous event under study can be obtained.

In actuality, it turns out that Kerr cell shutters transmit a minute amount of light even when supposedly "closed". This leads to a condition known as "bleedthrough" whereby light passes through the Kerr cell shutter when "closed" and exposes the film. When photographing propagating discharges which quickly sweep by the camera, there is a natural shuttering of sorts and bleedthrough is not a problem. However, bleedthrough can be serious when photographing a stabilized current distribution or a steady wedge flow pattern. In such an instance, the transmission of the "closed" shutter times the duration of the event i.e. the bleedthrough, can be a significant fraction of the transmission when "open" times the exposure time. Bleedthrough can be checked by having the photographic system view the particular process under study without "opening" the Kerr cell shutter. Since off axis light is the principal cause of bleedthrough, it can be minimized by carefully masking all parts of the apparatus except for the precise location of study. In all of the photographic work to be presented subsequently, bleedthrough has been checked and only photographs with insignificant bleedthrough are shown. In the majority of experiments conducted, bleedthrough has not been a very serious problem.

B. MAGNETIC INDUCTION COILS

Induction coils are diagnostic tools which derive their ulility from the Faraday Induction effect described by the equation

$$\nabla \times \vec{E} = -\frac{\partial \vec{B}}{\partial t} \qquad \text{(III-1)}$$

or in integrated form

$$\oint_c \vec{E} \cdot d\vec{l} = -\frac{\partial}{\partial t} \int \vec{B} \cdot d\vec{A}_c \qquad \text{(III-2)}$$

When applied to a fixed coil in space, the above simply states that an emf will be generated across the leads of the coil in proportion to the area of the coil, the number of turns of the coil and the time rate of change of the magnetic induction through the coil. If the output signal is integrated in time, one obtains the magnitude of the component of the magnetic induction, passing through the coil parallel to its axis, as a function of time.

Knowledge of the spatial distribution of the magnetic induction throughout space can lead to a determination of the current density distribution from Ampere's Law

$$\nabla \times \vec{B} = \mu_0 \vec{J} \qquad \text{(III-3)}$$

or to a determination of total current flow through an area from Ampere's Law in integral form

$$\oint_c \vec{B} \cdot d\vec{l} = \mu_0 I \qquad \text{(III-4)}$$

where the line integral is around the area of interest. Ampere's Law is a special case of the more general Maxwell equation

$$\nabla \times \vec{H} = \vec{J} + \frac{\partial \vec{D}}{\partial t} \qquad \text{(III-5)}$$

in which the displacement current, $\frac{\partial \vec{D}}{\partial t}$, has been neglected. For high conductivity plasmas, this is justified for time variations whose characteristic frequency is less than that roughly of microwaves.[37] Furthermore, the permeability of the medium is accurately given by μo, the permeability of free space, since currents resulting from magnetization in the plasma are very small compared with the conduction currents. Hence $\vec{B}$ and $\vec{H}$ are related by a multiplicative scalar, μo.

The judicious application of Faraday's and Ampere's Laws constitutes the philosophy of the magnetic induction coil diagnostic technique. Since time integration of the raw signals is an essential element of this technique, the integrators used will be discussed prior to discussing the various forms of induction coils.

1. Integrators

An integrator in the sense used here is a simple electrical circuit containing passive circuit elements which electronically integrates with respect to time a given input signal and places the integrated signal across its output terminals. The integrators used in this work are RC integrators and are diagrammed in Figure III-1. It can be easily shown that if $R_g \ll R$, and if $RC \gg t_i$, where t_i is the time of integration, then the output signal is directly proportional to the time integral of the input signal where the constant of proportionality is $^1/RC$.[38] RC is referred to as the time constant of the integrator and it is generally made an order of magnitude greater than the duration of the signal to be integrated. Integrators attenuate as they integrate. Consequently, in designing a probe which measures the time derivative of a quantity of interest, the probe must be made sensitive enough so that the output after integration is large enough to be monitored on the oscilloscope.

2. Rogowski Coil

The Rogowski coil is used in the linear pinch and the orifice pinch to monitor the total current in the discharge. A Rogowski coil is a toroidal coil of wire, shown in Figure III-2, whose output is directly proportional to the time rate of charge of total current flowing through the area enclosed by the torus. The coil, of course, records an emf related to the time derivative of the magnetic induction

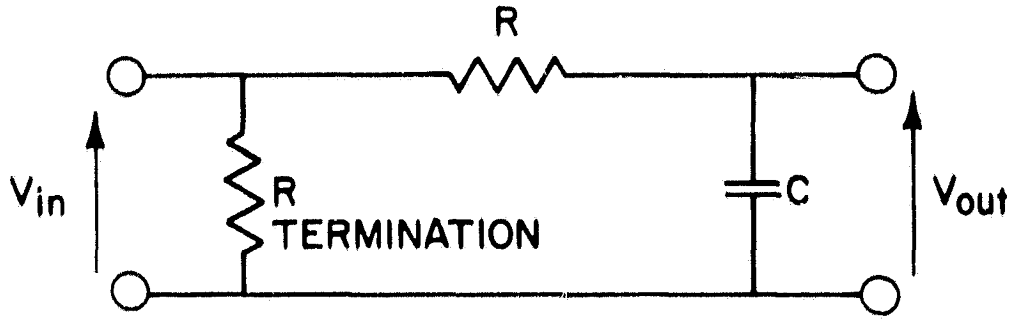

FIGURE III - 1 , RC INTEGRATOR

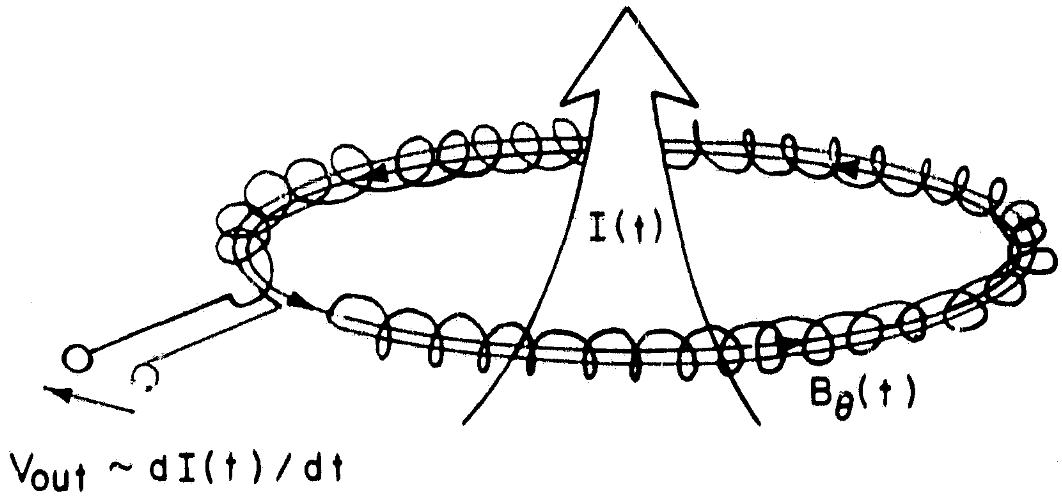

FIGURE III - 2 , ROGOWSKI COIL

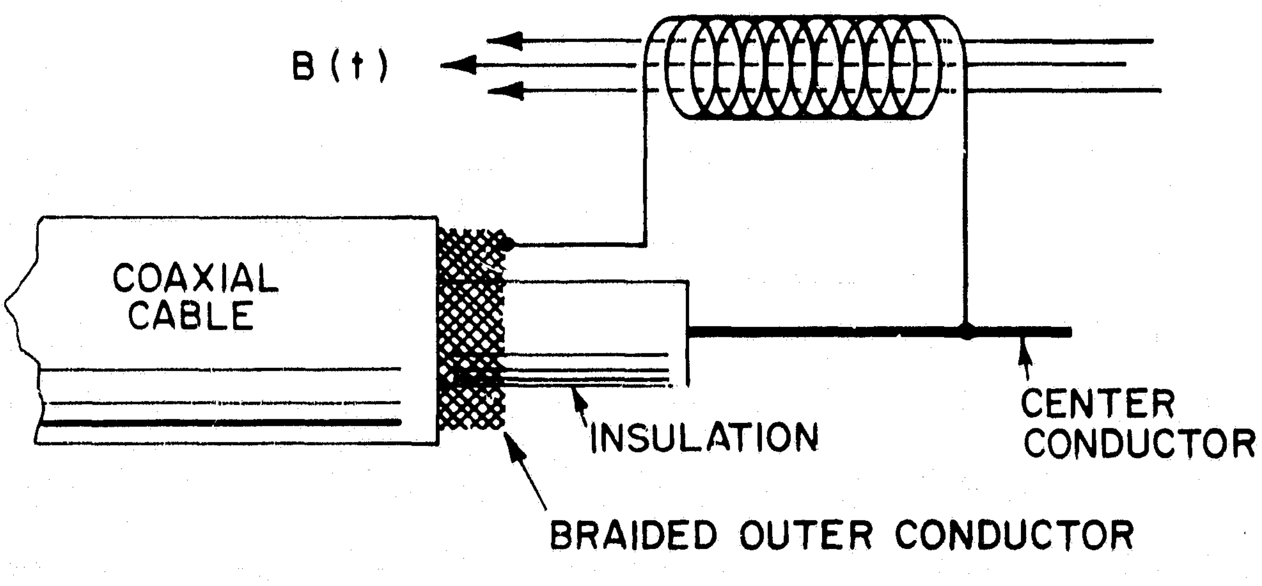

FIGURE III -3 , PICKUP COIL

generated by the current enclosed by the wire. By Ampere's Law, this magnetic field is proportional to the total current since the current is totally enclosed by the Rogowski coil. When the output is integrated, the total discharge current as a function of time is obtained. The Rogowski coil is best employed in cylindrical geometries surrounding a nearly axial current flow. Such a current distribution possesses an azimuthal magnetic field which threads through the loops of the torus, giving rise to a strong coupling between the field of the current and the diagnostic device. As seen in the Figure, the Rogowski coil is wound back on itself. This prevents it from acting like a large induction coil to any stray magnetic fields which thread through the area formed by the torus. Furthermore, the coil is generally shielded in such a way that it responds only to azimuthal fields.

3. Pickup Coil

The rectangular geometry of the parallel plate accelerator is not well suited to the use of a Rogowski coil to monitor total circuit current. The magnetic field between two long flat parallel plates whose width to separation ratio is large, is a pattern of straight field lines parallel to the plates and perpendicular to their sides. The magnetic field inside a long solenoid is a pattern of nearly straight field lines parallel to the axis of the coil. The total current to the parallel plate accelerator from the capacitor bank is fed by means of closely spaced, wide copper sheets in the high current pulses, $^{120}/20$ through $^{30}/80$ and by means of a #8 wire in series with a solenoidally shaped inductor for the low current pulses, $^{20}/125$ through 5/500. Both input connectors produce nearly straight magnetic field line configurations. To monitor the current in the parallel plate accelerator discharge, a "pickup coil" shown in Figure III-3 is used, which can be inserted between the parallel feed plates or axially into the input inductor in such a way that the magnetic field from the circuit current is aligned with the pickup coil axis. The integrated signal is proportional to the total current flowing and hence the current can be monitored.

4. Magnetic Probes

A very detailed treatment of this subject is given in [36] to which the reader is referred. A magnetic probe is an induction coil which itself is small relative to the dimensions of the phenomena under study and small enough that the spatial variation of the magnetic field over the area of the coil is negligible. A given component of magnetic field is measured by aligning the axis of the probe coil along that particular direction. The magnetic or B probe is generally used to map out the distribution of magnetic field in space by positioning the probe over a suitable spatial mesh. Where field gradients are steep, a fine mesh of positions is required and where gradients are small, a larger mesh can be employed. The oscilloscope records B as a function of time for a given location, and this process is repeated for each position in the mesh. By crossplotting the data, the spatial distribution of $\vec{B}$ is obtained at a series of times. Current densities, if desired, can then be obtained by application of Ampere's Law.

Magnetic probe design involves a series of judicious compromises. The sensitivity of the probe scales as the number of turns and the cross-sectional area of the coil and can be increased by either adding more turns or by enlarging the coil area. These measures, however, reduce spatial resolution and increase the inductance of the coil. It can be shown,[39] that in connection with RC integrators, another requirement that the output signal be proportional to the integral of the input signal, is that the inductance of the probe coil, $L_{coil} \ll R_s t_{rise}$, where R_s is the terminating resistance and t_{rise} is the desired frequency response expressed as a risetime. Large signals are desired to keep the noise/signal ratio very small but they are obtained at the expense of frequency response and spatial resolution.

In the course of the various experiments which will be described in the following chapters, many varieties of magnetic probes have been used and the specific details of the probes will be discussed when appropriate. The differences lie in the wire gauge, coil diameter, number of turns, number of coil layers, probe length, type of shielding and dielectric covering used. Generally, however, all the probes are alike. The basic probe consists of a coil whose leads are brought out as twisted pair which attach directly to a $93\,\Omega$ coaxial cable. The twisted lead is electrostatically shielded by a braided metallic sleeve or metal tube which attaches to braided shielding over the coaxial cable. This external shielding is grounded at the screenroom. This assembly consisting of the coil, twisted leads, shielding etc. is placed in a dielectric housing 1/4" in outer diameter, which is either a sealed pyrex tube, or an open glass tube or nylon sleeve filled with epoxy. A schematic diagram of the probes is shown in Figure III-4. Nylon probes are prefable to glass because of their relative durability but glass is prefable for long probes because of its rigidity which prevents drooping and hence ensures more accurate positioning.

The probes and integrators, as one unit, are calibrated by measuring the system response to a known magnetic field. This field may be produced with a metal calibration rig, where a metal short replaces the discharge, and an underdamped LC circuit. By knowing the capacitance and the initial charging voltage, by measuring the ringdown frequency and accounting for the decay, the current can be calculated. From geometrical considerations and Ampere's Law, the magnetic field which the probe sees can be obtained and compared with the signal output. For the rectangular current pulses, the pulse length, which can be measured, permits an accurate determination of the total discharge current which, in turn, allows for calculation of the magnetic field seen by the probe and its subsequent calibration. Theoretical calibrations are also possible, but generally are not as satisfactory as experimentally determined ones. This is due to the fact that it is not always possible to ascertain

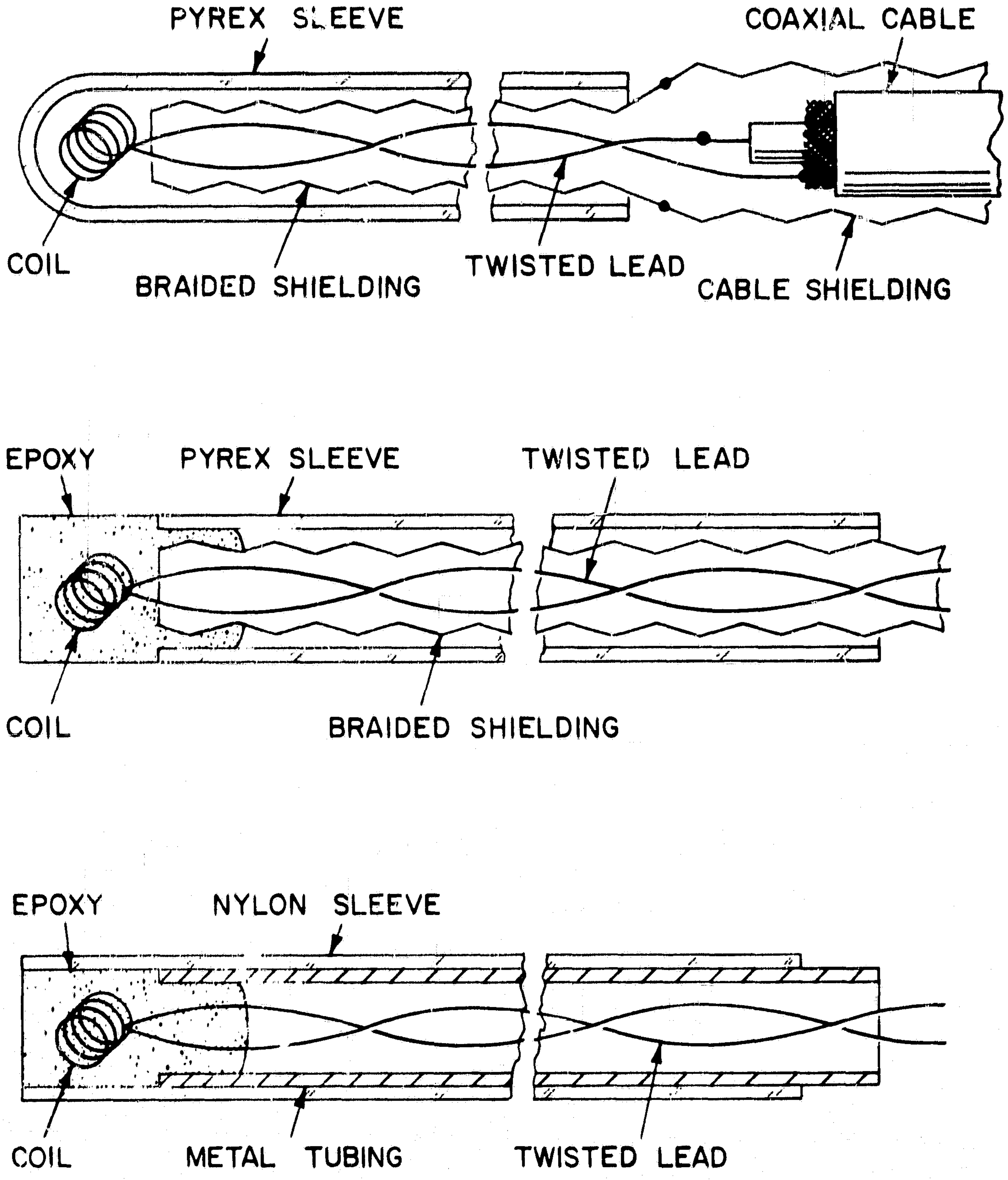

MAGNETIC FIELD PROBES (SCHEMATIC)

FIGURE III - 4

accurately enough key parameters needed in the calculations e.g. the effective cross-sectional area of a multilayered coil. Furthermore, when the probe is calibrated empirically in the geometry in which it is used, inherent errors, such as the lack of two dimensionality when assumed, can be cancelled out between the calibration and the data reduction.

Unlike the total current monitors which are external to the discharge and in no way affect it, magnetic probes are placed directly in the discharge and as with any such measurement it is important not to disturb significantly the property whose measurement is desired.

Lovberg [36] lists four perturbations of the plasma by the probe: 1) Plasma cooling 2) Boiloff of probe surface 3) Flux diffusion into the probe 4) Current stream perturbations, and treats each in detail. Only a few general comments will be made here.

Of the above, plasma cooling could probably be the most serious perturbation in the magnetic field measurement. Cooling results in a localized decrease of the plasma conductivity and consequently a lowering of the current density. Since the magnetic field at any one point does not arise solely from a localized source but is a function of the entire current distribution cooling of the plasma will not be serious as long as the current distribution as a whole is not significantly perturbed. Since the area of the probe is generally a very small fraction of the total area of the discharge, the plasma cooling perturbation is not too severe. There is evidence, however, that the current distribution with the low magnitude long duration current pulses e.g. $^{10}/250$ can be significantly altered if several probes are inserted into the discharge simultaneously and such a situation is to be avoided.

Localized current stream perturbations have little effect on magnetic field measurements as long as the entire current pattern is not severly altered for the same reasons mentioned in regard to the cooling perturbation.

Since a high plasma purity level is not a prerequisite for the experiments to be described and furthermore since any material blasted off the probe is probably minor relative to the insulator wall and electrode contributions, probe boiloff effects are likely to be insignificant.

For the time scales of interest in these experiments and following Lovberg's arguments, it can be shown that the magnetic flux diffuses into the probe in a time much shorter than the characteristic rise times encountered.

C. FLOATING DOUBLE PROBES - E FIELD MEASUREMENTS

Double Langmuir probes for use in gas discharges were first introduced by Johnson and Malter.[40] The double probes are used here only in the unbiased or floating mode very similar to the technique used by Burkhardt and Lovberg.[41] In contrast to a single Langmuir probe there are several advantages to the measurement of floating potential which Lovberg points out.[36][42]

Namely, one does not have to worry about the presence of magnetic fields, departures from thermal equilibrium and the determination of probe area and shape.

The floating double probe is used to measure internal electric fields in the plasma. This is done by measuring the difference in plasma potential at two adjacent points and dividing by the distance between the two points to obtain the field. Actually the difference in floating potential is measured, but, if electron temperature gradients are small compared with the difference in plasma potential between the two points, then the difference in floating potential is very nearly equal the difference in plasma potential. As Lovberg points out, it is extremely difficult to prevent a floating electrode from assuming the plasma potential minus about a kT_e/e sheath drop if the current drawn by the probe is negligible compared to the ion and electron fluxes entering the sheath. The electron temperature in the work described herein is probably a few e.v.[4] and hence the difference in electron temperature can only be a few e.v. in the worst possible case. Since a few volts is generally small compared with the difference in floating potential measured, electron temperature gradient effects should be unimportant and one can be reasonably assured that the difference in plasma potential is being measured.

For streamwise electric field measurements, a probe similar to that used by Burkhardt and Lovberg is employed possessing a conical tip and ring axially displaced as the electrode pair and shown in Figure III-5a. Such a coaxial geometry is attractive since it should not be able to pick up inductively, except in the case of very strong transverse magnetic field gradients, and, in addition, should possess smooth flow characteristics. For transverse electric field measurements a parallel set of needles or wires held straight is used as shown in Figure III-5b,c. Since it is difficult to ascertain the amount of inductive pickup of this probe geometry when plasma closes the loop across the electrodes, the transverse data is analyzed only at those times at a given location when $\dot{B}$ is zero. Since $\dot{B}$ is typically a sharply peaked function going to zero as the sheet sweeps by, this amounts to ignoring only the initial rise on the transverse E data. The connections to the electrode pair are brought out either with coaxial or twisted leads; both seem to work equally well.

Since the floating potentials in the discharge are quite high, 10^2 to 10^4 volts, direct coupling of the probe to the oscilloscope is not employed; this is a precautionary measure taken to protect the oscilloscope. The leads from the probe are fed into the primary of a ferrite core stepdown transformer [42] described in detail by Burton [4] for pulses up to a few microseconds in width. The transformer is capable of passing only the difference in floating potential and rejecting the high common mode signal. The E probe system is shown in Figure III-6.

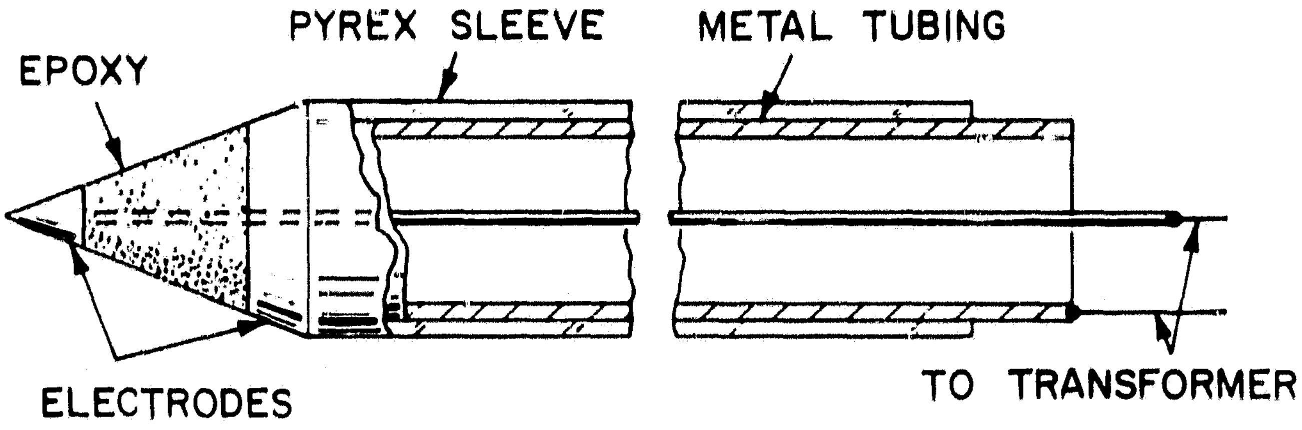

a) CONICAL PROBE (COAXIAL)

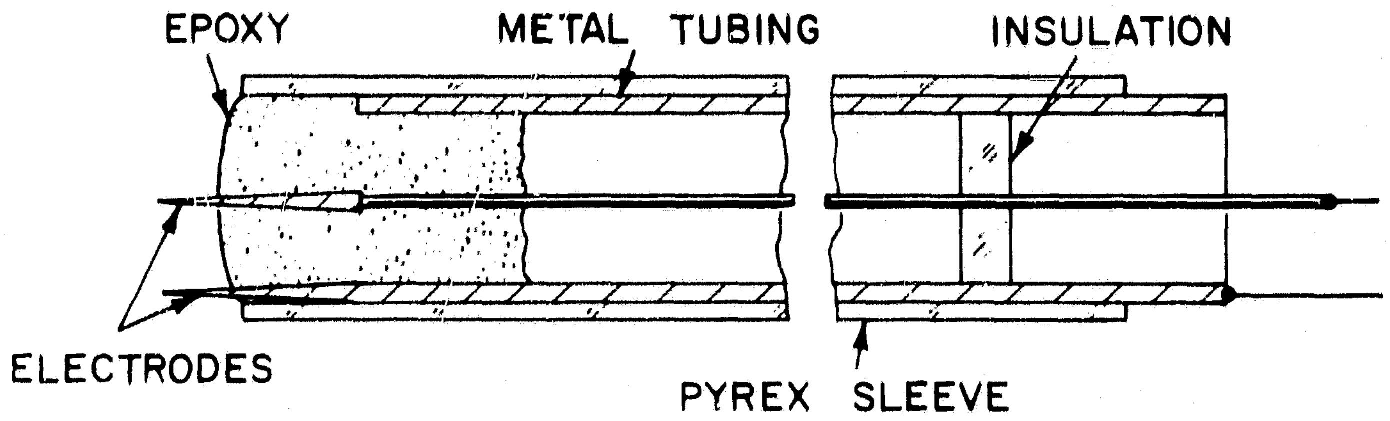

b) SHORT PRONGED PROBE (COAXIAL)

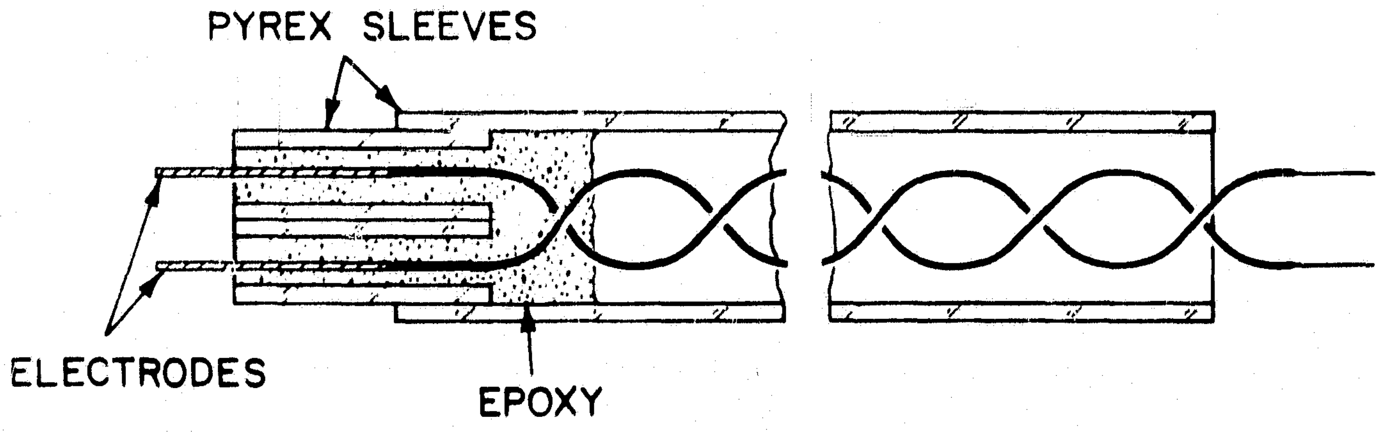

c) LONG TIPPED PROBE (COAXIAL)

ELECTRIC FIELD PROBES (SCHEMATIC)

FIGURE III-5

AP25-4055-66

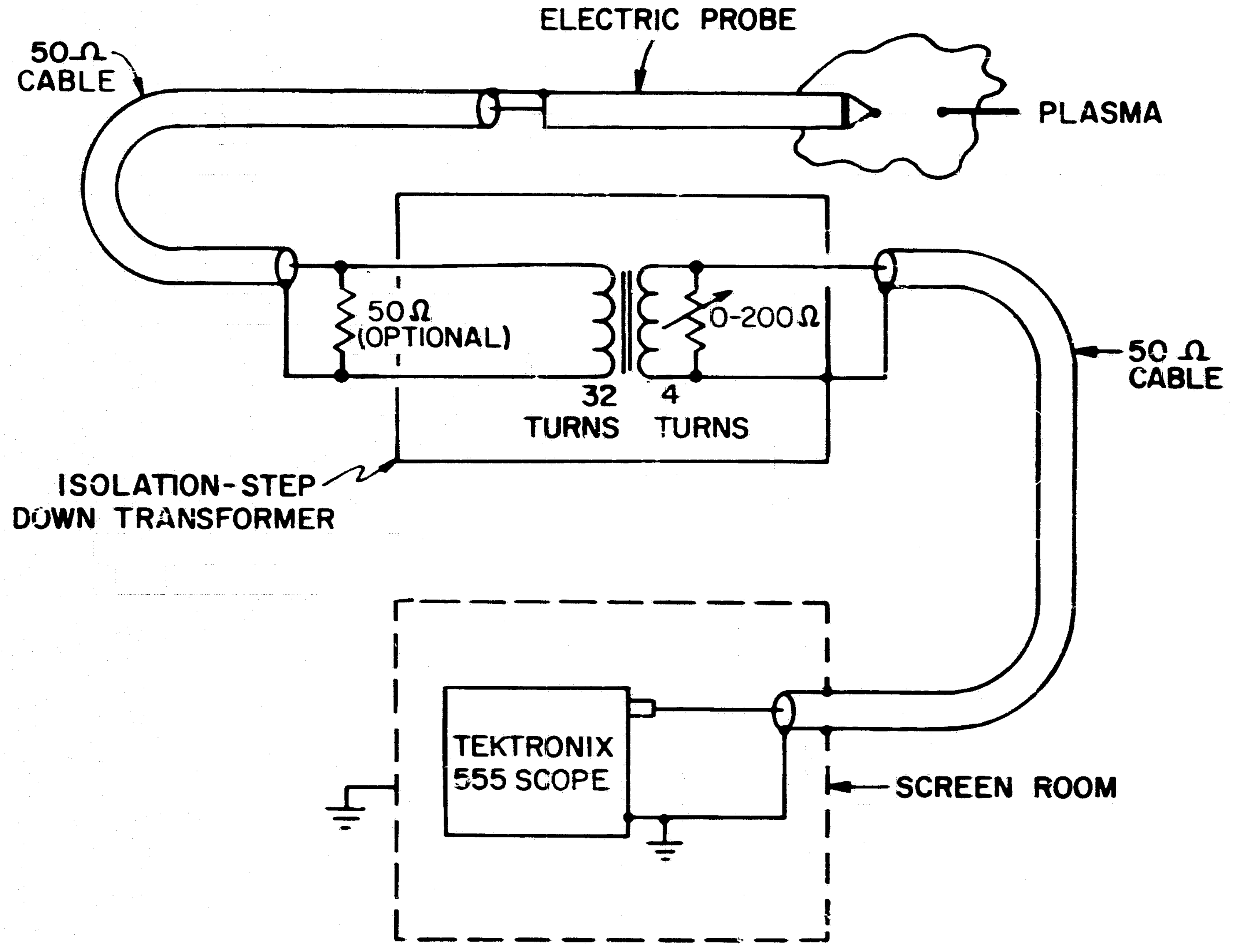

ELECTRIC PROBE DIAGNOSTICS

FIGURE III-6

For the very long current pulses which have durations of hundreds of microseconds, the transformer had to be redesigned since the coil inductances of the transformer shown are too small to handle a flat pulse of hundreds of microseconds extent. Also, with the lower amplitude current pulses, the electric fields in the discharge were expected to be smaller than those measured with the high current pulses and a stepdown transformer was not designed. Equal turns are placed on both the primary and secondary and the transformer is used only for isolation. Empirically it is found that 300 turns on both the primary and secondary and a 5600Ω terminator across the secondary are sufficient to handle pulses up to 300 µsec in duration. The risetime of this setup is 5 µsec which is less than the risetime of the long current pulses.

In contrast with the magnetic probe, the E probe measurement is dependent on localized physical quantities and the plasma perturbations, most notably the plasma cooling and current stream, are more serious in the case of the electric field measurement. Since the magnitude of these perturbations cannot be accurately evaluated, the probe data is generally interpreted as an estimate of the prevailing electric fields. Furthermore since the electric probe makes direct contact with the plasma, the output is subject to the same statistical fluctuations that the plasma undergoes. This results in the electric probe data being only fairly reproducible, generally ± 25% of some averaged value, whereas the magnetic probe data is generally within a few percent of the average.

D. VOLTAGE MEASUREMENTS

Voltage measurements are made using commercially available voltage probes, Tektronix Models 6013, 6013A or 6015. They are all essentially high impedance, RC compensated probes with high frequency response at high voltages with an attenuation ratio of 1000:1 operating on a divider principle. The center tap of the probe is connected to the point whose voltage relative to ground is desired. Interpretation of the measured voltages will be reserved for discussion in connection with the appropriate experiment.

Ground planes are found to be essential to obtain an accurate reading devoid of pickup. The voltage probe cable must be dressed very closely to the ground plane and, of course, there must not be any ground loops in the system. Braided shielding on the voltage probe considerably reduced the electrostatic hash encountered on the initial portion of a data trace.

E. PRESSURE MEASUREMENTS

Cold flow gas pressure measurements are made with piezocrystal pressure transducers in an attempt to determine the mass flow rates into the parallel plate chamber from the shock tube gas injection system for a series of orifice sizes.

Application of pressure to the face of a properly prepared crystal results in a surface charge on the crystal face.

This surface charge can be calculated by measuring the resultant voltage generated and by knowing the capacitance of the crystal. The pressure can be calculated since the surface charge created is related to the force applied through the piezoelectric constant.[36]

The probes employed here are essentially those developed at Princeton by York[6] for use in pulsed plasma discharges. A complete description of these probes is given in [6]. In the pressure measurements made in the parallel plate the capacitor bank is not discharged, and the sophistication involved in insulating the pressure probe from the discharge is not necessary.

A schematic diagram of the probe is shown in Figure III-7. For the sensitivity required, 1 millivolt for a pressure change of 100μ, an 1" diameter 1/8" thick PZT-5A crystal was purchased from the Clevite Corporation. The crystal is bonded to a stainless steel backing rod by means of conducting epoxy. The composite of crystal and rod is then housed in a brass cylinder and held in place with insulating epoxy and wax. This assembly is then epoxyed into a nylon vacuum fitting. Silver paint is used to make electrical contact between the exposed crystal face and the brass. Leads from a coaxial cable fitting are attached to the brass shell and stainless steel backing rod completing the probe. The probe connects directly to the oscilloscope through coaxial cable.

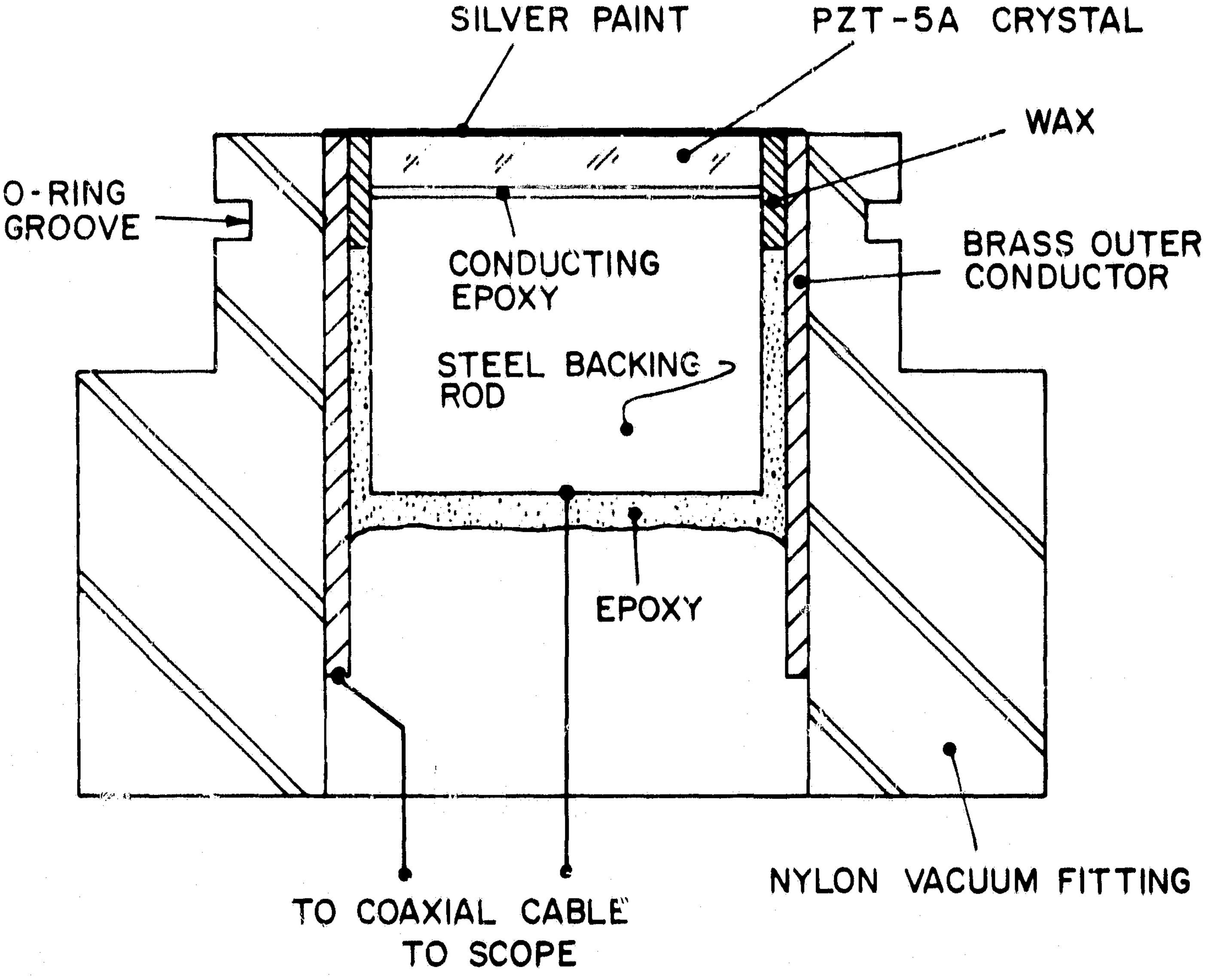

PIEZOELECTRIC PRESSURE PROBE (SCHEMATIC)

FIGURE III-7

AF 25 R 4446 68

This crystal geometry was not only selected for its sensitivity but also for its capacitance. The capacitance of the crystal and coaxial cable in conjunction with the megohm oscilloscope impedance yield a probe RC time constant of about 2400 μsec. Since a pressure history for about 300 μsec is required, the error in monitoring the pressure at 300 μsec will only be about 10% due to the RC decay of the probe system.

F. SPECTROSCOPIC STUDIES

Spectra are obtained in the $^{120}/20$ and $^{10}/250$ partially insulated electrode configurations by means of a McPherson Model 216.5 - 0.5 meter combination Scanning Monochromator Spectrograph and Polychromator.* This particular instrument is fitted with a Polaroid film holder so that the discharge spectra are quickly and conveniently obtained. Details of the experiments conducted and the results obtained will be discussed when appropriate.

G. DATA COLLECTION AND ANALYSIS

All data, other than Kerr cell photography and the spectroscopic investigations, are recorded by photographing the oscilloscope face during the discharge event. The data are recorded on Type 47 Polaroid Film ASA 3000. Data are read in mm to within 0.25 mm or 0.50 mm depending on the accuracy desired. This was also assumed to be the reading error.

---

*We would like to thank the Liquid Combustion Laboratory of Princeton University for their loan of this instrument.

Whenever possible large deflections, about 20 mm, are obtained on the film to minimize the effect of reading errors. Triple overlays of data when not perfectly reproducible are averaged and the errors in that case are the difference between the average value and the extrema. When the reproducibility is very good, triple overlays are not taken in general but only from time to time as a reproducibility check.

CHAPTER IV

PULSED PINCH EXHAUST STUDIES

As mentioned in Chapter I, a pulsed plasma accelerator must create a plasma, accelerate the plasma to velocities of interest for space missions, and finally, and very importantly, must efficiently exhaust the plasma. The exhaust process from a linear orifice pinch was first studied by Jahn, von Jaskowsky, and Burton[8] [16] [43] [44] and their initial efforts will be discussed in Sections A and B which follow.

A. ORIFICE STUDIES

The first exhaust studies were carried out with a 5" diameter plasma pinch driven by a 15 μfd capacitor bank, initially charged to 10 KV which rang down at 400 KC. The first half cycle delivered a peak of 300,000 amperes and had a half cycle time of 1.2 μsec. The solid anode was replaced by a anode containing a straight bored orifice centered on the anode. A 6" diameter by 2' long pyrex vessel served as the exhaust tank for this orifice pinch. The orifice diameter was systemically changed from 3/8", to 3/4", to 1 1/2", to 2", to 3" and to 4".

The exhaust from the orifice pinch was studied by observing the axial progression of the ejected luminous plasma via streak photography. Although this photographic technique was not treated in Chapter II, suffice it to say, that a streak photograph yields the luminosity trajectory, i.e. the locus of the luminosity front with time. The results of the streak photography studies are shown in Figure IV-1 where the velocity of the luminous gas is plotted against the downstream axial coordinate with orifice diameter as the parameter. In general, it can be seen that as the orifice size is increased, the velocity at the exit plane increases and the velocity downstream is higher for increasing orifice sizes.

To check the effect of orifice profile, simple conical nozzles with throat to exit diameters of 3/8" to 1 1/2" and 3/4" to 1 1/2" were tested and these data are also shown. Note that these results are nearly indistinguishable from the straight bore orifices of the same throat diameter.

For the 4" diameter orifice, the axial progression rate down the tank was 0.82 the velocity of the pinching current sheet, 1.5 inches/μsec. From this it was implied that much of the random thermal energy resident in the pinch heated plasma was recoverable as useful streaming motion. However, from Figure IV-1 and the known radial pinch velocity, only about 0.33 of the radial velocity is recovered in axial streaming for orifice diameters of 1 1/2" and less. Furthermore, in light of the nozzle data on the effect of orifice profile, it is believed that the above picture of the exhaust process as an implosion followed by an expansion of the pinch heated plasma is not totally correct.

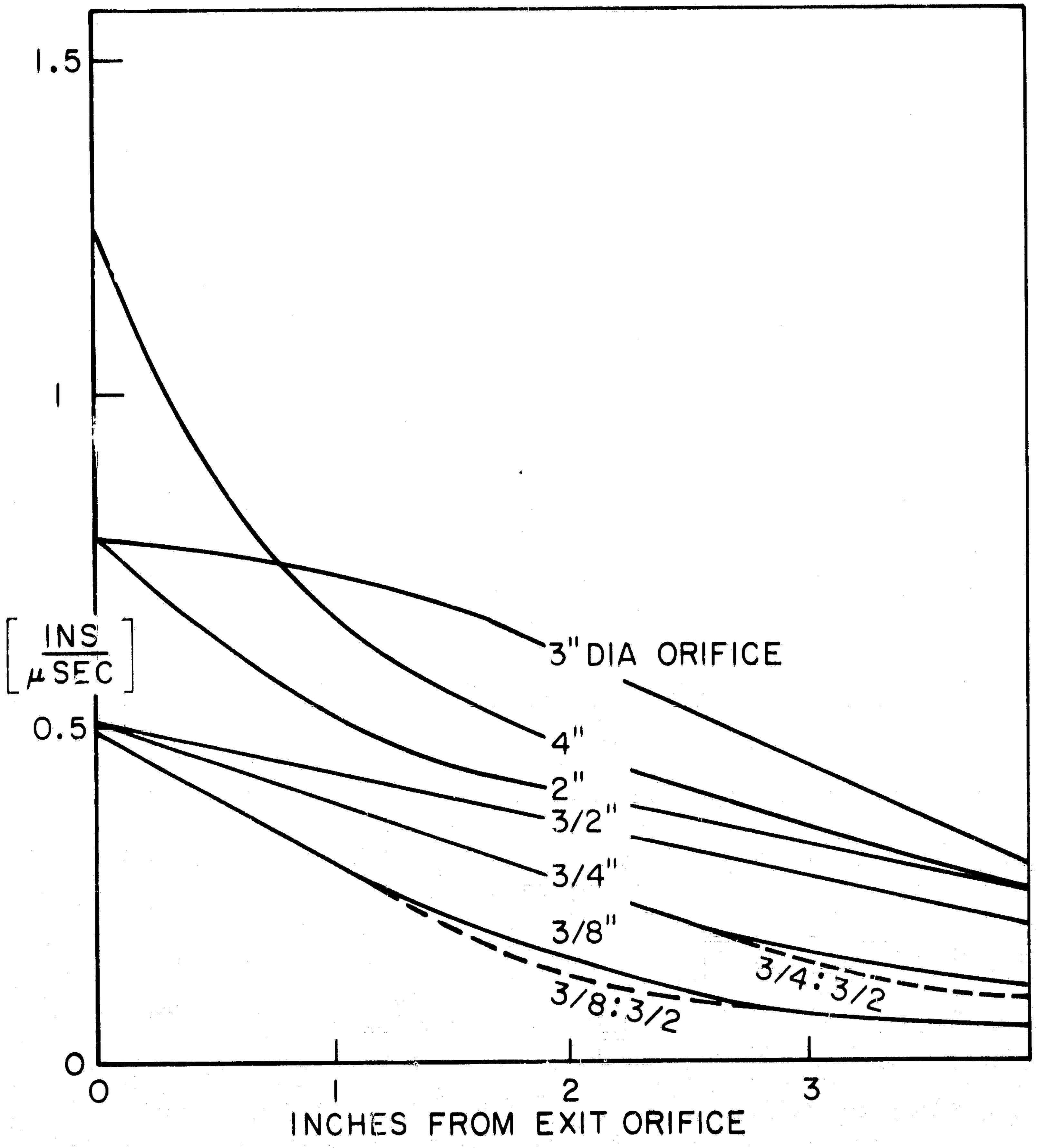

VELOCITY OF EXHAUSTED GAS FROM ORIFICES
OF DIFFERENT DIAMETER, IN 120 μ ARGON

FIGURE IV-1

AY25-JPR 4001-64

Perhaps a more plausible explanation is found in the manner in which the current distributes itself with increasing orifice size. Figure IV-2 shows the pattern of current streamlines reduced from magnetic probe data taken with the 4" diameter orifice in a 9" diameter x 18" long pyrex tank. With the very large anode orifices, a large portion of the current flows out through the orifice, bends around, and attaches to the downstream facing anode surface. This sets up the $\vec{j} \times \vec{B}$ body force distribution on the gas, which rather than being almost radially inward as in a closed chamber or chamber with a small orifice, curves outward through the orifice as suggested in Figure IV-3. It is hypothesized that this body force contour turns the flow through the orifice rather than the exhaust process being purely an implosion followed by a thermal expansion.

It is also known that in similar closed chamber discharges, there is a tilt of the current sheet from cathode to anode. This results in a $\vec{j} \times \vec{B}$ component directed axially inward toward the cathode, whereas in contrast the exhaust is axially outward. With larger and larger anode orifices, this disadvantageous tilt is eliminated.

Unfortunately, there is no magnetic field data other than that for the 4" diameter orifice but it might be speculated that with larger orifices, more of the discharge current flows in the exhaust plume. The higher velocities found downstream of the exit plane for the larger orifices are probably due to an increased $\vec{j} \times \vec{B}$ acceleration in this region.

AV25- JPR 4005-64

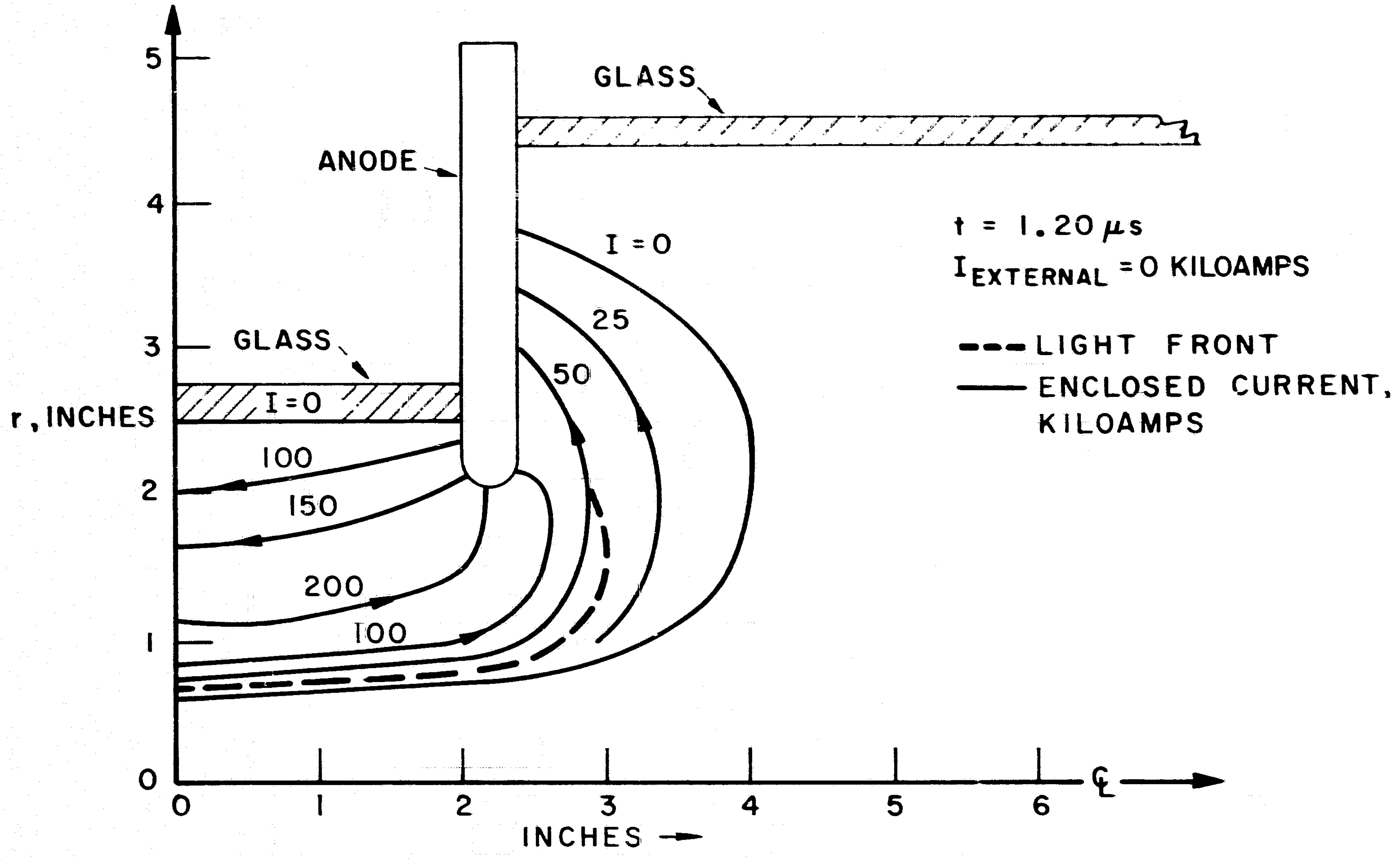

CURRENT PROFILES
120 μ ARGON, 4" ORIFICE

FIGURE IV-2

AP25 R 4461 68

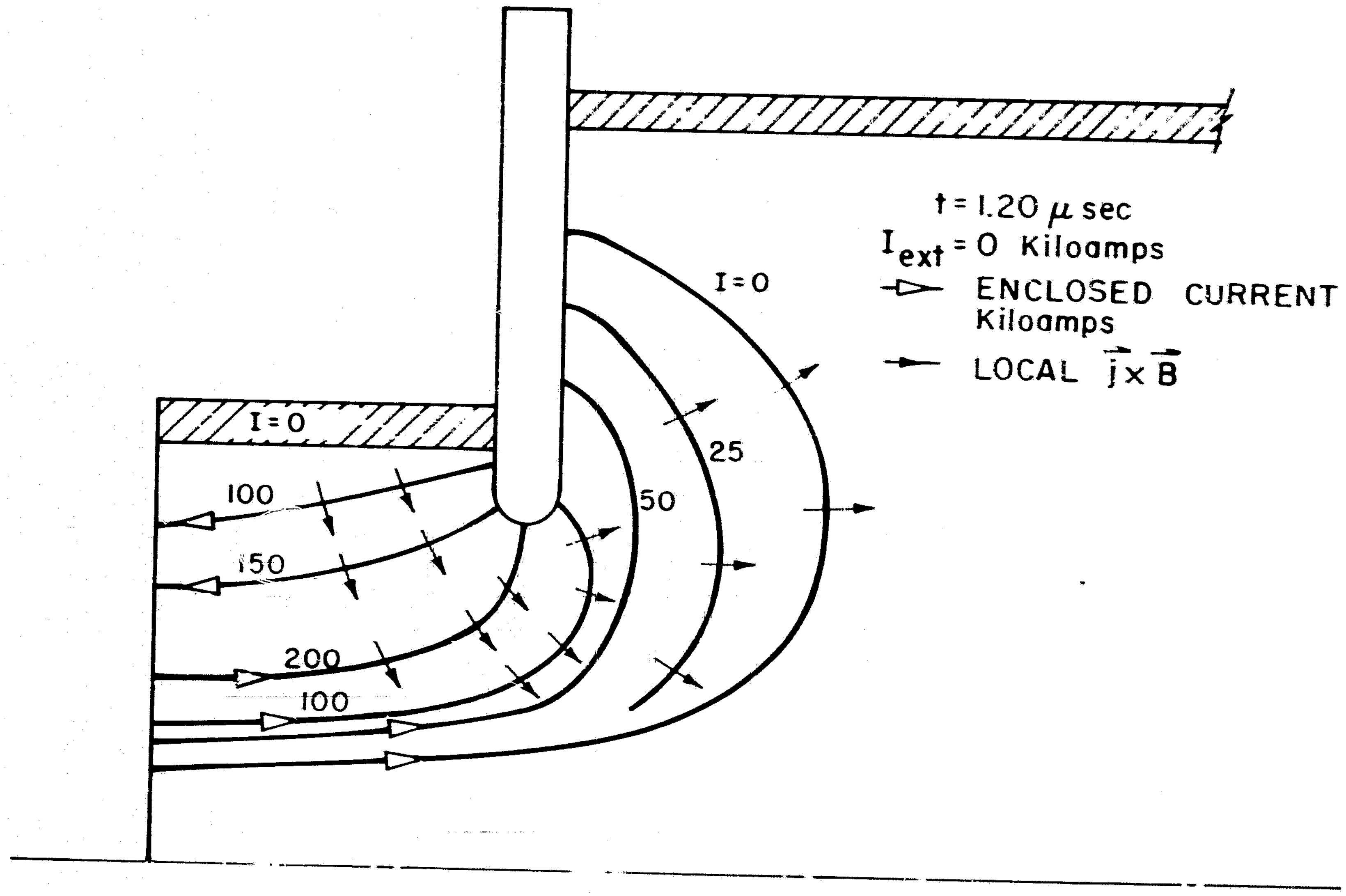

TURNING FLOW MODEL OF PINCH EXHAUST PROCESS

FIGURE IV-3

In actuality, the exhaust process probably embodies a combination of both the thermal expansion and turning flow mechanisms but it is believed that the data point to a domination of the electromagnetic mechanism over the electrothermal one.

B. EARLY EXHAUST WORK - SMALL TANK, SHORT DURATION PULSES

Having selected a 4" diameter orifice as the exhaust configuration, which is also attractive for photographic and probe accessibility to the details of the event, Jahn, von Jaskowsky and Burton performed detailed Kerr cell and magnetic probe studies of the exhaust phase with the orifice pinch driven by the 300,000 amp, 1.2 μsec half cycle time pulse into 120 μ argon. The photographic studies produced excellent results but the current density patterns in the chamber and exhaust plume were badly distorted by the "crow-bar" discharges due to the external current reversals. This was overcome by driving the pinch with a rectangular pulse of 200,000 amps amplitude and 5 μsec duration using one section of a pulse forming network developed by Black.[45] The luminous phenomena were qualitatively similar to the ringing pulse but significantly higher velocities were found in the exhaust. This is probably attributable to the fact that the current driving out in the exhaust was still connected to the external circuit and had not been short circuited by a crowbaring sheet. This again points to the exhaust process being predominantly an electromagnetic process rather than electrothermal.

To investigate the effect of the ambient back pressure on the exhaust process and to simulate a space environment more closely, Jahn and von Jaskowsky[44] photographically studied the exhaust process using a shock tube gas injection system described earlier for both the ringing and rectangular pulses for the 4" orifice. Quantitatively, there was little change in the axial velocities of the observed luminosity. Qualitatively, there was the absence of the so-called "diffracted front" probably due in the ambient case to the outward expanding current contours entraining ambient tank gas as they progress outward. In the absence of the ambient gas in the tank, this luminous diffracted front was not observed.

In viewing the magnetic probe studies and Kerr cell photographs in 120μ argon, and the Kerr cell work with the shock tube gas injection when the discharge is driven by the $^{200}/5$ pulse, it was clear that a transient process was being observed. If the current pulses were driven for a longer time, it was unknown whether the current pattern would disattach from the electrodes,[7] continue propagating outward and remain attached to the electrodes, or cease to propagate outward as found to be the case in some pseudo-steady coaxial guns.[46] Whatever happened, of course, is of great interest in the study of the pulsed exhaust process.

C. EXHAUST STUDIES - SMALL TANK, LONG DURATION PULSES

To investigate this latter aspect of the exhaust process, studies are first conducted on the 5" chamber diameter, 4" orifice diameter pinch with shock tube gas injection when the discharge is driven with the large 128 µfd capacitor bank set up to deliver the $^{120}/20$ current pulse.

Detailed magnetic probe studies of the exhaust so driven when reduced lead to contours of enclosed current as a function of time shown in Figure IV-5a and b. Figure IV-4 is an illustration to aid in explaining the concept of an enclosed current contour. Due to the azimuthal symmetry of the discharge only an azimuthal component of magnetic field, B_θ , results from radial and axial current densities, j_r and j_z . From Ampere's Law, equation III-4, in integral form

$$\oint \vec{B} \cdot d\vec{\ell} = \mu_0 \int_{A_\ell} \vec{j} \cdot d\vec{A}$$

one obtains with the assumption of azimuthal symmetry that

$$I_{\text{enclosed}}(r,z) = \frac{B_\theta(r,z)\, 2\pi r}{\mu_0} \qquad \text{(IV-1)}$$

The enclosed current is simply the total amount of current flowing through a circular area of radius r centered on the z axis and perpendicular to it. The magnetic probe is positioned where desired and the capacitor bank discharged; the integrated signal yields $B_\theta(t)$ for that location. By positioning the probe through the pinch chamber and exhaust region and crossplotting the data, one obtains the spatial distribution of $B_\theta(r,z)$. Multiplying $B_\theta(r,z)$ by $\frac{2\pi r}{\mu_0}$ gives $I_{\text{enclosed}}(r,z)$. Connecting points of equal $I_{\text{enclosed}}(r,z)$ yields the enclosed current contour. The enclosed contours are everywhere tangent to the current density and resemble streamlines of current flow.

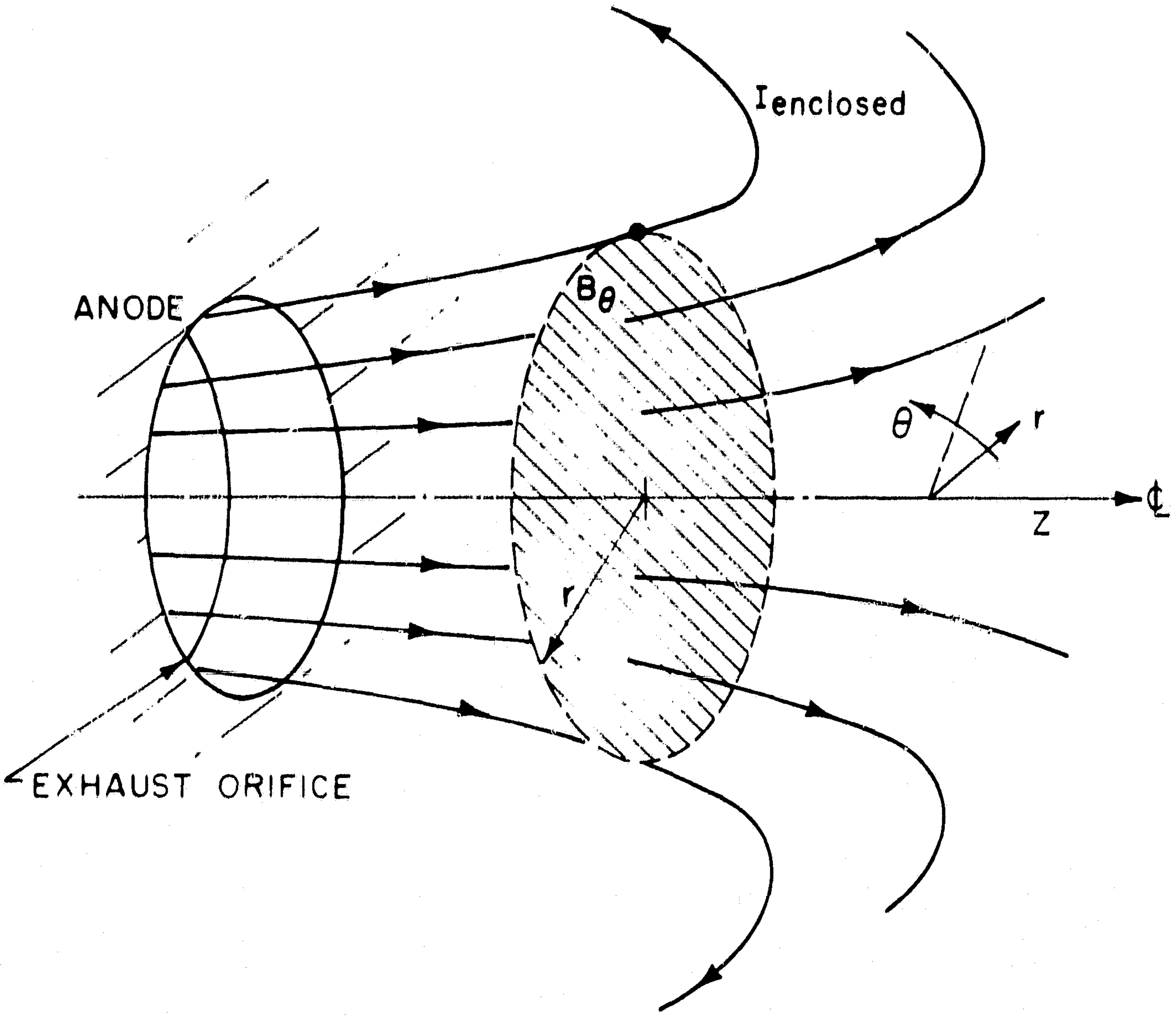

ENCLOSED CURRENT CONTOUR

FIGURE IV-4

AP 25 R 4463 68

AP25-R4075-66

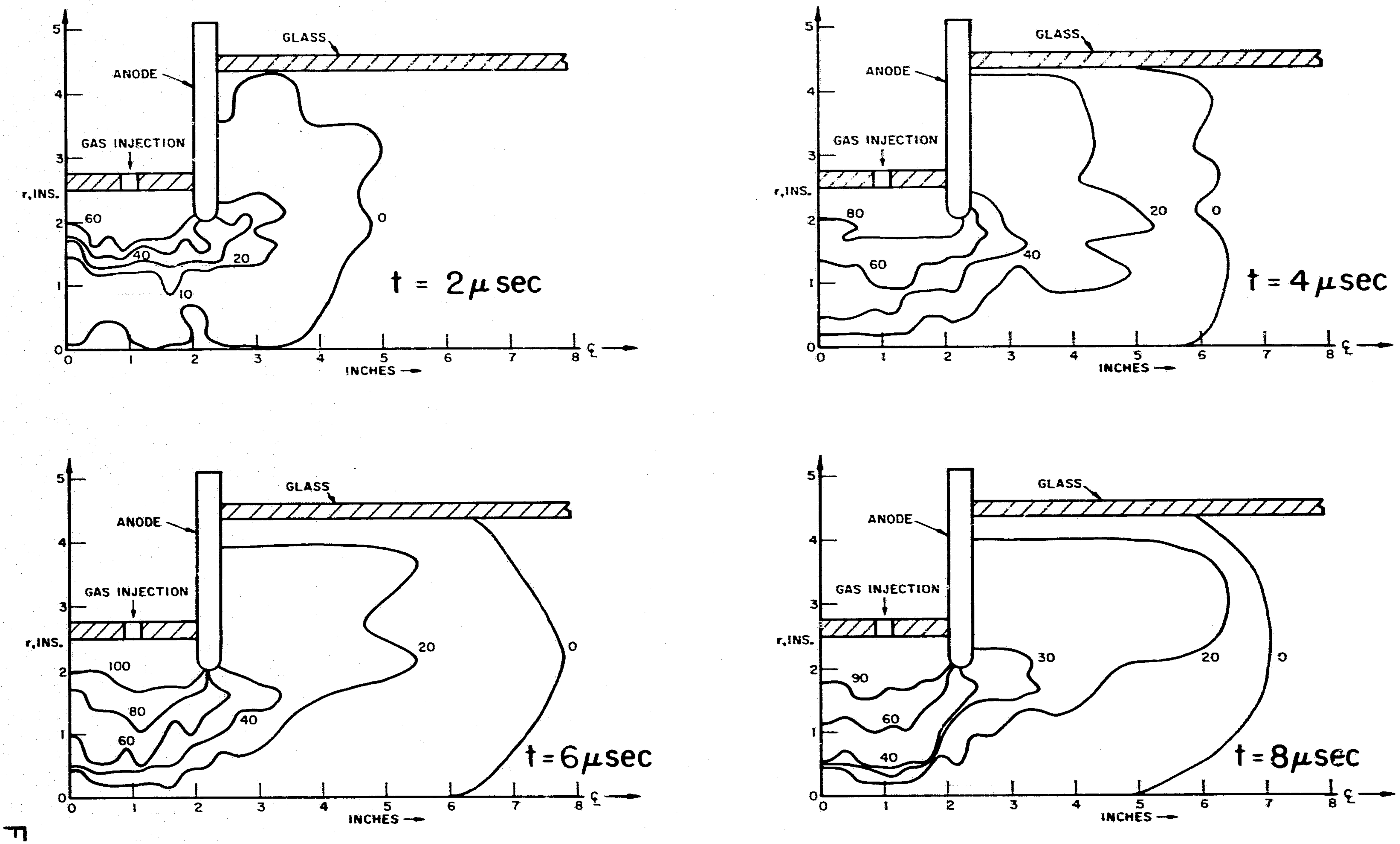

ENCLOSED CURRENT CONTOURS IN A 5" PLASMA PINCH
EXHAUST PLUME WITH SHOCK TUBE GAS INJECTION,
120 KA-20μs RECTANGULAR CURRENT WAVEFORM AT: 2, 4, 6, 8 μsec

FIGURE IV-5a

AP25-R4076-66

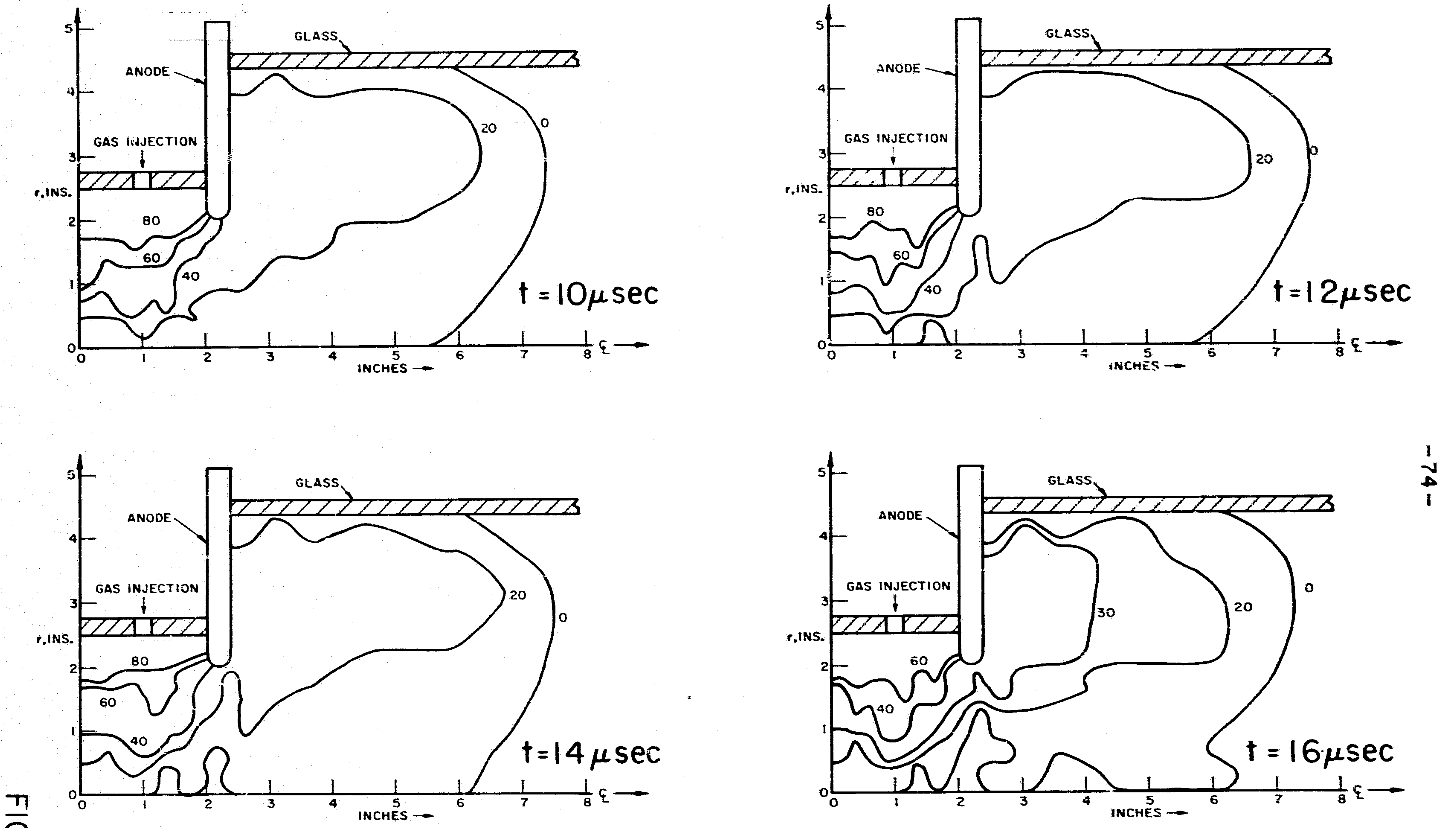

ENCLOSED CURRENT CONTOURS IN A 5" PLASMA PINCH EXHAUST PLUME WITH SHOCK TUBE GAS INJECTION, 120 KA-20μs RECTANGULAR CURRENT WAVEFORM AT:10,12,14,16μsec

FIGURE IV-5b

The magnetic probes used are two layered, 16 turn coils with a 2 mm ID enclosed in glass. The accuracy on the enclosed current contour valves is about ± 20% resulting from uncertainties in reading the probe data and positioning of the probes. The enclosed current contours thus obtained are compared with Kerr cell photographs of the discharge luminosity and the following conclusions are drawn: 1) The current is much more diffuse in structure than the photographs suggest, 2) The main current zone lags behind the luminosity, 3) Secondary breakdowns do not occur until the circuit current reverses, 4) The contours do not detach from the electrodes, nor continue to propagate downstream but rather stabilize spatially after about 6 μsec and remain in virtually the same position until the current reverses, 5) The exhaust plume current lies within 4", an orifice diameter, axially downstream of the anode, and 6) The exhaust vessel, which is only 9" in diameter appears to be confining the exhaust process. It is not at all clear whether the current pattern stabilization found is due to the confining effect of the small vessel or is a more fundamental property of the ejection process. It is also very important to ascertain whether acceleration of the gas stops with the cessation of current propagation or whether it continues through the generation of a new mechanism. These questions will be investigated in the next section.

Before going on, an additional comment should be interjected at this point. Previously, the axial velocity of propagation had been inferred from luminosity or B probe measurements, but no direct measurements have been made on the plasma. Using a simple Faraday cup probe [47] shown in Figure IV-6, biased negatively to repel electrons, ion current to the probe is monitored when the first exhaust plasma reaches the probe. A typical data trace is shown in Figure IV-7. Based on the arrival time of the plasma and the approximate distance the plasma has to travel, the exhaust velocity, taken to be the distance travelled divided by the time of flight, is found to be approximately 25,000 $^{m}/\mathrm{sec}$ which is comparable to the radial pinching rate suggesting that the plasma is able to make the 90° turn without a significant loss in velocity in agreement with the luminosity and magnetic field data conclusions.

D. EXHAUST STUDIES - LARGE TANK, LONG DURATION PULSES

It is apparent from the exhaust work described in the previous section that when long duration pulses, $^{120}/20$, are used in conjunction with the 9" diameter exhaust vessel, that the walls of the vessel may be interfering with the exhaust process and, perhaps, this wall interaction is the cause of stabilization. To eliminate this possibility, the large 3' diameter, 6' long plexiglass tank described in Chapter II was constructed in which to continue the exhaust studies. The 5" pinch chamber is fitted with a large 34" diameter anode containing a centered 4" diameter orifice. The diagnostic studies which are about to be presented demonstrate that the size of this tank is adequate to avoid exhaust plume-tank wall interactions.

AP25-4114-66

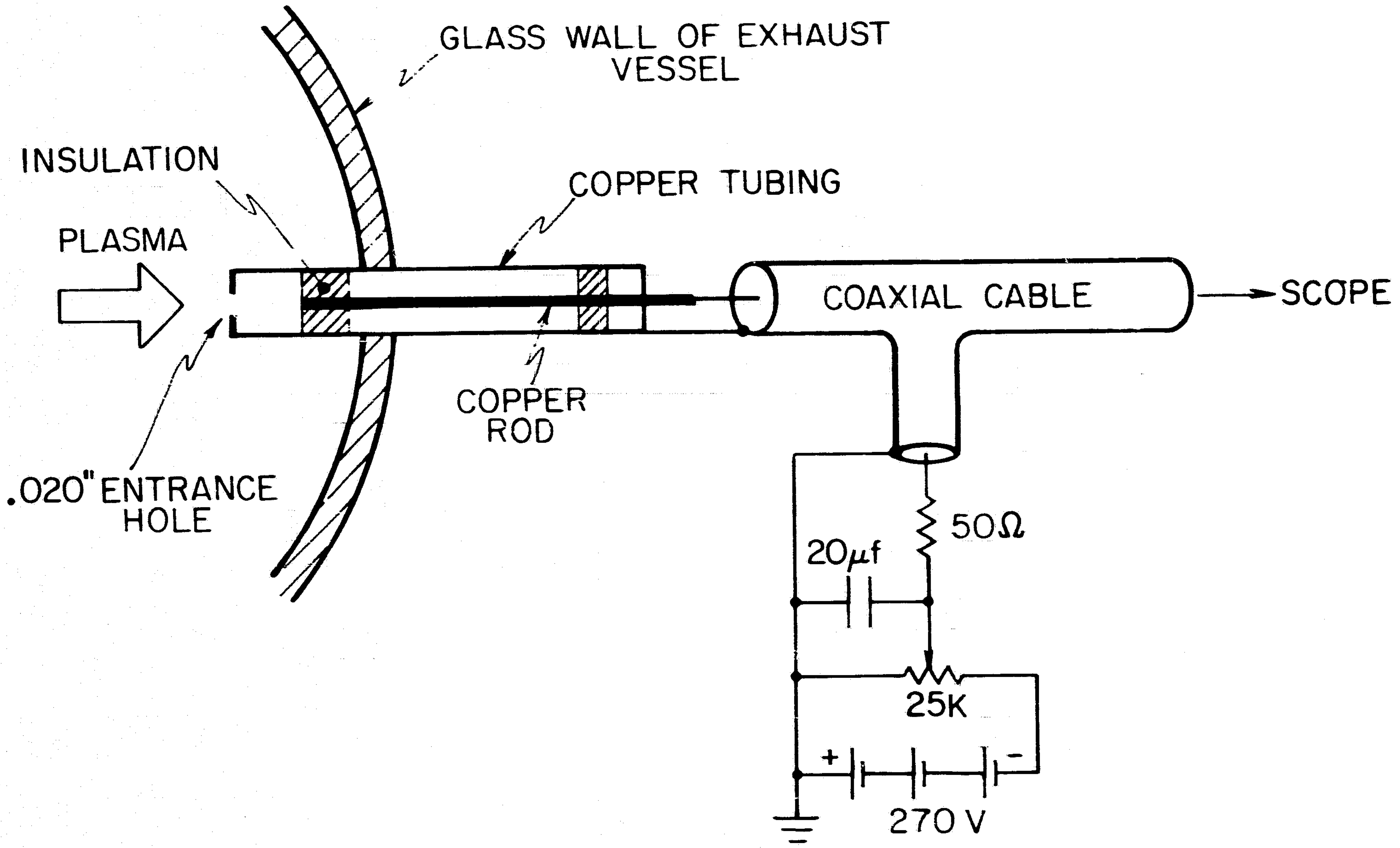

FARADAY CUP PROBE AND BIASING CIRCUIT
(SCHEMATIC)

FIGURE IV-6

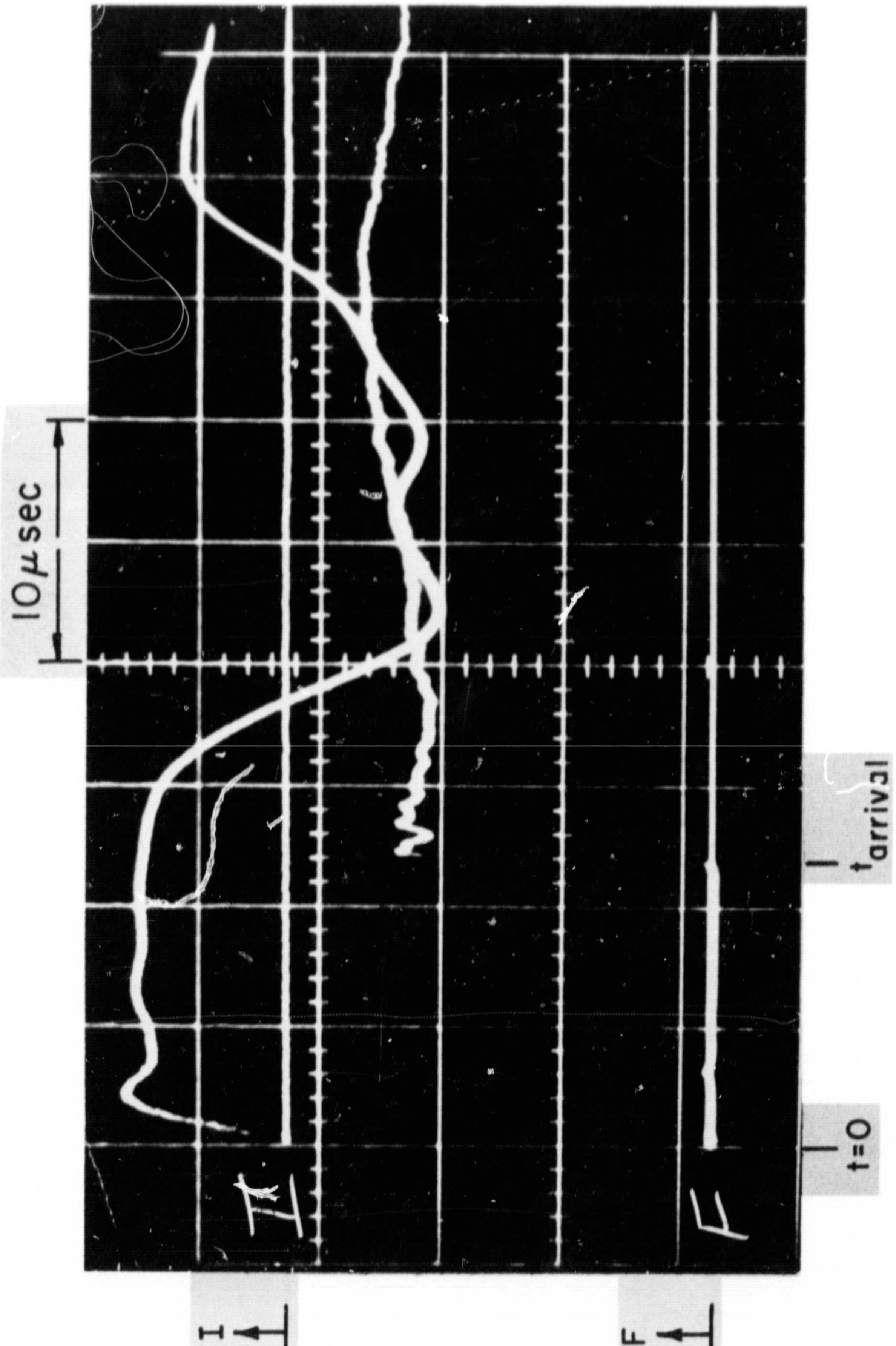

OSCILLOGRAM : DISCHARGE CURRENT I AND RESPONSE F OF FARADAY CUP

FIGURE IV-7

A matrix of 6 experimental studies on the exhaust of the pinch discharge shown in Table IV-1 has been conducted.

TABLE IV-1

τ I	20 μsec	80 μsec
120 Kamps	100μ ambient Shock Tube	╳
30 Kamps	100μ ST	100μ ST

1. Magnetic Probe Studies

As in earlier work, the main diagnostic technique is the magnetic probe and the final results are presented in the form of enclosed current contours. The magnetic probe responses in the exhaust are not perfectly reproducible as seen in Figure IV-8 where two triple overlays are presented. All the data are taken in the form of triple overlays and are averaged. From Figure IV-5a and b, one can note that the enclosed current contours are quite wiggly. The same wiggly contours are obtained in this work but due to the averaging incorporated in the data reduction which leads to an error of approximately 10% in contour value, the contours are drawn as smooth lines without any further loss in accuracy.

From a stabilization point of view, the most interesting cases are both filling modes for the $^{30}/80$ pulse. The enclosed current contours for these cases are presented in Figure IV-9a,b

I 414 B

a)

b)

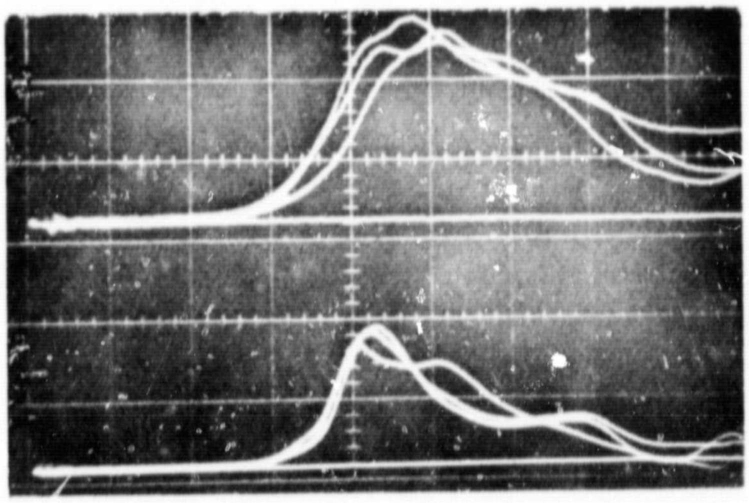

TYPICAL RESPONSE OF MAGNETIC PROBES

a) AT $R = 3\frac{1}{8}$ INCHES

b) AT $R = 1\frac{1}{8}$ INCHES

FIGURE IV-8

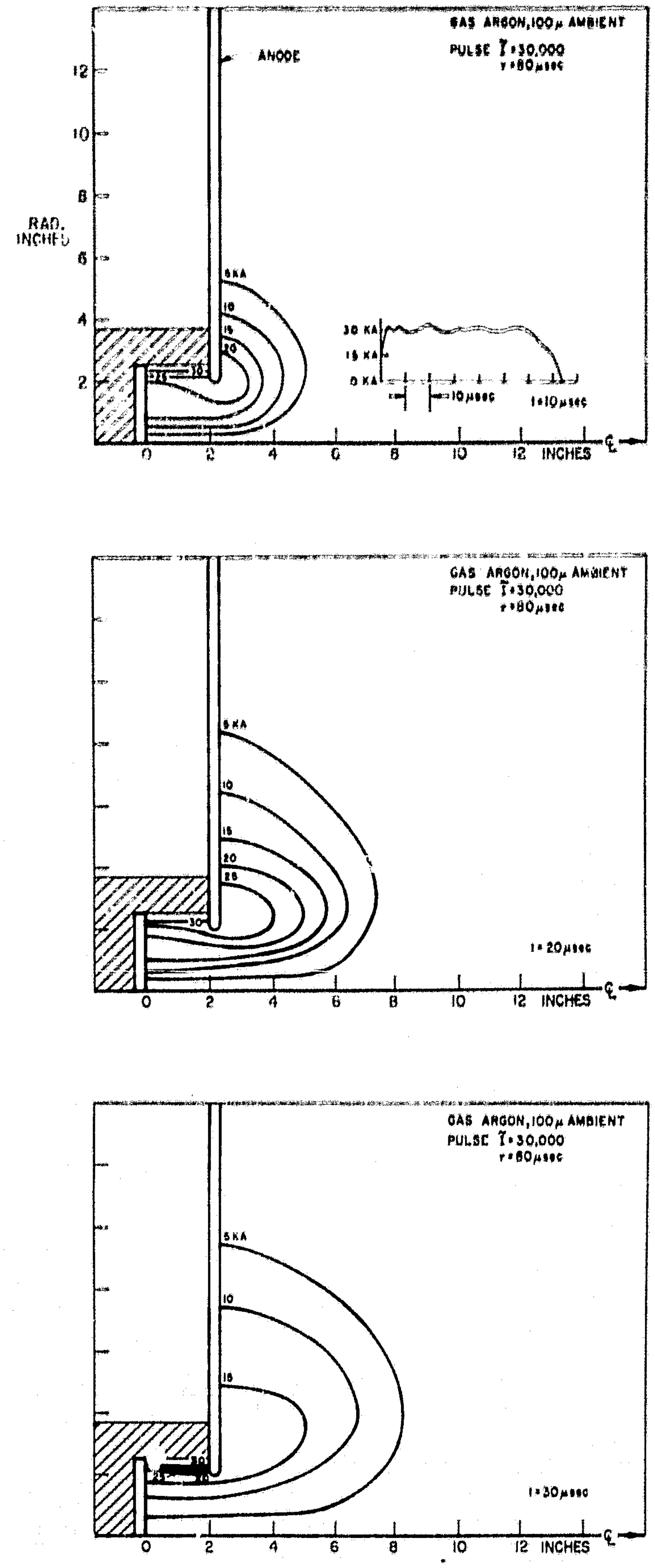

MAPS OF ENCLOSED CURRENT, AMBIENT FILL

FIGURE IV-9a

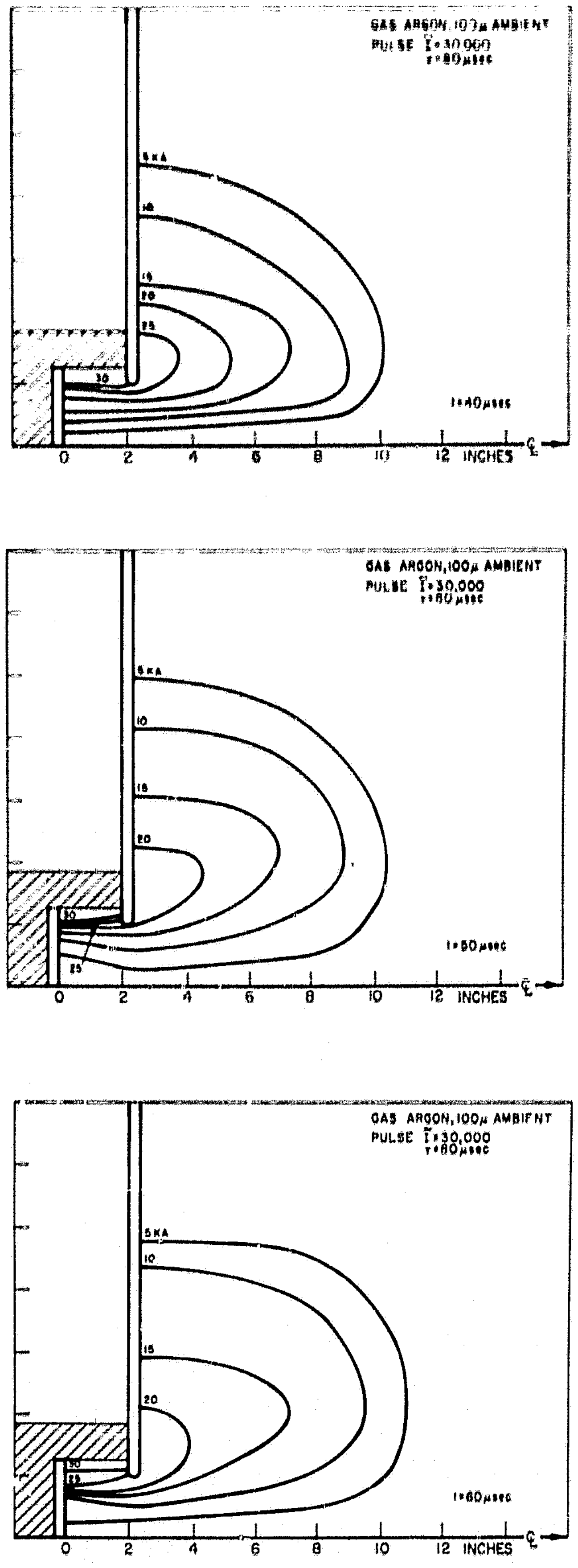

AP25 P236 68

MAPS OF ENCLOSED CURRENT, AMBIENT FILL

FIGURE IV-9b

and IV-10a, b. Detailed results for the other cases are presented in [48]. The enclosed current contours shown clearly reveal that the initial pulsed plasma expulsion event is followed after a transition period by a spatial stabilization of the current contours. This occurs for the results presented at times greater than 40 μsec. This current pattern stabilization is more vividly demonstrated in Figure IV-11a,b where the axial and radial trajectories of the leading edges of the current contours are presented. The spatial accuracy of the trajectories shown is about ± 10%. Table IV-2 presents a summary of the experimental results.

Based on detailed study of the exhaust patterns, the following generalizations can be made: 1) For the rectangular waveforms used, only a single "sheet" is created and pinched, but this current sheet does not contain the total circuit current. A sizable fraction of the current remains at the outer edge of the pinch chamber. No crowbarring, i.e. generation of additional current sheets, is found. 2) Only the current which participates in the pinching process eventually flows in the exhaust plume. 3) For a given pulse time and current amplitude, a greater portion of the discharge current appears to flow in the exhaust plume in the ambient case in contrast to the gas injection mode. This is due in part to a retrograde motion of the higher current contours from the exhaust plume back into the pinch chamber in the shock tube case. 4) For a given energy pulse, a greater fraction of current flows in the plume for the lower amplitude, longer pulses. 5) If the current magnitude is held constant and

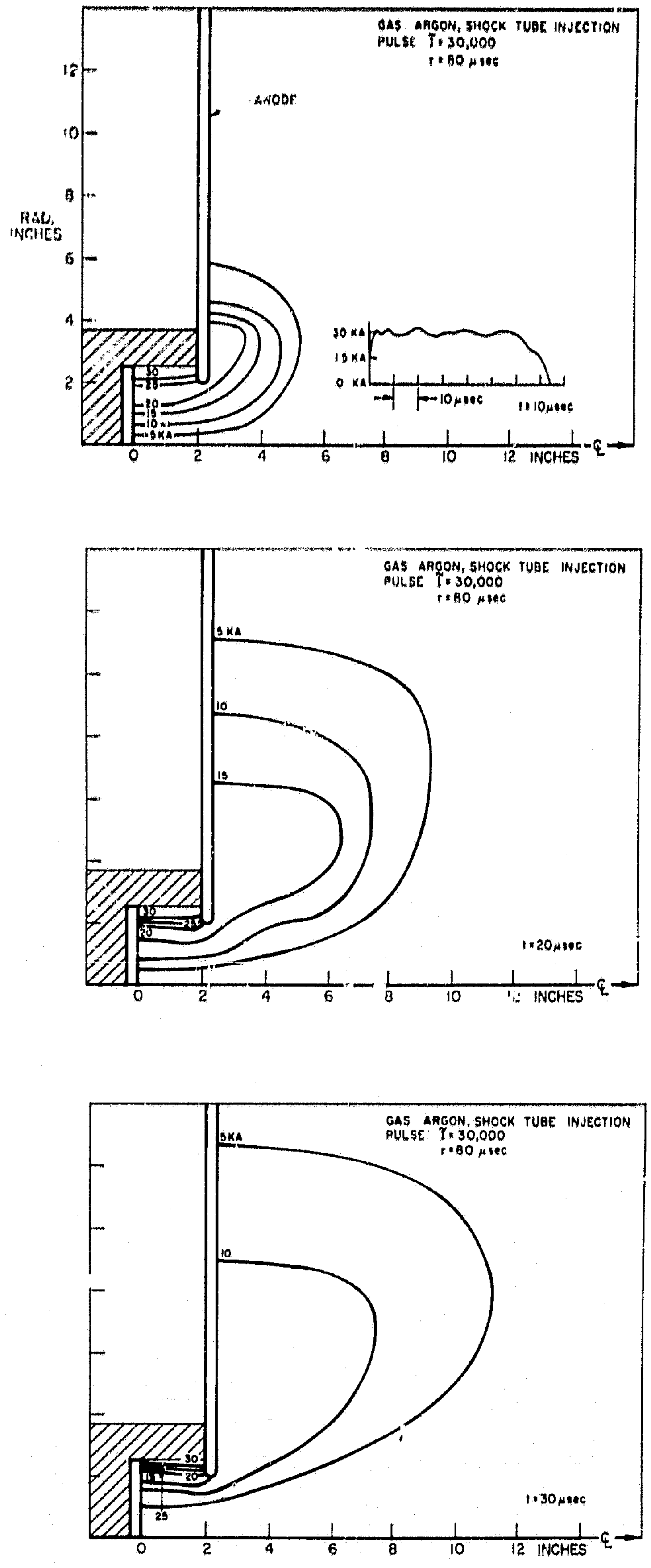

AP 25 P 237 68

MAPS OF ENCLOSED CURRENT, SHOCK TUBE INJECTION

FIGURE IV-10a

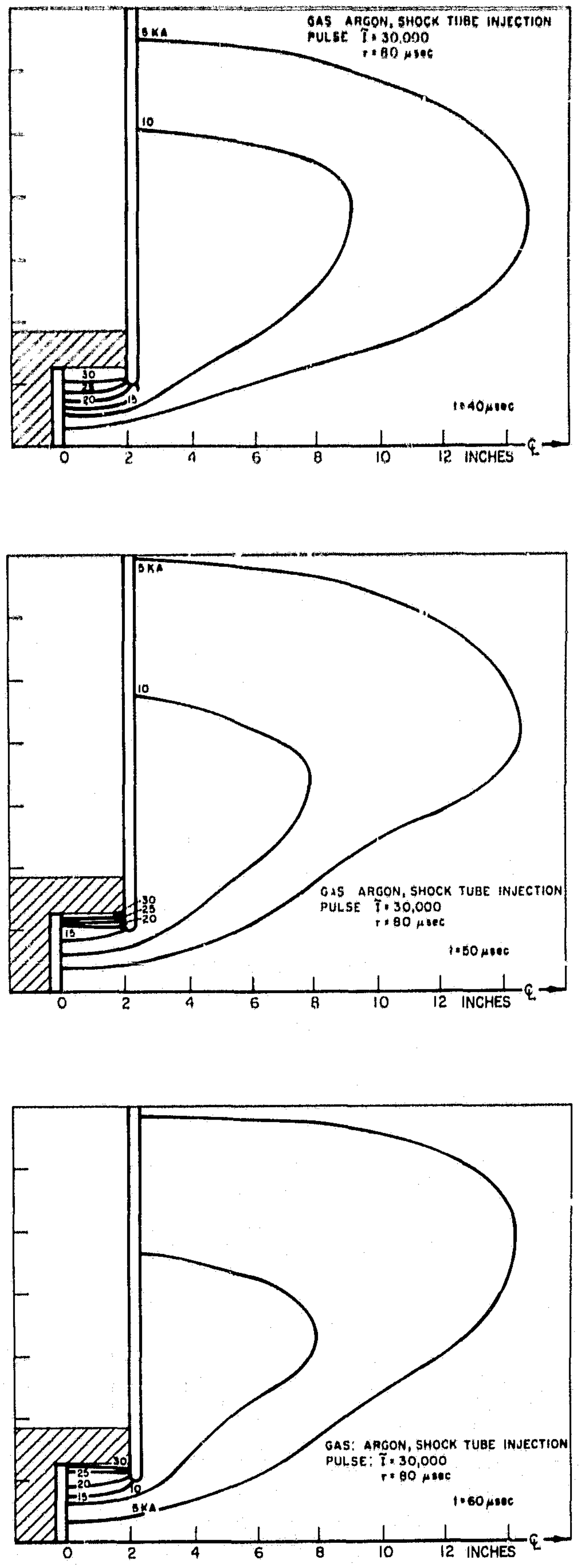

MAPS OF ENCLOSED CURRENT, SHOCK TUBE INJECTION

FIGURE IV-10b

AP 25 238 68

AP3 [illegible]

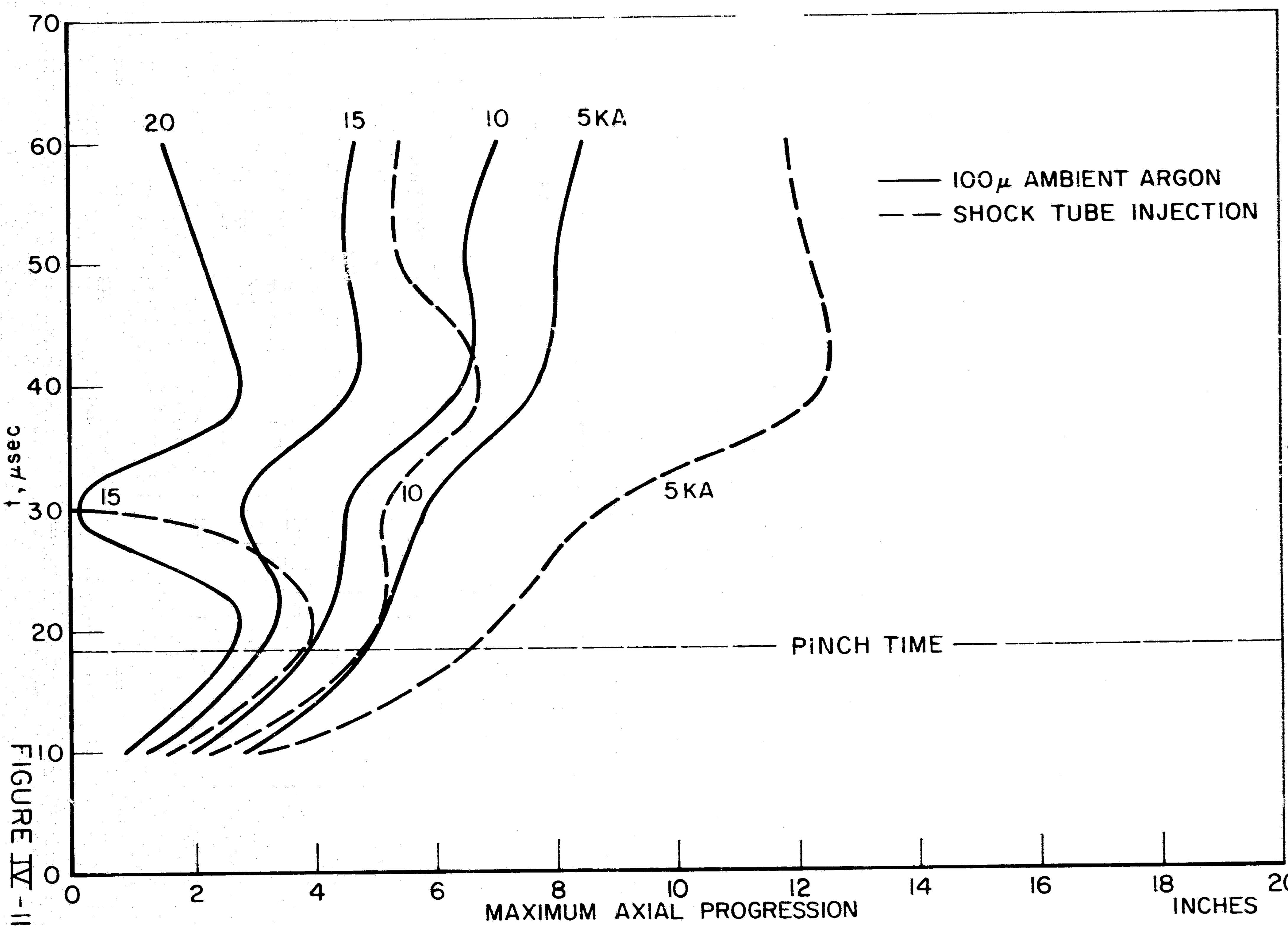

FIGURE IV-11a

DEVELOPMENT OF ENCLOSED CURRENT CONTOURS FOR 30 KA, 80 μsec PULSE

4P25 [illegible]

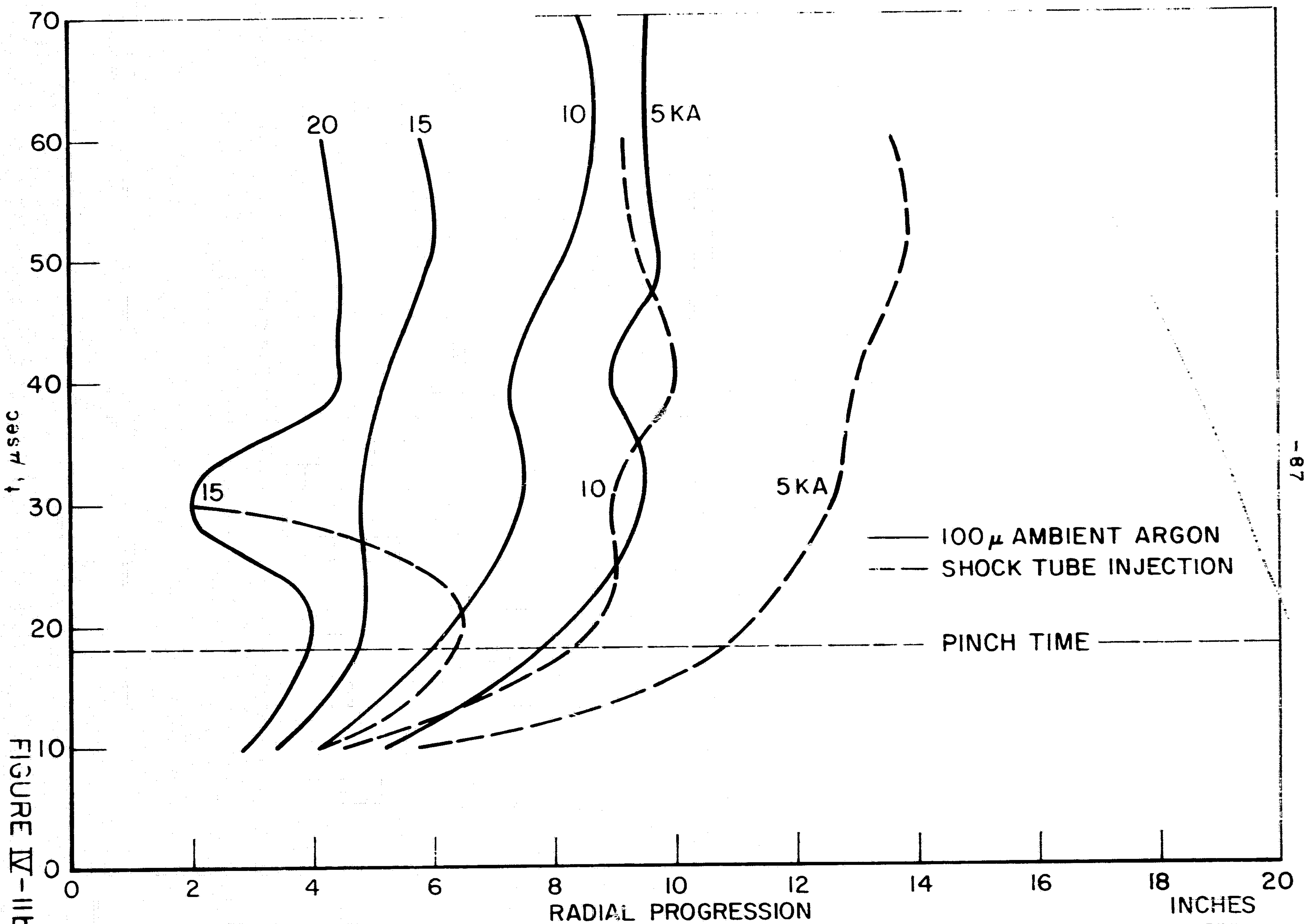

FIGURE IV-11b

DEVELOPMENT OF ENCLOSED CURRENT CONTOURS FOR 30 KA,80 μsec PULSE

TABLE IV-2

Gas Filling Made	Current Amplitude I, (kamps)	Pulse Length (μsec)	% Current Pinched	% Current In Exhaust Plume	Degree of Current Pattern Stabilization
100μ	120	20	30	30	Radial $t > 8$ μsec
"	30	20	60	60	none
"	30	80	60	60	Radial & axial $t > 40$ μsec
ST $(P_B\ .05\mu)$	120	20	30	30	none
"	30	20	data irreproducible	data irreproducible	none
"	30	80	data irreproducible $t < 20$ μsec	data irreproducible $t < 20$ μsec	Radial & Axial $t > 40$ usec

the pulse length increased, the pattern for the longer pulse is the same over the time span of the shorter pulse and the remainder is a continuation of the process from that point on.

6) Most importantly, it is found that the discharge process progresses through 3 phases: a) an initial, unsteady portion with well defined propagating current zones, b) a transition phase of a diffuse but unsteady current zone, and c) a stabilized phase with fixed current patterns, i.e. current pattern stabilization.

The stabilized phase is not attained in all cases within the testing times available. In particular, pinch times must be considerably less than the driving pulse length if current pattern stabilization is to occur.

2. Voltage Records

In Figure IV-12 are typical voltage measurements across the electrodes for the $^{30}/80$ pulse for both the ambient and shock tube filling modes. The average voltage across the electrodes is about 200 volts in the 10 to 60 μsec interval. The terminal voltage for a pulsed plasma accelerator can be given as [2]

$$V = IR + L\frac{dI}{dt} + I\frac{dL}{dt} \qquad \text{(IV-2)}$$

where I - total circuit current

L - discharge inductance

R - discharge resistance

For a rectangular current pulse $\frac{dI}{dt}$ is zero, and when stabilization occurs $\frac{dL}{dt}$ goes to zero. Despite the fact that stabilization is occurring, the voltage remains relatively

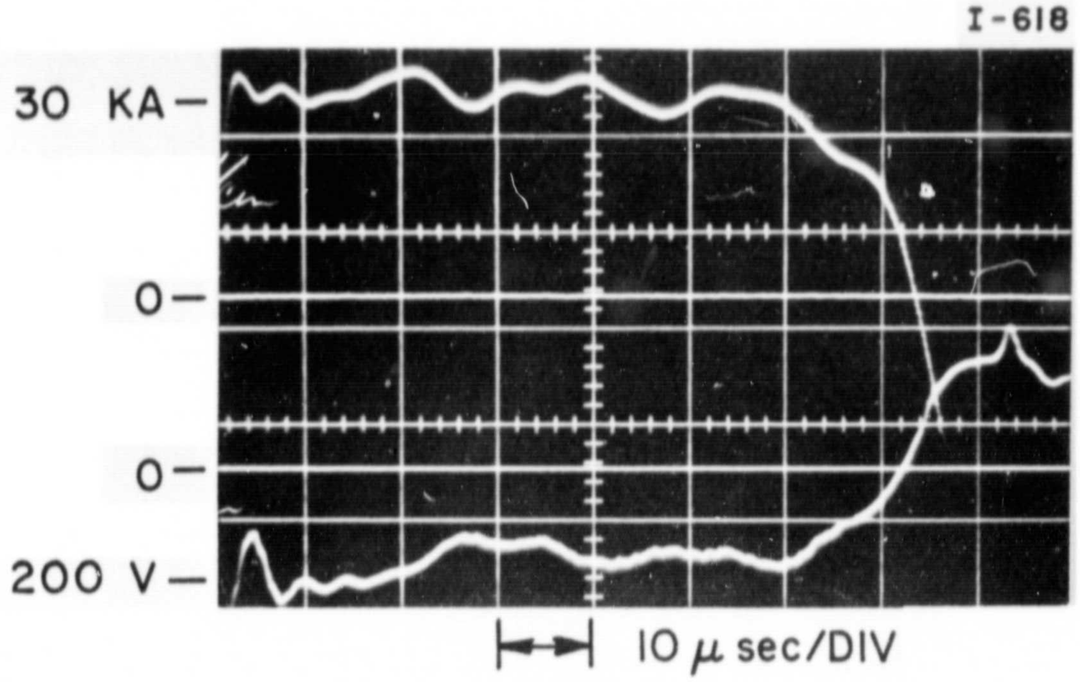

a) IN 100 μ ARGON

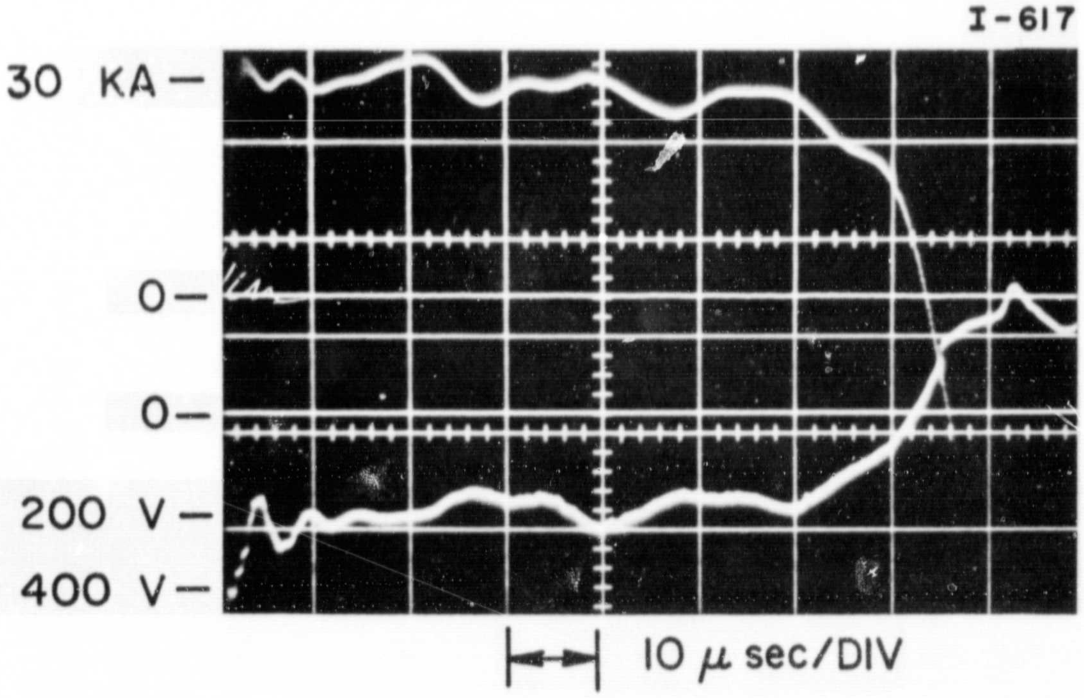

b) WITH GAS INJECTION

VOLTAGE ACROSS 30 KA, 80 μ sec DISCHARGE

FIGURE IV-12

constant. It is well known that steady flow accelerators generate a back $\vec{u} \times \vec{B}$ emf as plasma is accelerated across flux lines. It may be suggested that one is witnessing a steady flow mode of acceleration when current pattern stabilization occurs and that a back emf is generated which replaces the $I\dot{L}$ term. In a cylindrical geometry of this type with the additional complexity of the orifice, it would be very difficult to separate the various contributions to the total voltage. In later work with the parallel plate accelerator where the voltage contributions can be separated, it will be seen that the above hypothesis has considerable merit.

The purpose of presenting this work is to show in a chronological fashion how current pattern stabilization was first found in studying the exhaust phase of the orifice pinch. By introducing it in the context in which it was found, its importance as a phenomenon worthy of further investigation is easily demonstrated. The observation of current pattern stabilization with the diagnostics employed did not permit conclusive assignment of the cause of this transition nor indicate how it scaled. One may reasonably speculate that this is basically a geometrical effect associated with finite electrode dimensions and the corresponding limiting configuration to which the current pattern can expand before its driving mechanism fails. It is not clear whether this failure is an inability of the available interelectrode potential to sustain an arc column of greater length, a weakening of the local force density to the point that the plume can no longer sensibly progress against the ambient gas, an inherent limitation on the tolerable development of the discharge inductance, or a boundary condition limitation on the fields to remain at an adequate level for current conduction. The role of the gas density profile which modifies but does not inhibit the stabilization process is also unclear.

In an attempt to study stabilization more intensely, and in a simpler geometry, the parallel plate accelerator described in Chapter II was constructed. The next chapters focus on the investigations performed in that device and on their consequences.

CHAPTER V

PARALLEL PLATE ACCELERATOR
ALL METAL ELECTRODE CONFIGURATION

The parallel plate accelerator was specifically constructed to study current pattern stabilization in a simple, planar, two dimensional geometry. Prior to searching for a current pattern stabilization condition, the characteristics of the parallel plate geometry are first studied in the conventional pulsed or propagating sheet mode. These studies are performed using the full metal electrodes and are intended to accomplish three objectives: 1) To ascertain whether the current sheet will decelerate and stabilize if driven with a long duration pulse. 2) To study the two dimensionality of the device. 3) To provide a basis for comparison with the stabilized configuration if current pattern stabilization does not occur in this situation. In view of the results to be presented which demonstrate the absence of stabilization in this configuration and which confirm the two dimensionaltiy of the process, the primary importance of studying the all metal electrode configuration is to provide a basis for comparison with the partially insulated electrode case, which is the current stabilizing configuration. Accordingly, several of the results obtained with the all metal electrode case are presented in the next chapter so that comparisons between the all metal and partially insulated electrode configuration are more vivid.

For the initial work, three diagnostic methods are employed: Kerr cell photography, magnetic probe surveys, and voltage measurements.

A. KERR CELL PHOTOGRAPHY

Luminosity studies of both the 120/20 and 30/80 cases indicate no tendency of the current sheet to slow its propagation throughout the duration of the pulse. These studies do reveal, however, certain unexpectedly severe, two dimensional distortions of the current "sheet" geometry. These effects are illustrated in Figure V-1 for the 120/20 case. Similar results are obtained for the 30/80 pulse. The photographs shown are obtained by viewing the discharge through the plexiglass side wall normal to the direction of propagation; the camera is moved successively from adjacent positions between the bolts of the apparatus to follow the progress of the luminous front.

Of interest is the development of a diffuse "anode foot" which enlarges and grows as the sheet propagates down the channel. Inception of such a "foot" has also been observed in other experiments of this type,[27] but[30] here it is allowed to progress to the point where it completely dominates the entire luminous pattern, tilting it substantially with respect to the axis and diffusing it over a large dimension.

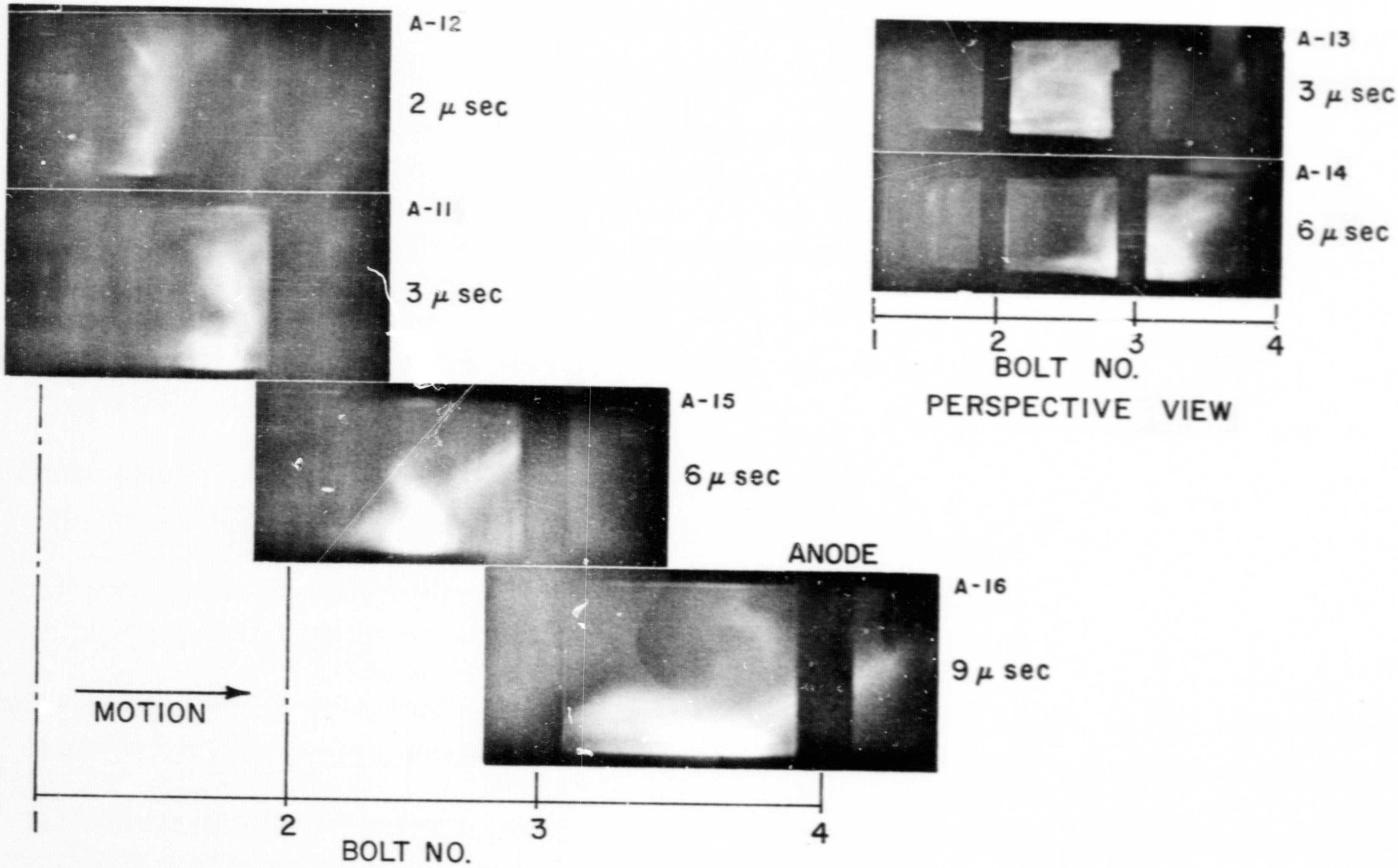

KERR-CELL PHOTOGRAPHS OF PROPAGATING LUMINOUS FRONT
IN PARALLEL PLATE ACCELERATOR ;
FULL ELECTRODES ; 100 μ ARGON ;
DRIVING CURRENT 120,000 amp × 20 μ sec.

FIGURE V-1a

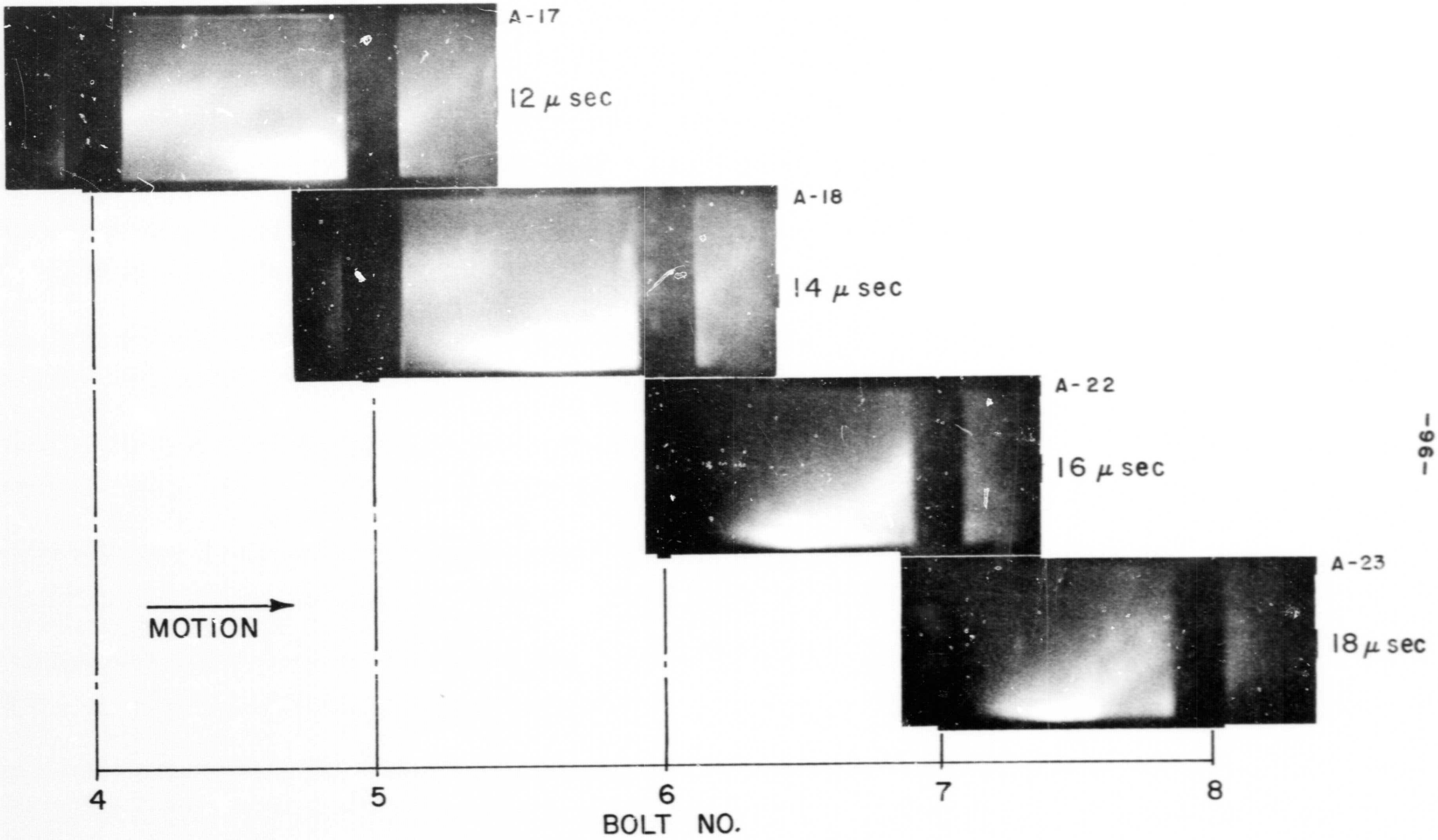

KERR-CELL PHOTOGRAPHS OF PROPAGATING LUMINOUS FRONT
IN PARALLEL PLATE ACCELERATOR ;
FULL ELECTRODES ; 100 μ ARGON ;
DRIVING CURRENT 120,000 amp × 20 μ sec.

FIGURE V-Ib

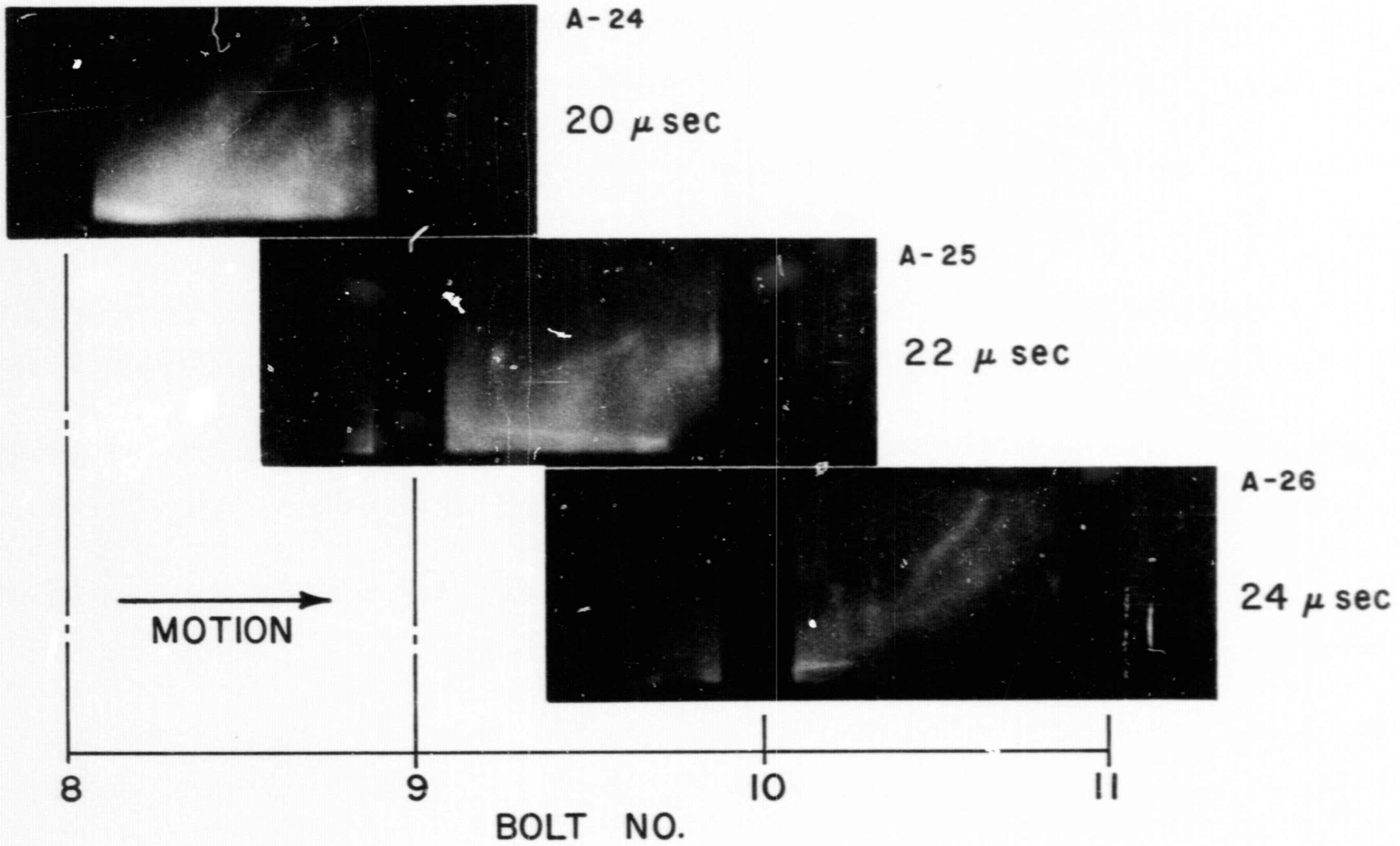

KERR-CELL PHOTOGRAPHS OF PROPAGATING LUMINOUS FRONT IN PARALLEL PLATE ACCELERATOR ; FULL ELECTRODES ; 100 μ ARGON ; DRIVING CURRENT 120,000 amp × 20 μ sec.

FIGURE V-1c

Perspective viewing of the discharge reveals that the process remains two dimensional, stretching from side wall to side wall across the electrodes. Because of the tilting and diffusing of the luminous pattern, it is difficult to define a mean trajectory precisely, but to a crude estimate, the propagation speeds are in the range of 40,000 m/sec for the 120/20 case and 20,000 m/sec for the 30/80 case. Luminosity trajectories can be seen in Figures V-2, 3. The spatial accuracy of the luminosity points shown is about ± 1".

B. MAGNETIC PROBE SURVEYS

The qualitative aspects of the luminous photographs are confirmed by magnetic probe data obtained in the conventional manner as described in Chapter III. The probes employed are Formvar wire coils epoxyed into sealed Pyrex tubes and inserted through access ports drilled in the anode.

The magnetic probe studies show that the current density patterns are quite reproducible and nearly two dimensional over most of the channel width. Typical profiles of magnetic field versus axial distance at channel half height, y=1", of the center vertical plane, z =3", at various times are shown in Figure V-4 for the 120/20 case. The magnetic field values shown are accurate to within ± 5%. Half height profiles in other vertical planes, z=1/2" and z=1-3/4" from the side wall are quite similar to those shown, and confirm the perspective photographs that the two dimensionality of the 120/20 current distribution is good. Since

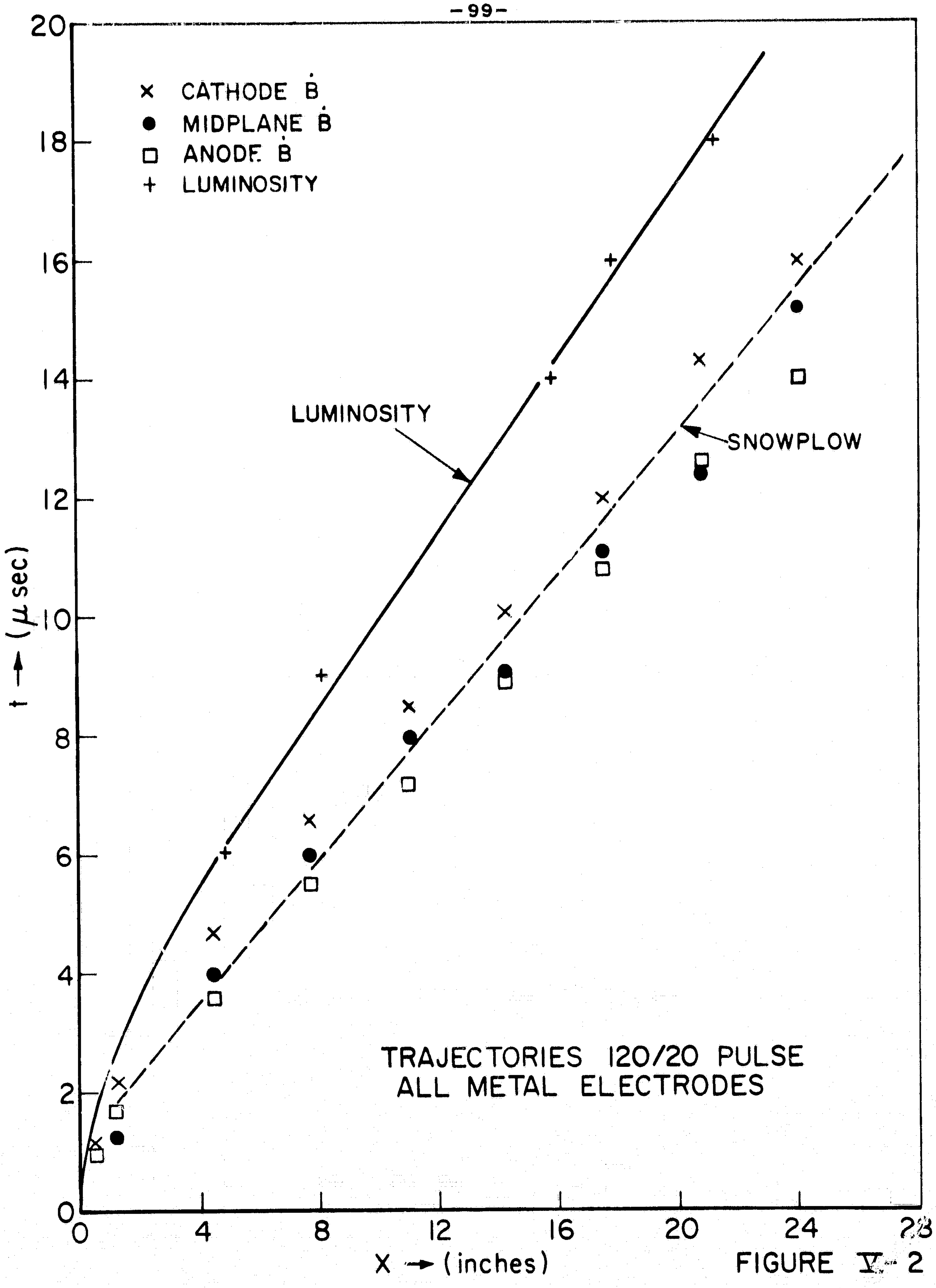

TRAJECTORIES 120/20 PULSE
ALL METAL ELECTRODES

FIGURE V-2

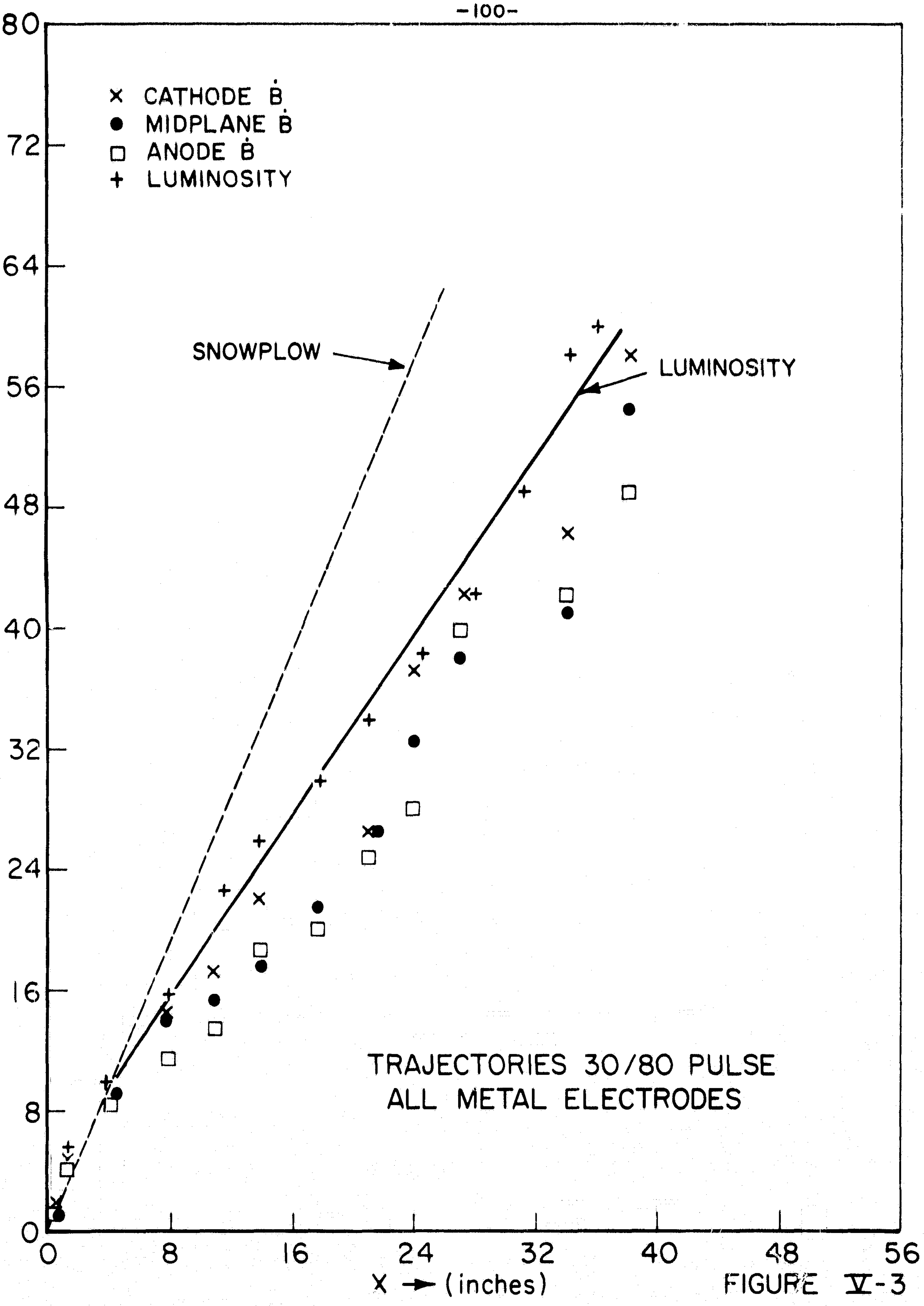

FIGURE V-3

AP 25 K 4452 68

AP 25 16 4322 67

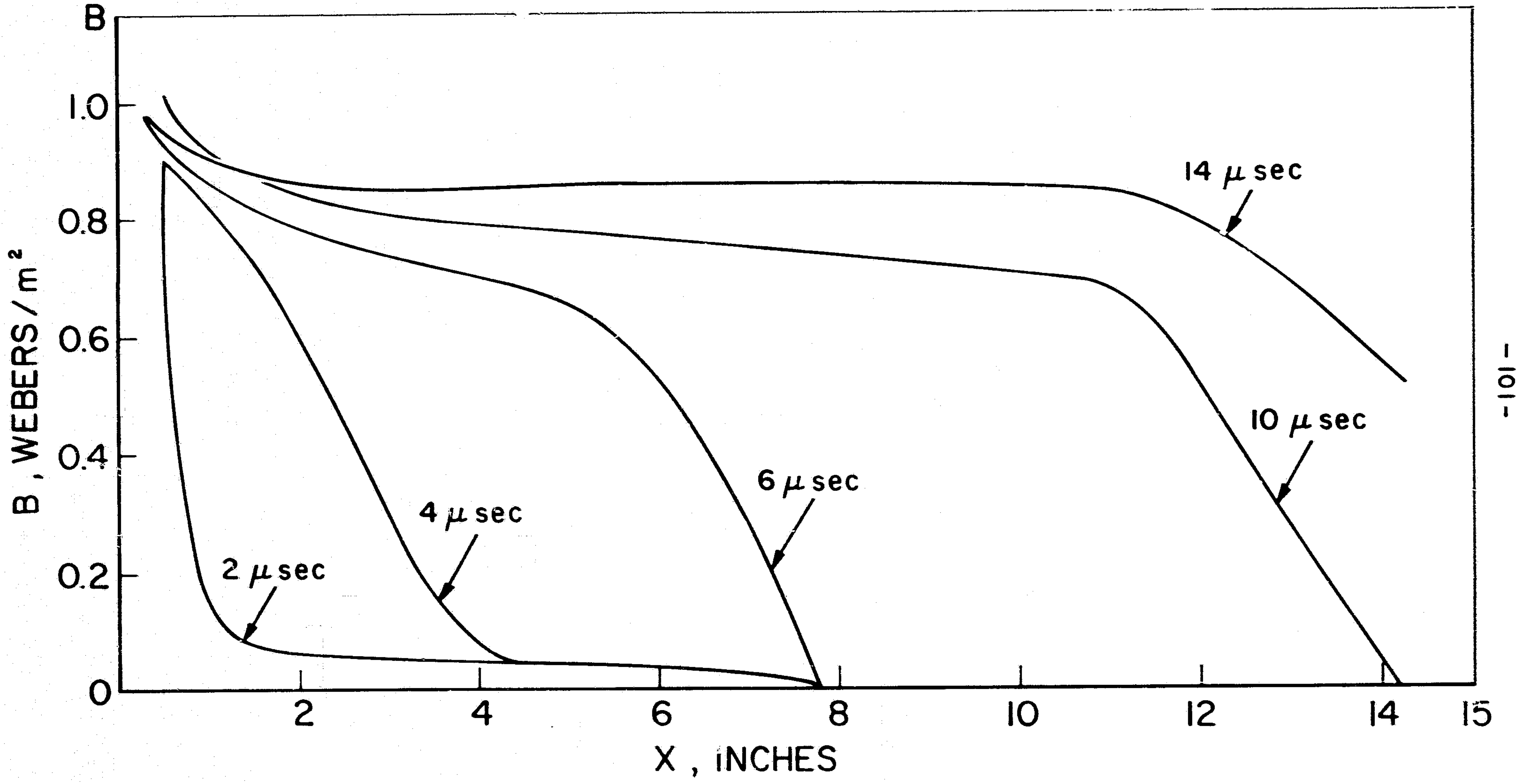

MAGNETIC FIELD PROFILES IN PARALLEL PLATE ACCELERATOR ;
FULL ELECTRODES ; 100 μ ARGON ;
DRIVING CURRENT 120,000 amp × 20 μ sec

FIGURE Ⅴ-4

the magnetic probe surveys verify the conclusion based on perspective viewing of the 120/20 discharge, and since perspective viewing of the 30/80 case indicates good two dimensionality, the 30/80 case is assumed also to be nearly two dimensional.

Differentiation of the spatial distribution of magnetic field curves with respect to x, or translation of the $\dot{B}$ records*, indicates that the current density profiles tend to be sharply peaked at the outset and then broaden as they propagate down the channel. Trajectory plots, x versus t, of the $\dot{B}$ peaks along with luminosity and snowplow trajectories are presented in Figures V-2 and 3 for the 120/20 and 30/80 cases respectively. Uncertainties in time are about ± 0.2 μsec for the 120/20 points and ± 0.5 μsec for the 30/80 data. Spatial accuracy of all the $\dot{B}$ data is about ± 1/16" Of note is the fact that the sheets propagate with nearly constant velocities which are in the same range as the luminosity. Also to be noted is the variation in sheet velocity across the interelectrode spacing corresponding to the tilting and diffusing of the current pattern seen in the luminosity photographs. Also appearing on these plots is the theoretical snowplow trajectory. The 120/20 case, which nearly fulfills the previously discussed em-

---

*From Ampere's Law it can be shown that $j_y \propto \dot{B}$ for constant amplitude current sheets:

$$j_y = -\frac{1}{\mu_0}\frac{dB_z}{dx} = -\frac{1}{\mu_0}\frac{dt}{dx}\frac{dB}{dt} = -\frac{1}{\mu_0}\frac{1}{u_{SHEET}}\dot{B}$$

pirical requirement of a lineal current density in the 10^6 amps/meter range for good sweeping sheets, shows good agreement with the snowplow model. On the other hand, the 30/80 pulse which falls well short of the criterion, shows poor agreement. The 30/80 current sheet runs ahead of the snowplow trajectory presumably due to a decreased mass loading of the sheet indicative of incomplete sweeping.

C. VOLTAGE MEASUREMENTS

Terminal voltage measurements are made by placing the voltage probe directly across the electrodes at the front of the accelerator, x = 48", or by employment of an inner divider. This device is simply a voltage tap which passes through an insulated port in the anode to electrical contact with the cathode and enables one to separate the resistive and inductive voltage drops in the plasma. Its geometry and simple analysis are sketched in Figure V-5. At any given position (A) along the channel, the inner divider first records only the resistive voltage drop through the plasma current sheet; if and when the current sheet sweeps by the probe position (B) it then records an additional voltage corresponding to the increase in magnetic flux, $\frac{d\phi}{dt}$, linked by the probe circuit. If the current sheet should come to rest and start accelerating gas through itself at a speed u, the probe will also record the corresponding motional emf, uB, regardless of its

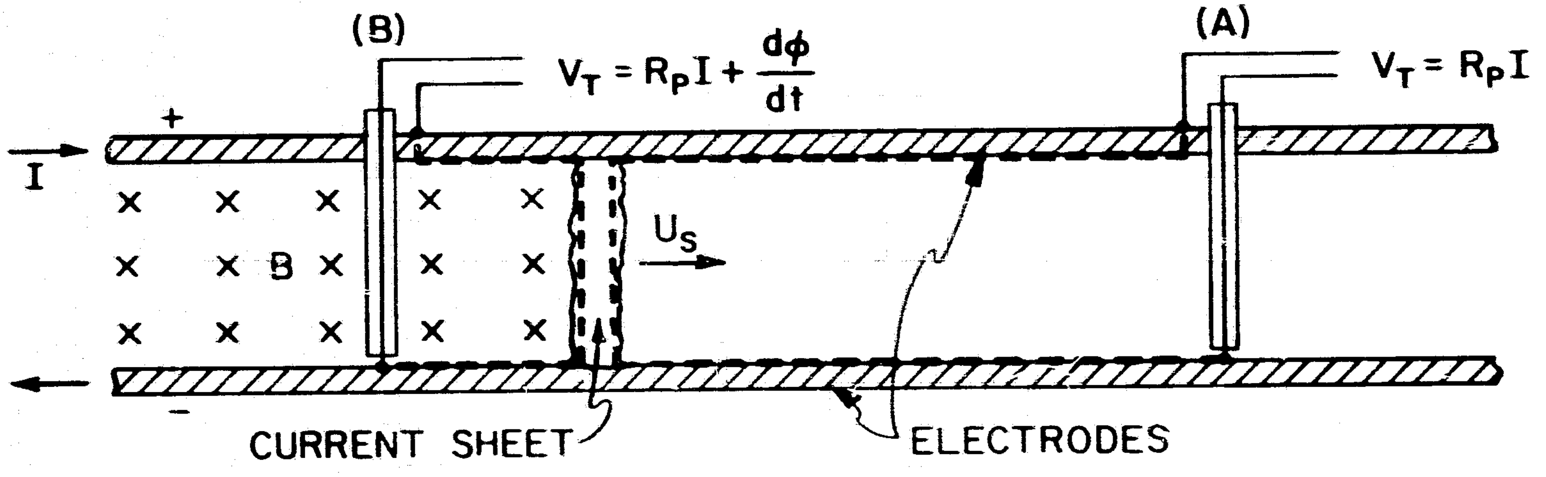

INNER DIVIDER AT TWO LOCATIONS IN PARALLEL PLATE ACCELERATOR

FIGURE V-5

location.

Figure V-6a shows the voltage signature at the front end of the accelerator for the 30/80 pulse. Since the current distribution never passes beyond the end of the device only the resistive drop, 50 to 60 volts in this case, is monitored. This corresponds to a maxium plasma resistance of 2 milliohms. In Figure V-6b the response of the inner divider at x = 24" is shown. The probe first records the resistive drop until the sheet sweeps by, at which time the inductive voltage drop is also recorded. For the constant amplitude current pulse employed, the inductive drop is proportional to the product of the current and sheet velocity. That the inductive drop remains relatively constant until the end of the current pulse is further proof that the current sheet continues to propagate down the channel for the duration of the pulse. Qualitatively similar signatures are obtained for the 120/20 case and are shown in Figure VI-6a, b; these are presented in Chapter VI in comparison with the stabilized voltage signatures.

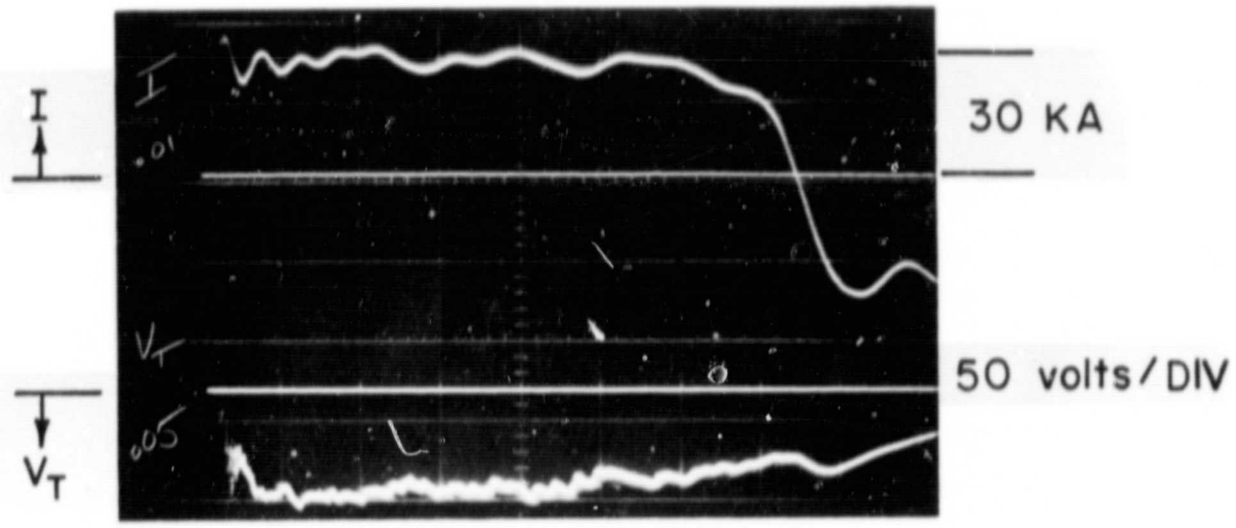

a) X = 45" 10 μ sec / DIV

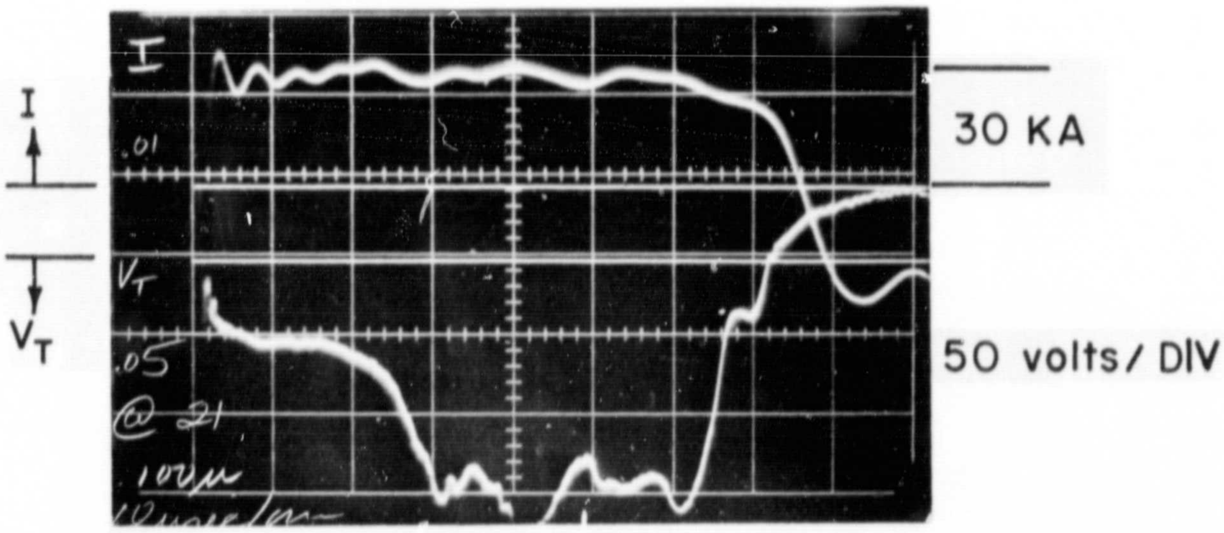

b) X = 24" 10 μ sec / DIV

100 μ ARGON; FULL ELECTRODES

VOLTAGE MEASUREMENTS, 30/80 PULSE

FIGURE V - 6

CHAPTER VI

PARALLEL PLATE ACCELERATOR
CURRENT PATTERN STABILIZATION STUDIES

A. STABILIZATION OF THE CURRENT SHEET

In an attempt to stop the propagation of the current sheet and precipitate transition to a current stabilized mode of operation, the channel is modified by covering both electrode surfaces with 0.003 inch Mylar sheet insulation from a position 9½" downstream of the discharge initiation location to the front end of the channel as previously shown in Figure II-8a. The propagating current sheet upon reaching the end of the conducting surface would be forced either to extend its length further and further while its ends remained attached to the electrodes, disattach itself in some manner, or lapse into a stationary pattern near the discontinuity. In all cases studied, the discharge elected the latter mode.

Using this partially insulated configuration, Kerr cell, magnetic probe, and voltage divider studies are repeated for otherwise identical conditions as the all metal electrode configuration. By comparison of the results for the full electrode and partially insulated electrode situations, transition from the pulsed to the pulsed flow mode is clearly established. These studies are then repeated by extending the mylar insulation from x = 2" to the front end wall, hence allowing only two inches of metal electrode. Again current pattern stabilization occurs with results qualitatively identical to those of the partially insulated configuration with a 9" electrode length.

Clearly, however, the thin mylar sheet must be considered a temporary measure by which the preliminary investigative studies can be carried out. For detailed study of the phenomenon, a partially insulated electrode was designed which called for ¼" thick inlaid nylon as the insulator. Furthermore it was decided to conduct the experiments with the 120/20 pulse where many of the results to be presented are more pronounced than with the 30/80 pulse. To provide nearly equal amounts of time for the propagating sheet, transition, and current stabilized phases during the 20 μsec current pulse, an electrode length of 5¼" was selected. A pair of partially insulated electrodes were constructed and employed in the experiments; their design is sketched in Figure VI-1.

Using the partially insulated electrode configuration described above, the transition from a sweeping current sheet to a stabilized current distribution is examined with a variety of diagnostics including Kerr cell photography of the discharge and plasma flow patterns, magnetic probes, electric probes and voltage probes. The results of these examinations will now be discussed; when more appropriate some of the initial 9" metal electrode

RP25 R 4350 68

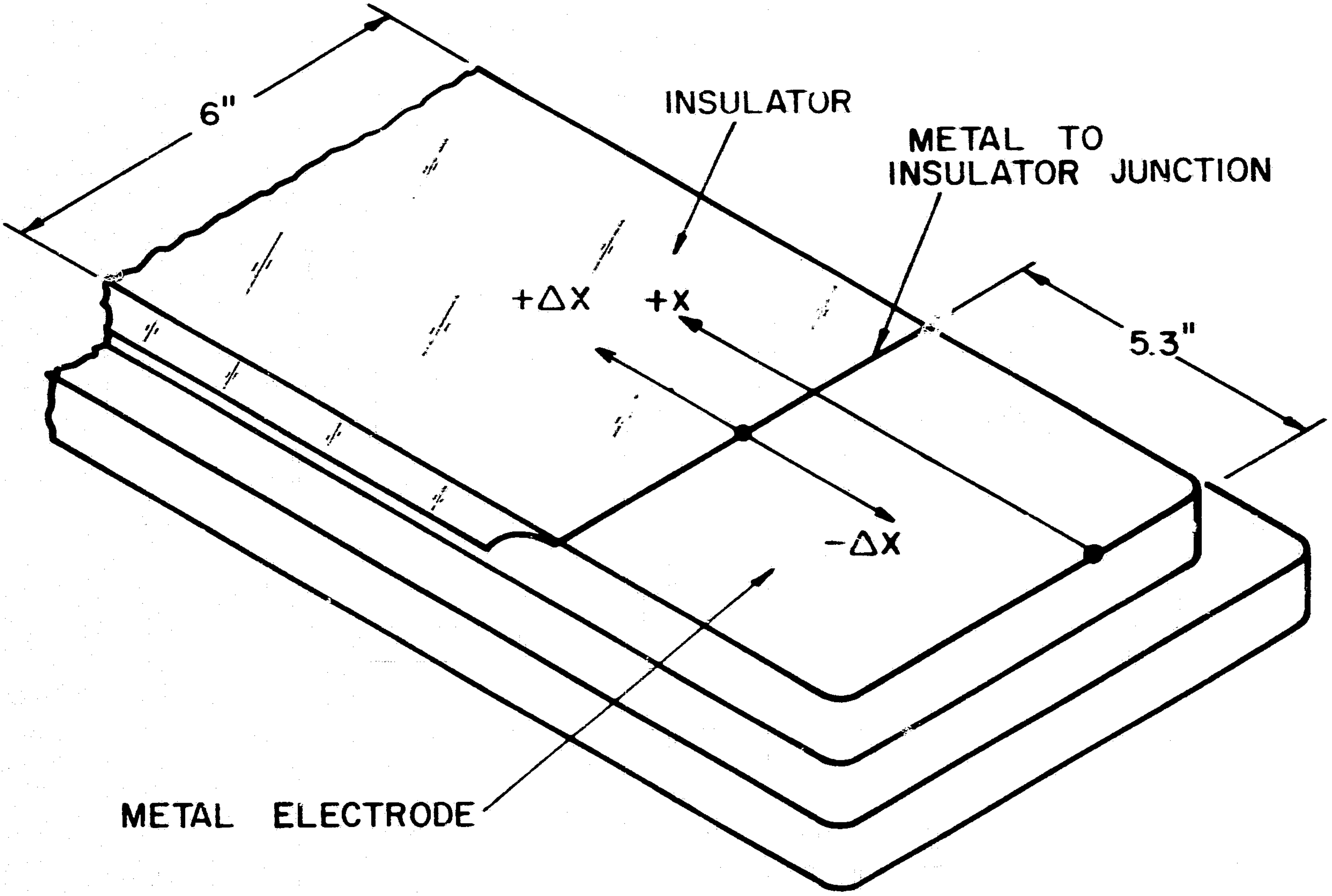

METAL ELECTRODE WITH INLAID INSULATION

FIGURE VI-1

length results will also be shown.

In the results to be displayed, the reference system employs x as the axial coordinate, such that the back wall where the discharge initiates is at $x = 0$ as has been the case to this point. The metal to insulation junction is at $x = 5\ 1/4''$ or $x = 9''$. The notation ΔX is used to denote position relative to the electrode to insulator junction; $\Delta X > 0$ runs along the insulation while $\Delta X < 0$ runs back along the metal electrode.

B. KERR CELL DISCHARGE PHOTOGRAPHY

Photographic studies of the discharge in the partially insulated electrode configuration are shown in Figures VI-2 and VI-3. Again, the discharge is viewed through the plexiglass side walls normal to the direction of propagation. The propagation of the sheet along the metal electrodes encompasses all the features previously identified in the all metal electrode configuration. When the propagating luminous front reaches the end of the exposed electrode, however, the luminosity pattern continues to propagate into the insulated channel unrolling as it were the stabilized pattern of two broad nearly axial and highly luminous bands emanating from the electrode discontinuity. One may speculate that these bright bands are analogous to the anode and cathode jets commonly seen in the magnetoplasmadynamic arcjet. Figure VI-4 summarizes the comparison of the luminous front trajectories in the various full electrode and partially insulated electrode cases studied. The 9" electrode length is presented; of

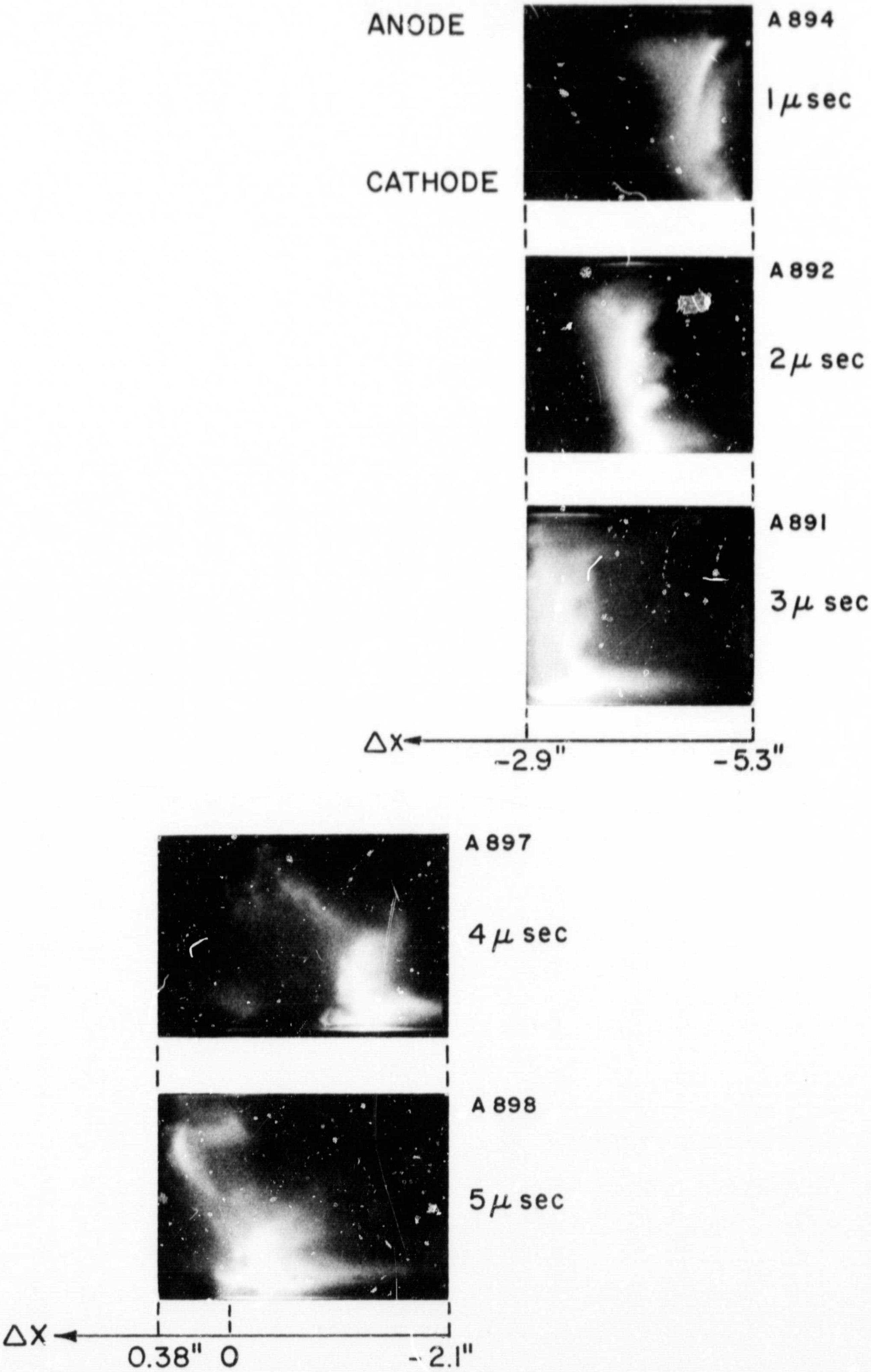

KERR CELL PHOTOGRAPHS OF PROPAGATING CURRENT SHEET

FIGURE VI-2

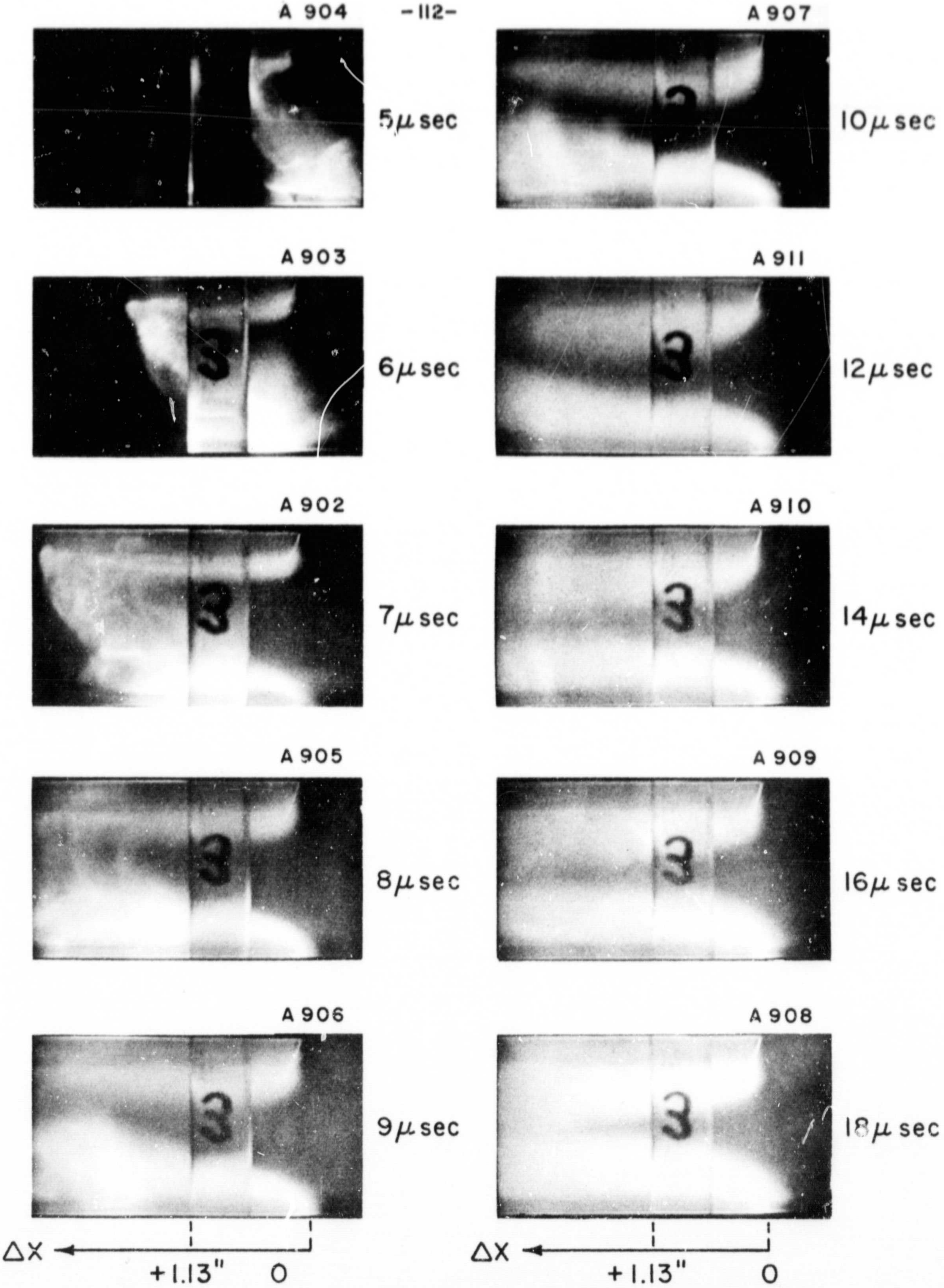

KERR CELL PHOTOGRAPHS OF TRANSITION TO STABILIZED CURRENT DISTRIBUTION

FIGURE VI-3

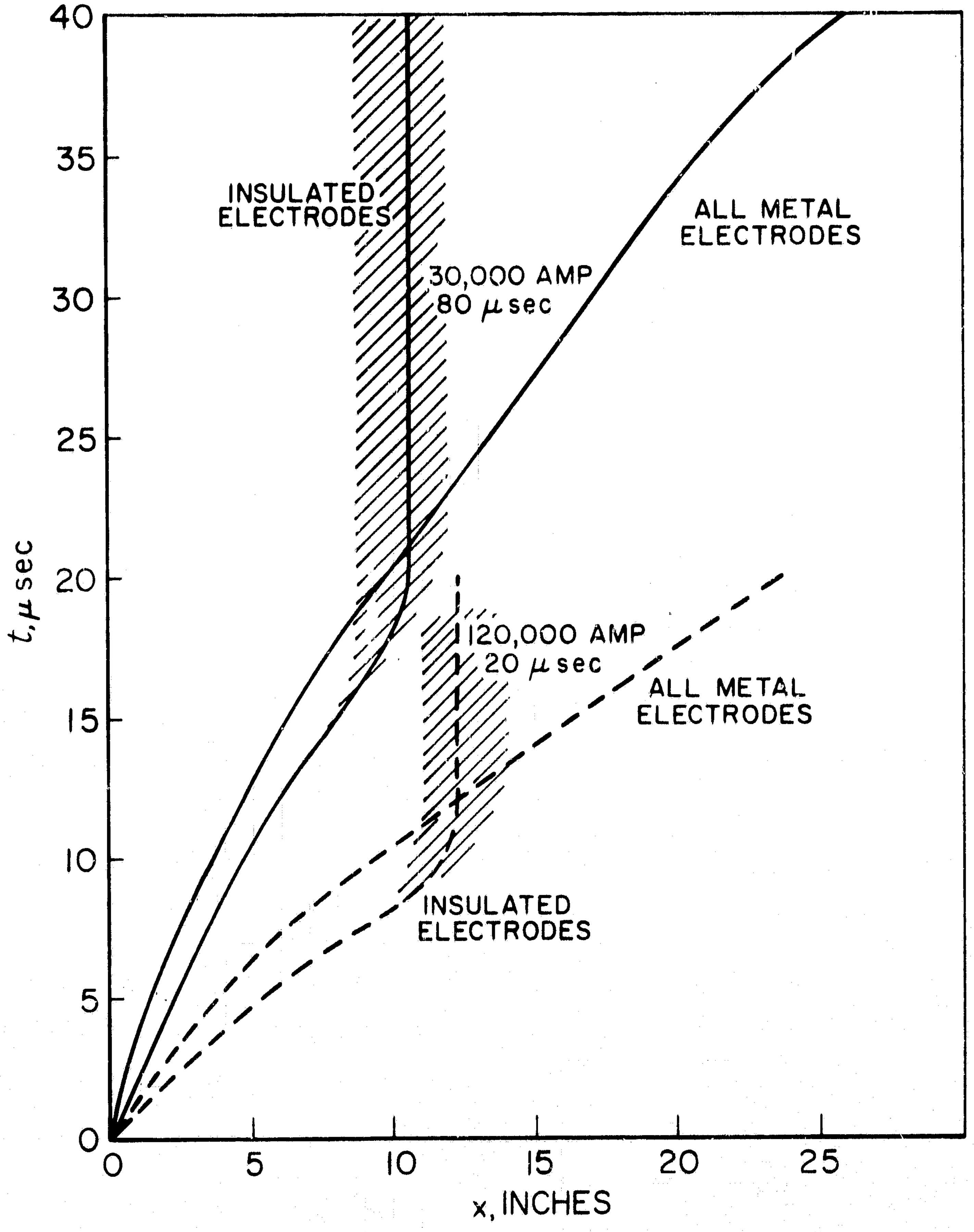

TRAJECTORIES OF LUMINOUS FRONT FOR VARIOUS ELECTRODE AND DRIVING PULSE COMBINATIONS; 100 μ ARGON

FIGURE VI-4

course similar trajectories are observed with other electrode lengths.

C. MAGNETIC FIELD STUDIES

Confirmation that the current carrying region has indeed ceased to propagate is best supplied by maps of enclosed current contours at a succession of times derived from magnetic probing of the entire discharge volume. Figure VI-5 displays such contours for the 120/20 current waveform and the 5 1/4" electrode length. The contour values shown are generally accurate to within ± 5%. The uncertainty results from data reading inaccuracies. In these illustrations, the individual contours conform to local current streamlines and their numeral indicates the cumulative current passing everywhere downstream. The slight tilt of the propagating current sheet, its broad anode attachment region, and its abrupt balloon-like arrest at the electrode discontinuity are again discerned in agreement with the luminosity studies. The stabilized pattern bows downstream in a hairpin fashion with the bulk of the current conducted across the midplane in the $0<\Delta x<6''$ region, i.e., within three channel heights downstream of the metal to insulation junction.

D. VOLTAGE MEASUREMENTS

Additional confirmation of current pattern stabilization and valuable indication that the pattern indeed continues to accelerate gas through itself in its stabilized phase is provided by a sequence of terminal voltage measurements with the inner divider discussed in the previous

AF25 2 7352 .8

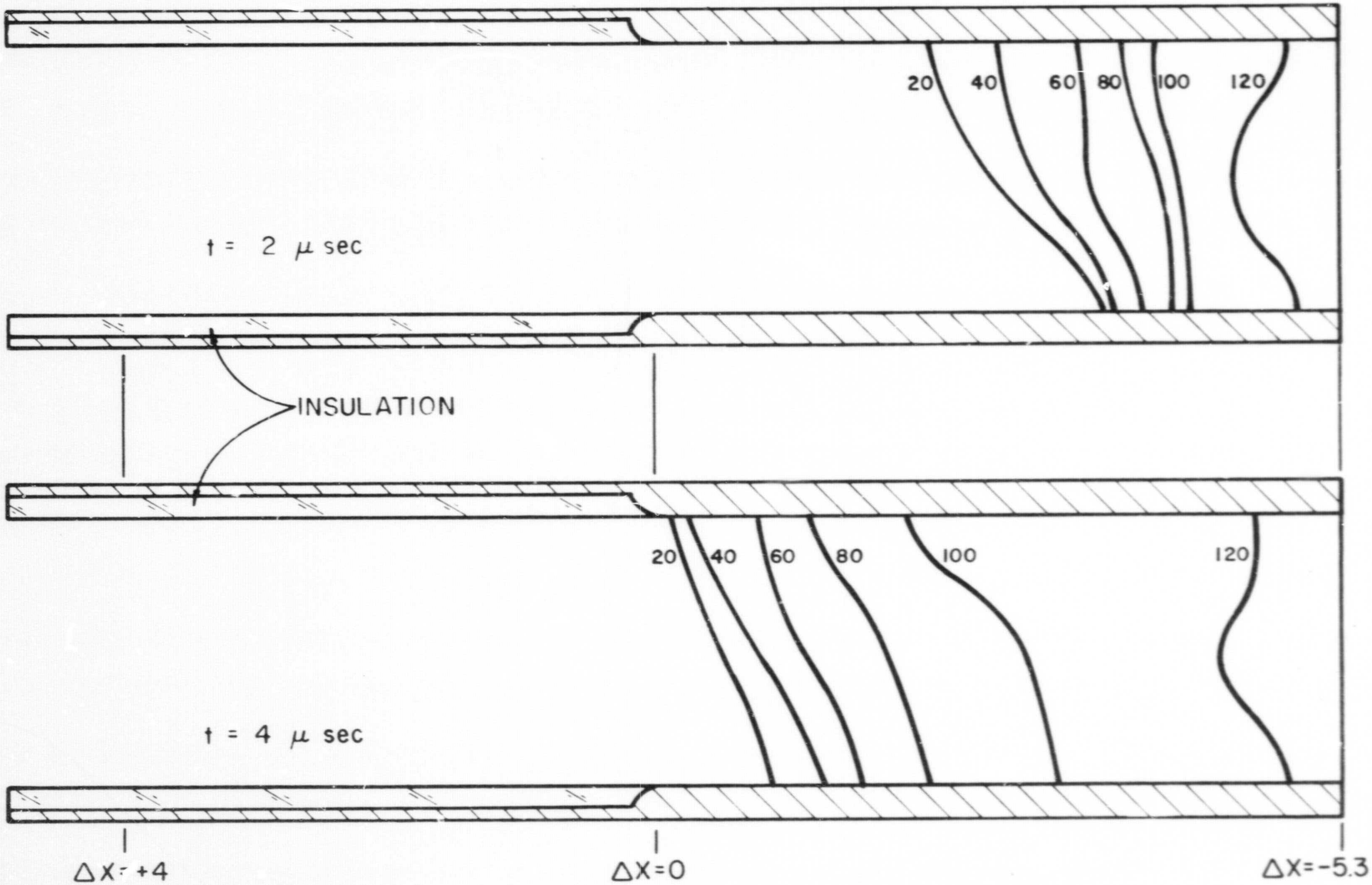

ENCLOSED CURRENT CONTOURS (K-Amp) IN PARALLEL PLATE ACCELERATOR

FIGURE VI-5a

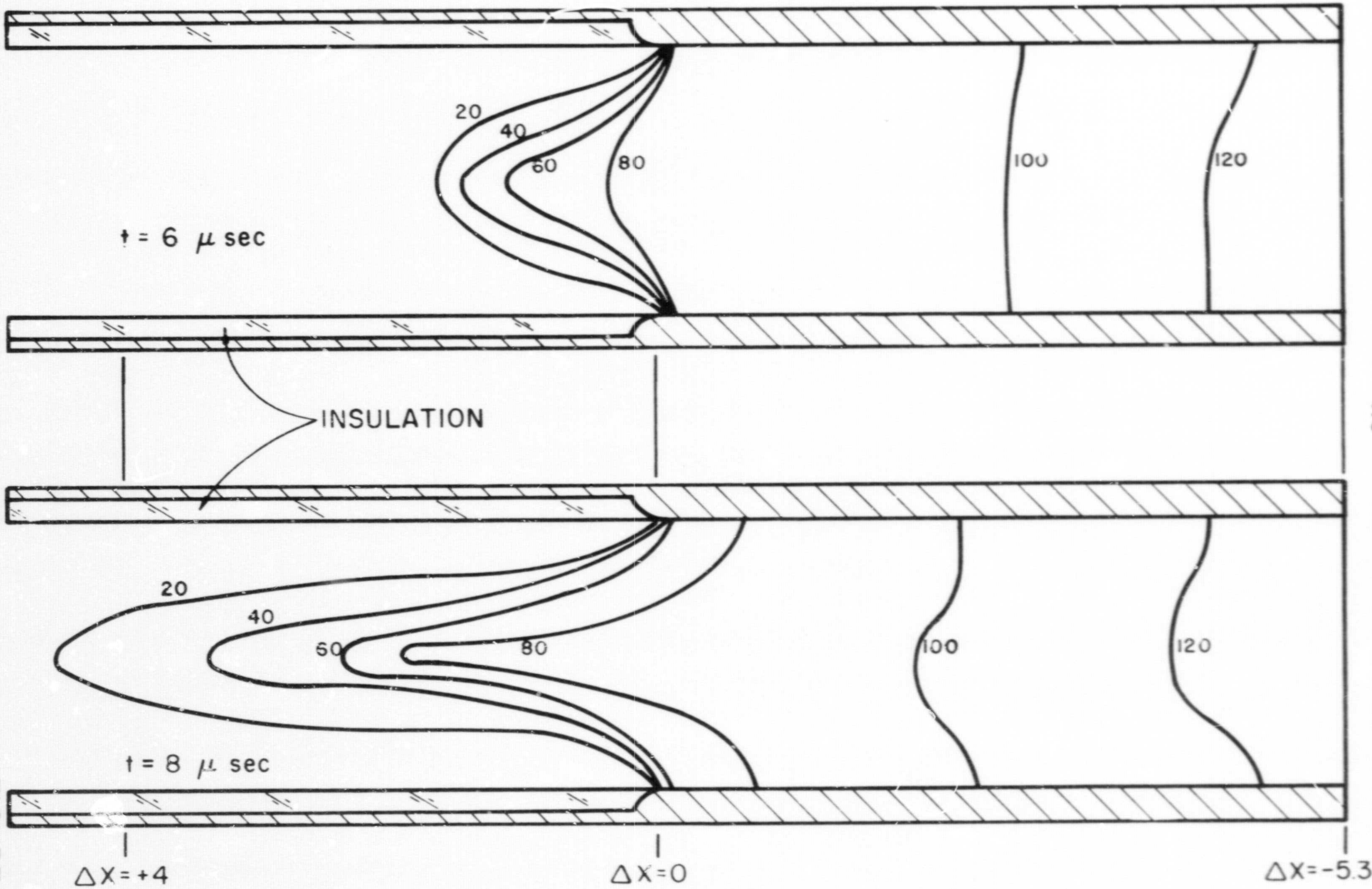

ENCLOSED CURRENT CONTOURS (K-Amp) IN PARALLEL PLATE ACCELERATOR

FIGURE VI. - 5b

AP25 12 4354 68

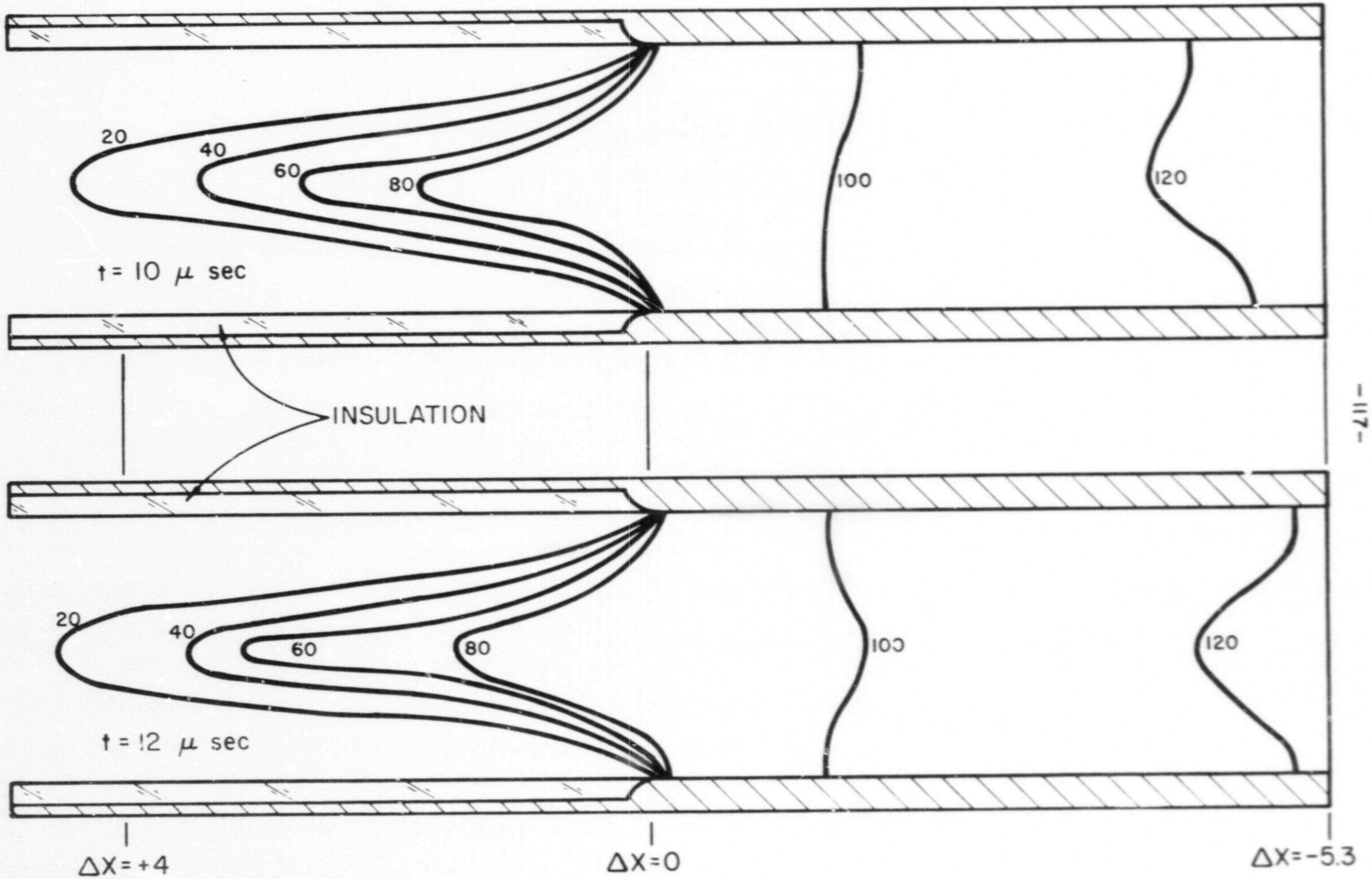

ENCLOSED CURRENT CONTOURS (K-Amp) IN PARALLEL PLATE ACCELERATOR

FIGURE VI-5c

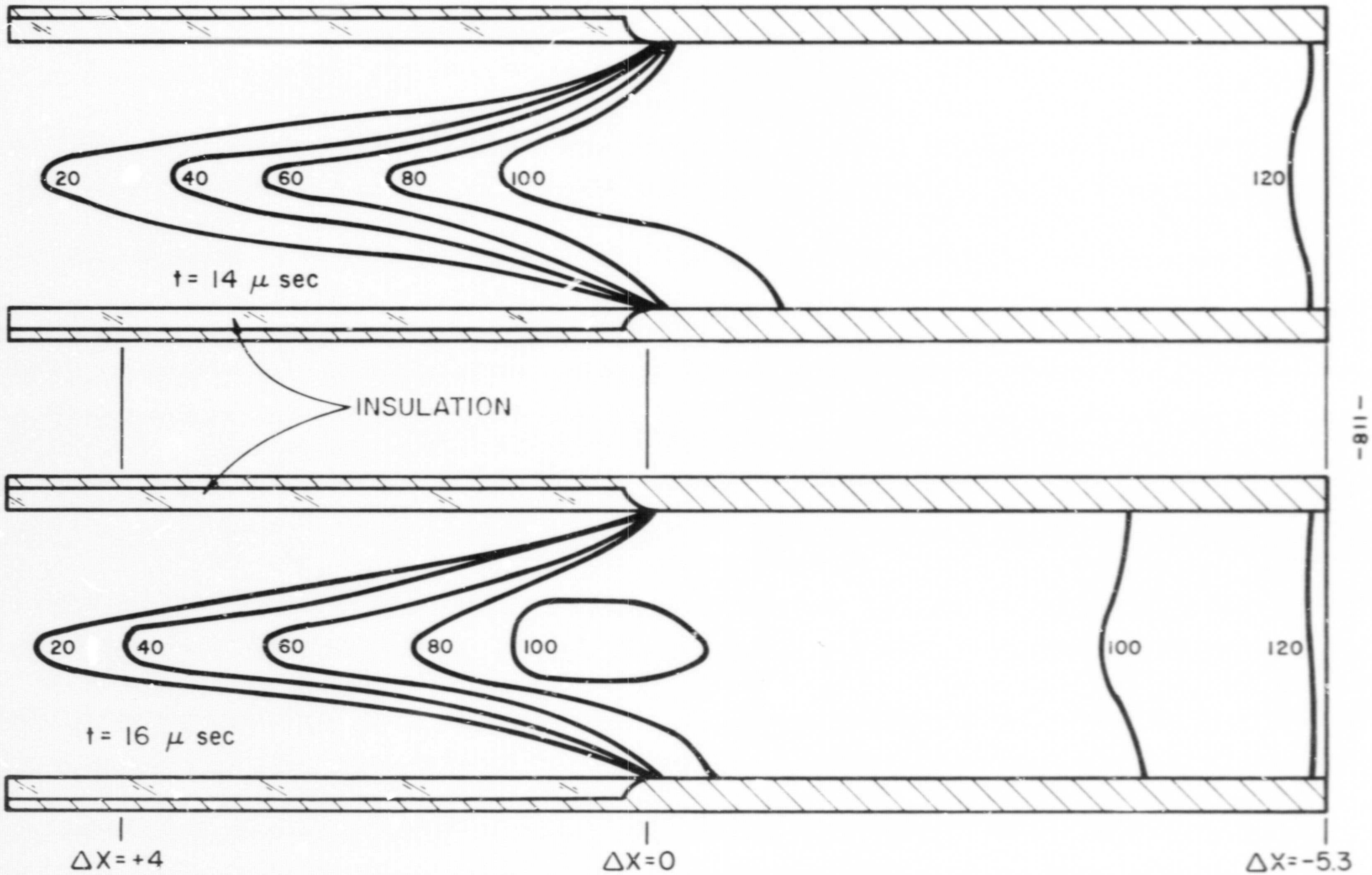

ENCLOSED CURRENT CONTOURS (K-Amp) IN PARALLEL PLATE ACCELERATOR

FIGURE VI-5d

AP 25 2 3352 .9

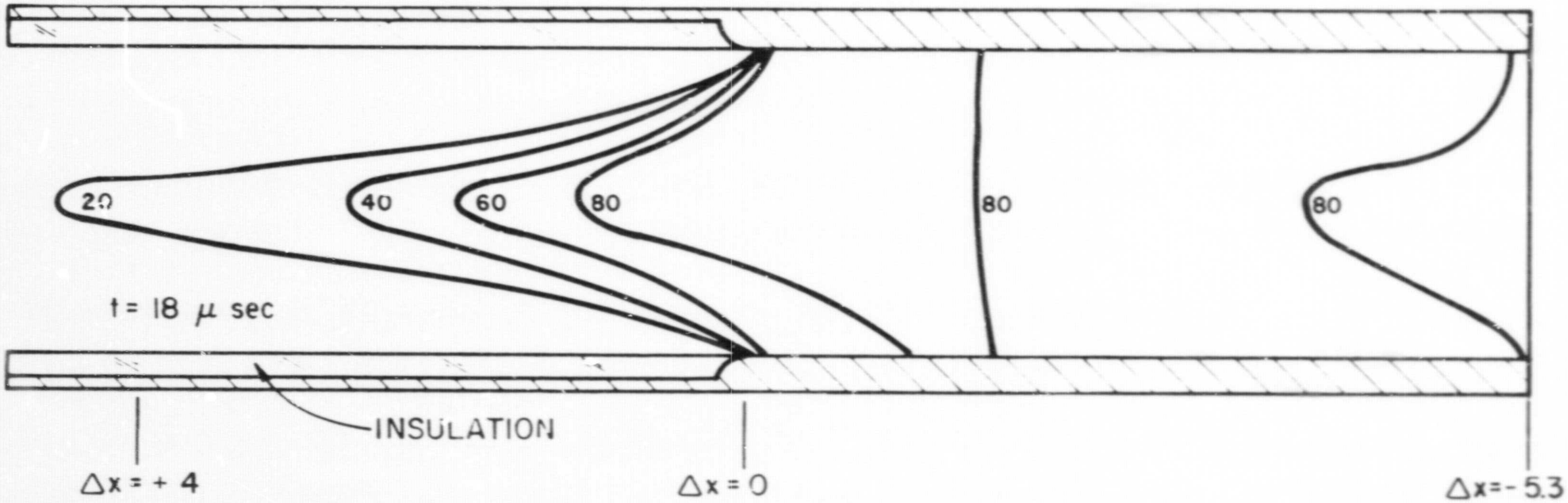

ENCLOSED CURRENT CONTOURS (K-Amp) IN PARALLEL PLATE ACCELERATOR

FIGURE VI - 5e

chapter. In Figure VI-6 a comparison of the probe responses obtained in the full metal electrode case and the partially insulated electrode case with 9" metal electrode length is presented. The 9" metal electrode length data is shown for comparison with the full electrode case so that the inner divider locations in the two contrasting situations coincide. In Figure VI-7 the probe responses in the 5¼" metal electrode length are shown. As is readily apparent, the voltage signatures for the two partially insulated electrode length cases are very similar; hence the comparisons of Figure VI-6 are quite general.

In Figure VI-6a the response of the probe when located about eight inches downstream of the initiation location is seen for the full electrode accelerator. Following a short burst of initiation noise the probe first records a resistive drop of about 60 volts for the first three μsec, corresponding to a plasma resistance of 0.0005 ohms. As the current sheet sweeps by, the inductive contribution is added, bringing the total voltage to some 700 volts where it remains relatively constant for the duration of the driving current waveform, corresponding to a constant speed propagation of the sheet down the channel. In contrast Figure VI-6b shows the response of the probe at the front end of the device so that the sheet does not reach this location during the lifetime of the pulse. Here, on an amplified scale, the resistive drop alone is recorded. The above 120/20 results are very

AP25 P119 67

ALL METAL ELECTRODES , 2 μ sec/DIV.

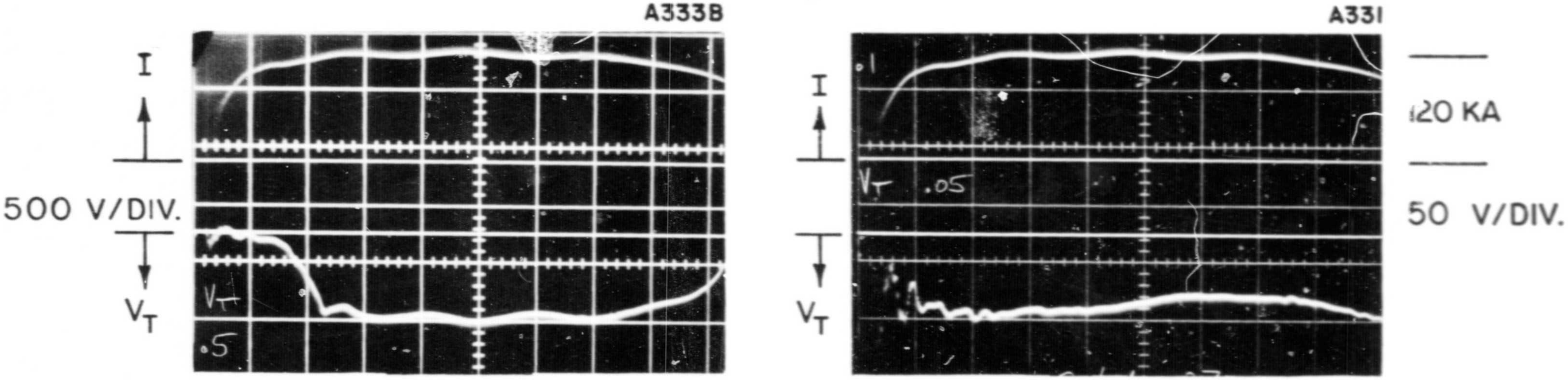

(a) x = 8"

(b) x = 45"

PARTIALLY INSULATED ELECTRODES ; 2 μ sec. / DIV.

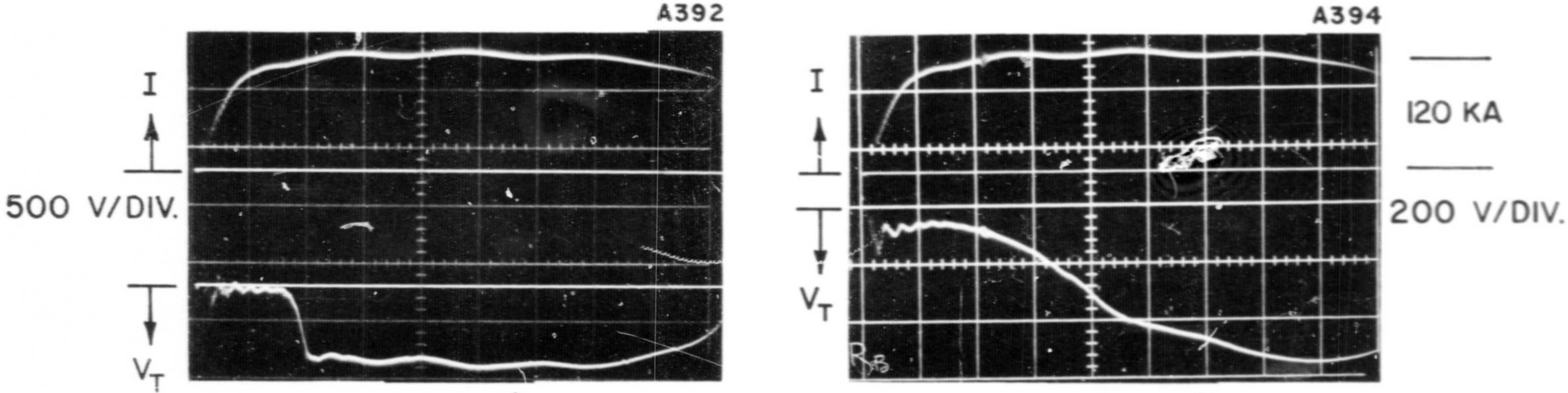

(c) x = 8"

(d) x = 45"

COMPARISON OF INNER DIVIDER RESPONSES IN PARALLEL PLATE ACCELERATOR

FIGURE VI - 6

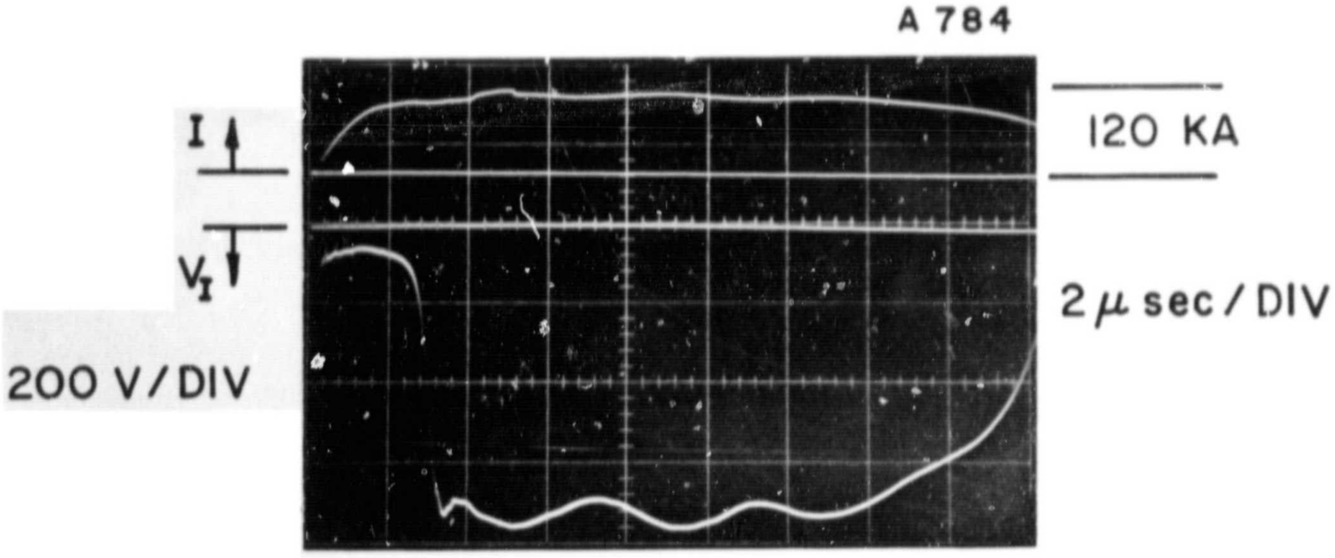

a) INNER DIVIDER AT ΔX=-2.3"

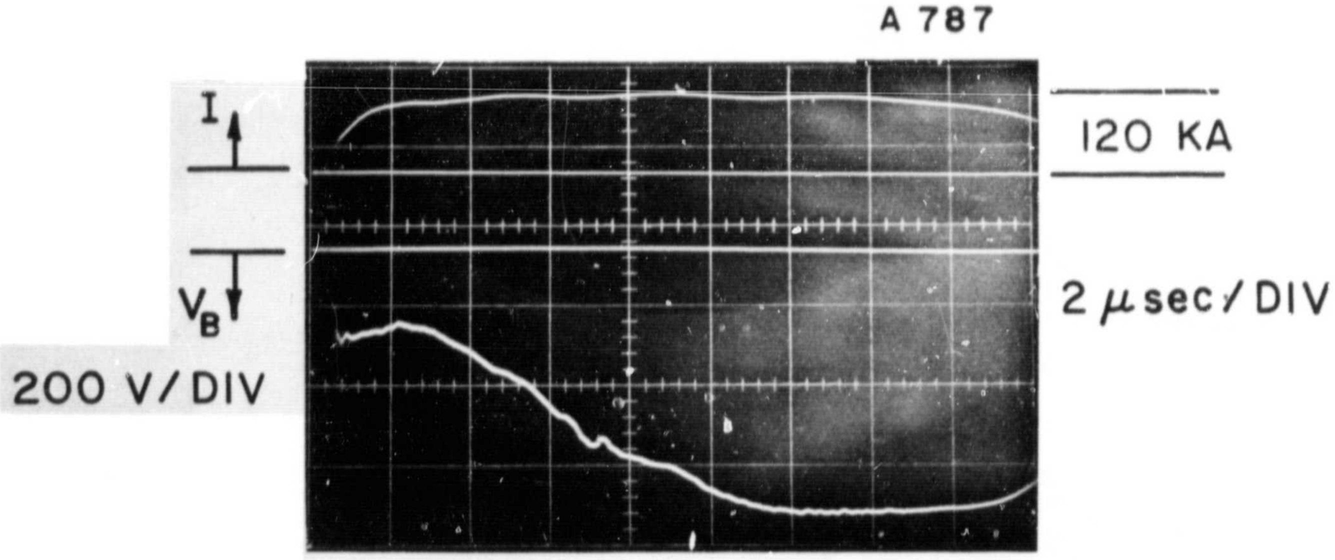

b) VOLTAGE ACROSS R_B

VOLTAGE SIGNATURES OF CURRENT SHEET STABILIZATION

FIGURE VI-7

similar in nature to the 30/80 results in the full electrode configuration shown in Figure V-6.

The above experiments are now repeated using the partially insulated electrodes. Curiously, the response of the probe eight inches from the back wall, Figure VI-6c, is almost identical to the full electrode case, Figure VI-6a, despite the fact that the current sheet stabilizes at the discontinuity some 10 μsec into the pulse, thereby eliminating the flux change contribution. One hypothesis is that the stabilization process is accompanied by an onset of gas acceleration through the sheet of just the right magnitude to provide a motional or back emf equal to the lost inductive contribution. But if this is the case, the motional emf component must also appear on the probe far downstream, since in a truly steady process, the voltage drop between electrodes should be the same everywhere along the channel. And indeed, referring to Figure VI-6d, unlike the corresponding signal in the full electrode case Figure VI-6b, the resistive contribution is supplemented by the motional emf at the time of sheet stabilization, bringing this voltage just to the value of the upstream divide, Figure VI-6c.

It thus appears that a new and rather powerful electromagnetic inertial mechanism is being observed; i.e., that when the motion of the conducting current sheet is arrested at the electrode discontinuity, the back emf generated in opposition to this change is just sufficient to maintain the terminal voltage at its previous level. The impressive feature of this effect is that the gasdynamic processes involved in its accomplishment are fundamentally quite distinct; that is, there has been a transition from the familiar unsteady mode of gas accumulation in a propagating current sheet, to the equally familiar but rather different steady mode of gas "blowing" through a fixed current pattern, <u>with no observable change in terminal voltage</u>.

E. KERR CELL WEDGE FLOW STUDIES

Although the current has ceased to propagate, acceleration of gas by the stabilized current distribution appears to continue as shown in the last section. The most vivid demonstration of flow acceleration is a photographic sequence of the flow patterns over small 15° half angle wedges set in three planes, 1/4 inch off the anode and cathode and in the midplane at various axial positions along the channel. The luminosity generated by placing the wedges in the flow is assumed to be generated by gasdynamic shocks and the luminosity patterns are further assumed to be coincident with the shock patterns.

For example, the status of the inlet flow to the stabilized current zone can be observed by placing the wedges upstream of the current stabilization region, $\Delta X < 0$. Such a series of pictures taken at 10, 14, and 18 μsec respectively is shown in Figure VI-8 where the wedge tips are located at approximately $\Delta X = -1\frac{3}{8}''$. Shocks are visible at each of these times indicating that the inflow is supersonic over the stabilized portion of the current pulse. The luminosity of

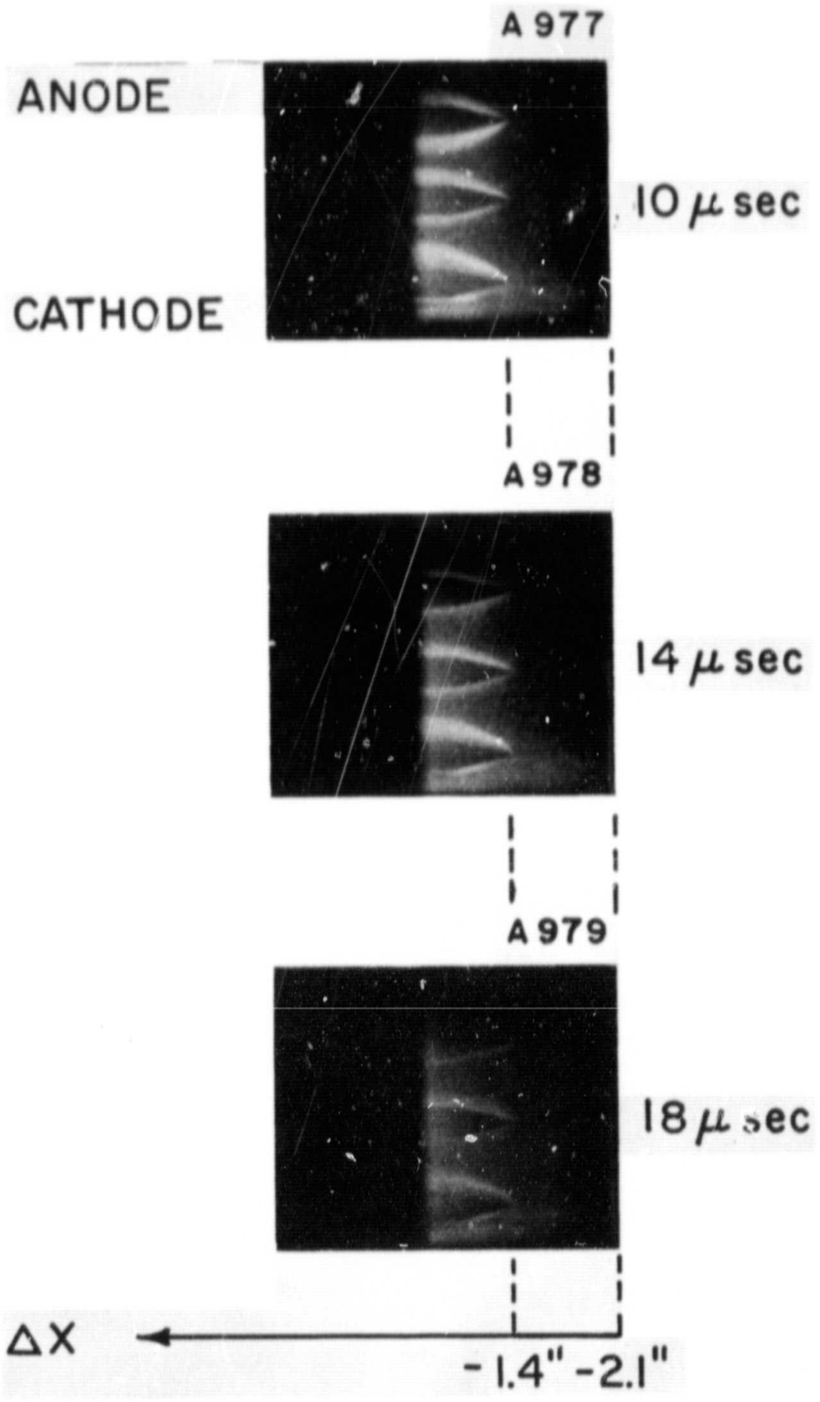

AIRFOIL VISUALIZATION OF GAS FLOW INTO STABILIZED CURRENT DISTRIBUTION

FIGURE VI - 8

these shocks, however, decreases with time suggesting that the mass flow into the stabilized current zone is decreasing. This is to be expected since no external source of mass is being supplied to the discharge.

Figure VI-9 displays the flow over the wedges at $\Delta x = +$ 2 3/8, + 5-5/8", and 8-3/8" for a series of times as shown during the pulse. Comparing these postions with the patterns of enclosed current shown in Figure VI-5, one sees that the above positions correspond respectively to the middle of the stabilized zone, to the downstream edge of the zone and to a completely exterior position. At the three times shown, 14, 16, and 18 μsec, it is apparent that the Mach number of the flow increases downstream through the stabilized current zone. At the first position, the shocks are somewhat detached; at the second, the shocks are attached; and at the third they are yet more inclined to the flow. Further interpretation is somewhat ambiguous since either a flow acceleration or a decrease in the local sound speed could produce the observed Mach number increase. However, since the effect of Joule heating, j^2/σ, in the current zone would tend to raise rather than lower the sound speed, and since the similarity in probe responses at the three transverse positions, speaks against major transverse gradients and excessive wall cooling, a valid flow acceleration through the current zone seems the more likely alternative.

F. ELECTRIC FIELD STUDIES

In an effort to unravel a bit more of the mechanisms

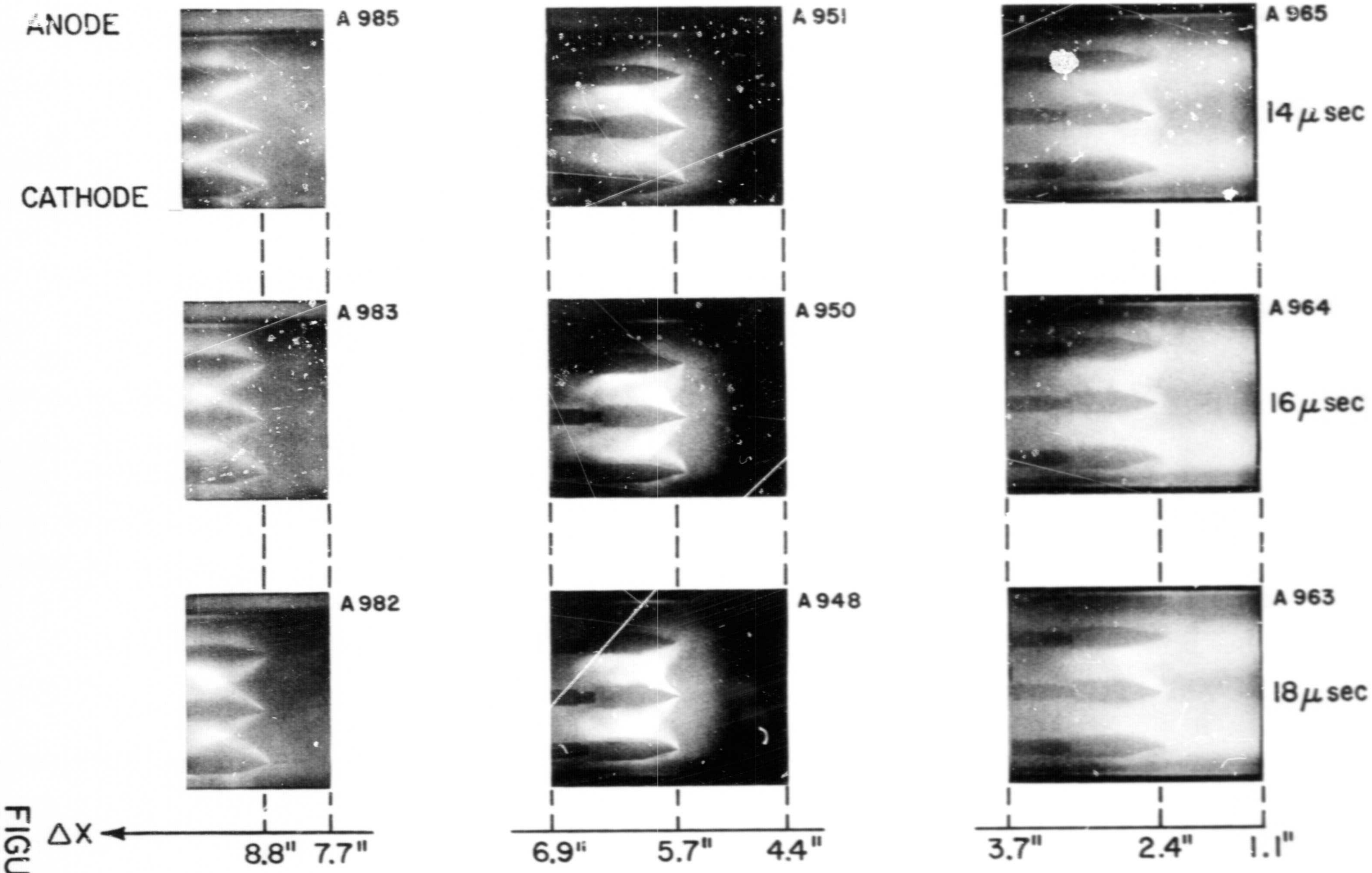

AIRFOIL VISUALIZATION OF GAS FLOW THROUGH
STABILIZED CURRENT DISTRIBUTION

FIGURE VI-9

of gas acceleration in the two phases, the patterns of streamwise and transverse electric field, E_x and E_y respectively, within the current carrying regions of the plasma are mapped. The E_x fields are monitored by means of a coaxial lead, conically shaped double electric probe, the E_y fields with a twisted or coaxial lead, straight tipped double electric probe. Examples of streamwise data are presented in Figure VI-10 while examples of the transverse field are shown in Figure VI-12.

The streamwise probe response along the metal electrode portion, Figure VI-10a, corresponds to that commonly observed [4] [41] for a propagating current sheet, namely, a "spike" of forward facing electric field. In contrast, E_x probe signatures obtained within the stabilized current distribution, Figure VI-10b, c, d, downstream of the metal to insulation junction, consist of a vestige of the current sheet spike, followed by a null period, followed by an abrupt rise to a plateau which lasts nearly to the end of the pulse. The amplitudes of the vestigial spike and of the plateau decrease with distance downstream of the electrode discontinuity. The former tends to decelerate once beyond the discontinuity but the leading edge of the plateau seems to maintain a uniform speed or even to accelerate somewhat as seen in Figure VI-11. The temporal uncertainty in the "spike" data is about ± .2 μsec whereas for the less sharply defined plateau arrival the uncertainty is roughly ± 1 μsec. Spatial uncertainties in probe positioning are approximately ± 1/16".

One may speculate that the first spike of E_x recorded by the probe announces the arrival of the snowplowed

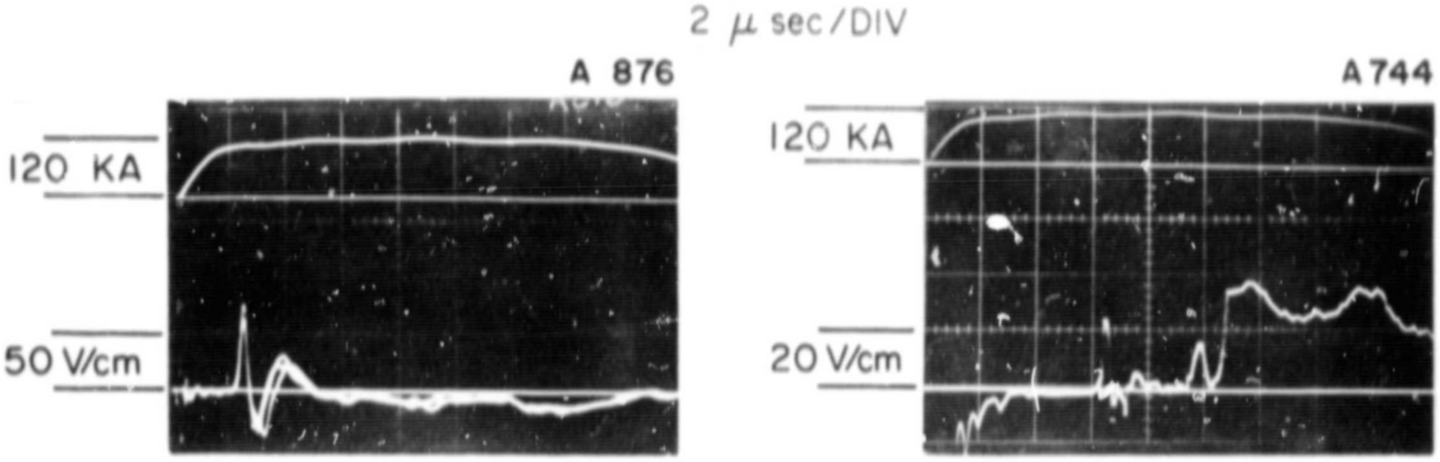

a) Δx= -3.3", MIDPLANE b) Δx= 2.8", MIDPLANE

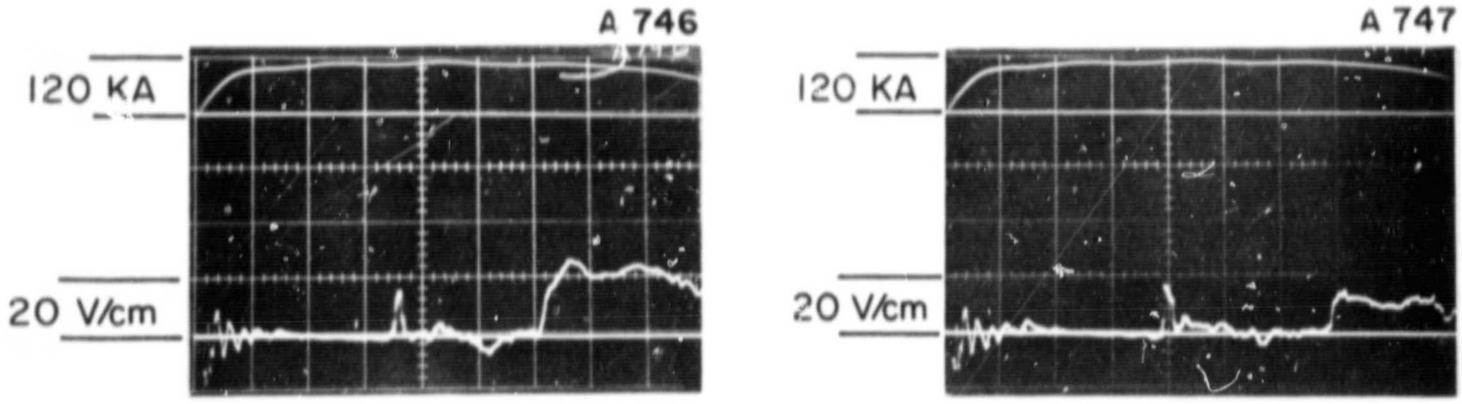

c) Δx= 3.8", MIDPLANE d) Δx= 4.8", MIDPLANE

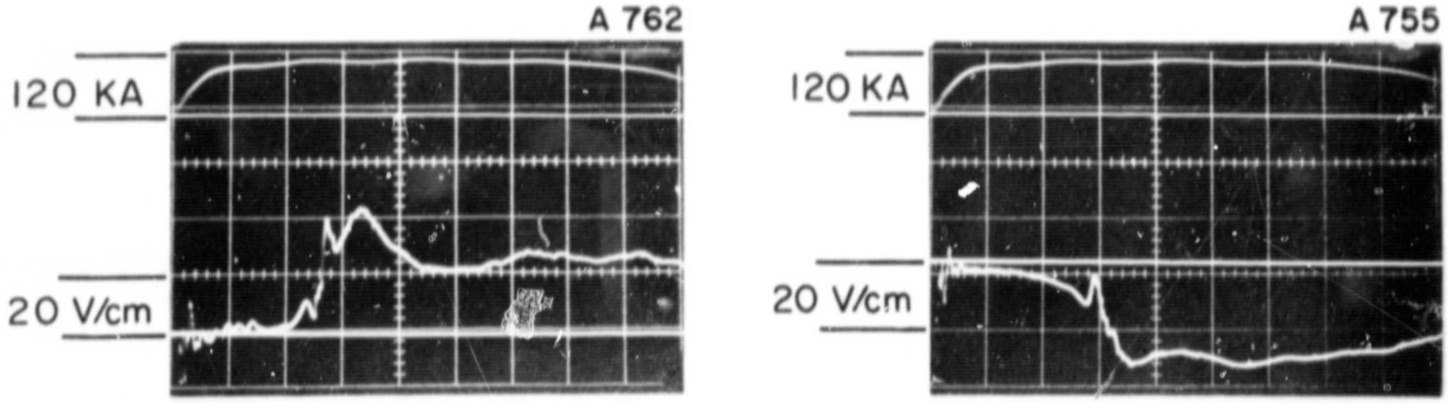

e) Δx= 0.75", 0.25" FROM ANODE f) Δx=0.75", 0.25" FROM CATHODE

ELECTRIC PROBE SIGNATURES OF CURRENT SHEET STABILIZATION; STREAMWISE ELECTRIC FIELD, E_x.

FIGURE VI-10

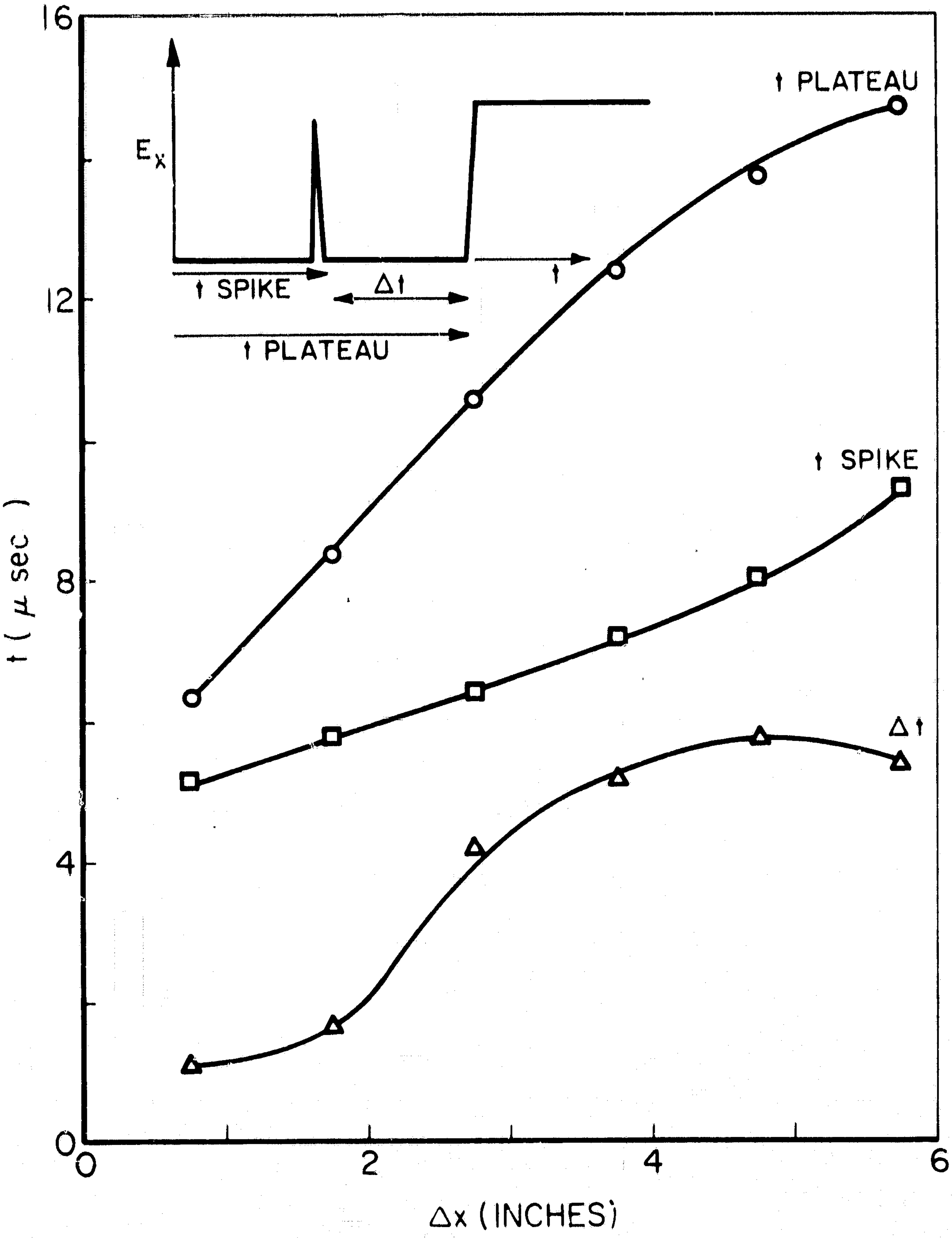

TRAJECTORIES OF CHARACTERISTIC FEATURES OF ELECTRIC PROBE SIGNATURES

FIGURE VI-11

plasma accumulated by the propagating sheet upstream in the conducting portion of the accelerator, now continuing on its own inertia as the current is arrested at the discontinuity and diffuses into the stabilized current conduction pattern. The plateau of electric field prevailing over the latter portion of the response presumably reflects the quasi-steady flow acceleration process in operation, possibly as a Hall voltage component of the total electric field. The rather well-defined null time between these two signals is somewhat puzzling particularly since no correspondingly abrupt processes are evident in the development of the discharge current distribution in this region.

Figure VI-10e, f display records of E_x obtained by a probe immersed in the conduction bands near the anode and cathode surfaces. Here the E_x field is essentially parallel to the current vector and hence is primarily a resistive component, nearly constant over the lifetime of the steady current pattern and opposite in sign near the anode and cathode. In the stabilized conduction bands, $t > 10$ μsec, E_y virtually vanishes; this can be seen in Figure VI-12a,b.

In Figure VI-12c,d E_y traces along the metal electrodes are presented. These traces rise as the sheet sweeps by and then fall off gradually during the remainder of the pulse. Figure VI-12e shows the E_y signal in the stabilized zone which, excepting fluctuations, remains relatively constant. The magnitude of E_y in the stabilized zone falls off with

120/20 PULSE, 100μ, $5\frac{1}{4}$" ELECTRODE LENGTH

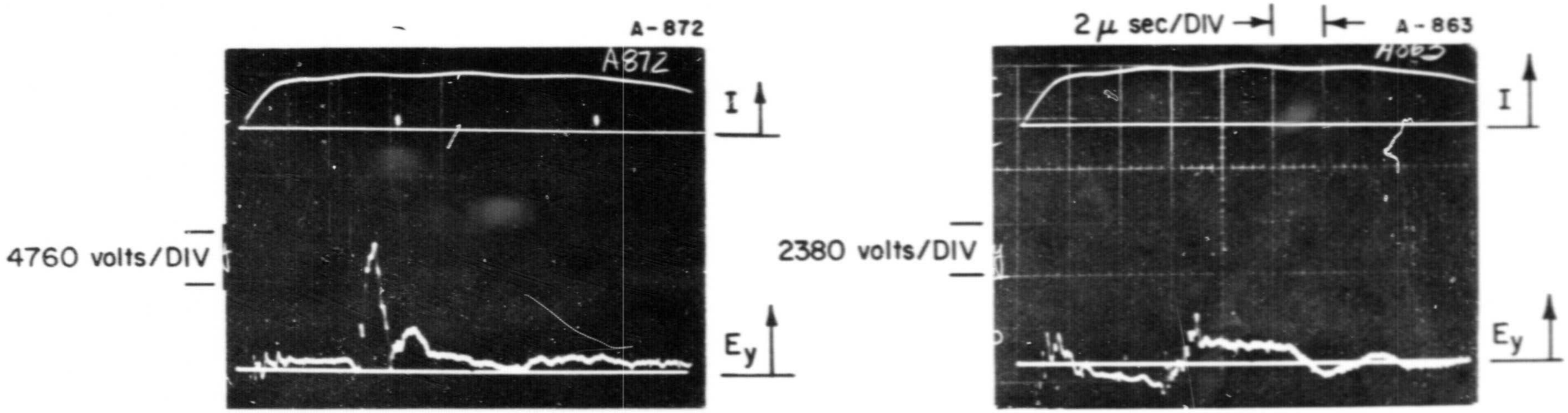

a) ΔX = 0.75", 0.25" FROM ANODE

b) ΔX = 0.75", 0.25" FROM CATHODE

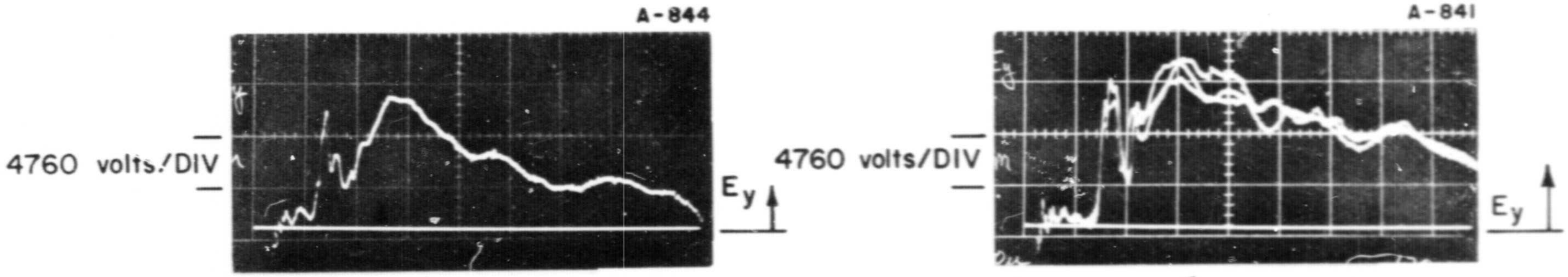

c) ΔX = -3.25", MIDPLANE

d) ΔX = -2.25", MIDPLANE

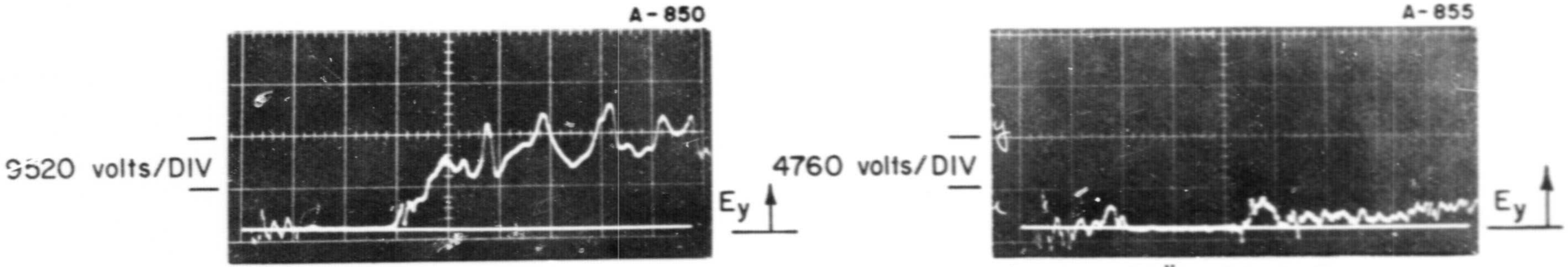

e) ΔX = 1.75", MIDPLANE

f) ΔX = 5.75", MIDPLANE

TRANSVERSE ELECTRIC FIELD SIGNATURES

FIGURE VI - 12

distance from the electrode discontinuity going to zero at the end of the stabilized current zone, Figure VI-12f.

The electric and magnetic field data are analyzed through the use of a generalized Ohm's Law and appropriate assumptions to examine the accelerating nature of the stabilized current zone and to explain the general behavior observed. This analysis is presented in Chapter VIII.

G. DISCUSSION

One may question how mass flow is provided for the stabilized phase, if the propagating sheet has effectively swept out the ambient fill of the conducting portion of the channel. Actually current sheets of this intensity and possessing large anode feet are known from earlier studies[5] to be "imperfect sweepers", a fact confirmed by the observed magnitude of the E_x spike too small to account for full acceleration of ions to sheet velocity. Rather it appears that the propagating sheet only partially accelerates the ambient gas it passes over, which later surges into, and is accelerated by, the stabilized current pattern. It is also probable that eroded insulator and electrode material provide some portion of the inlet mass flow to the acceleration zone. A spectrogram of the 120/20 discharge into 100μ argon is shown in Figure VI-13. As can readily be seen, many impurities are involved in the discharge process among them aluminum from the electrodes and carbon, oxygen and hydrogen from the nylon insulator and plexiglass sidewalls. Since the spectrum is not time resolved, it is not possible

AP 25 P-247 68

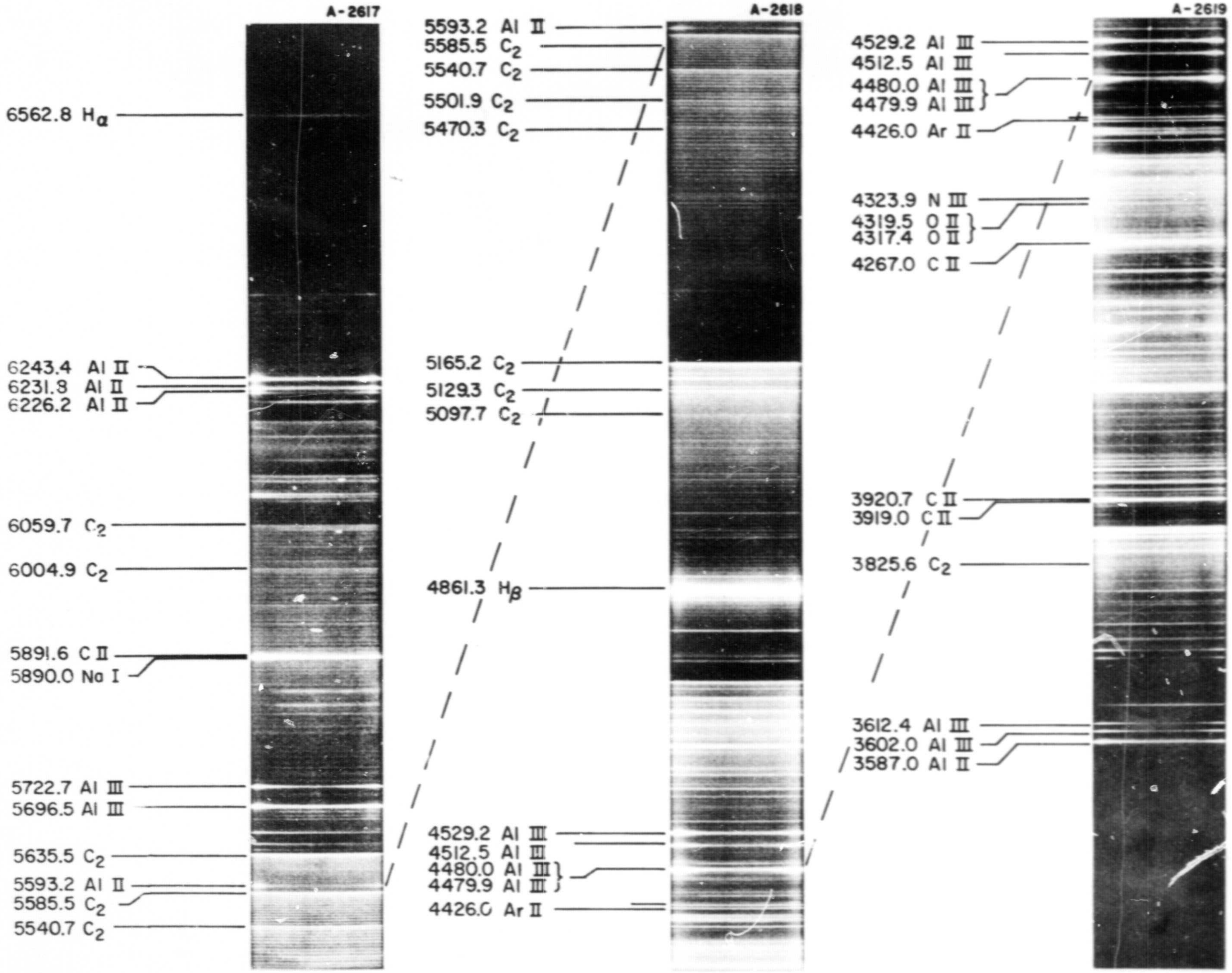

SPECTROGRAM OF 120,000 amp × 20 μ sec DISCHARGE
100 μ , $5\frac{1}{4}$" ELECTRODE LENGTH, SIDE ON @ $\Delta X=-4$"

FIGURE VI-13

to estimate the relative contributions of the impurities to the total mass flow.

Summarizing then, the diagnostic measurements on the partially insulated electrode configuration driven by the 120/20 pulse suggest the following picture of operation: electrodynamically, the current sheet breaks down, propagates along the metal electrodes imparting some fraction of its velocity to the gas it passes through, and, upon reaching the metal to insulation junction, decelerates quickly to a stabilized hairpin shaped current distribution. Gasdynamically, the flow set up by passage of the sheet lags behind the sheet somewhat until it stabilizes and then following a transition period, this gas provides the inlet flow to the stabilized acceleration zone.

As noted, there are three possible sources of mass flow for the stabilized current zone: (a) incompletely snowplowed gas, (b) ablated electrode material, and (c) ablated insulator material. If alternative (a) dominates, such a mass flow can persist for only a limited time before this mass supply is exhausted. For longer pulses, the outflow should decay at later times and such a tendency is indeed observed in the 30/80 case when wedge flow studies are examined.

If the stabilized current discharge is starved for inlet mass flow, one may expect some differences in behavior when provision for an external supply of gas is made. To make such a comparison, the shock tube gas injection system described in Chapter II has been installed on the parallel plate accelerator. However voltage signatures for the 120/20 and 30/80 current pulses show no convincing differences between 100μ ambient fill and shock tube injection set to provide 100μ channel pressure initially at breakdown. In retrospect, this is reasonable since the available time scale is probably too short for the injection flow to become properly established. In essence, the injected flow has the task of filling the channel void created by the sweeping current sheet as it propagates to its stabilized position. This filling process must require a time of the order of the channel length involved, divided by the sound speed of the injected gas, i.e., hundreds of microseconds.

In other words, while it appears that the electrodynamic aspects of steady, plasma acceleration, i.e., current pattern stabilization, can be simulated on a time scale of tens of microseconds, attainment of the corresponding quasi-steady gas flow from an external reservoir to the final accelerated stream will require an order of magnitude longer test times. Experiments extending the techniques described above to this longer testing time scale are presented in the next chapter.

CHAPTER VII

PARALLEL PLATE ACCELERATOR
GAS FLOW STABILIZATION STUDIES

In this chapter, a series of experiments designed to supply "fresh" gas to the current pattern stabilized discharge will be described. By "fresh" gas is meant gas which is not involved in the initiation of the discharge and which is not swept over by a propagating current sheet. The inlet flow to the stabilized 120/20 discharge is not "fresh" since it is set up by the sweeping action of the current sheet. To supply new gas to the current stabilized discharge involves extending the time scale of the experiment into the hundreds of microsecond time regime as shown by the simple arguments in the last chapter.

A. VOLTAGE MEASUREMENTS

Before performing any detailed interior diagnostics on the long current pulses*, voltage measurements are taken to see if any difference can be found between cases where the chamber is prefilled to an ambient pressure of 100μ argon and those where the shock tube injection is used to bring

---

*When referring to the long current pulses 20/125, 10/250, 5/500 the nominal design values are given. In actuality the pulses are approximately 20% lower in amplitude and longer in duration.

the pressure in the discharge zone from an initial hard vacuum to 100μ at the time of breakdown. In order to enhance any possible mass starvation effects, most of the data are taken with the length of the metal electrode portion reduced to 2" in contrast to the normal 5¼". The voltage is monitored at the downstream end of the parallel plate accelerator, where there are only two possible contributions to the total voltage, a resistive drop V_R representing the finite conductivity of the plasma, and a back emf component V_{uB} derived from plasma flow through the stabilized current distribution. Both of these components should behave in the same way to mass starvation of the discharge. In this pressure range the resistance of the discharge tends to decrease with increased gas pressure and hence will increase if mass flow is depleted. The V_{uB} contribution should vary inversely with mass flow rate, since the fixed $\vec{j} \times \vec{B}$ body force is applied per unit volume.

As longer and longer current pulses of correspondingly lower amplitude are employed, V_{uB} tends to become small compared to V_R which typically is on the order of 50 to 100 volts for this range of operation. Figure VII-1 displays a plot of V_{uB} versus current data for the case of 5¼" electrode length and 100μ prefilling. Note that in the range of 1,000 to 10,000 amps the V_{uB} term can be expected to be less than 20 volts so that any differences in the voltage signatures between shock tube gas injection and ambient prefill cases will most likely be due to changes in V_R.

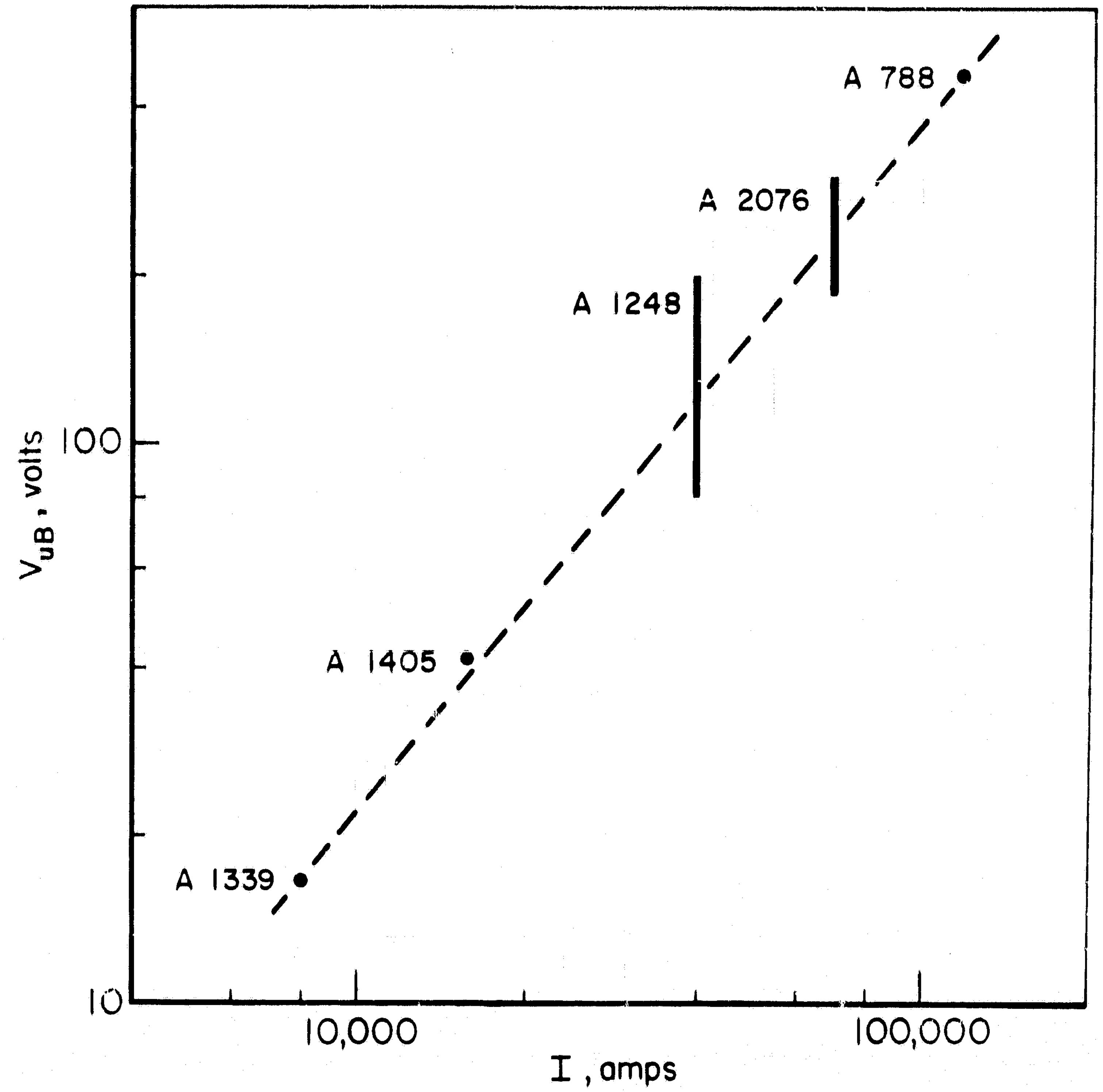

BACK EMF vs DISCHARGE CURRENT

FIGURE VII-1

This effect is shown in Figure VII-2 where the total voltage in the 10/250, 2" electrode length case which is nearly equal to the resistive drop is plotted against ambient prefill pressure.

In Figure VII-3 voltage measurements are presented for the permanently insulated electrode configuration, 5¼" electrode length, comparing 100µ ambient prefill with shock tube gas injection which simulates 100µ initially for both the 20/125 and 10/250 pulses. In Figure VII-4 voltage measurements are presented for a 2" metal electrode length comparing ambient and shock tube injection for three pulses 20/125, 10/250 and 5/500. Note that for the 20/125 pulse, for both the 5¼" and 2" electrode length cases, the voltage signatures for the shock tube and ambient cases are nearly identical. Also of note, however, is the very slight difference between the character of the voltage in the two fill modes as the electrode length is decreased to 2". Generally though it may be presumed that the shock tube is properly simulating 100µ initially, but for the balance of the pulse time it does not change the mass flow situation appreciably. However for both electrode lengths in the 10/250 case, a difference in the voltage level arises between the ambient and shock tube cases toward the latter half of the pulse. The effect is most noticeable in the 2" electrode case for the 5/500 pulse where, near the end of the pulse, the shock tube voltage is nearly 40% lower than the ambient value.

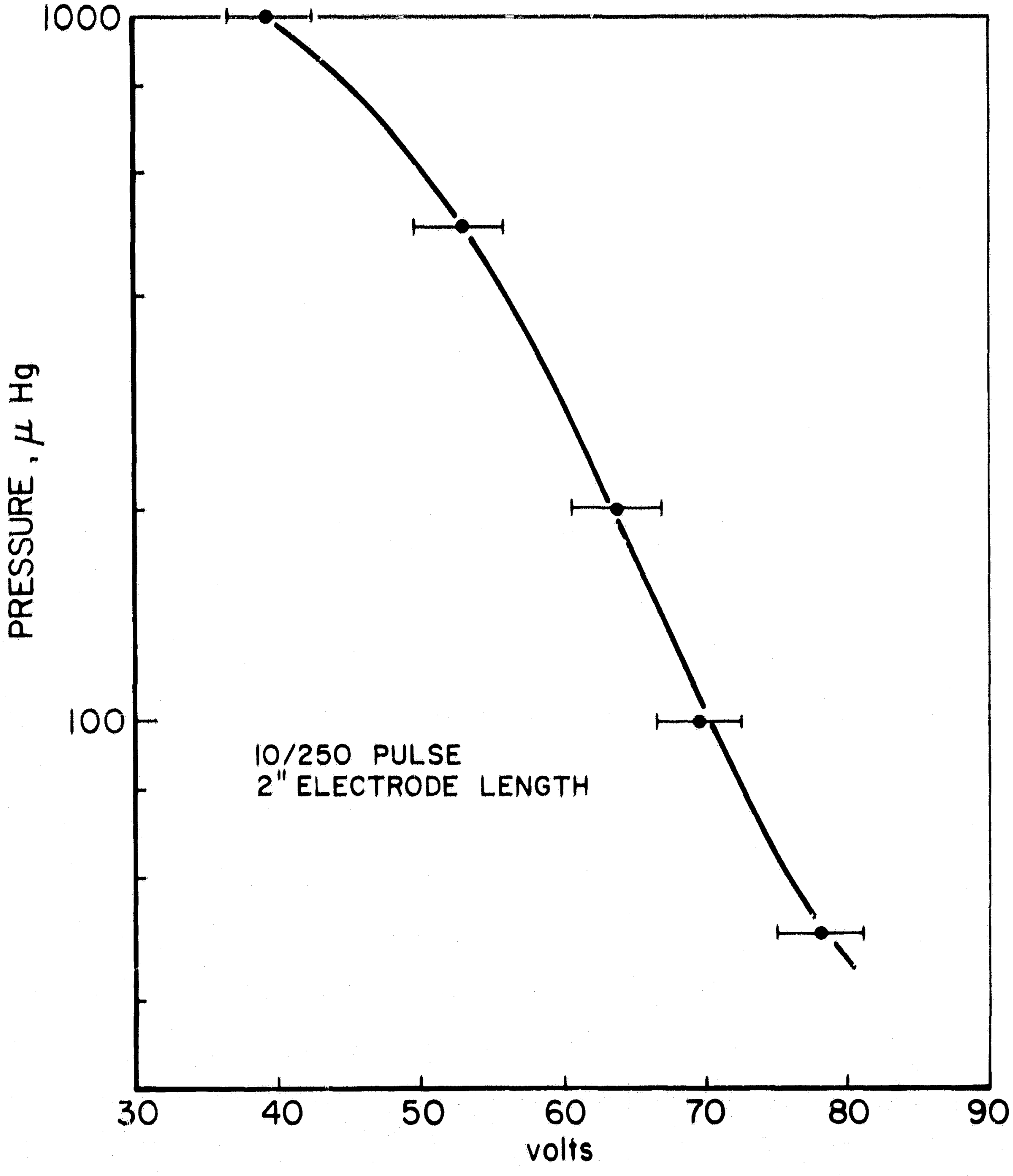

TOTAL ARC VOLTAGE vs AMBIENT PREFILL PRESSURE

FIGURE VII-2

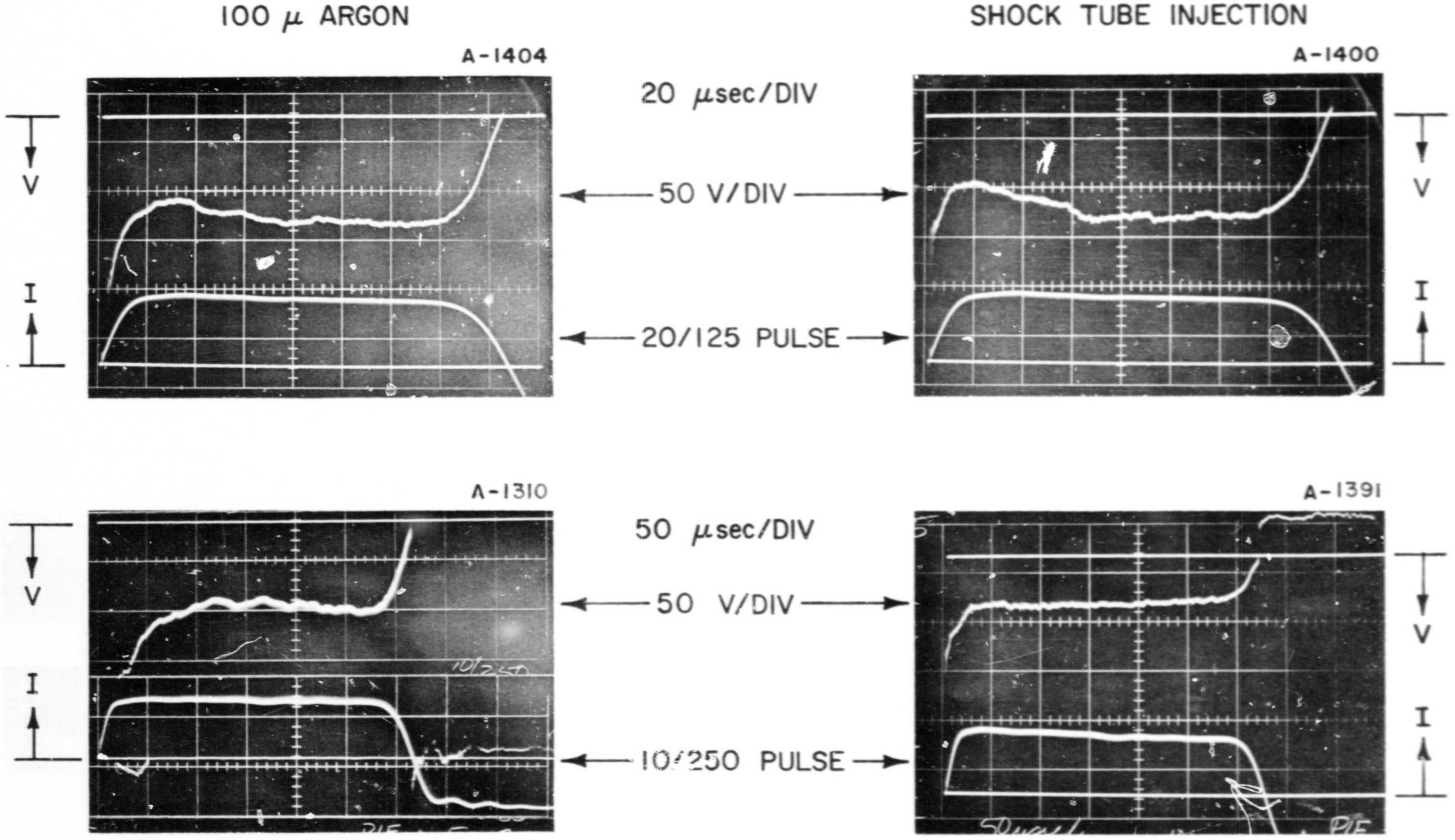

VOLTAGE SIGNATURES FOR 5 1/4" ELECTRODE LENGTH

FIGURE VII-3

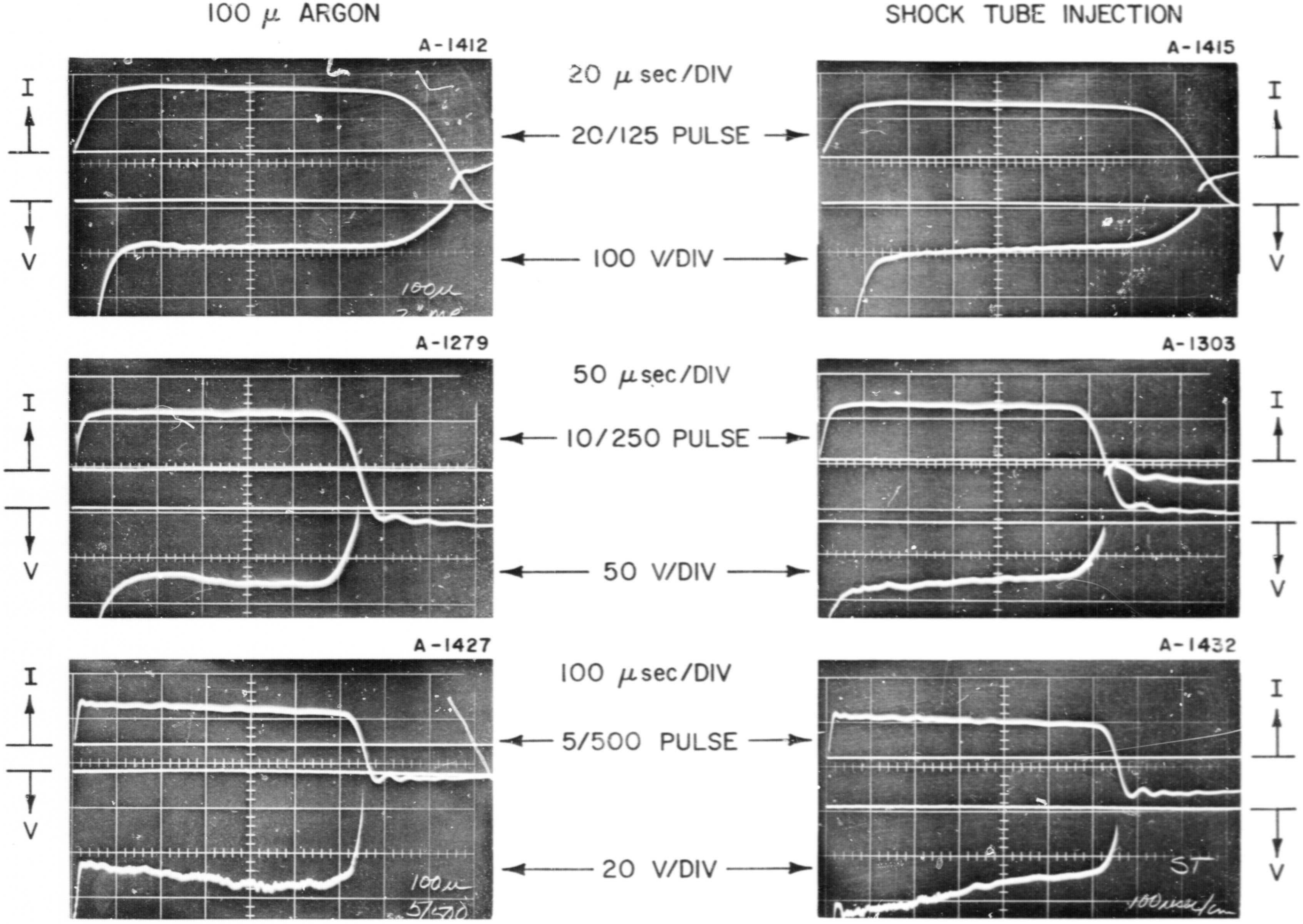

VOLTAGE SIGNATURES FOR 2" ELECTRODE LENGTH

FIGURE VII-4

In fact, the shape of the entire signature is markedly different for the long pulses. The shock tube fill voltage signatures decrease with time probably due to increased pressure in the discharge region because of the mass flow supply. On the other hand, the ambient signals increase with time presumably due to a mass starvation of the discharge. Thus based on voltage data, it appears that fresh gas can be supplied to the discharge from the existing shock tube injection system if the pulse length exceeds 150 μsec.

B. UNIFORMITY STUDIES

One possible difficulty with the long pulses in the parallel plate accelerator may be the lack of uniformity of the discharge. Fringing magnetic fields which exist because of the finite width of the accelerator may severely constrict the sheet discharge into an arc column when the current is maintained for very long periods of time. Such a constriction would impair the operation of the device as an effective gas accelerator. To check on this possibility, the uniformity of the discharge is studied in three ways: (a) Kerr cell photography, (b) magnetic probing, and (c) observation of electrode pitting.

To perform Kerr cell photography on the low amplitude current pulses, the 5 μsec pulse forming network is used to shutter the Kerr cell. Figure VII-5 shows

A-1594

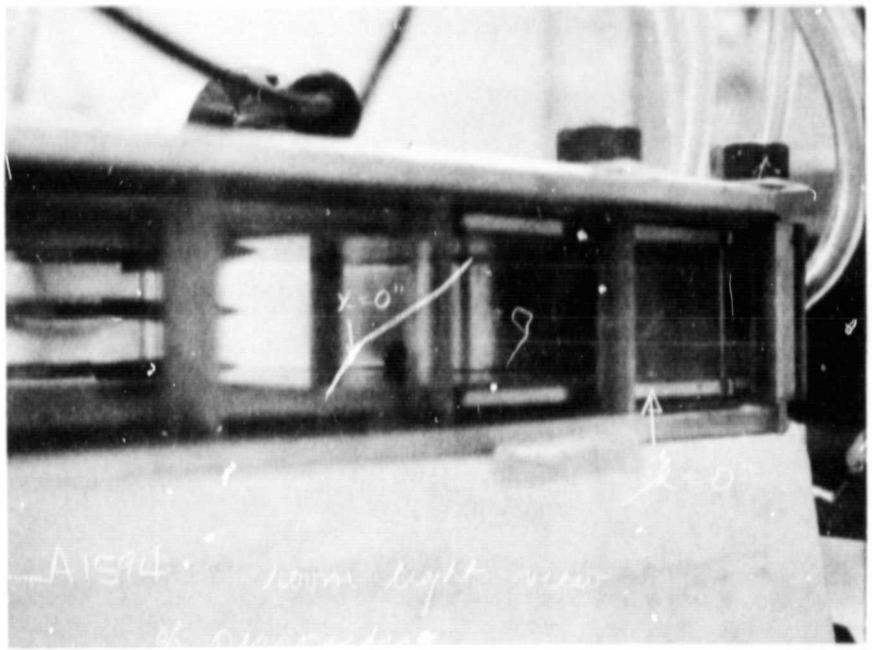

45° PERSPECTIVE

A-1595

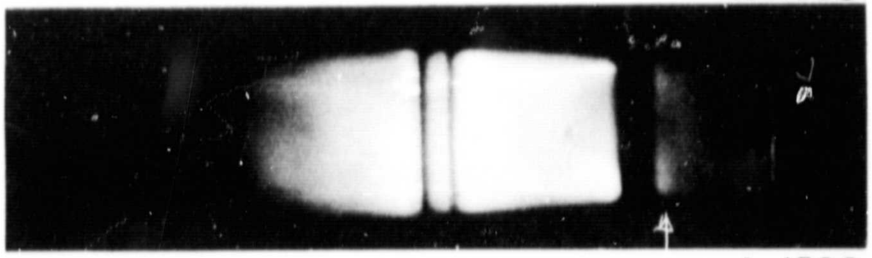

25 μsec

A-1596

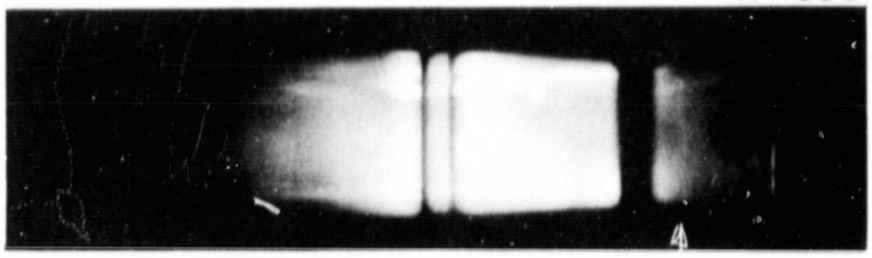

50 μsec

A-1597

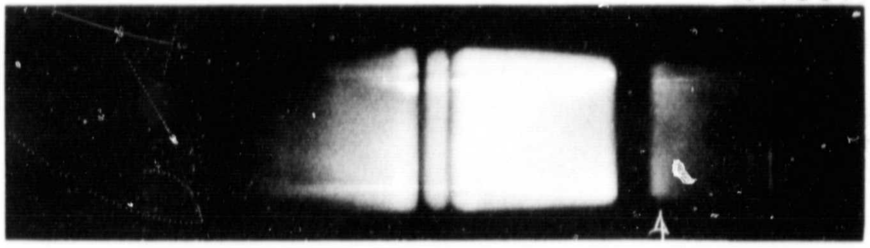

100 μsec

A-1598

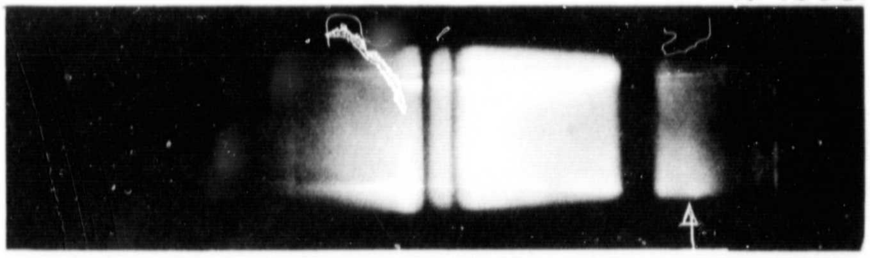

200 μsec

A-1599

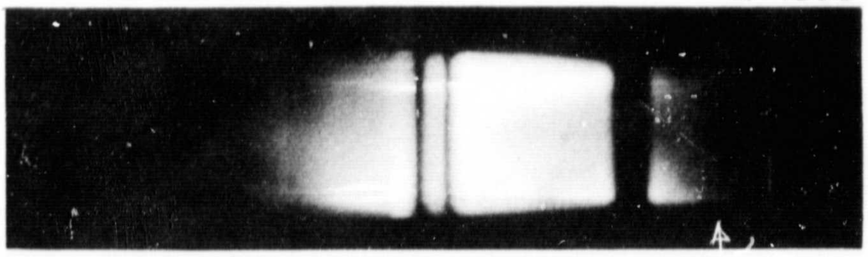

300 μsec

PERSPECTIVE PHOTOGRAPHS OF 10/250 DISCHARGE BETWEEN 2" ELECTRODES

FIGURE VII-5

a sequence of perspective photographs obtained for the 10/250 pulse, 2" electrode length with shock tube gas injection. Although some localization of the discharge luminosity can be discerned, it appears that the entire electrode width contributes to the discharge pattern.

The discharge uniformity is also studied with magnetic probes. A simple probe carriage enables one to position three magnetic probes in the midplane, y = 1", of the discharge at different distances from the side walls. The magnetic field data are reduced to give contours of enclosed current in the horizontal midplane. These patterns of enclosed current are geometrically identical with the magnetic field pattern generated by the current distribution. In the particular survey to be displayed, all of the data are taken on one side of the centerline of the device under a presumption of symmetry. The probes are all identical and equal calibrations are assumed for the probes. A calibration equating peak magnetic field with total discharge current is made and a single integrator is used. The results are shown in Figure VII-6a, b, c. The contour values shown are accurate to within about ± 5% based on reading errors alone. Errors induced because of probe perturbations on the discharge cannot be assessed.

From the data it is found that the discharge breaks down over the entire electrode surface and redistributes itself as a wave of current whose density is lowest near the walls and highest in the midplane. The wave of current propagates downstream as would a current sheet and also bows downstream slightly. The contours are smooth in the center of the

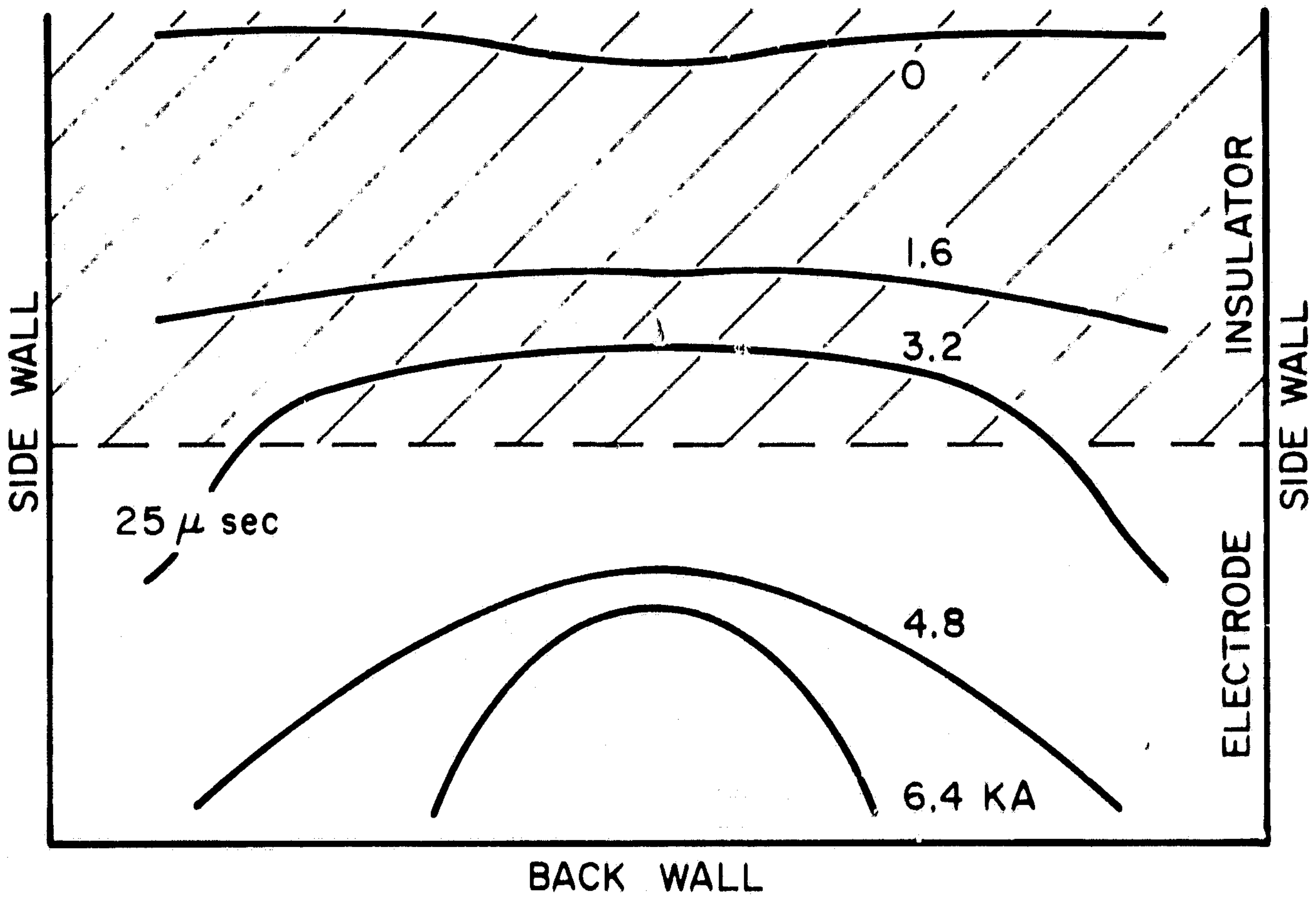

SHOCK TUBE INJECTION

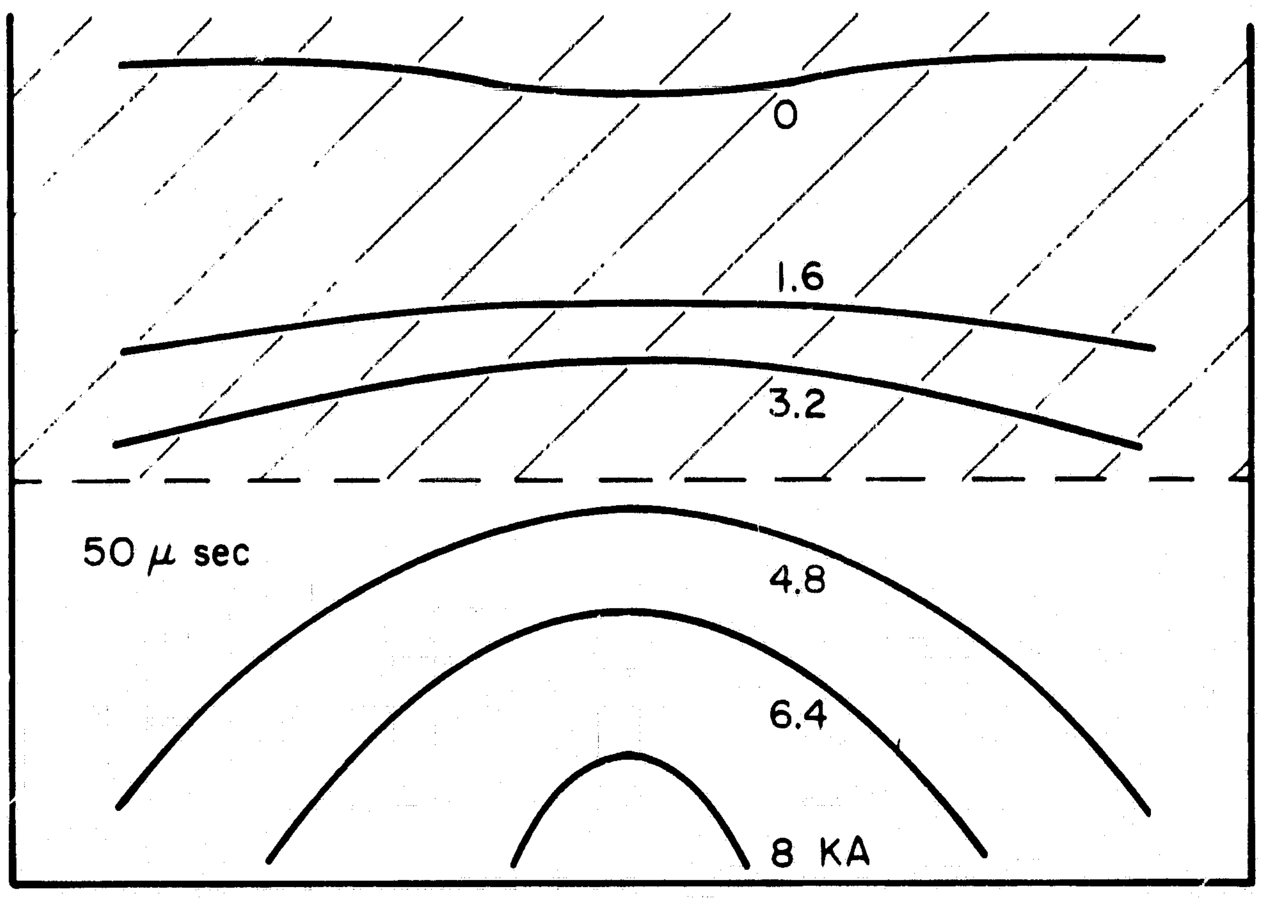

ENCLOSED CURRENT CONTOURS
FOR 10/250 DISCHARGE BETWEEN 2" ELECTRODES

FIGURE VII-6a

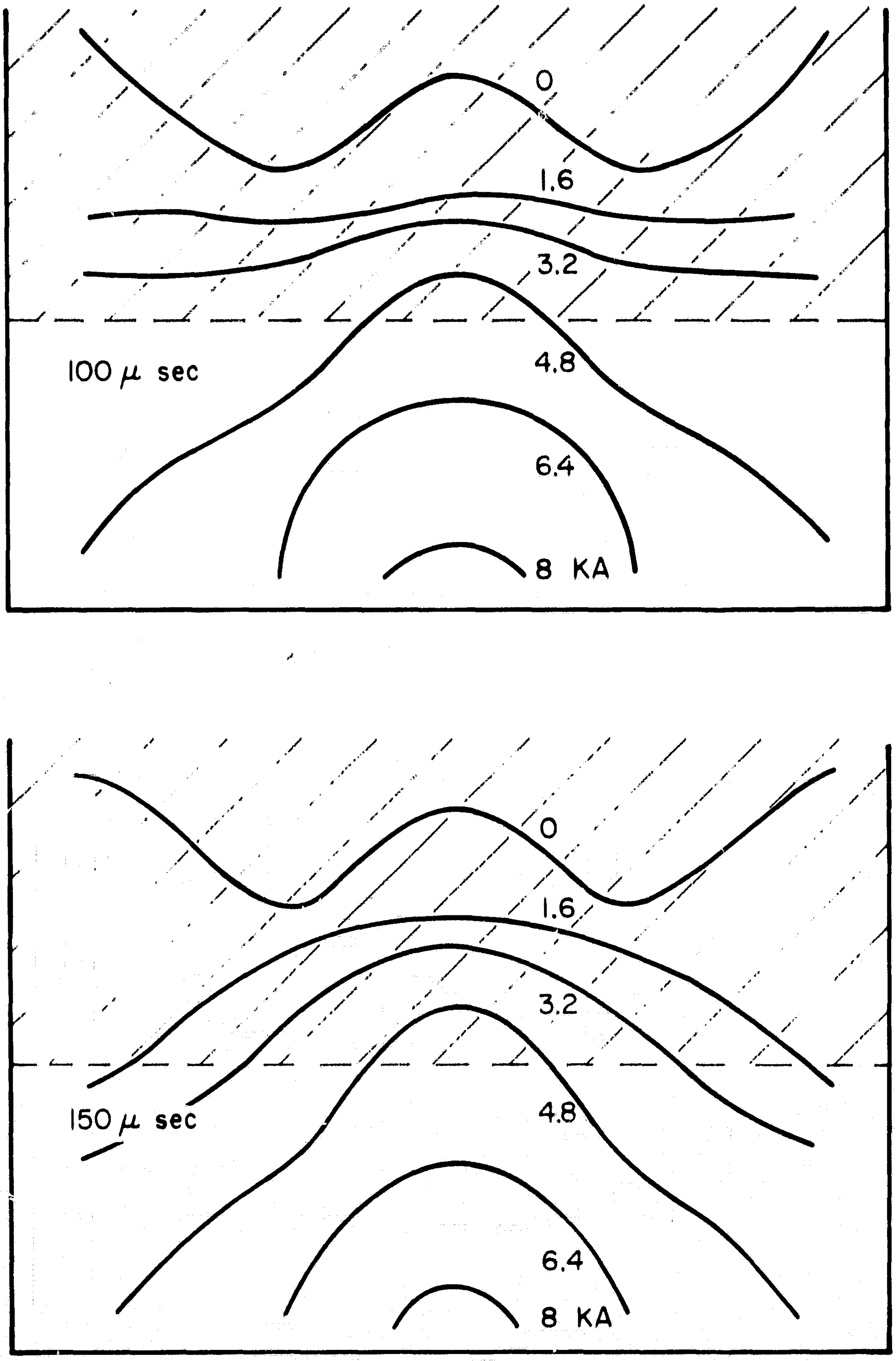

ENCLOSED CURRENT CONTOURS
FOR 10/250 DISCHARGE BETWEEN 2" ELECTRODES

FIGURE VII-6b

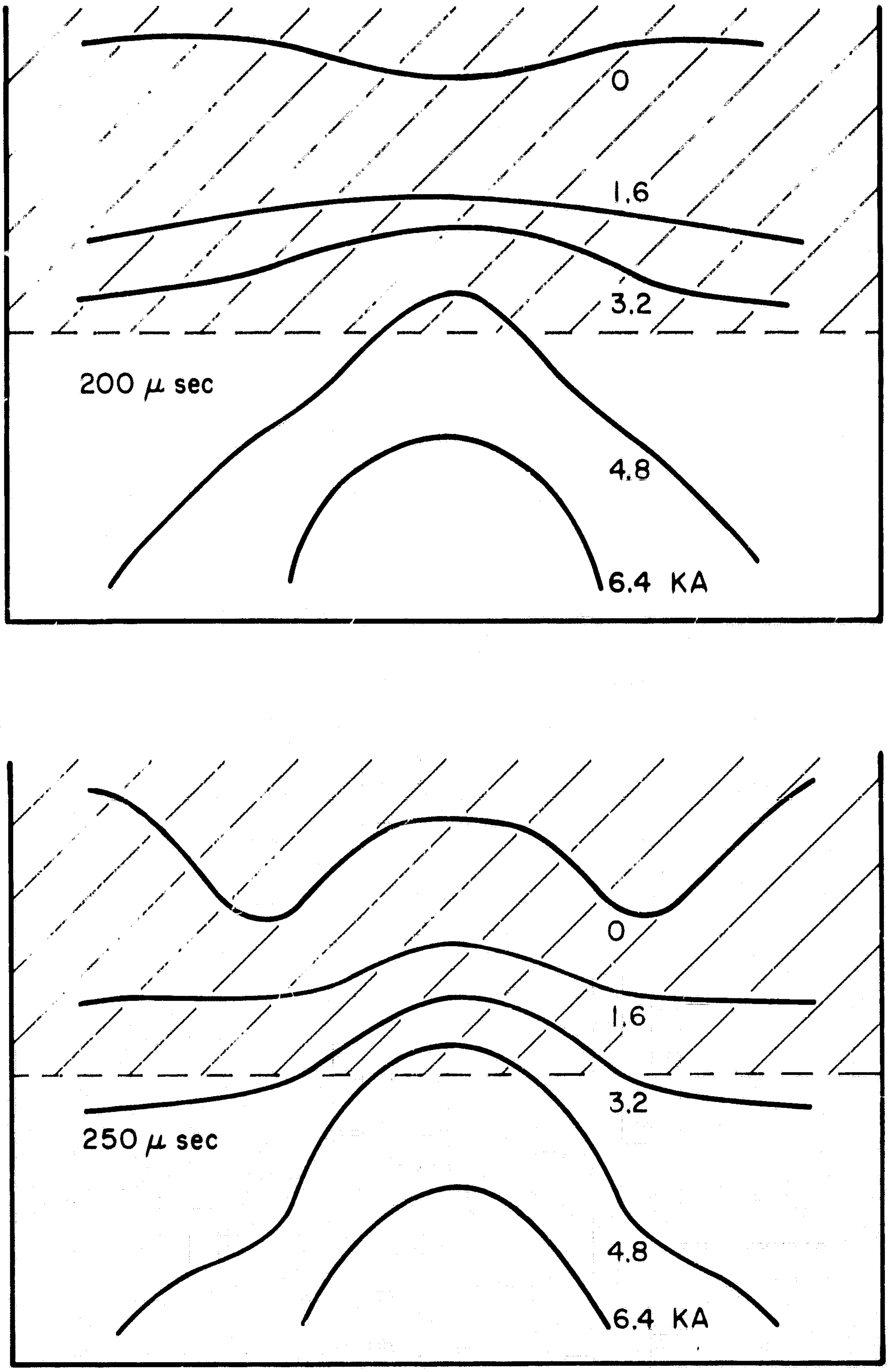

ENCLOSED CURRENT CONTOURS
FOR 10/250 DISCHARGE BETWEEN 2" ELECTRODES

FIGURE VII-6c

channel and indicate a distribution of current over the central region of the channel unlike a constricted arc column. Actually, the results shown are probably a bit pessimistic in their lack of one dimensionality. The presence of three probes on the one side of the channel clearly perturbs the current distribution as evidenced by electrode pitting and insulator deposition. Presumably the low current density at the insulator walls may be attributed to plasma cooling by the walls and a lowering of its conductivity. The evidence of diffuse discharge initiation over the entire electrode surface is contrary to previous experience with the fast rising, 2μsec, high current pulses where discrete current sheets arise near the minimum inductance location. The difference is probably attributable to the relatively long risetime, 20 μsec, of the long pulses, which predicates a skin effect comparable with chamber dimensions.

Observations of electrode pitting and deposition on the insulation adjacent to the electrode also support the above picture. Electrode pitting, as seen in Figure VII-7, is most severe in the central region of the channel and falls off nearer the walls. "Burn" marks on the insulation show a similar tendency. In no case is there a discrete arc column or spoke indicated.

C. WEDGE FLOW STUDIES

To ascertain whether the "fresh" gas, which appears to be feeding the stabilized discharge based on voltage

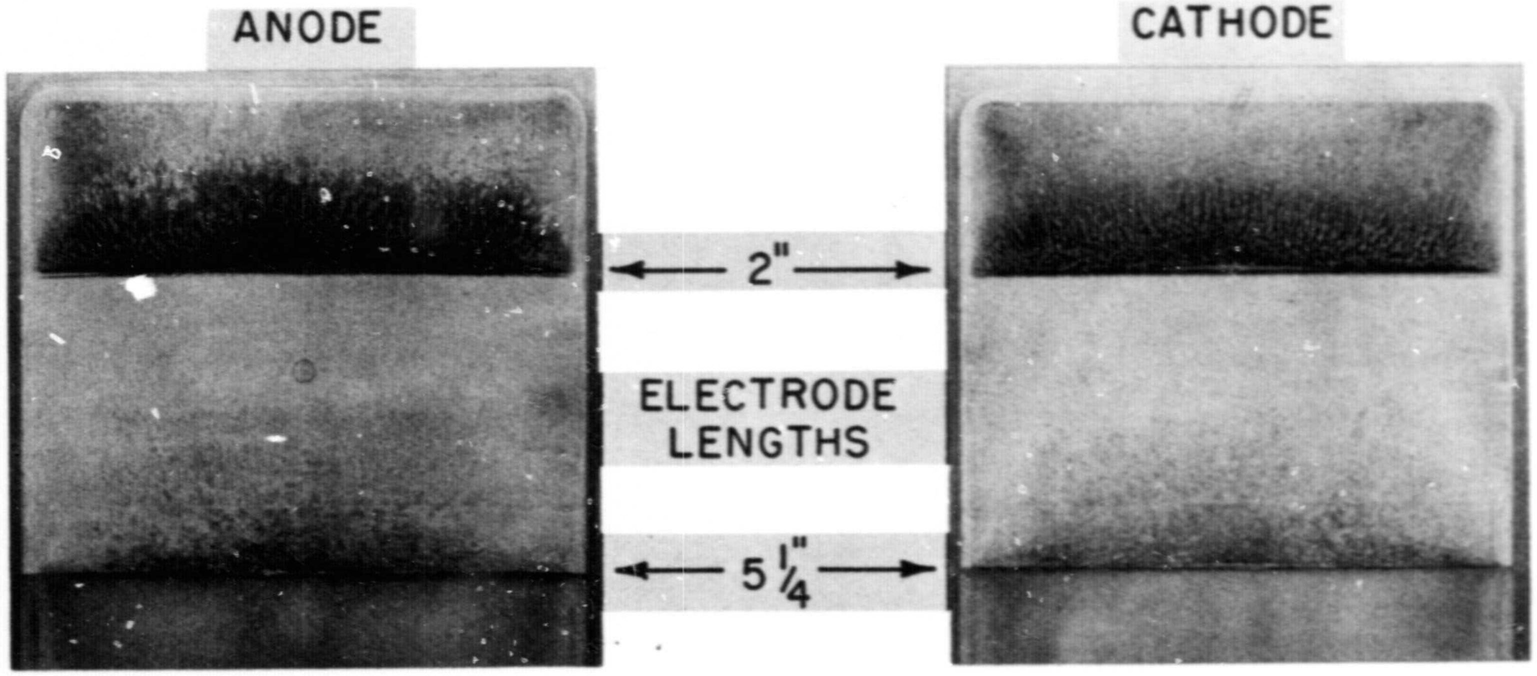

ELECTRODE PITTING PATTERNS FOR THE LONG PULSES

FIGURE VII-7

measurements, is being accelerated, a small 15° half angle wedge is placed 2½" downstream of the metal to insulation discontinuity. No results are obtained for the 5/500 pulse where the voltage differences between the flow modes are most striking, because the luminosity is too weak to be photographed with the currently available equipment. Based on the fact that the 20/125 pulse is too short in duration for the gas flow to become established and based on the insufficient wedge flow luminosity with the 5/500 pulse, gasdynamic flow stabilization studies are conducted with the 10/250 current waveform.

The initial pressure in the chamber at the time of breakdown and the mass flow rate to the discharge over the duration of the current pulse can be varied by altering the synchronization of the gas flows from the shock tube to the switch and chamber. This is mechanically accomplished by varying the length of the feeder tubes from the end of the shock tube and/or the size of the orifices within these feeder lines to the switch and main chamber. If the lengths of all feed lines and the orifice size to the switch are held constant, the initial pressure and mass flow rate can be varied by changing the size of the orifices in the feed lines supplying the chamber. By varying the mass flow rate in this manner, it is found that well-defined bow shocks on the wedges occur in only one range of values of the mass flow rate. Above and below this range no shocks are observed.

Although there is a variation in initial pressure as the orifice size to the chamber is altered to vary the mass flow rate, it is believed to be unimportant. Two comments can be made in support of this contention. First, wedge flow studies in ambient prefill cases where the initial pressure is varied from 50µ to 1000µ yield negative results regarding the observance of shock waves for the duration of the current pulse. Second, based on time of arrival studies of the luminosity at the wedge position, the initial pressure is known to be less than 200µ in the mass flow rate cases studied so that the variation in initial pressure cannot exceed this value. This spread in initial pressure is felt to be insignificant.

Although shock waves can be observed for a variety of orifice size and feeder line length combinations, which apparently all provide nearly the same mass flow rate, the particular set of parameters employed in the results to be shown are a 16" long ½" internal diameter switch line and 14" long ¼" I.D. chamber lines with orifices as noted when appropriate. With 1/8" diameter orifices in the chamber feed lines, shocks are observed throughout most of the pulse as seen in Figure VII-8. Even in this one visible shock wave case, the shocks are quite diffuse and suggest that the flow is rarified. However, the shock angles are nearly those observed with the high current pulses, e.g. 120/20 and 60/40. Based on time of arrival of the luminosity at the

10/250 PULSE, 2" ELECTRODE LENGTH

0.5" DIA ORIFICE TO SWITCH; 16" LONG SWITCH TUBE
0.125" DIA ORIFICE TO CHAMBER; 14" LONG CHAMBER TUBES

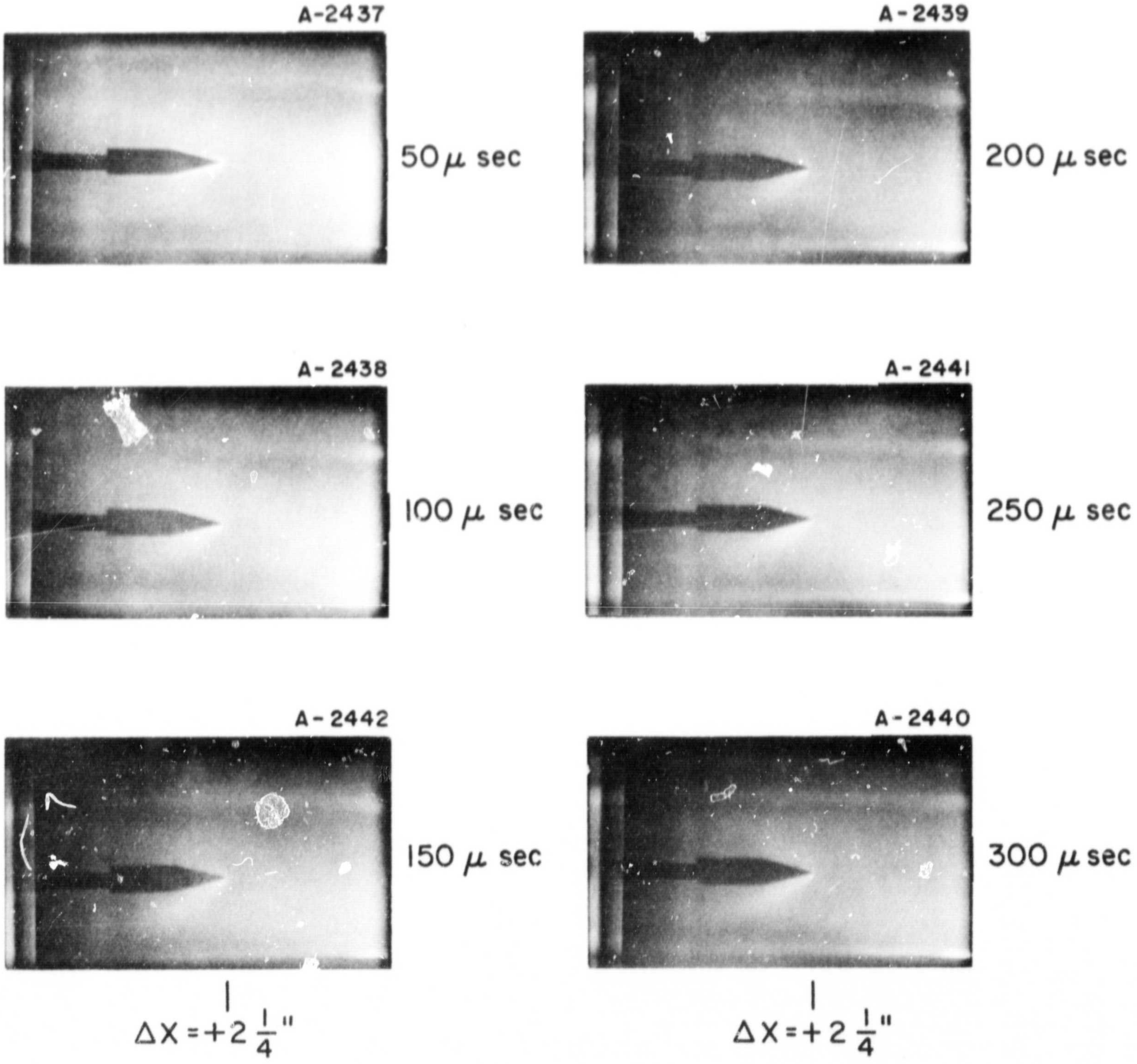

FLOW OVER WEDGE DOWNSTREAM
OF ELECTRODE DISCONTINUITY

FIGURE VII-8

wedge position and in comparison with similar studies in the ambient cases, the initial pressure is estimated to be between 50 and 100μ. Using highly sensitive piezocrystal pressure transducers and a technique described in APPENDIX A, the mass flow rate to the discharge for which shocks are discernible is experimentally determined to be about 3.6 grams/sec; this is with the 1/8" diameter orifices in the chamber feed lines. With 1/16" diameter orifices, the mass flow is found to be about 1.4 grams/sec and with no orifices at all, 7.5 grams/sec.

Although no shocks are visible for the lower or higher mass flow rate cases or for the ambient prefill case, an interesting new effect is seen in the form of an intensification of the luminosity extending downstream from the electrode discontinuity as the mass flow decreases. For example, Figure VII-9 shows a sequence of photographs with 1/16" dia. chamber orifices and a sequence with the 100μ prefill. When these photographs are compared with each other and with the 1/8" dia. orifices of Figure VII-8, this electrode effect is clearly illustrated. It is hypothesized that as the mass flow rate decreases, the discharge is starved for mass and begins ablating electrode and/or insulator material to run on with a resulting intensification of the luminosity near the electrode discontinuity. To check this hypothesis, the discharge is spectroscopically examined for the various mass flow rates available. These

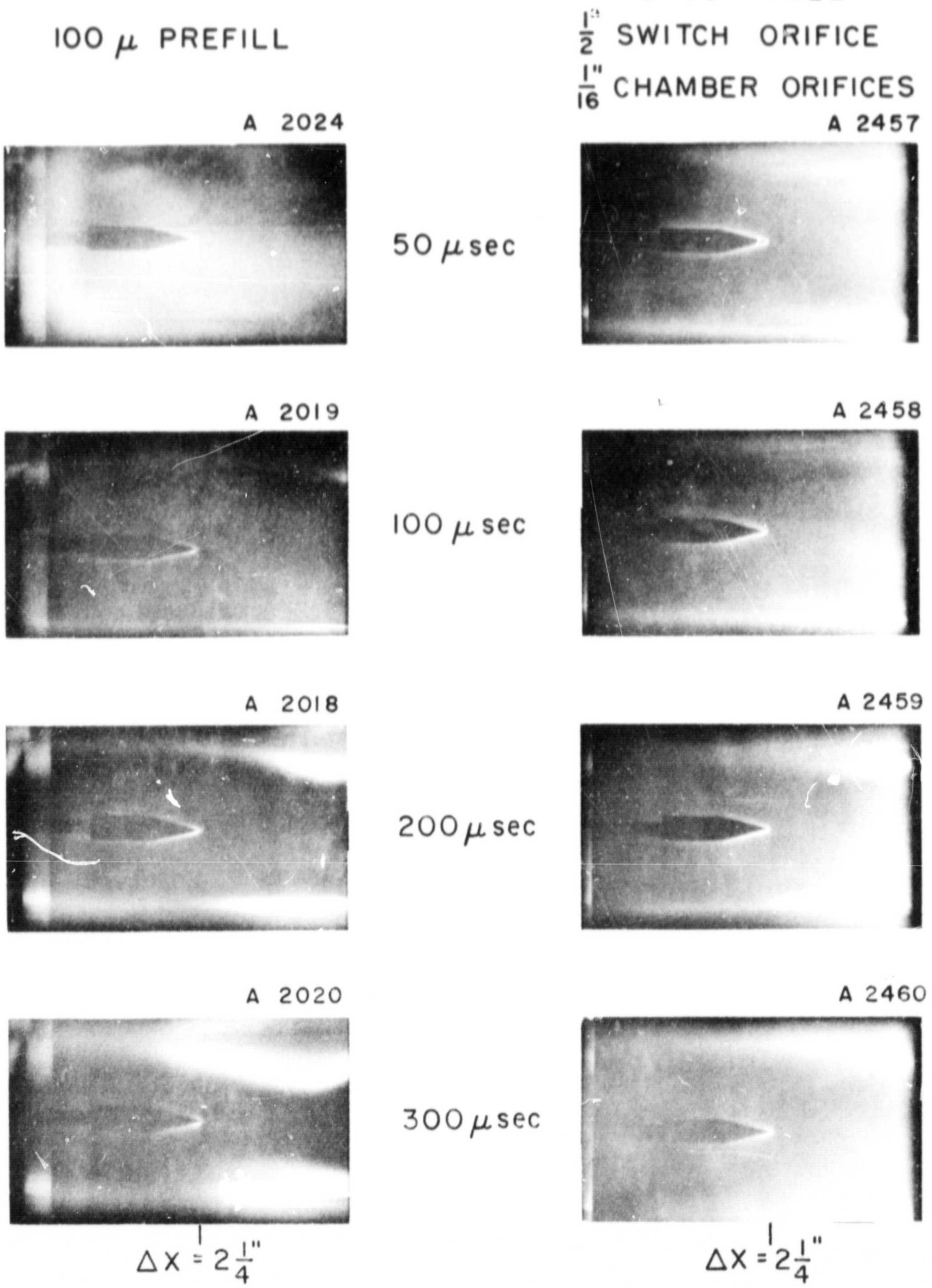

10/250 PULSE, 2" ELECTRODE LENGTH

ELECTRODE EFFECTS WITH DECREASED MASS FLOW RATES

FIGURE VII - 9

results are presented in Figure VII-10. As can readily be seen there is a dramatic decrease in the intensity of the molecular carbon bands as the mass flow rate increases. This carbon is most likely ablated plexiglass; small 1/16" thick plexiglass sheets are used to extend the insulation from the permanent x = 5¼" location to the x = 2" position used in these experiments. As the mass flow increases and the discharge has more and more argon to work with, the insulator ablation is significantly decreased. Also shown are several argon lines which become more prominent as the mass flow rate increases. These comparisons are particularly striking when the shock tube cases are compared with the 100µ prefill which apparently quickly runs out of argon on which to feed.

Having shown generally via the voltage measurements that fresh gas can be supplied to the discharge on a time scale of hundreds of microseconds, and having shown that long duration discharges are fairly uniform, detailed diagnostic studies, similar to those performed on the partially insulated 120/20 case, are now described for the specific mass flow rate case where the outflow can be photographically observed.

D. DIAGNOSTIC STUDIES

The case under detailed study is that for which bow shocks are visible on the wedge placed downstream of the stabilized current distribution; this occurs with the 1/8"

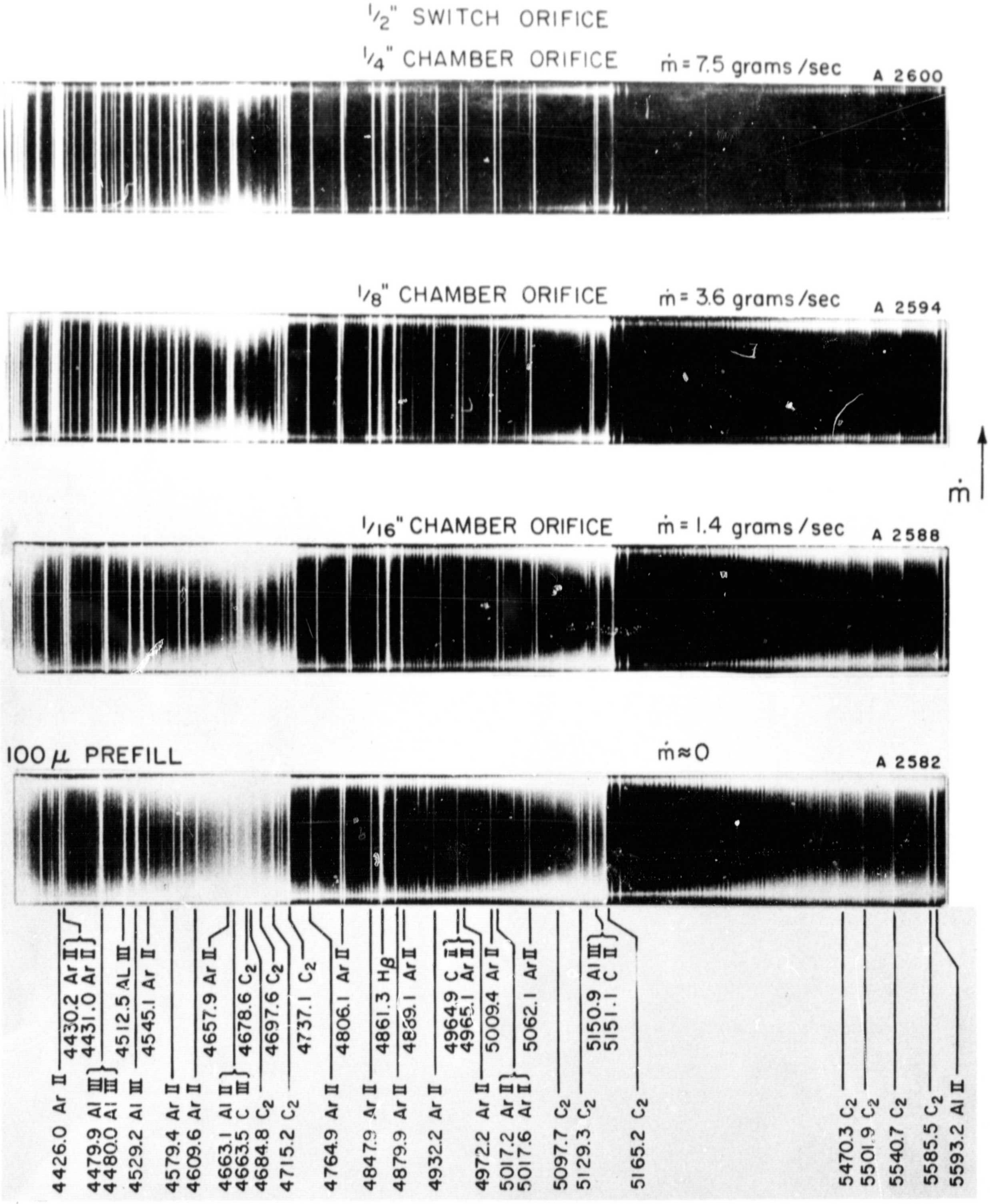

SPECTROGRAMS AT VARYING MASS FLOW RATES

FIGURE VII-10

diameter orifices in the chamber feed lines.

Voltage measurements comparing the shock tube gas injection mode and 100μ prefill are shown in Figure VII-11. At 50 μsec the signal levels are nearly equal but thereafter differ considerably as the discharge is supplied with fresh gas from the shock tube and starved for gas in the 100μ prefill case.

Magnetic probe studies in the vertical midplane demonstrate the nearly one dimensional character of the current distribution. Figure VII-12 shows contours of enclosed current at 250 μsec typical of the current distribution which prevails throughout the duration of the pulse. As the probe is withdrawn along the insulator, small negative signals are recorded. Such a signal can arise from current eddies being generated at the discontinuity or from a lack of complete two dimensionality. The latter interpretation has been adopted and negative signals are taken to be zero. The uncertainty in contour values is approximately ± 10% due to reading and probe positioning inaccuracies.

Both streamwise and transverse electric field data are obtained by means of twisted lead, conically shaped and pronged probes respectively, along the midline, $y = 1"$, $z = 3"$ of the accelerator. At any one probing location, both field components generally exhibit a nearly constant response with respect to time. Of interest, however, are the spatial variations in field strength, particularly in regard to the streamwise E_x distribution. These data

10/250 PULSE ; 2" METAL ELECTRODE LENGTH

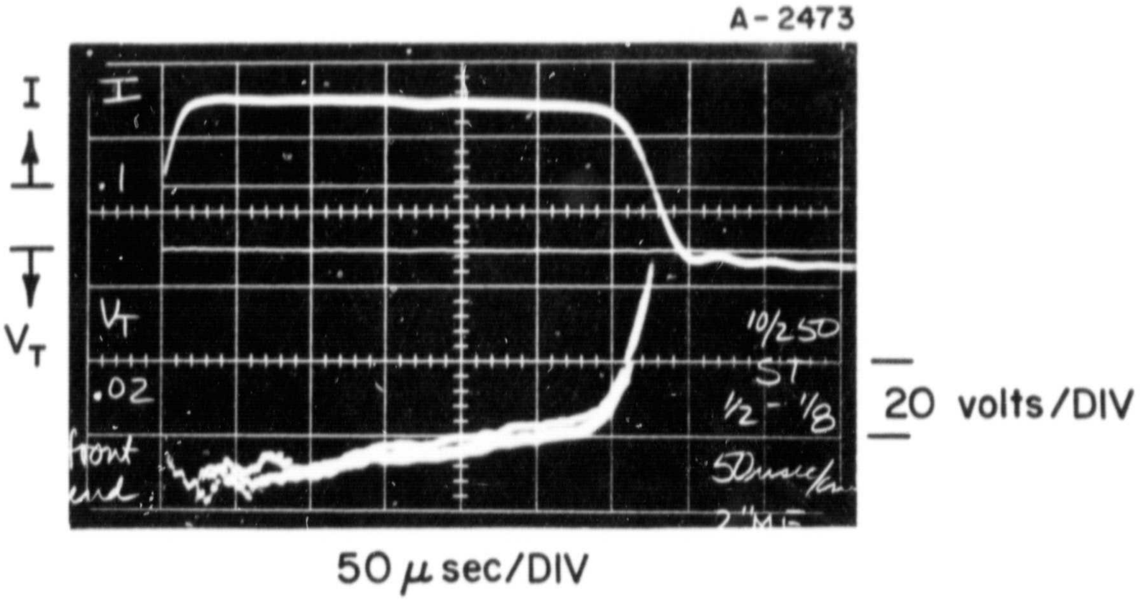

a) SHOCK TUBE { 0.5" DIA SWITCH ORIFICE ; 16" SWITCH TUBE
0.125" DIA CHAMBER ORIFICES ; 14" CHAMBER TUBES

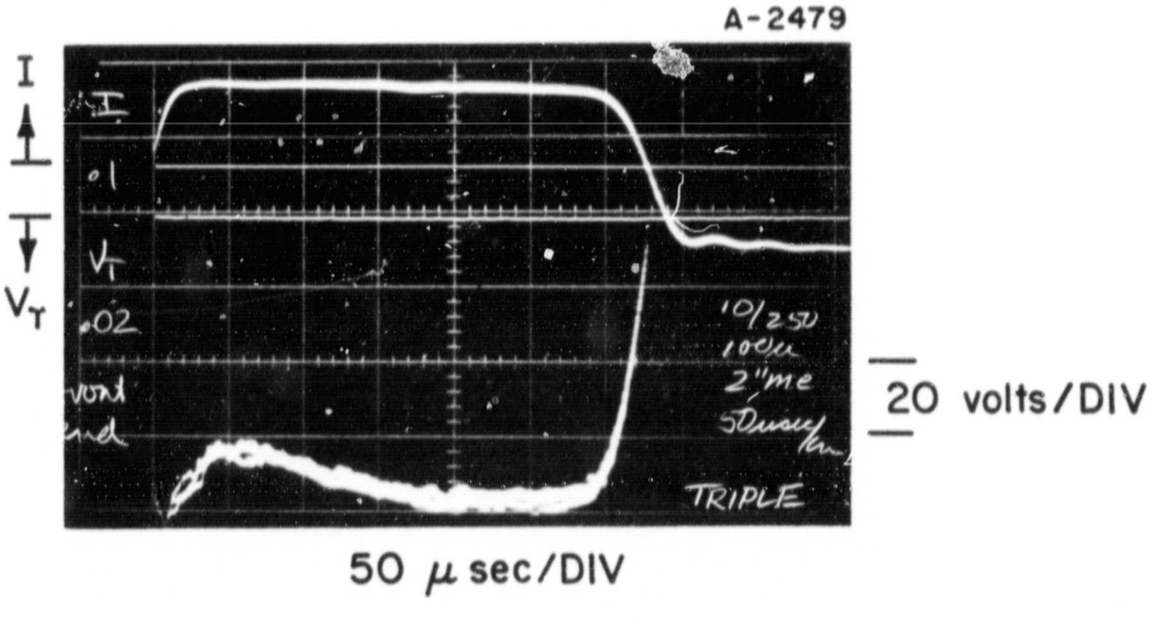

b) 100 μ PREFILL

COMPARISON OF VOLTAGE SIGNATURES WITH SHOCK TUBE
GAS INJECTION AND 100 μ PREFILL

FIGURE VII-11

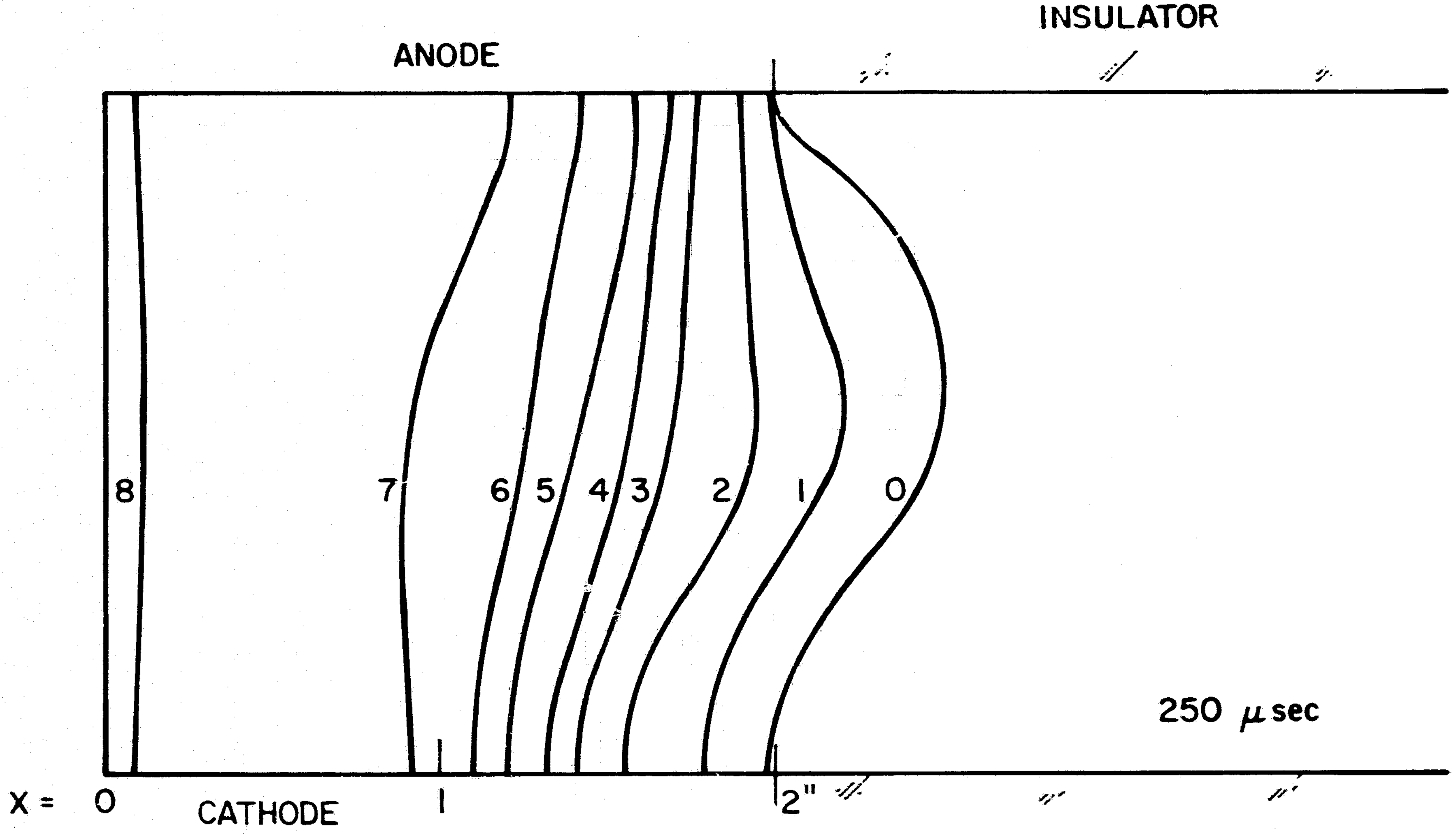

SHOCK TUBE 0.50" DIA SWITCH ORIFICE ; 16" SWITCH TUBE
0.125 " DIA CHAMBER ORIFICES ; 14" CHAMBER TUBE
2" METAL ELECTRODE LENGTH

CONTOURS OF ENCLOSED CURRENT, 10/250 PULSE

FIGURE VII - 12

are presented in Chapter VIII together with a joint analysis of the electric and magnetic field data.

CHAPTER VIII

DATA ANALYSIS

In Chapters VI and VII, data are presented for the most part in raw form as supporting evidence for the occurrence of the two physical phenomena of interest, namely, current pattern and gas flow stabilization. In this chapter, the raw data will be analyzed with the main intention of determining the accelerating nature of stabilized current distributions. Both the $^{120}/20$ and $^{10}/250$ cases are examined.

A. PULSED FLOW MODE ANALYSIS

The pulsed flow mode, as previously defined in Chapter I, is that mode in which only current pattern stabilization occurs. Clearly then, the $^{120}/20$ pulse, 100μ prefill, partially insulated electrode case will be examined.

1. Electron Density Profile

The electron number density can be determined from the electric and magnetic field data by the use of the generalized Ohm's Law [2] [37] which is given by the expression

$$\vec{J} = \sigma_c \left(\vec{E} + \vec{u} \times \vec{B}\right) - \frac{\Omega}{B}\, \vec{J} \times \vec{B} \qquad \text{(VIII-1)}$$

where σ_o - scalar electrical conductivity

Ω - electron Hall parameter

u - mass averaged flow velocity.

In the above equation, terms due to ion slip and the electron pressure gradient have been neglected. Ion slip can be neglected because the neutral particles are collisionally coupled to the ions in the density range and magnetic field strength prevailing in the experiment. Neglect of the electron pressure gradient effect has been justified a posteriori.

For the reference frame shown in Figure VIII-1, equation VIII-1 may be written in component form as:

$$j_x = \sigma_0 (E_x + u_y B_z) - \Omega j_y \tag{VIII-2}$$

$$j_y = \sigma_0 (E_y - u_x B_z) + \Omega j_x \tag{VIII-3}$$

The data will be analyzed along the centerline, y=1", z=3", of the accelerator and the following assumptions are made: 1) The plasma is quasi-neutral, $n_i = n_e$, where n is the number density and the subscripts i, e refer to ions and electrons respectively. Implicit in this assumption is that the ions are singly ionized; hence the ionic and electronic charges are equal. 2) $j_x = 0$ in the midplane. This is based on the photographically observed symmetry of the current bands even though the current distribution is highly bowed. 3) $u_y = 0$ in the midplane. The zero u_y assumption is based on the symmetry of the shock waves which appear on the wedges, indicative of a nearly axial flow field.

It must be pointed out that the last assumption has an important manifestation, namely, that electrons carry all of the midplane j_y current. Since the electron mass m is nearly 10^{-5} of an argon ion mass, M_i or atom mass M_a, the mass average

AP25 R 4449 68

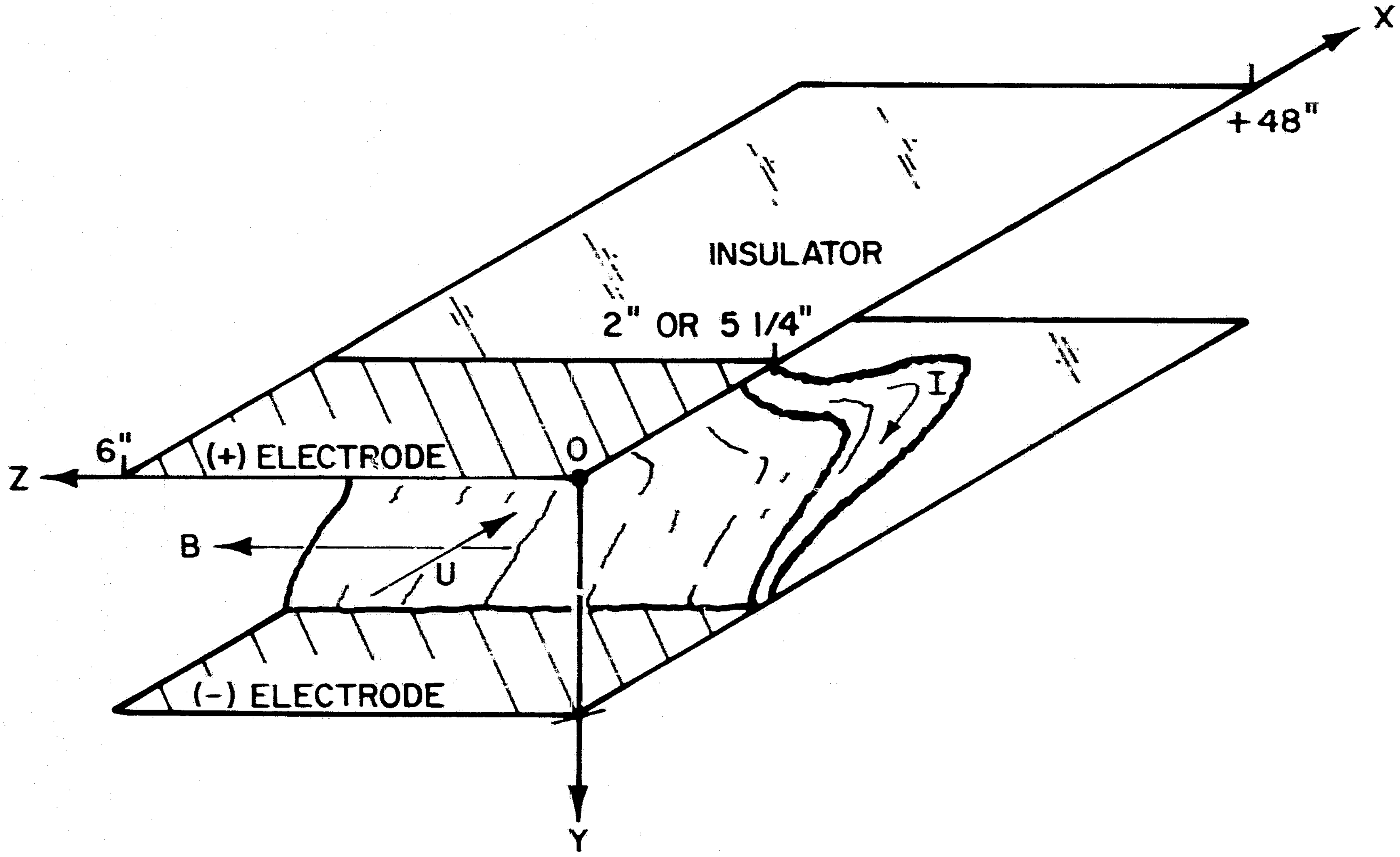

COORDINATE SYSTEM FOR ANALYSIS

FIGURE VIII-1

flow velocity may be regarded as the heavy particle velocity. Since the ions have no transverse velocity component, they cannot conduct any of the transverse current.

With the above assumptions, VIII-2 reduces to

$$\sigma_0 E_x - \Omega j_y = 0 \qquad \text{(VIII-4)}$$

The scalar electrical conductivity is given by

$$\sigma_0 = n_e e^2 / m\nu_c$$

where ν_c is the total electron collision frequency with heavy particles, i.e. ions and neutrals. The electron Hall parameter defined as the ratio of the gyro frequency to collision frequency is

$$\Omega = eB / m\nu_c$$

Inserting these relations into VIII-4 and solving for the electron density one obtains

$$n_e = j_y B_z / eE_x \qquad \text{(VIII-5)}$$

Since the distributions of B_z and E_x are experimentally determined and since j_y can be obtained from the spatial distribution of B_z through Ampere's Law, the distribution of n_e can be determined. The analysis of the data will be performed at one time, 16 μsec.

Since it is assumed that electrons carry all of the stabilized current in the midplane, the streamwise E_x fields generated are truly Hall fields. The E_x data used in the analysis are recorded with a coaxial lead, conically shaped

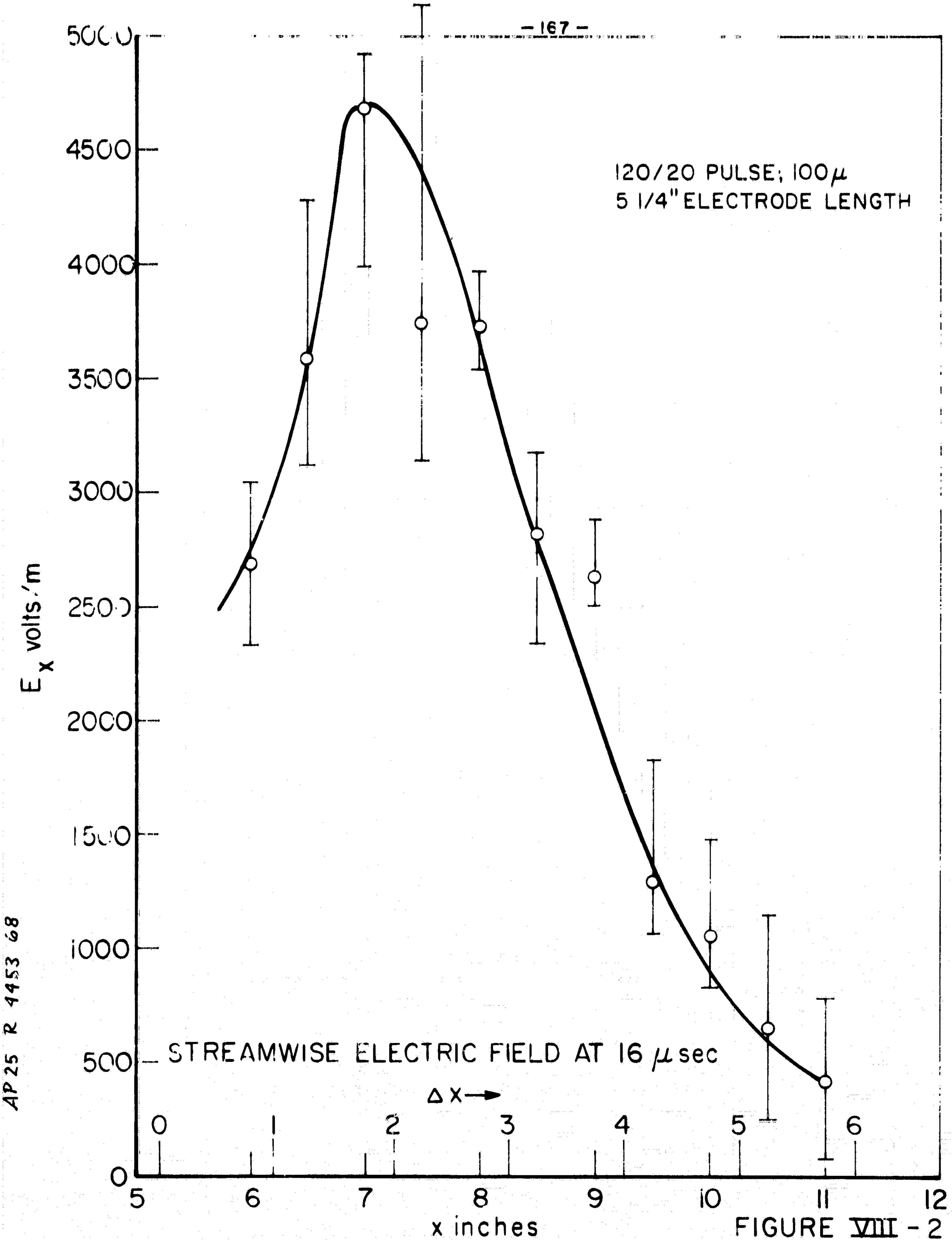

FIGURE VIII-2

AP25 R 4453 68

probe with a 5/16" tip separation. Readings are taken 1/2" apart. Triple overlays of the data are taken and averaged. The probe is cleaned after each triple overlay. The spatial distribution of streamwise electric field through the stabilized current pattern at 16 μsec is shown in Figure VIII-2. The error bars shown reflect the scatter in the data; the points shown are the average field values.

The magnetic field distribution at the same time in the stabilized zone is shown in Figure VIII-3. The magnetic probe employed consists of a 5 turn - #26 formvar wire coil with an internal diameter of 3/32" housed in a 6 mm OD glass tube sealed with epoxy. The data is very reproducible and the error bars displayed are due to reading errors, ± .25 mm. As in the E_x data, a 1/2" grid spacing is used.

The current density is determined from the magnetic field data from Ampere's Law in finite difference form

$$j_y(x) = -\frac{1}{\mu_0}\frac{dB_z(x)}{dx} \simeq \frac{1}{\mu_0}\frac{B(x-\Delta x) - B(x+\Delta x)}{2\Delta x}$$

Since the magnetic field variation spatially is quite smooth, this linearized technique for determining j_y is fairly accurate. The distribution of j_y is shown in Figure VIII-4. The error bars arise from the reading errors in the B data which become significant relative to the difference in the magnetic field at alternate positions.

Having obtained the spatial distributions of E_x, B_z and j_y, the electron density distribution may be calculated

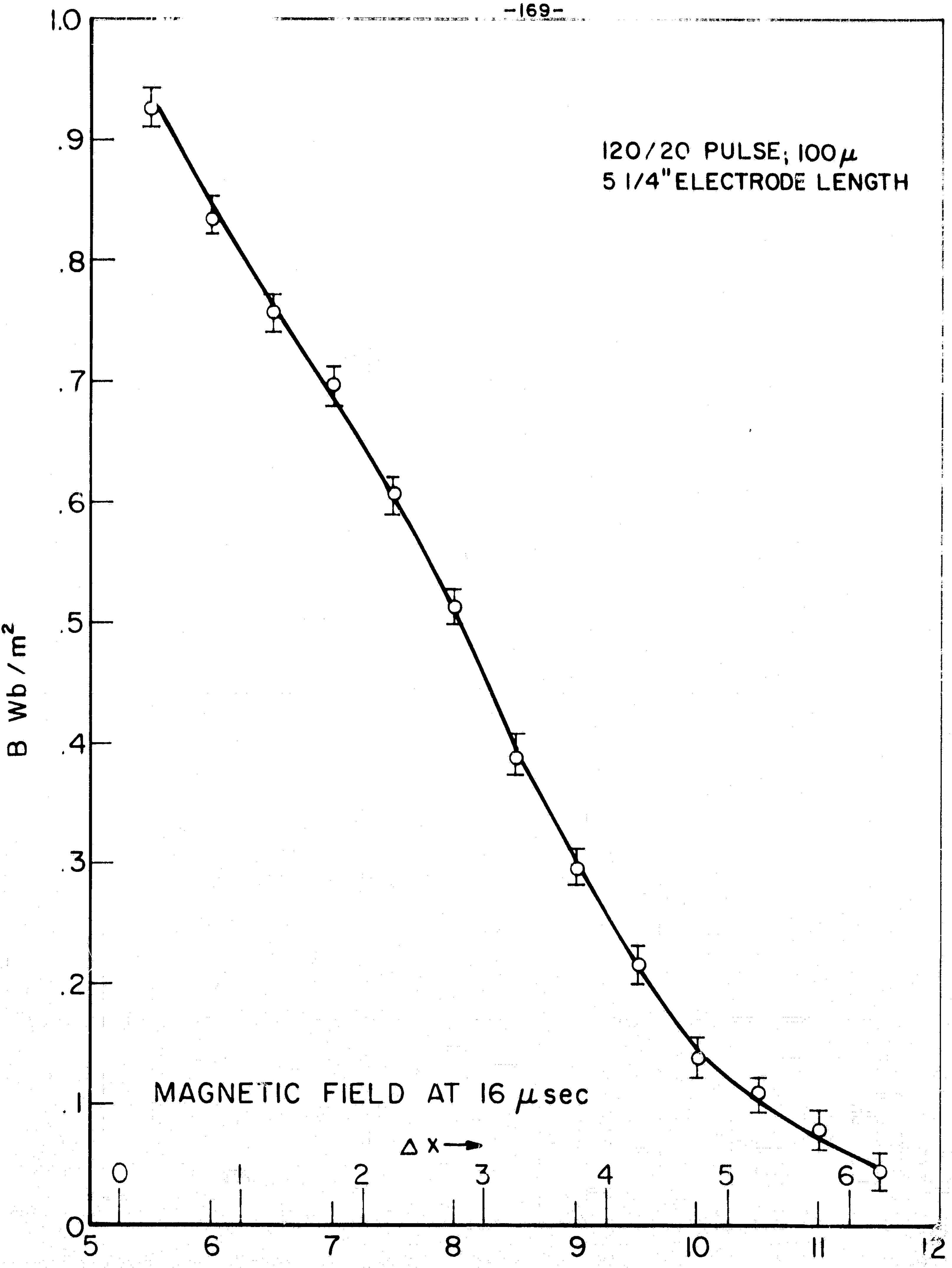

FIGURE VIII - 3

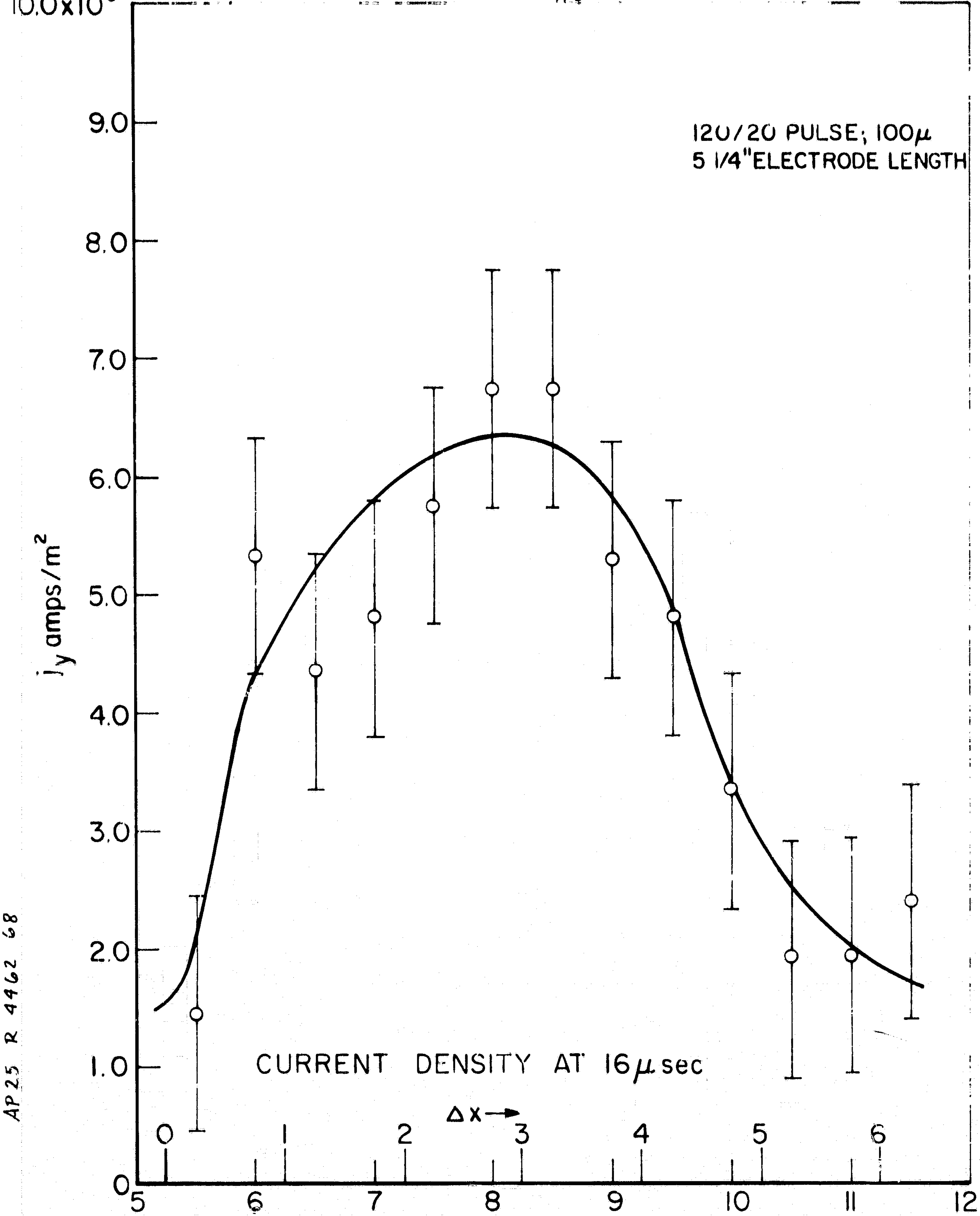

FIGURE VIII-4

AP25 R 4462 68

in accordance with VIII-5 and results can be seen in Figure VIII-5. The error bars shown result from a combination of the reading errors in B, the analysis errors in j and the scatter in E_x and of course do not reflect on the validity of the assumptions made or on the reliability of the probes.

Of note is the peak electron density calculated, approximately $10.3 \times 10^{21} m^{-3}$. The particle density of 100μ room temperature argon is $3.3 \times 10^{21} m^{-3}$. The inflow electron density into the stabilized current zone is thus about three times higher than the prefill density. Also of interest is the electron density falloff through the stabilized zone, the significance of which will be treated in the following section.

2. Velocity Profile

The velocity profile of the flow through the zone can be obtained if the electron density can be related to the total mass density which in turn is related to the flow velocity from the one dimensional steady state continuity equation. The total mass density ρ is

$$\rho = n_e m + n_i M_i + n_a M_a \qquad \text{(VIII-6)}$$

The degree of ionization α is defined as

$$\alpha \equiv \frac{n_i}{n_i + n_a}$$

which when rearranged and solved for n_a gives

$$n_a = \frac{n_i(1-\alpha)}{\alpha}$$

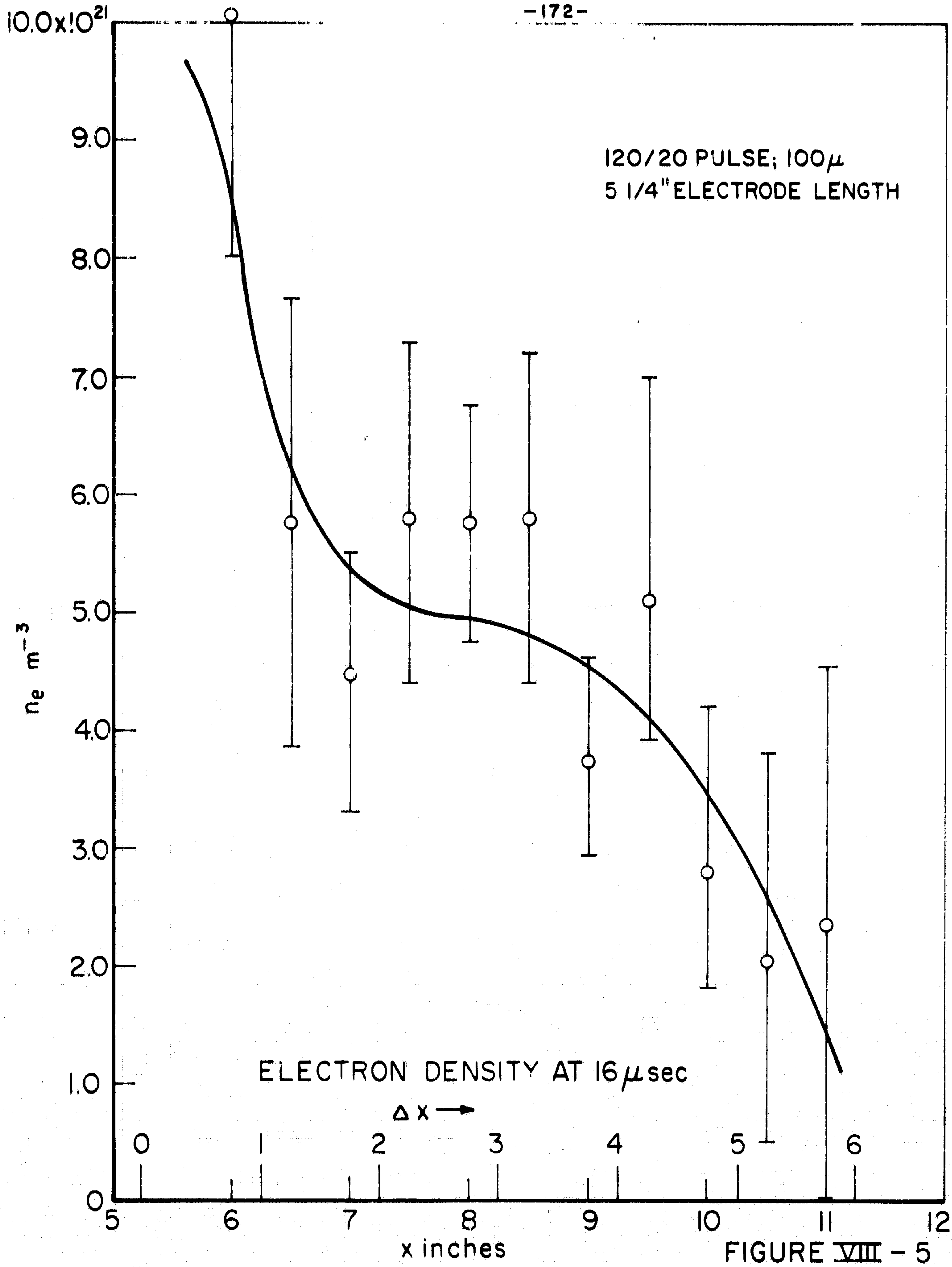

FIGURE VIII - 5

Since $m \ll M_i$, $M_i \approx M_a$, and $n_i = n_e$, VIII-6 becomes

$$\rho = \frac{n_e M_i}{\alpha} \qquad \text{(VIII-7)}$$

Substituting for ρ from VIII-7 into the one dimensional steady state continuity equation

$$F = \rho u = \text{constant}$$

one obtains

$$u = \frac{\alpha F}{n_e M_i} \qquad \text{(VIII-8)}$$

The velocity profile can be obtained from VIII-8 knowing the electron density distribution previously determined if the spatial variation of α is known. The variation of α through the zone cannot be determined on the basis of the measurements which have been made. To circumvent this impasse, α will be assumed to be constant. Physically, the current sheet is envisioned as setting up an ionized gas flow which subsequently feeds the stabilized zone, the flow remaining frozen in its passage through the current region. With α constant, equation VIII-8 shows that the reciprocal of the electron density should resemble the velocity profile; $\frac{1}{n_e}$ is plotted in Figure VIII-6. The error bars are very large and are not displayed. Hence the significance of the electron density decrease through the stabilized zone is its correspondence to an acceleration of the flow in this region. From VIII-6 it appears that there may be as much as a fivefold increase in the incoming velocity after acceleration through

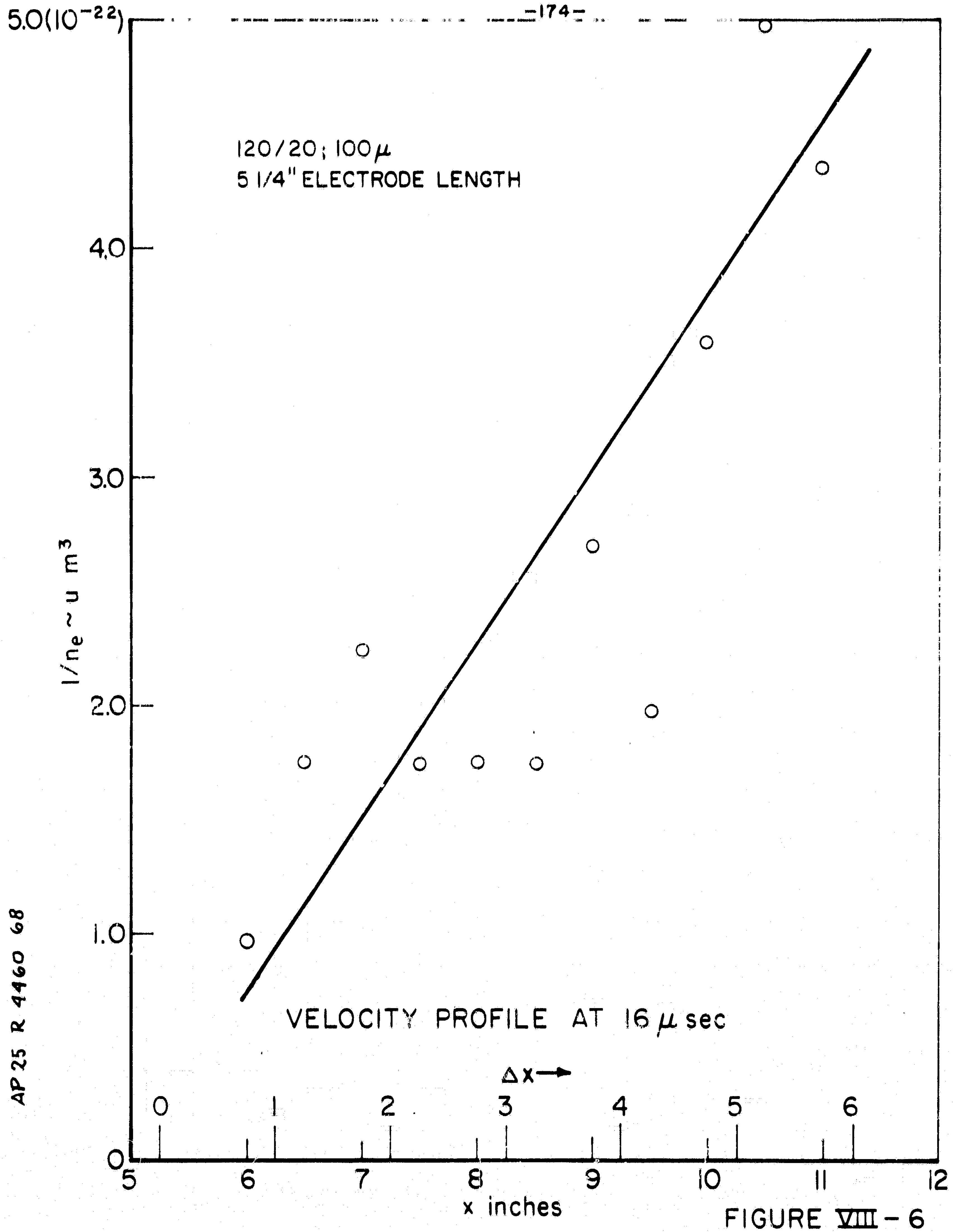

VELOCITY PROFILE AT 16 μ sec

FIGURE VIII - 6

AP25 R 4460 68

the zone. Later analyses indicate that the velocity ratio is only about half this value.

Before the outflow velocity u_f can be calculated, however, the inflow velocity u_o must be determined.

3. Inflow Velocity

The inflow velocity can be obtained in the following manner. With j_x assumed zero, VIII-3 when solved for u_x gives

$$u_x = \frac{1}{B_z}\left(E_y - \frac{j_y}{\sigma_0}\right) \qquad \text{(VIII-9)}$$

All quantities on the right hand side of the above equation can be experimentally obtained at any point except for σ_0. It will now be shown, however, that along the metal electrode portion of the channel that j_y/σ_0 can probably be neglected relative to E_y.

From the voltage measurements, the resistive drop which is first monitored before stabilization occurs will be assumed to remain constant throughout the duration of the pulse even when stabilization occurs. The resistive drop, typically 60 volts, when divided by the 2" interelectrode spacing gives a field of 1200 volts/meter. This value is well below 1/10 of the lowest E_y fields measured in the midplane along the metal electrode region. Furthermore the 1200 volts/meter is probably an upper estimate since voltage drops of about 20 volts can be expected to occur at each electrode sheath[2] and consequently the midplane resistive field is even much lower. Further evidence is had by comparing the resistive drop with the back $\vec{u}\times\vec{B}$ emf contribution to the total voltage in this case. The V_{uB} generated is about an order of magnitude greater than the resistive drop. Hence neglect of jy/σ_c in VIII-9 seems quite justifiable.

The transverse electric field, E_y, is monitored with a twisted lead, extended double tip probe with a 1/16" electrode separation. The reproducibility of the data is very good. Dividing E_y by B_z gives u_x in accordance with VIII-9 after neglecting jy/σ_o. The $\frac{E_y}{B_z}$ values at five positions, x = 1" through x = 5", along the metal electrode portion of the channel range from 13,900 $^m/\text{sec}$ to 20,600 $^m/\text{sec}$. The average value is found to be 18,200 $^m/\text{sec}$ and this value will be assumed to be the inflow velocity, u_o, into the stabilized current zone. This value is approximately .57 of the sheet velocity, 32,000 $^m/\text{sec}$ in this case, determined from the $\dot{B}$ trajectory.

4. Outlet Velocity and Degree of Ionization

The outlet velocity u_f may be determined in two different ways; each way, however necessitates knowledge of α. With the assumption that α is constant, the two techniques result in two equations for the two unknowns of interest, u_f and α.

One technique is to determine how much energy an ion acquires as it accelerates through the streamwise electric field. The outflow velocity can be determined by equating the amount of work done on the ion to its change in kinetic energy. The force acting on the ion at any point is eE_x and the amount of work performed is simply the integral of the force over the appropriate path length, hence the outlet velocity is given by the equation

$$u_f = \left[u_c^2 + \frac{2e}{M_{eff}} \int_{\substack{\text{Stabilized} \\ \text{zone}}} E_x \, dx \right]^{1/2} \tag{VIII-10}$$

Note that in VIII-10 that the ionic mass is not used but rather an effective mass $M_{eff} = M_i/\alpha$

Although the electric field acts only on the ions, the neutrals are collisionally coupled to the ions and this collisional drag due to neutrals can be accounted for through the guise of "heavier" ions since $\alpha \leq 1$. Hence equation VIII-10 may be written

$$u_f = \left[u_c^2 + \frac{2e\alpha}{M_i} \int_{\substack{\text{Stabilized} \\ \text{zone}}} E_x \, dx \right]^{1/2} \tag{VIII-11}$$

The integral in the radical is simply the area under the curve in Figure VIII-2 between x = 6" and x = 11".

The second technique of u_f determination is to apply a momentum balance to the flow. For a one dimensional, self field accelerator, the momentum equation is

$$\rho u \frac{du}{dx} = jB - \frac{dp}{dx}$$

Neglecting the pressure gradient relative to the very much larger $\vec{j} \times \vec{B}$ force and substituting for j from Ampere's relation, the momentum equation can be directly integrated to

$$u_f = u_o + \frac{B_o^2}{2\mu_c F} \qquad \text{(VIII-12)}$$

where the subscripts o and f refer to the inlet and outlet conditions and B_f is assumed zero which is experimentally verifiable. Replacing F by $\rho_o u_o$ and substituting for ρ_o from VIII-7, one obtains

$$u_f = u_o + \frac{\alpha B_o^2}{2\mu_o M_i u_o n_{eo}} \qquad \text{(VIII-13)}$$

In VIII-11 and 13 all quantities are known except for u_f and α. Simultaneous solution of these equations yields the results that $\alpha = .82$ and $u_f = 40,800$ m/sec. It is clear that the flow is highly ionized. Less than 1 per cent of the total electrical energy input into the discharge is required to provide this level of ionization. Furthermore the velocity ratio is found to be 2.25. This is less than half the velocity ratio found previously from $1/n_e$. One final comment can be made concerning this discrepancy in the velocity ratio. Preliminary, untimeresolved Doppler shift experiments* have been performed in which the discharge is viewed head on and side on by the spectrograph in successive discharges. The highest velocity found for Ar II, singly ionized argon, through this technique is 39,200 m/sec ± 25%. Hence the indications are that the velocity ratio through the stabilized current distribution does not exceed approximately three. This is roughly in agreement with the simple theory presented in Appendix B.

---

*I would like to express my thanks to Mr. Michael Boyle for his analysis of the Doppler shift data.

It may well be that the constancy of the degree of ionization assumption is not strictly valid. A decrease in the degree of ionization in the downstream region of the current zone where the current density falls off from its peak value would result in a decrease in electron density which could wrongly be interpreted as an acceleration of the flow in this region. Determination of the velocity ratio from the reciprocal of the electron density is more sensitive to variations in α than the velocity calculations based on the momentum balance or streamwise electric field integration techniques. In the latter cases, the increments to the integrals of interest become relatively smaller with distance as the fields fall off sharply and changes in α in this region do not predicate profound variations in the total value of the integral. In summary, then, determination of the velocity ratio from the reciprocal of the electron density distribution, in contrast to the other methods, is more likely to be in error when the constancy of the degree of ionization assumption is not totally correct.

5. Mass Flow Rate

Having calculated the degree of ionization in addition to the inlet electron density and flow velocity, the mass flow rate through the current distribution can now be obtained. The mass flow rate per unit area, F, can be determined from VIII-8 and is found to be $15.3 \frac{\text{kgm}}{\text{m}^2\text{sec}}$. For the cross sectional area of the channel, this corresponds to a mass flow rate of $.118 \frac{\text{kgm}}{\text{sec}}$.

The total amount of gas passed through the current zone may be estimated by assuming the flow exists for about ten microseconds and multiply the mass flow rate by this amount of time. Such a calculation gives 1.2 x 10^{-6} kgm. The initial amount of gas in the interelectrode region can be calculated and is found to be 8.5 x 10^{-6} kgm. The amount of gas passed through the stabilized zone is about 14% of what is in the interelectrode region from the prefilling. Hence even if the sheet is 85% efficient in sweeping up mass as it propagates down the channel, there should still be enough residual mass to feed the stabilized current zone. Since the velocity of a snowplowing current sheet scales as $\rho^{-1/2}$, the trajectory of the sheet is relatively insensitive to small amounts of leakage. Hence even though the $\dot{B}$ trajectory of the sheet shows good agreement with the theoretically predicted snowplow trajectory, this agreement does not preclude the existence of a small amount of gas left behind by the current sheet.

Finally it is of interest to estimate the duration of the flow through the stabilized zone. If it is assumed that the current sheet sets up the 5 1/4" electrode length of residual gas moving at 18,200 $^{m}/$sec the flow can be expected to last for about the electrode length divided by the inflow velocity or approximately 7.3 μsec. The trailing edge of the gas will take about 7 μsec to reach the current zone and then another 7 usec or less to be accelerated through it. Hence there is enough time for the gas to be accelerated through the current zone, but it is also clear that the current zone will likely run out of mass flow during the duration of the pulse as is indeed observed from the wedge flow studies upstream of the stabilized current region. Although steady flow analyses have been applied, this flow can persist for only a limited time, and hence the accelerator is operating in a pulsed flow mode.

B. QUASI-STEADY MODE ANALYSIS

The quasi-steady mode is that regime where both current pattern and gas flow stabilization are present. The analysis for this mode will now be presented using the $^{10}/250$ pulse, 2" metal electrode length and the shock tube gas injection technique adjusted for the mass flow rate for which shock waves are visible on the downstream wedge. The analysis will be performed at one time, 250 μsec, near the end of the pulse and along the centerline, $y = 1"$, $z = 3"$ of the channel.

1. Field Distributions

The magnetic field is recorded with a 100 turn multilayered coil with an internal diameter of 1/8" enclosed in a pyrex tube and sealed with epoxy. The spatial distribution of the field is shown in Figure VIII-7 along with the corresponding current density distribution obtained from the magnetic field in the manner discussed earlier. The error bars in B result from data reading errors and those in j from the analysis of the B data.

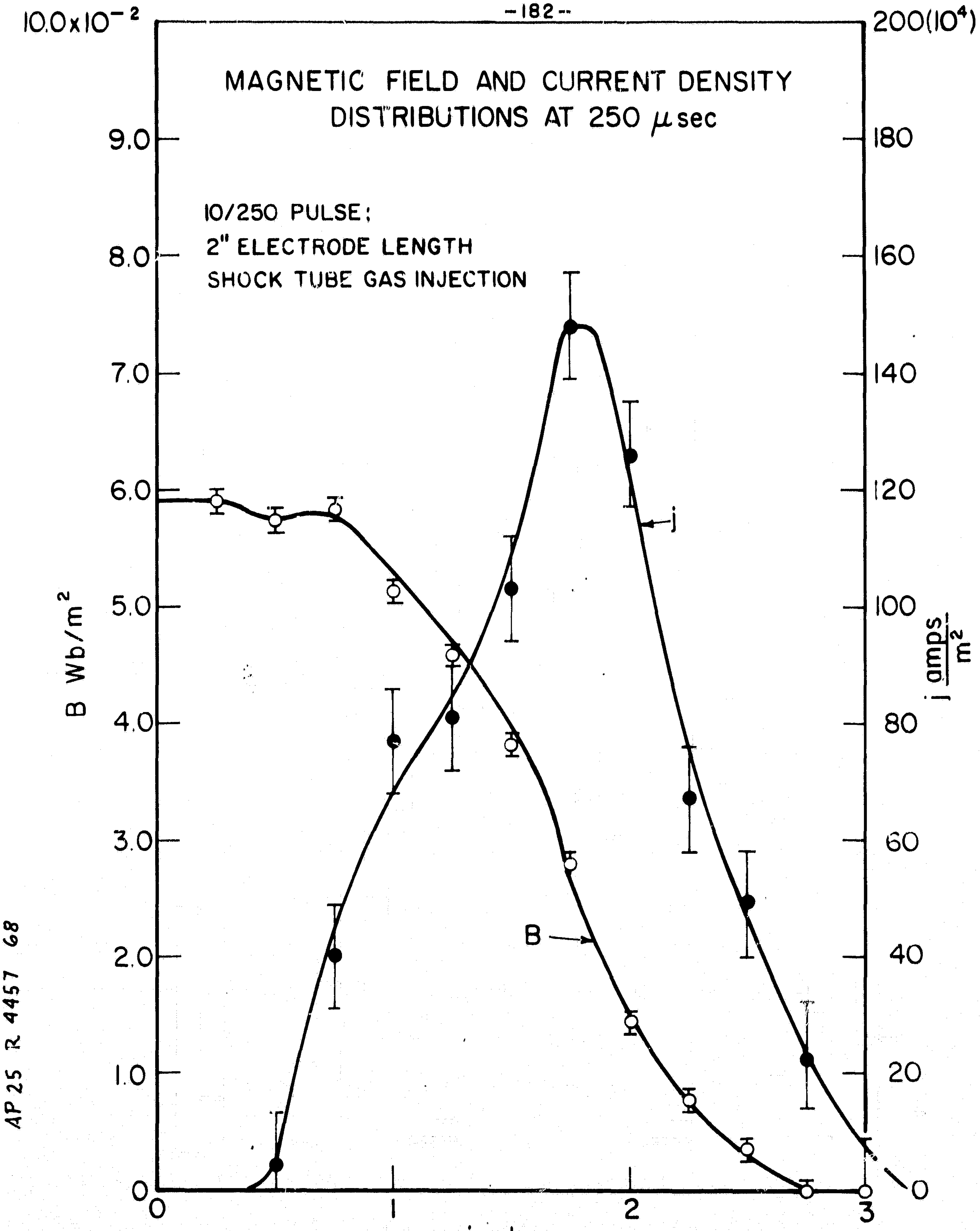
MAGNETIC FIELD AND CURRENT DENSITY DISTRIBUTIONS AT 250 μsec

10/250 PULSE;
2" ELECTRODE LENGTH
SHOCK TUBE GAS INJECTION

FIGURE VIII-7

AP 25 R 4457 68

The streamwise electric field is monitored with a twisted lead, conically shaped probe with a 1/4" electrode separation. For fairly reproducible data, it is necessary to clean the probe after every discharge; otherwise, the signals obtained in successive discharges differ drastically. Three recordings are made at each probing position and the data are averaged. The E_x distribution is plotted in Figure VIII-8; the error bars arise from scatter in the data. Of special note is the very rapid falloff of the E_x field in the region from x = 1" to 2", the region in which the current density j_y peaks. If j_x is assumed to be zero as is nearly the case as can be seen in Figure VII-12, and, if E_x goes to zero, equation VIII-2 when solved for j_y with the appropriate expressions substituted for σ_o and Ω, gives the result that

$$j_y = n_e e u_y$$

Hence all of the current is carried by ions and there must be a transverse heavy particle velocity. Hence in the midplane region from x = 1" to x = 3" it appears that there is a significant u_y and the zero u_y assumption used previously in the $^{120}/20$ analysis cannot be made.

With $j_x = 0$ the only legitimate assumption that can be made, equations VIII-2 and 3 represent 2 equations in 4 unknowns σ_o, n_e, u_x and u_y and as such are insoluble. Hence the electron density distribution cannot be obtained in the manner used earlier.

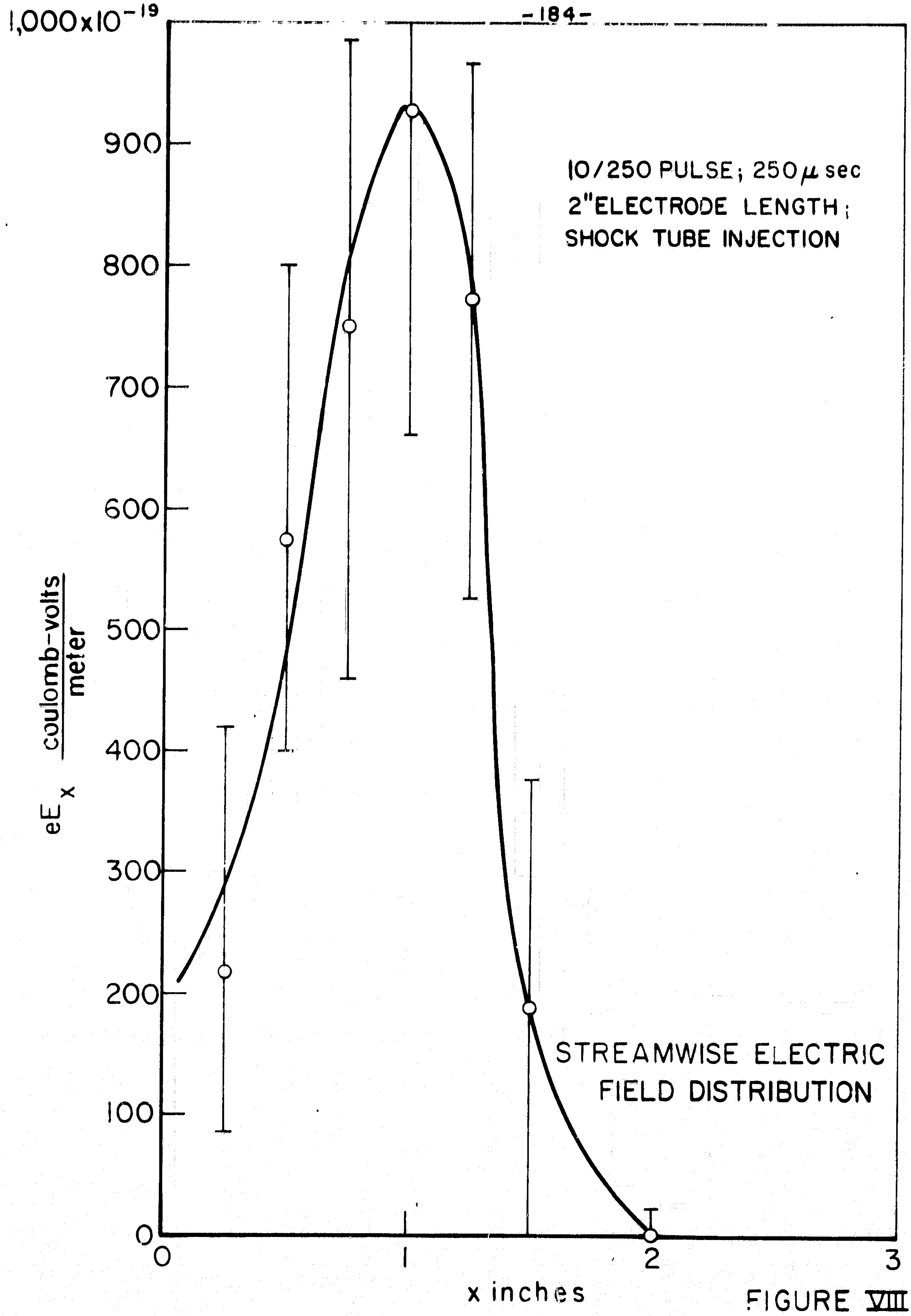

FIGURE VIII-8

AP25 R 4455 68

The striking difference between the character of the stabilized zone in the $^{120}/20$ case and this $^{10}/250$ case is probably due to the nature of the inflow. In the $^{120}/20$ case the flow into the distribution is set up by passage of the current sheet and is probably highly ionized as shown from the previous calculation of α. In the $^{10}/250$ case, fresh argon is being supplied to the discharge which must first be ionized to some extent before acceleration of the flow can occur. It can be shown for instance that when $j_x = 0$, equation VIII-2 and the definition of the transverse current density

$$j_y = n_e e (u_y - u_{ey})$$

may be combined and solved for u_{ey} with the result that

$$u_{ey} = - E_x / B_z$$

Because of the monotonic nature of B, u_{ey} peaks when E_x does. One may speculate that this u_{ey} peaking well before the current density, is part of the mechanism to provide for ionization of the fresh gas feeding the discharge. Clearly, however, further investigation is called for. It would be particularly instructive to study the character of the zone as the mass flow rate to the discharge is varied.

2. Velocity Determiniations

Some streamwise velocity information can be obtained if j_y/σ_0 is again small compared with E_y as is the case in the $^{120}/20$ analysis. The E_y fields measured are generally less than 10^3 volts/meter. The total voltage drop across the electrodes is about 48 volts and most of this as shown previously is resistive drop. For the 2" interelectrode spacing this corresponds to a field of 10^3 volts/meter. Furthermore, the V_{uB} term is known to be much smaller than the resistive drop V_R. Hence at first glance j_y/σ_o cannot be simply neglected. However, if one considers equation III-9

$$u_x = \frac{1}{B_z}\left(E_y - j_y/\sigma_o\right)$$

neglect of j_y/σ_o will lead at worst to upper estimates of u_x. Furthermore, since most of the resistive drop may be in the anode and cathode fall regions,[2] neglect of j_y/σ_o in the midplane may not be bad at all.

In Figure VIII-9, the transverse electric field E_y is shown. E_y is measured with a twisted lead, extended double tip probe with a 1/16" electrode separation. The probe is cleaned after every discharge and the error bars shown represent the scatter in the data. The data at x = 1/2" are very irreproducible and are not shown. Also plotted on Figure VIII-9 is E_y/B_z. If j_y/σ_o is truly negligible, the change in E_y/B_z represents a velocity ratio u_f/u_o of about 2.7 and an outlet velocity of about 3900 m/sec.

If E_y/B_z at x = 1", 1430 m/sec, is assumed to be the inlet velocity into the current zone, a momentum balance, equation VIII-12, can be applied to determine u_f. In this case the mass flow rate has been determined from cold gas flow experiments and it is not necessary to know the degree

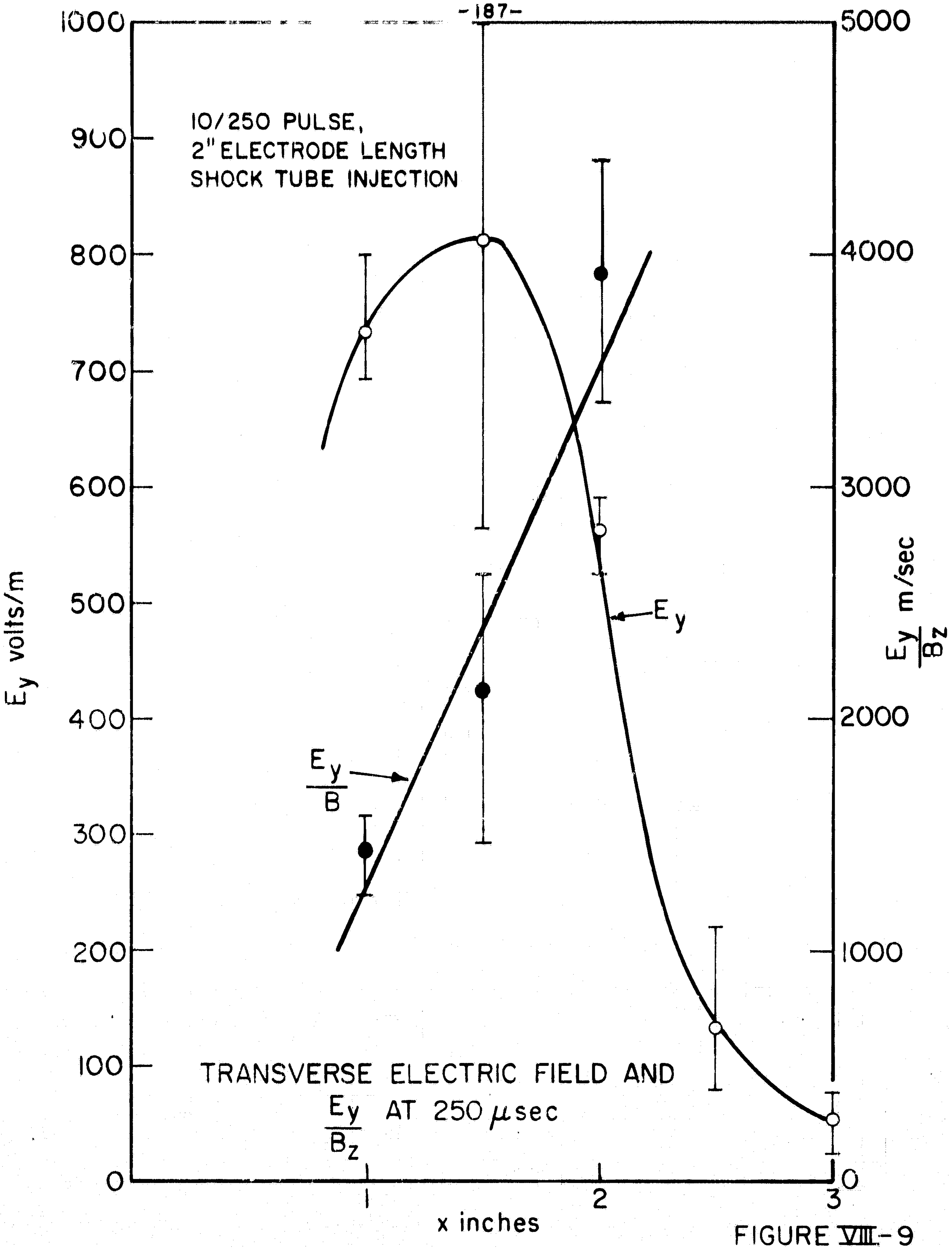

TRANSVERSE ELECTRIC FIELD AND $\frac{E_y}{B_z}$ AT 250 μsec

FIGURE VIII-9

AP 25 R 4454 68

of ionization. Using the known mass flow rate of 3.6 x 10^{-3} $^{kgm}/sec$, the outflow velocity u_f is found to be 3,670 $^{m}/sec$. This corresponds to a $^{u}f/u_o$ of 2.6. The agreement between the momentum balance and the $\frac{E_y}{B}$ calculation, which are essentially independent of one another, lends some credance to the neglect of $^{j}y/\sigma_o$ in the E_y analysis.

3. Degree of Ionization

If the integration of the streamwise electric field, equation VIII-11, is applied to obtain u_f the degree of ionization α must be known. If u_f is known, and α assumed constant with the same reservations expressed previously, VIII-11 can be solved to determine α . Such a calculation gives α = .23. To provide this degree of ionization, less than 10 per cent of the total energy delivered to the discharge during the duration of the pulse is required.

CHAPTER IX

CONCLUSIONS AND RECOMMENDATIONS

Based on the experimental studies which have been conducted and reported in this work, several of the questions posed in Chapter I can now be partially answered. The recommendations which will be made are directed toward answering these questions more completely.

A. ELECTRODYNAMIC STABILIZATION

Stabilization of the current pattern will occur at electrode to insulator junctions whether they are artificially created as in the parallel plate accelerator, or exist naturally because of the termination of the electrodes as in the orifice pinch or coaxial gun. The insulator referred to above may be nylon, mylar, or simply the exhaust vacuum. Stabilization is the achievement of the steady state current conduction pattern as determined by the electrodynamic boundary conditions. For rectangular current pulses, current pattern stabilization will occur if the pulse duration is long enough to permit the convecting current distribution to assume the final steady state configuration. In the experiments performed, the current pattern is generally able to reach the steady state distribution on a time scale of tens of microseconds which determines the characteristic time scale for current pattern stabilization.

That the current pattern should be two-dimensional and assume a hairpin like shape in the stabilized phase can be shown by the following example. Consider two parallel plates each containing a metal to insulation junction at the same axial location, in between which is immersed a static uniformly conducting medium. Assume that a steady state current flow is established whose spatial distribution is now sought. The pertinent equations are:

$$\vec{j} = \sigma \vec{E} \qquad \text{Ohm's Law}$$

$$\nabla \times \vec{E} = 0 \qquad \text{Faraday's Law}$$

$$\nabla \cdot \vec{E} = 0 \qquad \text{Gauss' Law.}$$

Since $\vec{j}$ can be substituted for $\vec{E}$ in the last two equations, the current streamlines can be determined from Laplace's equation since both the curl and divergence of $\vec{j}$ are zero. This problem is completely analogous to determining the fringing electric fields at the ends of a parallel plate capacitor whose field is known to bow out from the edges of the plates.[49]

If the highly conducting medium is moving, i.e. has a flow velocity, the current pattern will bow out even further, being blown downstream as it were by the flow.[50] Although this simple model does not rigorously apply to a self field electromagnetic accelerator where $\vec{E}$ is dominated by $\vec{u} \times \vec{B}$ and not $\vec{j}/\sigma$ it is indicative of the general shape of the current distribution which would occur in the latter.

B. EXHAUST OF A PULSED PLASMA ACCELERATOR

In driving the orifice pinch with rectangular current pulses whose pulse length is much greater than pinch time, or the parallel plate with pulses larger than the sheet transit time along the electrodes, the current remained attached to the electrodes and stabilized spatially as has been seen. Unlike previous experience with rapidly varying pulses which create successive current sheets or shed the exhaust plume current via a short circuiting and current vortex generation mechanism, no such tendency has been observed when the circuit current remains constant with time.

For a pulsed plasma accelerator which operates for a few tens of microseconds or less, a time generally too short to supply fresh gas to the discharge, stabilization of the current pattern is probably disadvantageous. This is based on the premise that perfectly sweeping current sheets can be created. If they cannot, stabilization would be beneficial since any residual gas left behind by the sheet would be accelerated by the stabilized phase. If perfectly sweeping sheets can be created, however, operation in the pulsed flow mode is unattractive for two reasons:
1) Unless the mass flow rate is properly programmed to the stabilized discharge, inefficient operation of the thruster is likely to result. If the discharge is starved for mass, most likely the case to occur, most of the input energy will go into resistive dissipation and not into useful acceleration of the gas.
2) If current continues to flow at the time of plasma ejection, not only will there be increased dissipative losses, but there could be considerable energy stored inductively in the magnetic field which is not available for gas acceleration.

Pulsed plasma exhaust studies should be continued particularly with current pulses whose pulse duration is roughly equivalent to pinch time or transit time along the electrodes. These experiments should utilize the optimal energy transfer techniques developed by Wilbur at Princeton[51], and, in addition to independent velocity determinations similar to those made in the past, should now include the capability of determining the fraction of the initial mass exhausted, i.e. mass utilization. Such an empirical determination could be made by means of a thrust balance whose output is integrated with respect to time to obtain the total impulse. Of particular interest would be the scaling of such parameters as mass utilization and exhaust efficiency as the ratio of pulse length to ejection time is systematically varied.

C. QUASI-STEADY PLASMA ACCELERATION

It has been seen that the quasi-steady mode of plasma acceleration can be established on a time scale of hundreds of microseconds and that acceleration of the gas occurs roughly in agreement with the simple model of Appendix B.

The experiments described here have been performed by going to very long duration pulses at the expense of current amplitude. The long time is necessary for the gas flow to become established through the discharge. Many of the difficulties encountered with the present setup can be circumvented and many of the effects seen can be enhanced, if a much larger capacitor bank is provided with the capability of delivering large amplitude current pulses for long durations, e.g. $^{100}/_{500}$. If such a pulse were available, many advantages would be gained: 1) The V_{uB} generated at stabilization would dominate the resistive drop, V_R . Since V_{uB} theoretically is flow sensitive, more accurate determinations of minimum times necessary for gas flow establishment could be made. This is especially important when various gas injection techniques are studied. 2) The outflow velocity would be in an electric propulsion range of interest unlike the long duration pulses studied here. 3) With higher current discharges, signal strengths would be much higher, probe perturbations of the discharge would be reduced, and smaller probes could be employed, all contributing to more accurate probing of the discharge and a truer description of its physical operation. 4) The flow luminosity would be much more intense and flow visualization, particularly the wedge flow studies, should be greatly improved, and 5) the two dimensionality of the discharge would be highly improved.

Appendix A

MASS FLOW RATE DETERMINATION

To determine the mass flow rates into the discharge from the shock tube during the duration of the current pulse, a simple cold gas flow technique is employed. The term "cold" refers to the fact that the capacitor bank is not electrically charged and then discharged through the gas. The parallel plate accelerator is pumped down as usual below 1μ and the shock tube diaphragm is ruptured, initiating the switch and chamber filling flows. The pressure in the main chamber is monitored as a function of time at a series of positions by means of highly sensitive piezoelectric pressure gauges described in Chapter III. The gauges enter the channel through access ports milled in the anode and are placed with their flat sensing surfaces flush with the anode surface. In this orientation, only the static pressure is measured. The gauges are an inch in diameter and can be centered at x = 2 7/8", 6 1/8", 9 3/8", 12 5/8" and 15 7/8".

Two nearly identical probes are used; one probe is always located at x = 2 7/8" while the second probe may be placed in any of the four remaining probing locations. In the main case of interest i.e. 1/8" diameter orifices in the chamber feed lines, the chamber pressure at the breakdown location is nearly 100μ when the discharge initiates. Time t = 0 in the cold flow experiments is assumed to occur when the pressure at the first probing location, x = 2 7/8", equals 100μ. Using this point as a time reference, the pressure versus time data at the five probing positions can crossplotted to yield the spatial distribution of pressure in the channel at a series of times from 0 to 300 μsec, the duration of the current pulse.

Assuming that the gas is at room temperature and having determined the pressure distribution, the total mass of gas in the chamber can be calculated at each time. The mass flow rate to the chamber for each time interval is simply $\Delta m/\Delta t$. Using 50 μsec time intervals, the mass increments are found to be nearly constant over a time equivalent to the duration of the current pulse. This indicates that the mass flow rate to the discharge is relatively constant throughout the duration of the current pulse. The mass increments are averaged and an average mass flow rate is calculated. If the mass flow rate is nearly constant, the mass flow rate can be calculated by determining the mass increment supplied during a time equal to the pulse duration and dividing this mass increment by the pulse length.

Using this technique, the mass flow rate is found to be 3.6 grams/sec for the 1/8" chamber feed line orifices, 1.4 grams/sec for the 1/16" dia. orifices, and 7.5 grams/sec with no orifices in the 1/4" dia. lines. Based on the assumptions made, these values can be considered, at best, estimates of the actual mass flow rates to the discharge.

The pressure measurements also reveal that the channel does not fill uniformly but by means of a broad pressure wave propagating down the channel. Based on the times of arrival of the leading edge of this wave at the various probe locations its propagation speed is found to be about 750 ^{m}/sec. The escape speed of room temperature argon is 960 ^{m}/sec [52] and hence the above value is not too unreasonable.

APPENDIX B

A CONTROL VOLUME MODEL OF STEADY FLOW, SELF FIELD, ELECTROMAGNETIC GAS ACCELERATION

From a propulsion standpoint, it is of interest to be able to forecast the limiting velocity increment which can be imparted to an ionized gas flow. In Figure B-1 is shown the model to which the following simple analysis will be applied. The model is based on the experimental observations that have been made in this work. A gas flow with the initial parameters shown enters the current zone, interacts with it, and leaves the zone with the terminal values shown. The inlet and outlet flows are assumed to be one dimensional and uniform across the channel; the flow in the current zone may or may not be one dimensional. However, the field distributions in the current zone must be two dimensional due to the electric field boundary conditions posed and Maxwell's steady state relation that

$$\nabla \times \vec{E} = 0$$

If the flow field is one dimensional throughout, the steady state conservation laws, continuity, momentum, and energy, together with the perfect gas law result in the following differential equations,[2]

continuity $\quad \frac{d}{dx}(\rho u) = 0$

AP 25 R 4461 68

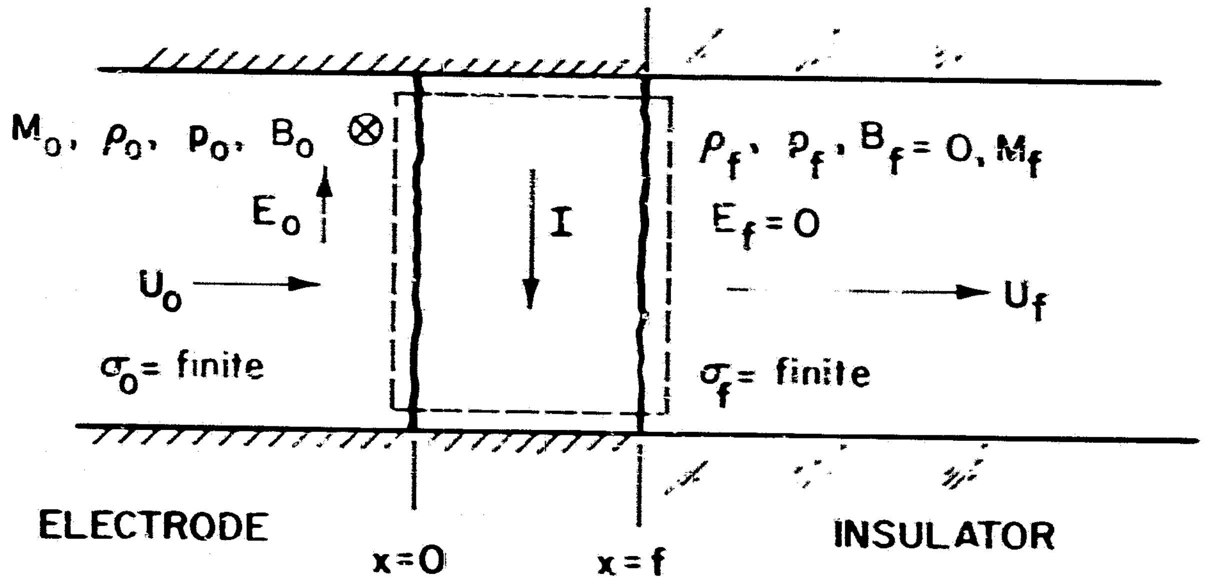

THEORETICAL MODEL

FIGURE B-1

momentum $$\rho u \frac{du}{dx} + \frac{dp}{dx} = -\frac{B}{\mu_c}\frac{dB}{dx}$$

energy $$\frac{d}{dx}\left(\frac{\gamma}{\gamma-1}pu + \rho\frac{u^3}{2}\right) = \vec{j}\cdot\vec{E}$$

wherein much of one's ignorance concerning the precise internal state of the gas, e.g. degree of ionization, is absorbed in γ. The differential equations for conservation of mass and momentum integrate exactly to algebraic expressions. Integration of the energy equation to an algebraic form is possible only if the detailed structure of the current zone, i.e. the distributions of $\vec{j}$ and $\vec{E}$, is known. If the structure is known and the integration performed, the three conservation laws result in three algebraic equations which can be solved for the three unknowns of interest, u_f, p_f, and ρ_f assuming the inlet parameters are known. This difficulty, i.e. the necessity to know the detailed structure of the zone, can be avoided by using a control volume approach [53] in which the current zone is essentially treated as a black box.

Applying conservation of mass, momentum, and energy to the dotted control volume of Figure B-1, the conservation laws in control volume form lead to the following three equations

$$\rho_o u_o A = \rho_f u_f A \qquad \text{(B-1)}$$

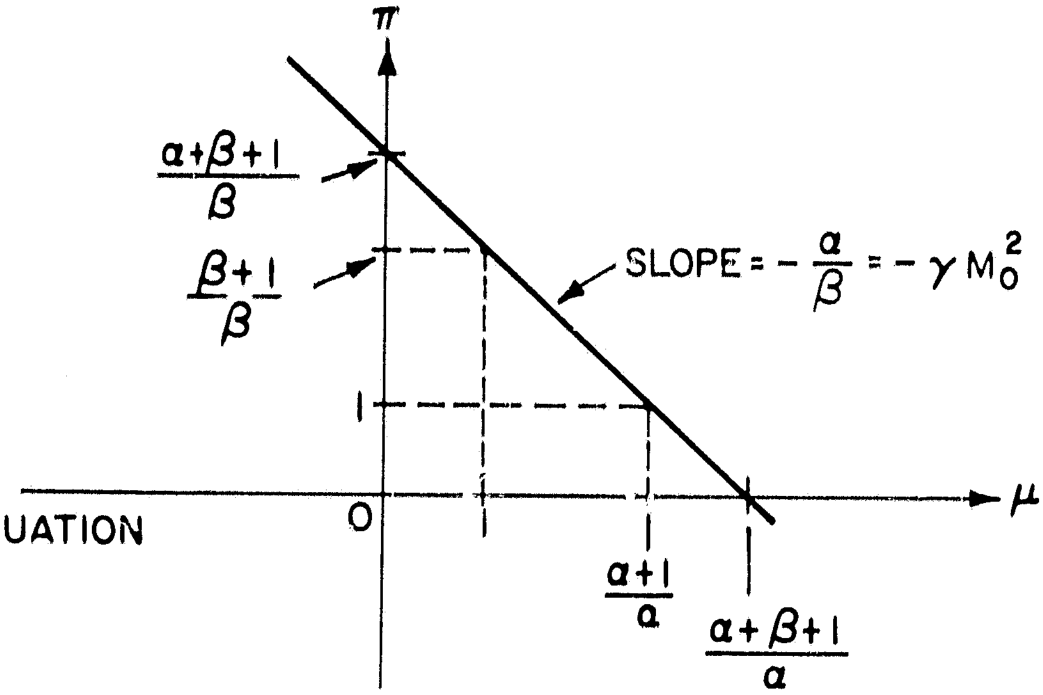

A) MOMENTUM EQUATION

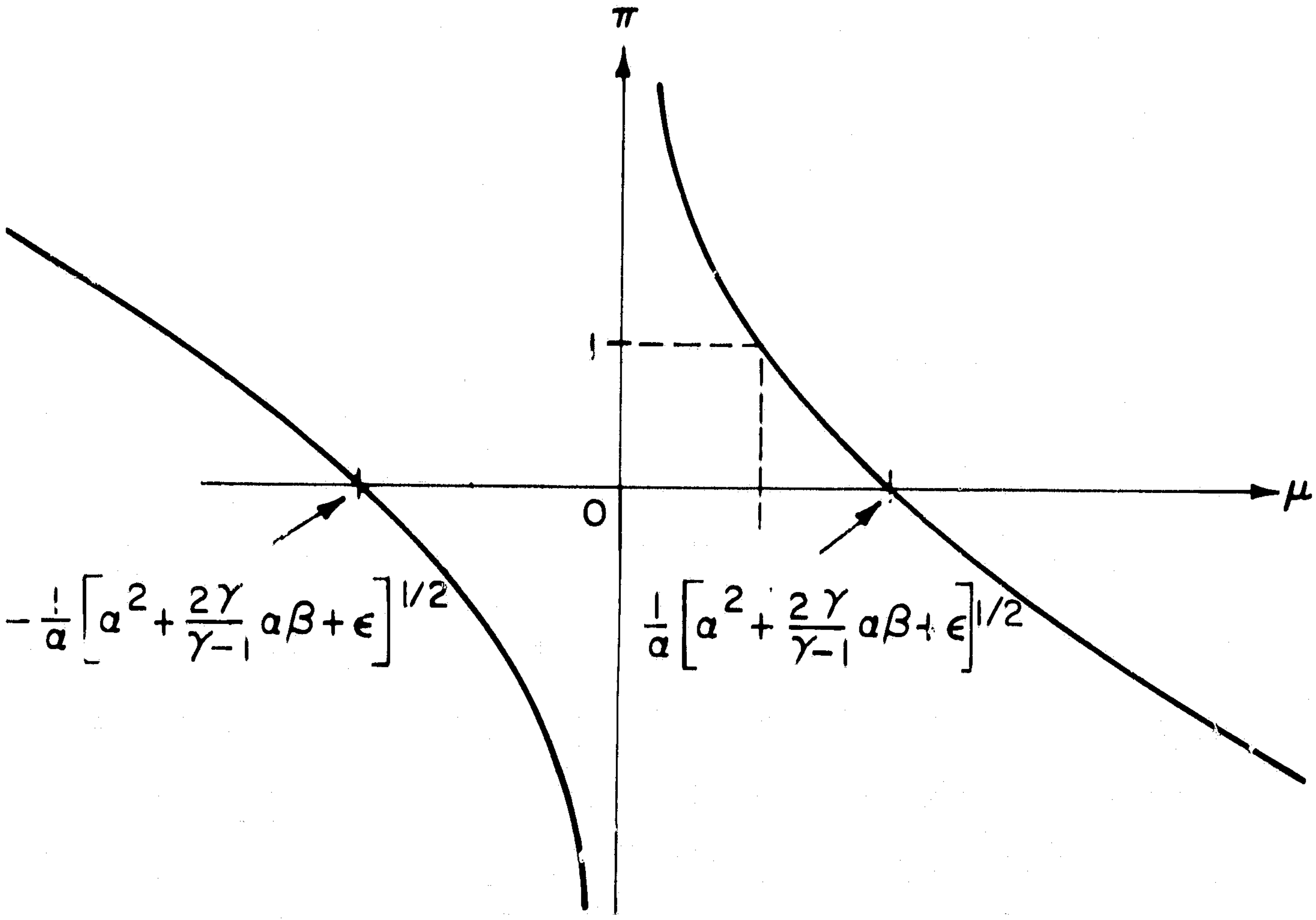

B) ENERGY EQUATION

GRAPHS OF FLOW EQUATIONS

FIGURE B-2

$$(p_o + \rho_o u_o^2)A + \int_{C.V.} (\vec{j}\times\vec{B})_x \, dv = (p_f + \rho_f u_f^2)A \qquad \text{(B-2)}$$

$$\left(\frac{\gamma}{\gamma-1} p_o u_o + \rho_o \frac{u_o^3}{2}\right)A + \int_{C.V} \vec{j}\cdot\vec{E} \, dv = \left(\frac{\gamma}{\gamma-1} p_f u_f + \rho_f \frac{u_f^3}{2}\right)A \qquad \text{(B-3)}$$

where the inlet and the outlet flows are assumed to be one dimensional and uniform over the inlet and outlet area,, A, of the control volume. No assumptions need be made concerning the interior of the control volume. The integral of the streamwise component of the $\vec{j} \times \vec{B}$ force throughout the control volume is easily evaluated for a two dimensional current distribution by first noting that

$$(\vec{j}\times\vec{B})_x = j_y B_z$$

and that from Amperes Law

$$j_y = -\frac{1}{\mu_o}\frac{dB_z}{dx}$$

Substituting into the integral of equation (B-2) one obtains that

$$\int_{C.V.} (\vec{j}\times\vec{B})_x \, dv = \int_0^w \int_0^h \int_0^f \left(-\frac{1}{\mu_o}\right) B_z \frac{dB_z}{dx} \, dx\,dy\,dz = \frac{B_o^2}{2\mu_o} A$$

The integral of $\vec{j}\cdot\vec{E}$ throughout the control volume is just the electrical power into the gas, i.e. the product of the total current I and voltage drop across the control volume, V, which can be obtained experimentally. It should be pointed out that the V to be used is the total voltage drop across the electrodes minus the electrode sheath drops. It is assumed here that the power dissipated in the thin sheaths is lost to the electrodes. Having so identified the integrals, and making the identification that

$$F = \rho_c u_o = \rho_f u_f$$

the mass conservation equation can be eliminated from the system of equations resulting in the following two equations for the two unknowns of interest, u_f and p_f,

$$p_o + F u_c + \frac{B_c^2}{2\mu_c} = p_f + F u_f \tag{B-4}$$

$$\frac{\gamma}{\gamma-1} p_o u_o + \frac{F u_c^2}{2} + \frac{IV}{A} = \frac{\gamma}{\gamma-1} p_f u_f + \frac{F u_f^2}{2} \tag{B-5}$$

Equations (B-4) and (B-5) can be solved for p_f and u_f if the input parameters of the flow are known. In the experiments described in this work, however, the input flow parameters are generally unknown. In the special case of experimental interest here, in which the magnetic pressure $B_o^2/2\mu_c$ greatly exceeds the gasdynamic pressure p_o, it can be shown that there is an upper limit on the velocity ratio which can be achieved. To obtain this upper limit and see how it compares with the experimentally determined values obtained in Chapter VIII, it is convenient to nondimensionalize equations (B-4) and (B-5) in terms of the following definitions:

$$\mu \equiv \frac{u_f}{u_c} \qquad \pi \equiv \frac{p_f}{p_o} \qquad \beta \equiv \frac{p_o}{B_c^2/2\mu_c} \qquad \alpha \equiv \frac{F u_c}{B_c^2/2\mu_c} \qquad \epsilon = \frac{2FIV}{A\left(B_o^2/2\mu_c\right)^2}$$

One can easily show that

$$\alpha = \gamma \beta M_o^2 \tag{B-6}$$

where M is the Mach number. In terms of the above, the momentum and energy balance equations become respectively

$$\alpha + \beta + 1 = \alpha\mu + \beta\pi \tag{B-7}$$

$$\alpha^2 + \frac{2\gamma}{\gamma-1}\alpha\beta + \epsilon = \frac{2\gamma}{\gamma-1}\alpha\beta\pi\mu + \alpha^2\mu^2 \tag{B-8}$$

The momentum equation (B-7) and the energy equation (B-8) are sketched in the π-μ plane in Figure B-2a,b. The momentum equation is a straight line with intercepts and slope as noted; the energy equation is hyperbolic with the intercepts as noted and the vertical asymptote along the π axis. Physically meaningful solutions occur when the two equations intercept in the first quadrant above the isentropic as shown in Figure B-3. Relaxing the requirement that the curves intercept on or above the isentropic, it is clear that the momentum equation can only intercept the energy equation in the first quadrant and yield accelerator solutions, $\mu > 1$, if and only if, the μ axis intercept of the momentum equation is less than or equal the μ axis intercept of the energy equation. Invoking this condition one finds the following requirement

$$\frac{(\gamma-1)\left[(1+\beta)^2 - \epsilon\right]}{\beta - \gamma + 1} \leq 2\alpha \tag{B-9}$$

In the limit as $\beta \ll 1$, this leads to the condition on α that

$$\frac{\epsilon - 1}{2} \leq \alpha \tag{B-10}$$

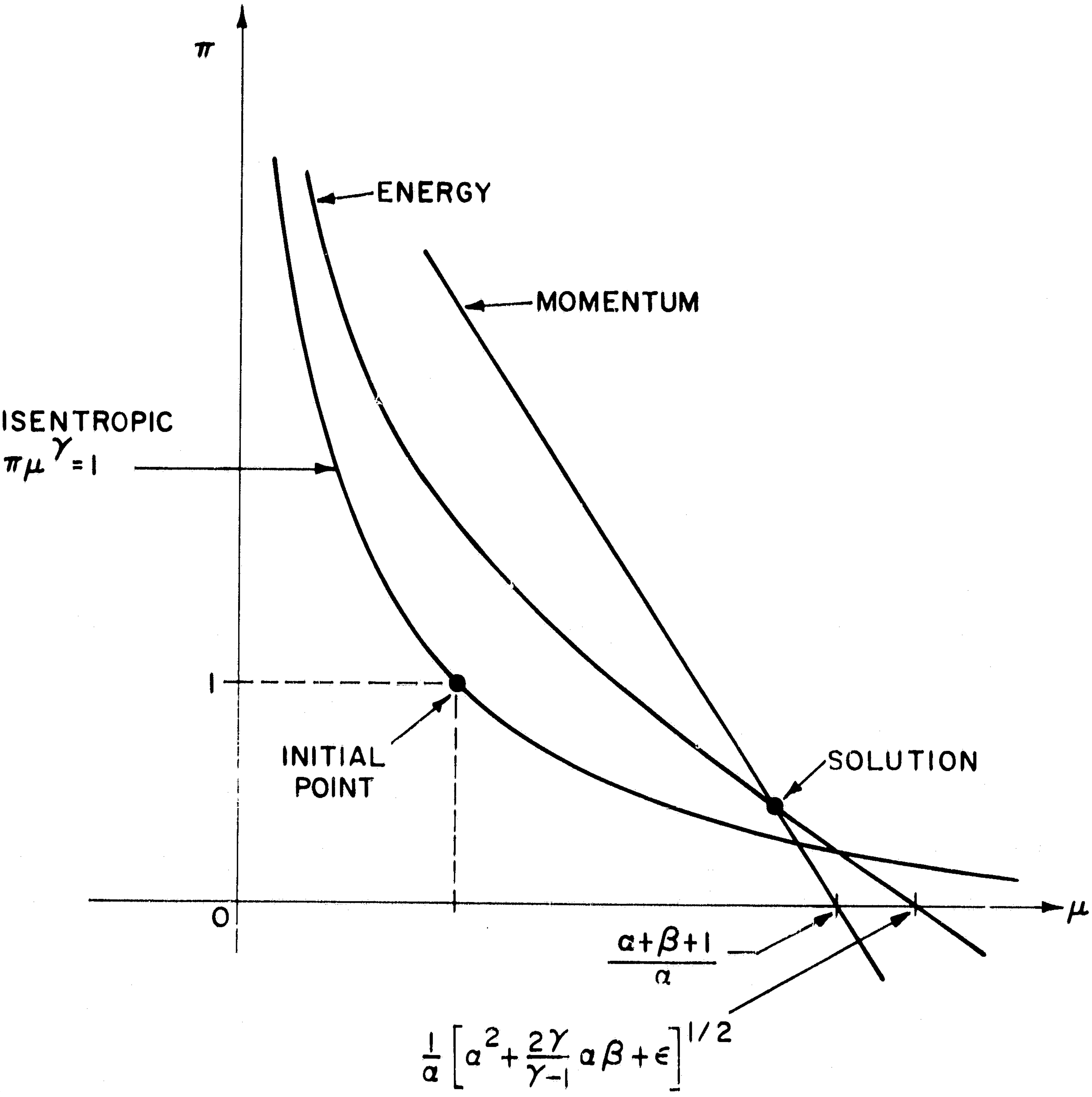

DEMONSTRATION OF THE INTERCEPT CRITERION

FIGURE B-3

Inserting this into the momentum equation with $\beta << 1$ imposed, one obtains the result that

$$\mu \leq 1 + \frac{2}{\epsilon - 1} \tag{B-11}$$

Once ϵ is evaluated, the upper limit on μ can be obtained.

To obtain V from the total voltage, the sheath drops must be estimated and subtracted out. The sheath drops have been estimated by plotting the experimentally determined resistive voltage drops in 100μ argon as a function of discharge current and linearly extrapolating to zero current. The voltage intercept at zero current is taken to be the total of the sheath drops. Essentially the assumption is made that the sheath drops are independent of discharge current. There are experimental indications that this may indeed be the case.[53] At the anode of some magnetoplasmadynamic arcjets the power to the anode is found to scale linearly with the discharge current.

For the $^{120}/20$ 5 1/4 " electrode length case an exact determination of the sheath drops is somewhat academic. The total voltage drop is 700 volts and the sheath drops are estimated to total 40 volts via the abovementioned method. Twenty-five per cent errors in the determination of the sheath drops lead to less than a 2 per cent variation in the calculated ϵ value. Using the experimentally determined value of 15.3 $^{\text{kgm}}/\text{m}^2 \cdot$ sec for F from Chapter VIII along with I, V, P_o and A in the expression for ϵ , one obtains $\epsilon = 2.1$; this corresponds to $\mu \leq 2.8$. The velocity ratio experimentally obtained in Chapter VIII is 2.25 which, of course, does not exceed the limiting value predicted by the model.

For the $^{10}/250$, 2" electrode case, the total voltage drop is 48 volts. From the extrapolation technique the sheath drops are estimated to be about 30 volts for this electrode length. The determination of ϵ is very sensitive to the value of the sheath drop chosen. For instance, a 25 percent error in the determination of the sheath drops in this case leads to a variation in ϵ of more than 40 percent. F is simply $\dot{m}/A$, where $\dot{m}$ is 3.6 (10^{-3}) $^{kgm}/sec$ as determined in Appendix A. Substituting this value of $\dot{m}$, a V of 18 volts along with I, B_o and A, ϵ is calculated to be about 4.0, which leads to $\mu \leq 1.7$. The velocity ratio experimentally determined in Chapter VIII is 2.7, exceeding the upper limit calculated. If this ratio, i.e. 2.7, is assumed to be the upper limit, the calculation can be performed in reverse and the sheath drop calculated. This leads to a sheath drop of about 40 volts, roughly 33 percent higher than the value chosen, but within the error involved in the linear extrapolation of the data to zero current.

Before this model can be reliably used to predict upper limits on the velocity ratios achievable in pulsed flow and quasi-steady flow accelerators, it is clear that the total sheath voltage drop should be accurately determined experimentally.

REFERENCES

1. E. Stuhlinger, Ion Propulsion for Space Flight, McGraw Hill, New York (1964).

2. R. G. Jahn, The Physics of Electric Propulsion, McGraw Hill, New York (1968).

3. M. Rosenbluth, et al., "Infinite Conductivity Theory of the Pinch", Los Alamos Scientific Laboratory Report LA-1850.

4. R. L. Burton, "Structure of the Current Sheet in a Pinch Discharge", Princeton University Ph.D. Thesis (1966).

5. W. R. Ellis, Jr., "An Investigation of Current Sheet Structure in a Cylindrical Z Pinch", Princeton University Ph.D. Thesis (1967).

6. T. M. York, "Pressure Distribution within the Structure of a Propagating Current Sheet", Princeton University Ph.D. Thesis (1968)

7. W Bostick, "Experimental Study of Ionized Matter Projected Across a Magnetic Field", Physical Review, 104, p. 299 (1956).

8. R G. Jahn, W. von Jaskowsky, and R. L. Burton, "Ejection of a Pinched Plasma from an Axial Orifice", AIAA J., 3, 10, p. 1862 (October 1965).

9. K E. Clark and R. G. Jahn, "The Magnetoplasmadynamic Arcjet" Astronautica Acta, 13, pp. 315-325, (1967).

10. K. E. Clark, " Quasi-Steady Plasma Acceleration", Princeton University Ph.D. Thesis (1968).

11. D. E. T. F. Ashby, L. Liebing, and A. V. Larson, "Quasi-Steady State Pulsed Plasma Thrusters", AIAA J, 4, 5, pp. 831-835, (May 1966).

12. N. A. Black and R. G. Jahn, "On the Dynamic Efficiency of Pulsed Plasma Accelerators", AIAA J., 3, 6, pp. 1209-10 (June 1965).

13. R. G. Jahn and W. von Jaskowsky, "Structure of a Large Radius Pinch Discharge", AIAA J., 1, 8, pp. 1809-1814 (August 1963).

REFERENCES-cont'd

14. R. G. Jahn, W. von Jaskowsky, and A. L. Casini, "Gas Triggered Pinch Discharge Switch", RSI, 36, 1, pp. 101-102 (January 1965).

15. "Pulsed Electromagnetic Gas Acceleration", First Semi-Annual Progress Report, Princeton University, Guggenheim Laboratories for the Aerospace Propulsion Sciences, Report No. 634 (1962).

16. "Pulsed Electromagnetic Gas Acceleration", Fourth Semi-Annual Progress Report, Princeton University, Guggenheim Laboratories for the Aerospace Propulsion Sciences, Report No. 634c (1964).

17. R. G. Jahn and K. E. Clark, "A Large Dielectric Vacuum Facility", AIAA J., 4, 6, p. 1135 (June 1966).

18. "Pulsed Electromagnetic Gas Acceleration", Tenth Semi-Annual Progress Report, Princeton University, Guggenheim Laboratories for the Aerospace Propulsion Sciences, Report No. 634i (1967).

19. C. K. Chu, "Kinetic-theoretic Description of the Formation of a Shock Wave", Phys. Flds., 8, 1, pp. 12-22 (January 1965).

20. G. Bienkowski, "Propagation of an Initial Density Discontinuity Fourth Symposium of Rarified Gas Dynamics, Volume I (Toronto, 1965).

21. J. K. Wright, "An Apparatus For the Production of Intense Shock Waves", Proceedings of the IVth International Conference on Ionization Phenomena in Gases, Volume II, p. 1105 (1959).

22. T. H. Jensen and V. O. Jensen, "Description of an Experiment with a Magnetically-driven Shock", Research Establishment Risö Report No. 20 (Nov. 1960).

23. V. O. Jensen, A. H. Sillisen, F. H. Vinther and C. F. Wandel, "An Experiment on Magnetically Driven Shocks", Research Establishment Risö Report No. 28 (June 1961).

24. J K. Wright and M. C. Black, "A Theory of Electromagnetically Driven Shock Waves", Jrnl. Fld. Mech., 6, p. 219 (1959).

25. T. F. Morse, "Electromagnetic Acceleration of a Shock Wave in a Constant Area Duct", Phys. Fluids, 5, 2, p. 596 (May 1962).

REFERENCES cont'd

26. M. F. Maes, "Experimental Investigation of the Confined Parallel Rail Pulsed Plasma Accelerator", Proceedings of the Third Annual Symposium on the Engineering Aspects of MHD. Gordon and Breach, Science Publishers, New York, pp. 439-465 (1964).

27. L. Liebing, "Motion and Structure of a Plasma Produced in a Rail Spark Gap", Phys. Fluids, 6, 7, p. 1035 (July 1963).

28. O. M. Friedrich and A. A. Dougal, "Current Sheath Dynamics and Magnetosonic Oscillations in Magnetoplasmas", NASA CR-309 (October 1965).

29. T. N. Lie, A. W. Ali, E. A. MacLean, and C. C. Chang, "Diagnostics of Accelerating Plasmas", Catholic University of America, Dept. of Space Sciences and Applied Physics, Report No. 66-021.

30. J. R. MacLelland, A. S. MacKenzie and J. Irving, "Schlieren Photography of Rail Tube Plasmas", Phys. Fluids, 9, 8, p. 1613 (August 1966).

31. R H. Lovberg, "Acceleration of Plasmas By Displacement Currents Resulting From Ionization", Proceedings of the VIth International Conference on Ionization Phenomena in Gases, Paper IX 6 (Paris, 1963).

32. D. H. Winicur, "Electric Propulsion Characteristics of a Pulsed Plasma Rail Accelerator," AIAA J. 2, 9, p. 1673 (September 1964).

33. R. L. Burton and O. Chang, "Acceleration Processes in a Stabilized High Current Arc", University of California at San Diego, Report IPAPS 67/68-214 (April 1968).

34. G. N. Glasoe and J. V. Lebacqz, Pulse Generators, McGraw-Hill, New York, Chapter 6 (1948).

35. S. Ramo, J. R. Whinnery and T. Van Duzer, Fields and Waves in Communications Electronics, Wiley, New York, Chapter 1 (1965).

36. R. H. Huddlestone and S. T. Leonard, Editors, Plasma Diagnostic Techniques, Academic Press, New York (1965).

REFERENCES-cont'd

37. G W. Sutton and A. Sherman, Engineering Magnetohydrodynamics, McGraw-Hill, New York, (1965).

38. E Brunner and M. Javid, Analysis of Electrical Circuits McGraw-Hill, New York, pp. 218-220 (1959).

39. W Koeppendorfer, "Induction Coils for Fast High Current Gas Discharges", Institute for Plasma Physics, Munich-Garching, Report IPP p. 12 (November 1961).

40. E. O. Johnson and L. Malter, "A Floating Double Probe Method for Measurements in Gas Discharges", Physical Review, 80, 1, p. 58 (October 1950).

41. L. C. Burkhardt and R. H. Lovberg, "Current Sheet in a Coaxial Gun", Phys. Fluids, 5, 3, p. 341 (March 1962).

42. R. Lovberg, "Inference of Plasma Parameters from Measurements of E and B Fields in a Coaxial Accelerator", Phys. Fluids, 7, Part 2, 11, p. 557 (November 1964).

43. "Pulsed Electromagnetic Gas Acceleration", Fifth Semi-Annual Progress Report, Princeton University, Guggenheim Laboratories for the Aerospace Propulsion Sciences, Report No. 634d (1964).

44. "Pulsed Electromagnetic Gas Acceleration", Sixth Semi-Annual Progress Report, Princeton University, Guggenheim Laboratories for the Aerospace Propulsion Sciences, Report No. 634e (1965).

45. N. A. Black, "Dynamics of a Pinch Discharge Driven by a High Current Pulse-Forming Network", Princeton University Ph.D. thesis (1966).

46. F. W. Mezger, "Stationary Current Sheet Model For Plasma Acceleration", General Electric Space Sciences Laboratory, Report R65SD21, pp. 1, 2 (May 1965).

47. D. E. T. F. Ashby, T. J. Gooding, B. R. Hayworth and A. V. Larson, "Exhaust Measurements on the Plasma from a Pulsed Coaxial Gun". AIAA J., 3, 6, pp. 1140-1142 (1965).

48. "Pulsed Electromagnetic Gas Acceleration", Ninth Semi-Annual Progress Report, Princeton University, Guggenheim Laboratories for the Aeropace Propulsion Sciences, Report No. 634h (1966).

REFERENCES-cont'd

49. R. P. Feynman, R. B. Leighton, and M. Sands, The Feynman Lectures on Physics, Addison-Wesley, Reading, Mass., Vol. II, pp. 6-12 (1963).

50. A. Sherman and H. Yeh, "Blowing of Current Patterns in Nonequilibrium Plasmas", AIAA J., 5, 9, pp. 1689-1690 (September 1967).

51. P. J. Wilbur, "Energy Transfer From a Pulse Network to a Propagating Current Sheet", Princeton University Ph.D. thesis (1968).

52. A. Shapiro, The Dynamics and Thermodynamics of Compressible Fluid Flow, Ronald Press, New York, Volumn II, p. 947 (1957).

53. A. Shapiro, The Dynamics and Thermodynamics of Compressible Fluid Flow, Ronald Press, New York, Volume I, (1953).

54. A. V. Larson, "Experiments on Current Rotation in an MPD Engine", AIAA J. 6, 6, pp. 1001-1006 (June 1968).